La Rivista del Nuovo Cimento (2023) 46:163–291
https://doi.org/10.1007/s40766-023-00042-9

REVIEW PAPER

50th anniversary review of the Mediterranean desiccation hypothesis

William B. F. Ryan[1]

Received: 22 February 2023 / Accepted: 17 April 2023 / Published online: 13 June 2023

Abstract

The first deep-sea drilling expedition in the Mediterranean chanced upon unanticipated discoveries when recovering deeply buried sediments of Late Miocene age that had once accumulated in ultra-shallow water and had later experienced subaerial exposure. Among these deposits were potassium and magnesium chlorides, desiccation cracks, fluvial gravels and shale bearing bottom-dwelling diatoms requiring sunlight, all indicative that the Mediterranean had evaporated one or more times to near dryness during what became called the Messinian Salinity Crisis. The initial presentation of these findings in 1973 was met with hesitancy. Had the present 2 to 4 km deep Mediterranean Basins been much shallower? How does one explain sediment sandwiched between beds of anhydrite and gypsum that hosted microfossils belonging to both ocean seawater and species that lived in fresh-to-brackish water lagoons? Did all of the evaporites originate on salt pans rimmed by alluvial aprons, or was there a deep-water period during which most of the 1 to 2 km thick layer of salt layer had arrived? How do the Late Miocene evaporites and mudstones outcropping in mobile belts along numerous Mediterranean margins fit with the scenario of a near empty Mediterranean? These inquiries are addressed in the style of a historical narrative reviewing 50 years of investigations by researchers turning their attention to the peripheral deposits, including those from the Paratethys. The stable isotopes of oxygen, carbon, sulfur, deuterium and strontium become crucial evidence in support of a substantial Mediterranean desiccation that harmonizes what appears to be unresolved conflicts among prior and even contemporary interpretations.

Keywords Mediterranean · Messinian · Lago-Mare · Desiccation · Evaporites · Halite · Anhydrite · Gypsum · Erosion surfaces

✉ William B. F. Ryan
billr@ldeo.columbia.edu

[1] Lamont-Doherty Earth Observatory of Columbia University, 61 Route 9W, Palisades, NY 10964, USA

1 Introduction: Early thoughts of an evaporating Mediterranean Sea

The first hints of a possible evaporation of the Mediterranean Sea can be traced to the Leicester Codex of Leonardo da Vinci (1452–1519) in text accompanying his drawing of a method for measuring the rate of evaporation of water as it is being heated. Actual evidence of evaporation came centuries later when in the process of investigating the proliferation of gastropods from margins of Algeria, Spain, Sicily and the Italian peninsula Giuliano Ruggieri recognized "*a clearly evaporitic situation … with gypsum and salt extending throughout the western Mediterranean.*" [1]. He doubted that any fauna could have survived in the abyss where all marine life was likely to have been "*totally destroyed by the adverse environmental conditions*" [2]. For Ruggieri, the replacement of the *Melanopsis* species on shores of evaporating lagoons by the sudden introduction of new marine life from the Atlantic, including deep-water corals, led him to propose a rapid transgression at the commencement of Charles Lyell's Pliocene Epoch [3].

Raimando Selli linked the evaporative and lacustrine events to the Messiniano of Mayer–Eymer and placed them together in the latest stage of the Miocene that he named the Messinian [4, 5]. Selli introduced the term 'crisis of salinity' (crisi di salinitá) that is now called the Messinian Salinity Crisis (MSC). He used the MSC to encompass not only a dramatic environment change in the Mediterranean, but also throughout the eastern European region known as the Paratethys that remained fresh when the Mediterranean became hyperhaline.

In the Mediterranean region, Selli's Messinian stage began with pre-evaporitic euxinic sediments rich in diatoms that he labeled the Formazione Peliti Eusiniche, followed by an extreme saline interval represented by the Formazione Gessoso Solfifera, and ending with a fresh-to-brackish interval called the Formazione a Colombacci. The Gessoso Solfifera, consisted of repetitious beds of gypsum in the crystal appearance of selenite that had been described by Pliny the Elder in his first volume of Natvralis Historiæ (77 AD) as lapis specularis, or mirror stone for its reflective surface and glass-like transparency.

In the deepest subsurface of the Caltanissetta basin in Sicily the Gessoso Solfifera also entailed sodium and potassium–magnesium rich salts (halite and kainite) reaching 400–600 m in thickness in subsurface mines [6–8]. These salts were thought to have precipitated in land-locked bodies of super-saturated brine. They were overlain unconformably by earliest-Pliocene marls of the Formazione Trubi [9, 10]. The Trubi marls were populated by planktonic foraminifera (97–99%) with species that lived in a relatively deep and fully-marine environment.

2 Discovery of an abyssal salt layer

The possibility that layers of salt, like those in the subsurface of Sicily, might also exist beneath the floor of the Mediterranean Sea was first revealed by Cousteau and Alinat [11]. Using echo-soundings while aboard the vessel Calypso of the Musée Océanographiqie de Monaco, they discovered small knolls (called petits accidents) on the otherwise flat seabed in the Ligurian Sea at water depths exceeding 2.5 km. When

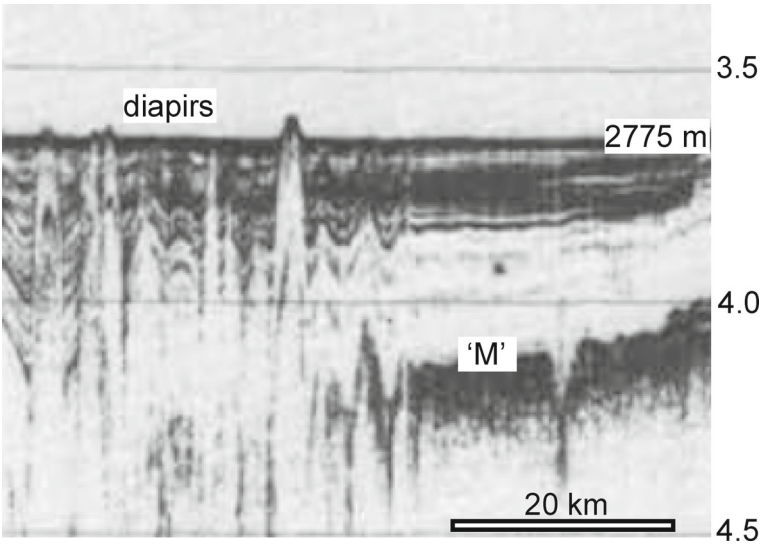

Fig. 1 Vintage 1965 reflection profile with diapirs protruding through Reflector 'M' and reaching the seabed to form knolls. Vertical scale is reflection time in seconds two-way travel time (twtt)

later viewed in seismic reflection profiles these knolls turned out to be piercement diapirs (Fig. 1) that arose from a presumed layer of salt [12–19]. The diapirs penetrated through the highly reverberant sub-bottom reflector 'M' that had been observed throughout deeper regions of the western and eastern Mediterranean [20].

Seismic refraction measurements showed that Reflector 'M' corresponded to the top of consolidated material [21–24]. A deep cleft in the seabed southwest of Crete had allowed a piston-coring device to sample earliest-Pliocene foraminifera-rich limestone close to the top of Reflector 'M'. The limestone had the same foraminiferal assemblage as present in the Trubi Formation in Sicily, the first indication that the salt might be an abyssal equivalent to the Gessoso Solfifera [20, 25].

At the same time this limestone had been sampled by piston-coring, the U.S. National Science Foundation entered into a contract with the Regents of the University of California to fund the Deep-Sea Drilling Project (DSDP). Its objective was to drill much deeper into the sediment cover of the ocean floor and date with microfossils the sediments recovered in successive cores. The age of the bedrock would come from the age of the oldest overlying sediment.

The success of the new drillship Glomar Challenger was immediate. On its first expedition in 1968 the recovered cores confirmed the existence of Jurassic-age salt domes in the Gulf of Mexico [26]. On the third expedition core samples provided convincing proof of seafloor spreading and continental drift [27]. On its thirteenth expedition in 1970 the drilling technology enabled comparable discoveries in the Mediterranean Sea: samples from its salt layer in the Algero-Balearic Basin [28], a youthful Miocene age for bedrock in the Alboran Basin and Valencia Trough [29, 30], and recovery of dewatered sediment from the interior of an accretionary prism in the eastern Mediterranean [31].

3 Initial signs of once dry Mediterranean

3.1 Discoveries from the first deep-sea drilling in 1970

Scientific drilling in the Mediterranean Sea began in the Alboran Sea. There at DSDP Site 121 Reflector 'M' (Fig. 2) corresponded to a widespread unconformity [32]. Upon reaching it at 682 m below the seafloor (mbsf), the drill bit hit a hard interface, inducing increased and erratic torque on the drill pipe. When recovered the formation below the 'M' Reflector was substantiality more indurated than the softer marl and sands above. The sediment above the reflector was early Pliocene in age. The sediment below belonged to the Tortonian stage of the Late Miocene. The lack of microfossils belonging to foraminiferal zones N17-18 [33, 34] and nannofossil zones of NN-12-13 [35] revealed that the Messinian stage of the Late Miocene was missing and only indirectly represented by a thin hardground. However, the cause for the hard ground and missing sediments at the unconformity would only become apparent later in the expedition after the discovery of evidence indicating partial desiccation of the entire Mediterranean.

The next drill site, 122, was located in the Valencia Trough (Fig. 3). The strategy here was similar: sample the 'M' reflectors, continue into the presumed underlying salt layer, and terminate in the flank of an adjacent bedrock peak [36].

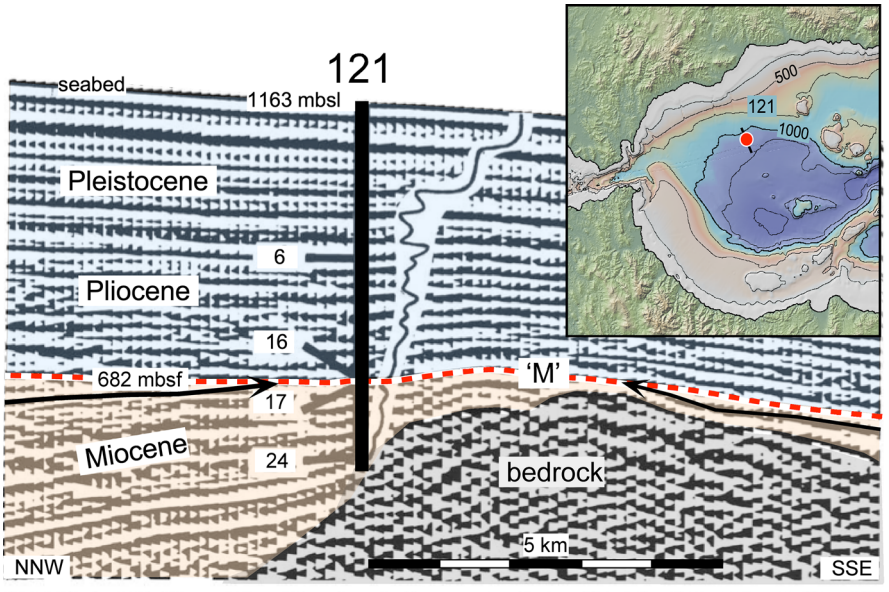

Fig. 2 Reflection profile with location of DSDP Site 121 in the Alboran Sea. The unconformity labeled Reflector 'M' is shown with red dashed line, truncating pre-Messinian Miocene-age reflectors and draped by early Pliocene marls. The graph is the rate of drill pipe penetration displaying decreased penetration rates when reaching strong reflections. Numbers 6–24 are core identifications

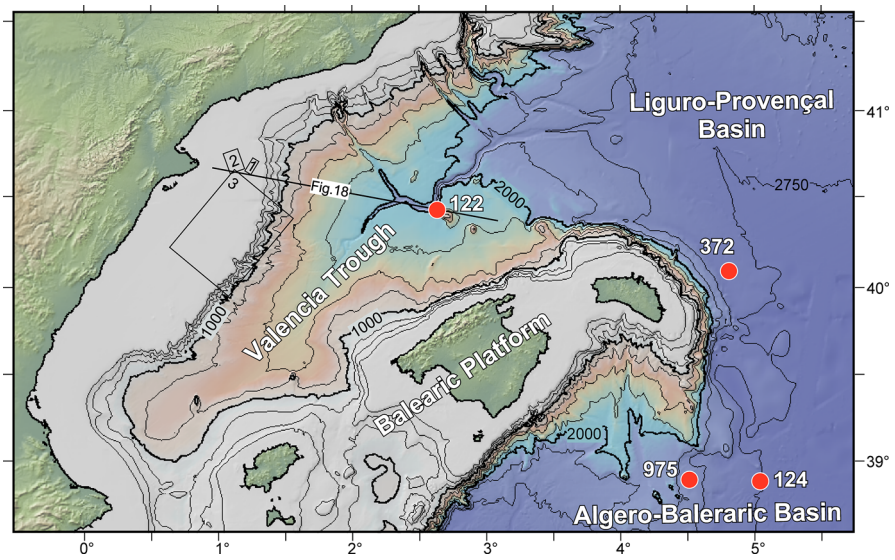

Fig. 3 Bathymetric contours (250 m interval) in the northwestern Mediterranean. Labeled drill sites are discussed in the text. Labeled boxes are 3D seismic surveys. Line is location of profile in Fig. 18

Again, when reaching Reflector 'M' the drill bit encountered a resistant formation. But this time, as it was entered, the drill bit plugged. The recovered core contained only sand with crystals of selenite. The attempt for another core proved futile. However, when the drill collars containing the core barrel were raised on deck, the collars and core barrel were found to be packed with buckets-full of gravel mixed with sand and pebbles (Fig. 4).

Although a disappointment to not have reached the salt layer, the effort spent at this site proved valuable. From the selenite crystals in the gravel, alabaster gypsum caught between the teeth of the drill bit and detrital gypsum in the sand came the first clues to a pre-Pliocene evaporite series. The gravel was composed of 70% basalt fragments, 25% selenite crystals, 5% limestone of mid-Miocene age (Serravallian and Langhian Stages), and shell fragments of mostly dwarfed gastropods, pelecypods, brachiopods, and lamellibranches once living in environments of unusual low salinity and shallow water. The absence of rocks of continental origin (e.g., granite, greywacke, schist) in the gravel was explained in the expedition reports by postulating the gravel had derived from erosion of the Miocene seabed, its underlying strata and volcanic bedrock.

At DSDP Site 124, located on the foot of the continental margin southeast of Balearic Platform (Fig. 3), an unusual formation was met for the third time at Reflector 'M' (Fig. 5). It adhered to the drill collars and suddenly increased the torque on the rotating drill pipe. The sediment in the first two cores turned out to be a sticky and stiff dolomitic marl with occasional lenses of detrital gypsum and barren of microfossils. However, further below, the marl began to reveal a few planktonic foraminifera. Though indicative of a Miocene age, most of the specimens were dwarfed and of uniform size. The remaining normal-sized specimens were already extinct. Of particular

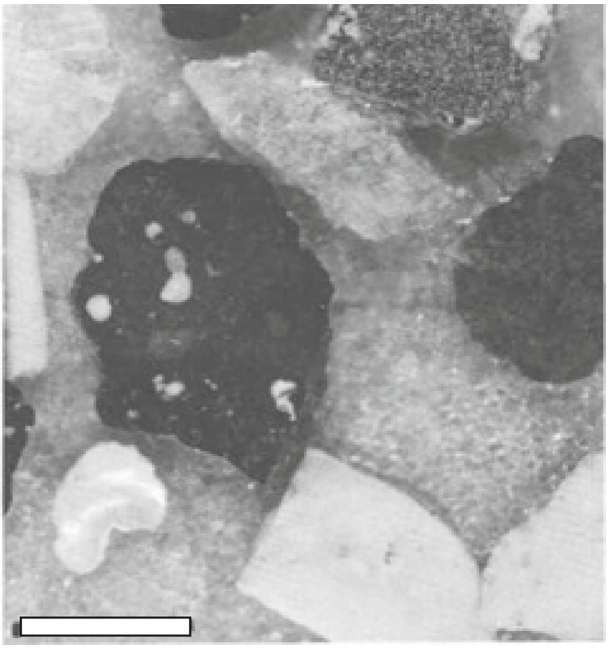

Fig. 4 Gravel composed of rounded and sub-rounded vesicular basalt, limestone of Middle Miocene age, selenitic gypsum, and shells belonging to shallow-water mollusks. Scale bar represents 1 cm

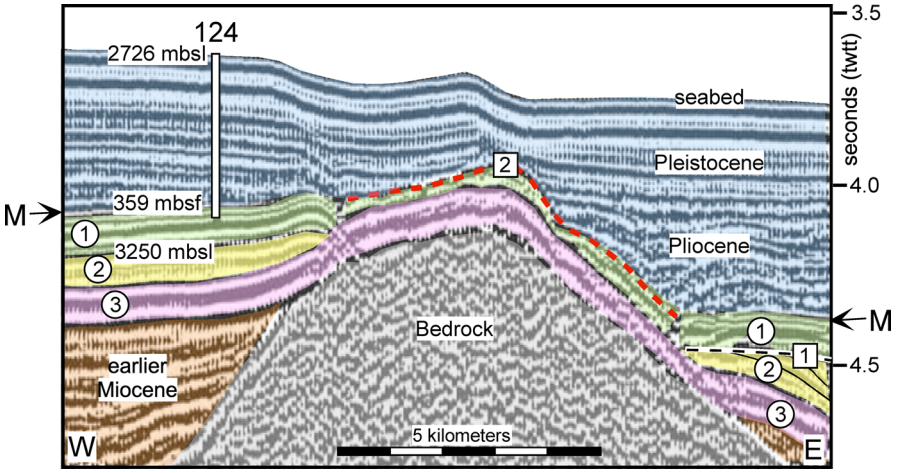

Fig. 5 Reflection profile crossing a buried bedrock ridge. Note that informal Unit 1, sampled in drill cores at DSDP Site 124 is partly eroded on the crest and eastern flank of the ridge (red dashed line), but intact and identical in its internal reflections on both sides. Unit 2 is absent on the ridge, whereas Unit 3 drapes the ridge. The truncation of internal reflectors in Unit 2 is unconformity #1 and erosion on the surface of Unit 1 is unconformity #2

note were numerous thin and finely laminated dark layers rich in pyrite and holding an abundance of siliceous microfossils (diatoms, Radiolaria, and sponge spicules).

Below was solid rock: thinly laminated anhydrite (Fig. 6, upper left) reminiscent of the 'balatino' facies in the Formazione Gessoso Solfifera in Sicily [9]. Under microscopic examination, the light bands consisted of parallel-bedded anhydrite laths while dark bands contained rounded and abraded crystals of gypsum in a mud matrix. Tiny white blobs were anhydrite spherules that had initiated growth along partings in the original sediment.

Further below, the anhydrite displayed a coarser texture with nodules large in some bands and small in others (Fig. 6, upper right). Each band was separated from the next by detrital sand containing sparce tests of dwarfed foraminifera with mud-filled tests. There was no evidence of size-grading in the detrital layers, but instead, marked size-discrimination between individual layers. Questions arose: had the anhydrite nodules grown in place like those in the thinly laminated facies in Fig. 6, upper left or were they detrital?

As the drill hole continued to deepen the nodules became larger until they obscured all the intervening matrix and presented a texture called 'chicken-wire' (Fig. 6, lower

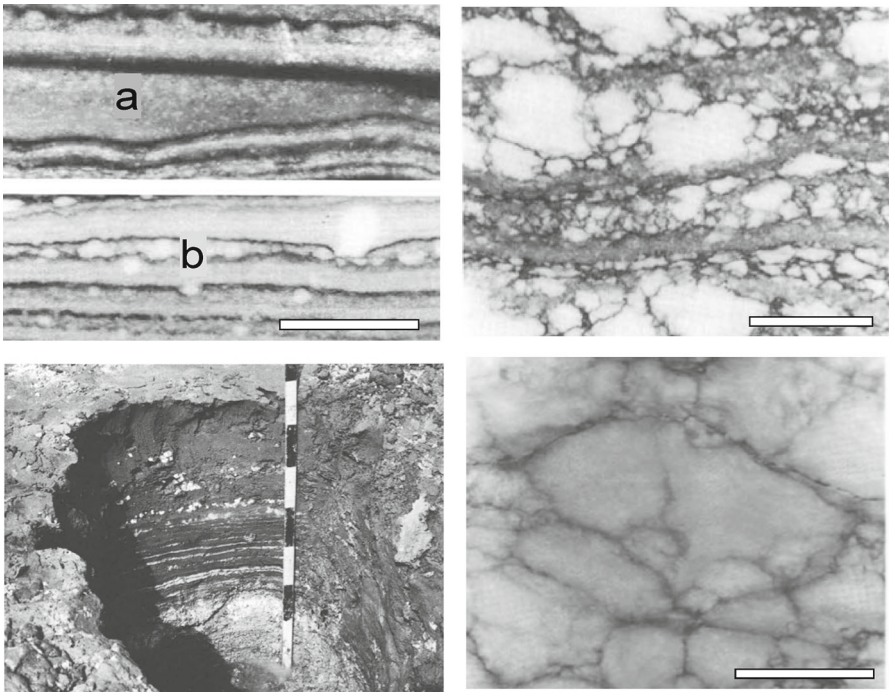

Fig. 6 Top left: thinly laminated (balatino) anhydrite displaying **a** preferential infilling of depressions; **b** spherules grown within the light bands and deforming the bounding dark bands. Top right: larger anhydrite nodules in bands separated by detrital sand. Bottom left: Anhydrite nodules in shallow pit dug into the sabkha sediments of the Persian Gulf [40]. Units on the rod have 10 cm spacing. Bottom right: chicken-wire anhydrite with only a wisp of mud. Core pictures from DSDP Site 124 [41]. Scale bar in pictures represents 1 cm

right) by geologists working in the petroleum industry. 'Chicken-wire' anhydrite had been considered a product of subaerial crystallization [37]. This anhydrite, recovered in beds several meters thick, was separated by finely laminated dolomitic mudstone again hosting diatoms and siliceous sponge spicules. The diatom assemblage included benthic and epiphytic species similar to those living today in stagnant waters of landlocked marches [38, 39].

The anhydrite nodules recovered by the Glomar Challenger more than 3 km below the surface of the Mediterranean Sea resembled those found in shallow pits dug into the supratidal flats of the Persian Gulf (Fig. 6, lower left) [40, 42–44]. There, in the subsurface of the supratidal zone, called sabkhas, anhydrite nodules grew in the hypersaline capillary zone as evaporation drew in groundwater sourced from the adjacent saltwater sea. As the nodules expanded, they displaced the surrounding sediment.

The apparent similarity between the DSDP Site 124 nodular anhydrite and that of the modern Persian Gulf triggered animated discussions among the shipboard scientists. Had the absence of Messinian deposits in the Alboran Sea, gravel with selenite mixed with fragments of shallow-water mollusks in the Valencia Trough, and anhydrite at this deeper location in the Algerian Basin taken place when water levels dropped hundreds to thousands of meters below the surface of the adjacent Atlantic Ocean [45, 46]? The steady downhole increase in Na and Cl measured from porewaters confirmed that halite existed at greater depths than achieved by the drilling [47, 48]. The Cl/Br ratio indicated leaching of relatively pure NaCl [49]. The downhole increase in porewater salinity confirmed that Unit 2 on both sides of the bedrock ridge (Fig. 5) was likely to be the halite layer that had produced the previously-recognized salt diapirs. However, the absence of Unit 2 on the bedrock ridge required explanation. The truncation of its internal reflectors on the eastern side suggested that halite may once have draped the ridge and was later removed prior to the dolomitic marls and anhydrite in Unit 1. If so, the drape would imply that the halite crystals had settled from a thick layer of brine capable of submerging pre-existing relief, rather than precipitation confined to shallow salt pans to each side of an exposed ridge. The subsequent shallow and brackish environments required cessation of new saltwater from the Atlantic and evaporation of the remaining brine. Near complete evaporation would expose halite on the ridge to erosion and could have been responsible for truncation of the internal halite reflectors in Unit 2 that created unconformity #2 in Fig. 5. A second episode of erosion produced unconformity #2.

Further confirmation of shallow and brackish environments came from the eastern Mediterranean at Sites 125 and 129 (Fig. 7). At Site 125 on the crest of the Mediterranean Ridge in the Ionian Sea, the sticky and stiff dolomitic marls contained the same faunas as found at Site 124: bottom-dwelling foraminifera considered to have lived in shallow water and diatoms conditioned to fresh and brackish environs. The drill hole terminated in a gypsum conglomerate that plugged the drill bit (Fig. 8, left). From the Cl/Br ratio in porewaters it became apparent that halite had not been present there, but instead had been preserved only in deeper enclosed regions.

At Site 129 in the eastern Mediterranean, the dolomitic marl contained not only an abundance of shallow-water benthic foraminifera (*Ammonia beccardii, A. tepida*), but entire carapaces of ostracods belonging to *Cyprideis pannonica* (Fig. 8, right).

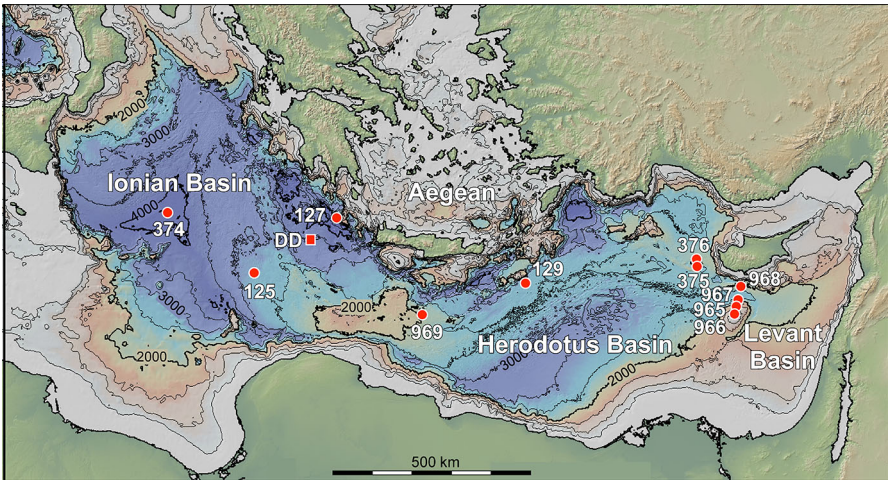

Fig. 7 Drill sites in the eastern Mediterranean. DD is the Discovery Deep brine pool. Bathymetric contours at 500 m intervals

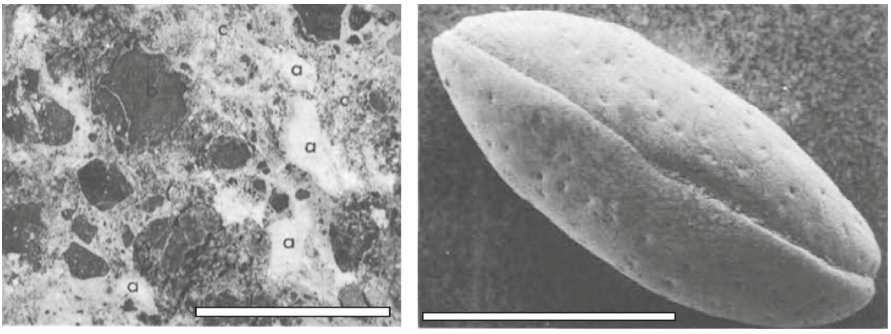

Fig. 8 Left: Conglomerate at DSDP Site 125 with pebbles of dolomite (black) in a matrix of gypsum sand with pockets filled with white anhydrite (**a**). Scale bar = 1 cm. Right: *Cyprideis pannonica* from DSDP Site 129, eastern Mediterranean. Scale bar = 0.5 mm

Cyprideis pannonica appeared for the first time around 8 Ma in Maeotian-age sediments in the Paratethys where it was associated with lake and flood plain environments [50–53]. Identical assemblages of this ostracod had been observed in the mudstones separating gypsum belonging to the 'Pasquasia Gypsum Beds' in Sicily [5, 54, 55].

The Pasquasia formation in Sicily is comprised of seven cycles of gypsum alternating with ostracod-bearing marls. The same sequence of beds had been traced over distances exceeding 85 km throughout the Caltanissetta Basin in Sicily (Fig. 9). Each cycle began with the *Ammonia beccardii tepida* and *Cyprideis* in dolomitic marls, followed upwards by gypsum. This cycle was well known to one of those aboard the Glomar Challenger who interpreted it as evidence of shoaling upwards (regressive)

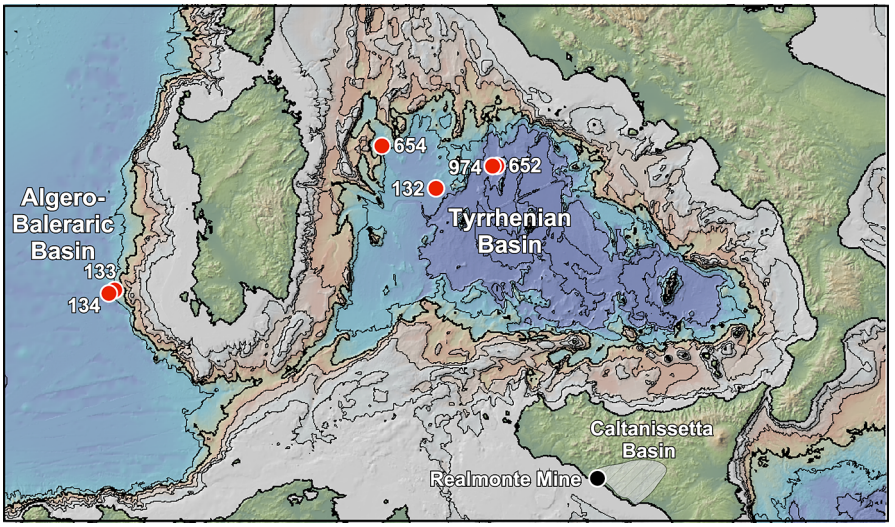

Fig. 9 Selected locations of drill sites in the Tyrrhenian Sea and west of Sardinia investigated during DSDP Leg 13 in 1970, ODP Leg 107 in 1986 and ODP Leg 161 in 1995. Bathymetric contours are at 500 m spacings

and increasing salinity when brackish lakes shrank by evaporation to become nearly-dry salt pans rimmed by arid margins. It became apparent to the shipboard scientists that cycles of gypsum and dolomitic marls with benthic foraminifera and ostracods in the drill cores were analogous to those in the Pasquasia Formation in Sicily.

3.2 Signs of subaerial exposure

In a quest to find further supporting evidence of a shrinking Mediterranean Sea, two locations were visited on return to the western basins: Site 132 in the Tyrrhenian Sea and Sites 133 and 134 on the distal margin of western Sardinia (Fig. 9).

An unusual rust-red sandy silt was found at Site 132. It caught attention because it was extremely rich in plant pollen and spores and had no remains of aquatic organisms [56]. Pollen in the red sediment included plants representative of marsh environments (*Liquidambar* co-occurring with *Viburnum*) as well as grasses living in proximity to dry coasts (*Chenopodiaceae* and *Ephedra*) [38]. The rust-red bed rested directly on anhydrite that had hydrated to gypsum by the introduction of meteoric water. The volume changes that had taken place during hydration had shattered the laminae into slivers (Fig. 10, middle). Further below, the gypsum displayed stromatolite-like wavy bedding (Fig. 10, right) reminiscent of algal mats that bind detritus swept onto tidal flats during storms [57].

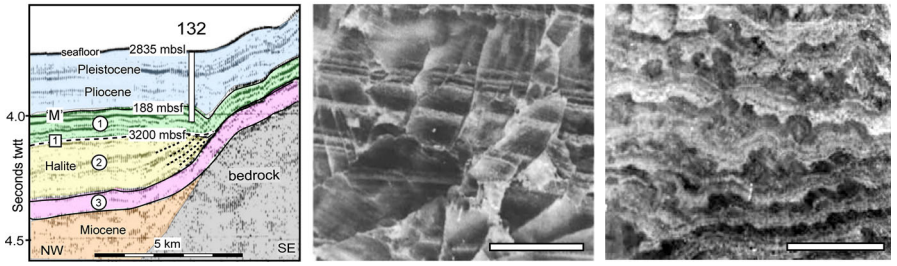

Fig. 10 Left: Reflection profile with location of DSDP Site 132 in the Tyrrhenian Sea. Unit 1 (green) was sampled. Unit 2 (yellow) is the presumed halite layer, absent on higher elevations, but with truncated reflectors on uniformity #1 suggestive that it had once been there, but subsequently eroded or dissolved. Middle: laminated gypsum layer shattered by volume change during hydration from anhydrite. Right: Stromatolite-like wavy laminations. Scale bars are 1 cm

3.3 Alluvial fan and desiccation crack

With evidence growing of brackish lakes that from time to time became subject to extreme evaporation leading to precipitation of anhydrite and terminating in a terrestrial soil, the shipboard scientists turned their attention to the deepest region of the western Mediterranean located at the foot of the Sardinia margin. Could evaporation have been so extensive that even this region dried out?

At Site 133, just 300 m above the floor of the adjacent Algero-Balearic Basin, the formation below Reflector M presented an appearance similar to the red silt encountered at the previous site. However, at Site 133 the formation consisted of both rusty-red and aquamarine siltstone and sandstone interbedded with variegated shale. Carbonates, evaporite minerals and aquatic microfossils were conspicuously absent. The shales contained rounded pebbles and cobbles of metamorphic phyllite and greywacke, presumably derived from upslope exposures of the bedrock [28]. The most abundant mineral in the silt and sand was quartz followed by goethite in the shale [58], a common component of soil. Poor size-sorting excluded the possibility that the siltstones were aeolian loess. Some siltstones contained gravel-size flattened pebbles of sandstone and schist. The composition was consistent with the postulate that the reddish beds making up Unit 4 in Fig. 11 had been deposited on either a terrestrial flood plain or on an alluvial fan.

Six holes were drilled at nearby Site 134 in an east to west transect at the edge of the Algero-Balearic Basin floor. Holes 134 a, b and c penetrated through Quaternary marine marls and then reached bedrock without encountering any Messinian deposits. Hole 134 d sampled nodular gypsum prior to reaching bedrock. Hole 134 e contained no Messinian sediment before reaching bedrock.

The drilling at hole 134 proper recovered the full range of Pleistocene, Upper Pliocene and Lower Pliocene pelagic oozes and marls before reaching Reflector'M'. There it recovered flat pebbles of Messinian dolomitic mudstone with rounded edges (Fig. 12, top left). Pebbles of this shape are diagnostic of surf that abrades them as they wash up and down the shore face. The next core returned the same cycles of laminated anhydrite as found at Site 124 on the opposite side of basin, interbedded

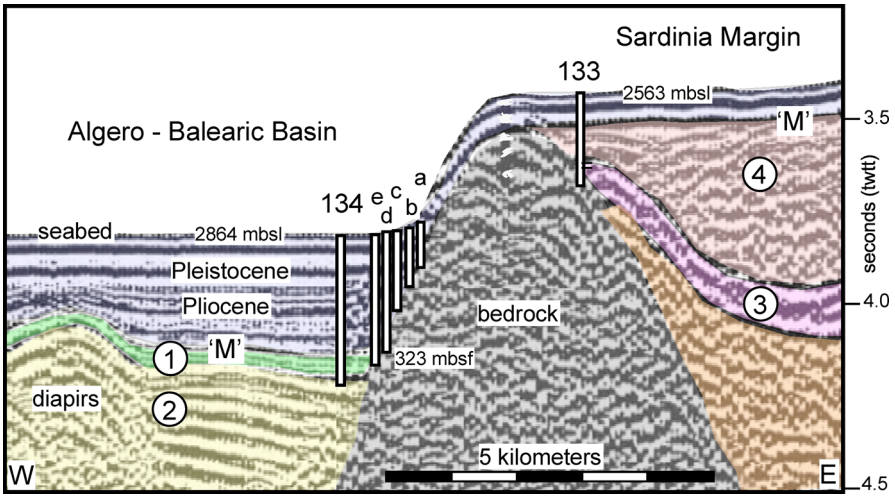

Fig. 11 Sites 134, a, b, c, d, e and 133 at the foot of the western margin of Sardinia. Units 1, 2 and 3 are colored the same as in Fig. 5 at the foot of the Balearic Platform. Where sampled at Site 133, the top of Unit 4 is a reddish siltstone with cobbles of metamorphic bedrock

with dolomitic marls containing ostracods and mudstone with Radiolaria, diatoms and sponge spicules.

However further below the drilling encountered translucent and banded halite intercalated with detrital sandstones. One detrital bed had an erosive top cut by a 3.5-cm deep crack [59] (arrow in Fig. 12). Several slices through the crack showed that it was an elongate vein that could have been produced by the shrinkage that accompanies desiccation.

The detrital layers contained abraded and broken tests of foraminifera indicative of transport from elsewhere. Mineral grains of the same size as the foraminifera were all nearly rounded and frosted, typical of aeolian origin. Clay and fine-grained silt were only present as infillings of the foraminifera chambers. Most detrital grains were coated with or stained by goethite, a component of laterite soil from which they may have arrived.

The translucent halite included two distinct types of crystals, cloudy bands with pyramid-shaped hopper crystals that had been recognized long ago in the manufacturing of granular salt in shallow evaporation ponds [61] and clearer bands with euhedral crystals containing dusty interiors hosting the remains of incompletely dissolved hopper crystals. The alteration between precipitation and dissolution is a common feature of banded halite belonging to the Salina Salt from the center of the Michigan Basin [62, 63].

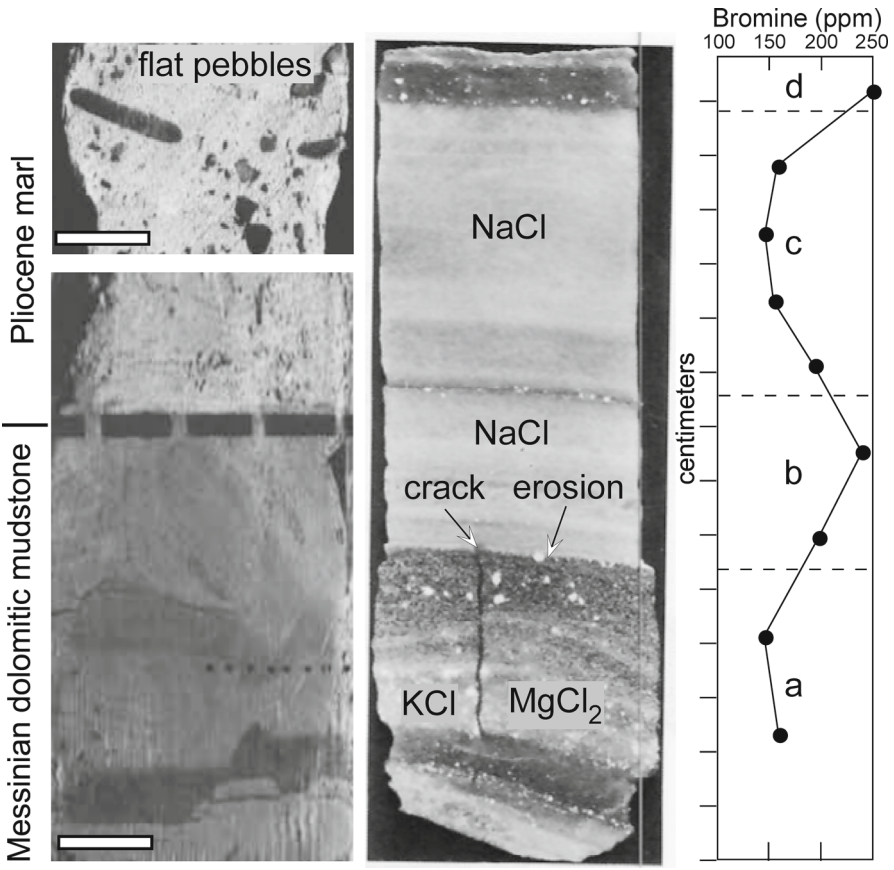

Fig. 12 Left: Sharp contact between soft Pliocene marl above Messinian dolomitic mudstone in Core 7, Site 134. Left top: Scattered flat pebbles of dolomitic mudstone imbedded in a Pliocene marl matrix < 10 cm above the Pliocene/Miocene contact. Scale bars are 1 cm. Middle: Translucent halite in Core 10, Site 134 sandwiched between dark detrital beds. The bottom detrital layer has a beveled top surface cut by a 3.5-cm deep crack (arrow) that offsets laminae in the detrital layer, but not its base. Right: Bromine content that shows remarkably large variations at a sample spacing of ~ 1.5 cm, with bromine values dissimilar from each other in both the detrital layers (**a**, **d**) as well as in the halite (NaCl) intervals (**b**, **c**). Matrix in the detrital layer includes potassium and magnesium chlorides indicative of a super-saturated brine residue [60]

4 Formulation of a desiccated deep-basin hypothesis

4.1 Lithology evidence

To the shipboard scientists and those chosen to further investigate the collected samples from DSDP Leg 13 in shore-based laboratories the strongest lithologic evidence of periodic subaerial exposure of the Messinian seabed was the similarity between the nodular and chicken-wire anhydrite at Sites 124 and 134 d and deposits beneath the supratidal flats of the Persian Gulf [40, 64, 65]. If produced by shrinkage during desiccation, the crack in the halite-cemented sandstone was supporting evidence.

Highly-flattened pebbles are commonly used as environmental indicators of intertidal deposition. Although these pebbles were recovered in a matrix of earliest-Pliocene foraminiferal ooze, they were found only 10 cm above the Messinian dolomitic mudstone from which they may have been derived. It was also possible that they had been transported from some distance upslope. Yet, on the other hand, they could have been mixed into the overlying ooze by the rotating drill bit as it encountered the mudstone upon which they had been originally deposited. Red sandstone, siltstone and shale with pebbles and cobbles is more commonly associated with terrestrial environments than subaquatic marine environments.

4.2 Faunal evidence

The most striking faunal evidence of severe evaporitic drawdown was the discovery of benthic and epiphytic diatoms in thinly laminated mudstones. Diatoms are unicellular organisms belonging to the genera of algae. In addition to nutrients, they require sunlight. Analogous to plants, diatoms convert light energy to chemical energy by photosynthesis. For the benthic diatoms at Site 124 to have flourished, sunlight must have reached either the sediment/water interface, as would occur in a shallow lagoon or lake or illuminated floating plants upon which the diatoms were attached. The diatoms at Site 124 co-occurred with silicoflagellates. The most common species, *Distephanus speculum*, blooms in the ultra-shallow and oxygen-depleted bottom waters in the Gulf of Trieste, northern Adriatic Sea [66]. Intense respiration and decomposition of silicoflagellates and diatoms would have contributed to the anoxic conditions indicated by the high organic carbon in the dolomitic mudstones. Benthic diatoms required a sunlit substrate and epiphytic species needed attachment to plants rooted in the substrate.

4.3 Bromine evidence

Measurements of the bromine content in the halite (Fig. 12) were performed by Robert Küehn after conclusion of the DSDP Leg 13 expedition [60]. Bromine concentrates during evaporation of seawater. Thus, the early halite would be expected to have relatively low concentrations (< 20 ppm), but as brine enriches further to co-precipitation of the more soluble salts, bromine values may reach very high values for the magnesium and potassium salts (> 200 ppm). In a deep pool of brine, such as a nearly-filled Mediterranean, the evaporation of a halite-saturated brine necessary to precipitate 1.5 cm of NaCl would neither alter the brine concentration nor its bromine content to any detectable amount [67, 68]. Thus, the rapid variations of bromine content between samples spaced 1.5 cm apart in core 10, Site 134 is not indicative of a deep brine pool. The lowering of the brine surface just a few meters in a shallow playa lake can increase the level of saturation from that of sodium chloride to those of magnesium and potassium chlorides. MgCl2 and KCl were detected in the detrital layer cut by the crack in Unit a of Fig. 12.

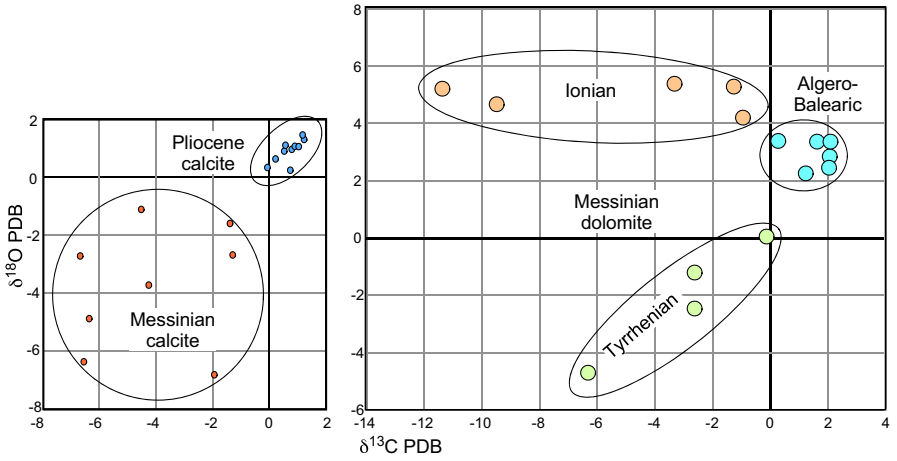

Fig. 13 Left: Carbon vs oxygen isotopes for Pliocene calcite (blue dots) and Messinian calcite (orange dots). Right: Carbon vs oxygen isotopes for dolomitic marls and marlstone

4.3.1 Oxygen and carbon isotope evidence

Additional evidence for ephemeral lakes came from post-expedition investigations of the stable isotopes of calcite and dolomite in the Messinian deposits [69–71]. Measurements on the Messinian calcites all resided in the negative quadrant of $\delta^{18}O$ and $\delta^{13}C$ when compared to the Pliocene saltwater calcites that cluster tightly in the opposite positive quadrant (Fig. 13, Left). The broad scatter of Messinian calcites was similar to calcites in lacustrine deposits from the Pleistocene lakes from West Texas [72].

The Messinian dolomitic marls and marlstones were not just isotopically distinct from the calcites, but unique to each region, with a tight cluster of positive $\delta^{18}O$ and $\delta^{13}C$ values at Sites 124 and 134 d on the edges of the Algero-Balearic Basin, negative $\delta^{18}O$ and $\delta^{13}C$ in the Tyrrhenian Sea and uniform positive $\delta^{8}O$ with negative $\delta^{13}C$ at Site 125 in the Ionian Sea (Fig. 13, Right).

If the dolomitic marls and calcites had preserved the original primary isotopic composition of the waters in which they crystalized, their distinct differences implied that that the western, central and eastern basins of the Mediterranean had not been submerged under the same body of water at the time these sediments were deposited.

4.3.2 Strontium isotope evidence

Strontium isotopes were investigated from Messinian carbonates and sulfates at three of the expedition drill sites [73]: 122 in the western Mediterranean, 132 in the central Mediterranean (Tyrrhenian Sea) and 125 in the eastern Mediterranean. All samples showed a depletion in isotope 87 compared to that of Miocene-age marine strontium [74, 75]. This depletion is due to the supply of strontium from continental waters. Depletions can only be as large as those measured on the Messinian samples when

the supply of the continental waters is dominate, because the strontium content is generally more than ten times less in river water than in sea water.

4.3.3 Oxygen isotopes in sulfate ion

Marine oceanic sulfates (SO_4^{--}) have a very narrow $\delta^{18}O$ of 9.5 ± 0.25‰ relative to SMOW [76, 77]. Therefore, values as high as 15.8 and 16.7‰ for the anhydrite at Site 124 had required brines when > 90% of original seawater had been evaporated. In contrast, the extremely low value of 3.8‰ for gypsum at Site 132 in the Tyrrhenian Sea was indicative of hydration of former anhydrite by the introduction of meteoric water.

4.4 Geomorphology

At the announcement of the preliminary results of the Glomar Challenger expedition at a Congress on the Mediterranean Neogene Stratigraphy in September 1971, Georges Clauson brought attention to an earlier 'eustatic hypothesis' by Denizot [78, 79]. Denizot's evidence of a pronounced fall in sea level came from a 1950's drilling program in southern France. The boreholes revealed an unexpected large thickness of marine sediments (> 1000 m) of Pliocene-age filling an older valley of the Rhône River and its tributaries, whose Miocene limestone margins had been cut by subaerial erosion. The deep riverbed incisions led Denizot to propose a total isolation of the Mediterranean, a substantial drop in its sea surface, and its floor "*occupied by brackish ponds and saline lagoons*." Denizot further suggested that when the Strait of Gibraltar opened, the Atlantic seawater invaded the fluvial network and raised the entire sea surface in what he termed the "*transgression Pliocèné*." The earliest clays to fill the network had the same foraminifera assemblage with abundant *Sphaeroidinellopsis* as found in the earliest-Pliocene marls at Site 132 [80].

I.S. Chumakov learned of the Glomar Challenger preliminary results from an article in the New York Times newspaper, translated in Moscow by the Soviet news agency TASS. He communicated his publication [81] describing the discovery of early Pliocene sediments filling a paleo estuary of the Nile River. At Wadi Halfa in Sudan, some 1200 km from the present seacoast, the thalweg of the Nile had been notched > 100 m into granite bedrock and then filled with marls having an absence of facies characteristic of a transgressive series.

In his invited chapter in the DSDP Leg 13 Initial Reports, Chumakov attributed the incision of the river network to a "*new and very low base level of erosion*." [82]. He proposed a drop in the surface of the upper Miocene Mediterranean Sea as great as 1 to 1.5 km. For Chumakov, the Pliocene transgression had to have been "*instantaneous*" to transform the over-deepened river valleys into saltwater estuaries.

During the late 1960's another large fossil drainage system of Miocene age had been revealed in northern Libya. Here it had been cut into middle Miocene limestone to a depth of over 400 m, but was now completely buried [83]. Given the name Sahabi channel, the incision had been traced more than 300 km inland from the Gulf of Sirte coast using seismic reflection techniques. The absence of any reported Messinian age

sediment in these paleo valleys, even as fluvial lag deposits, was a tantalizing indication that prior to the Pliocene transgression both the western and eastern Mediterranean had been in a state of severe regression.

5 Early reaction to the desiccation hypothesis

5.1 Issues raised at the 1973 Utrecht symposium

In March 1973, Carl Drooger hosted a symposium in Utrecht, Netherlands titled "Messinian Events in the Mediterranean" and attended by > 170 participants [84]. The 1972 publication by Kenneth Hsü in the magazine Scientific American titled "When the Mediterranean dried up" had already created controversy. To most participants, it seemed more reasonable to dry up shallow basins only 200 to 500-m deep [85] rather than those several kilometers deep. These greater depths could be achieved by subsequent collapse of the sea floor [86–90].

The depth of the Mediterranean during the Messinian needed to be quantified to become persuasive. In his presentation William Ryan reported a personnel communication in 1971 from P. F. Burollet and Ph. Magnier of the Compagnie Française des Pétroles describing a widespread unconformity just discovered by exploration drilling in the subsurface of the Gulf of Lions. The unconformity descended from 0.9 to 2.4 km below the seabed and separated marine shales of Tortonian age below from Pliocene calcareous marls above, rich in planktonic foraminifera. The unconformity was littered with gravels and pebbles of crystalline and metamorphic composition along with beds of lignite indicative of either a fluvial or alluvial deposits [91].

This unconformity did not receive wide attention until the 1972 meeting of the Mediterranean Science Commission (CIESM) in Athens. There it was recognized that the unconformity continued all the way down the continental margin of France to the landward edge of the salt layer at a depth of 3.5 km below the sea surface and at a distance exceeding 150 km from the coast (Fig. 14). In places beneath the shelf pre-MSC sediment as thick as 1 km had been removed. Such a large thickness could not have been stripped from the edge of basins only 200 to 500-m deep.

Additional personal communications from H. Hay-Roe of the Belco Petroleum Corporation in 1971 and from J. E. Webb of the Phillips Petroleum Company in 1973 announced another extensive erosional event in the offshore regions of Israel [93, 94] and Egypt [95] which had resulted in the sculpting of dendritic drainage systems buried beneath a Pliocene–Pleistocene cover exceeding 1 km in thickness (Fig. 15).

Another issue raised at the Utrecht symposium was the presence of planktonic foraminifera in the dolomitic marls. Had the planktonic foraminifera been supplied during repeated fillings of the Mediterranean? In reply, Maria B. Cita cautioned that the sparse, dwarfed and specialized foraminiferal assemblage in the dolomitic marl of the DSDP cores represented either abnormal environments or mechanical size-sorting [38]. Arvedo Decima and Rodolfo Sproveri added to the discussion [96]. In their study of the last seven marl levels in the Gessi di Pasquasia Formation in Sicily they noted that all normal-sized planktonic foraminifera were reworked from elsewhere. The specimens were broken, partly dissolved, and stained by red iron oxides. Furthermore,

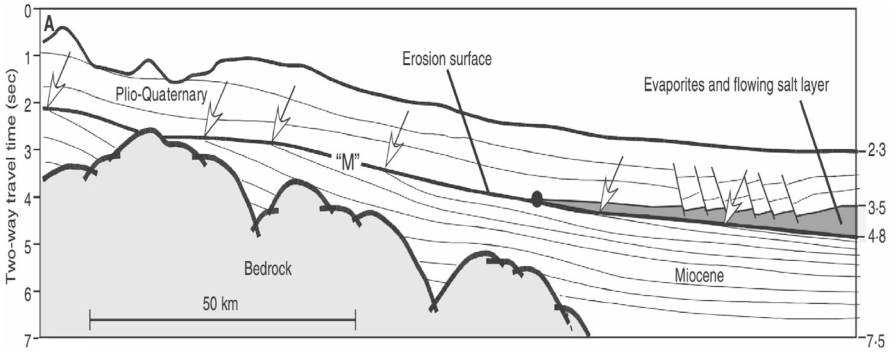

Fig. 14 Tracing of a reflection profile from the shelf edge in the Gulf of Lions to the foot of the continental margin [92]. Arrows mark successive truncations Miocene sediments by the erosion surface corresponding to Reflector 'M'. The dot marks the maximum onlap of Messinian evaporites. Numbers on the right are calculated elevation referenced to sea level in kilometers

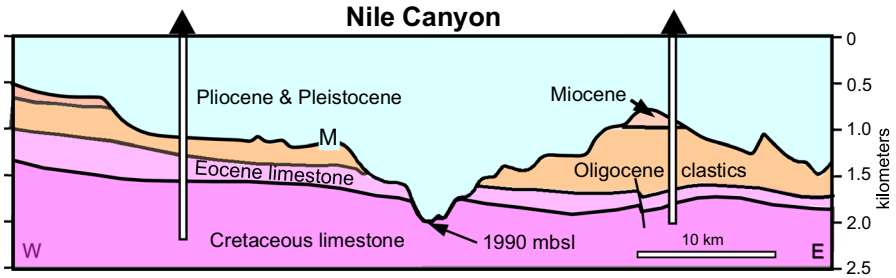

Fig. 15 Tracing of a Phillips Petroleum Company reflection profile across the Nile Delta revealing the thalweg of the buried Messinian Nile Canyon [95]. Profile crossing is located 25 km seaward of Cairo

the assemblages were inconsistent in stratigraphic distribution from sample to sample. Many species had already become extinct. The dwarfed specimens were all of the same size: a sign of traction transport from elsewhere. The only autochthonous species were the fresh- and brackish-water benthic foraminifera and ostracods.

As to the inquiry of whether there had been many fillings and dryings, Gerhard Richter-Bernberg offered his knowledge of the Cattolica Member of the Gessoso Solfifera Formation in Sicily [97]. He described repeated beds of selenite, each up to several meters in thickness. The beds were built by "*upright standing gypsum crystals*" that he called "*crystal swords*". There were as many as a dozen selenite beds stacked one upon the other and reaching a combined thickness of 150–200 m. They were rooted on top of the diatomaceous Tripoli Fm, signaling the gradual rise in salinity to saturation for gypsum. He was able to trace the same succession of beds from outcrop to outcrop over distances exceeding 80 km. But, in some places younger beds were missing. Those preserved were capped and sealed by the Pliocene Trubi marls, implying removal of the youngest selenite beds by erosion during the Messinian. It became apparent that these considerable thicknesses of gypsum could

be not explained by accumulation in the tidal zone. Instead, Richter-Bernberg proposed a "*reef-like platform*" on margins surrounding deep-water areas where gypsum and salt co-precipitated. The more than a dozen beds belonged to a hypersaline stage of the MSC prior to any fall of sea level. Since individual beds of selenite showed no signs of emersion, there must have been a sufficient accommodation space and continuous supply of Atlantic seawater to keep the Mediterranean full.

A full Mediterranean during the hypersaline stage fit with deep-water evaporite model of Robert Schmalz [98]. Discussions at the symposium concerned whether the salt had co-precipitated with the selenite beds or accumulated afterwards. Reflection profiles had displayed a band of strong reflections (Unit 3 in Figs. 5, 10 and 13) immediately below the acoustically transparent and ductile layer assumed to be halite [86, 99, 100]. If the selenite beds had preceded halite, these reflections would most likely correspond to the selenite beds that Selli termed 'lower evaporites' [101]. As many as 14 consecutive selenite beds had been precipitated not only in Sicily, but along the eastern margin of the central Apennines and on the margins of the Adriatic foretrough [101–103]. In outcrop these 'lower evaporites' were almost always observed to be at disconformable contact beneath the Gessi di Pasquasia formation in Sicily and the Colombacci formation in the Apennines that Selli referred to as the 'upper evaporites' [101].

According to the presentation of Decima and Sproveri [96] the 'upper evaporites' had accumulated in restricted basins under conditions of brackish water as shown by the presence in the interbedded marls containing *Cyprideis* and *Ammonia beccardi tepida* and mollusks such as *Dreissena* sp. and *Melanopsis*. Episodes of evaporation resulted in beds of gypsum in some places and limestone in others. Decima and Sproveri concurred with the DSDP Leg 13 scientists that during the concluding interval of the MSC the Mediterranean had become divided into numerous lakes of uncertain size and depth, which collected great quantities of detritus from strata of different ages that had become exposed around the borders of the lake-basins during episodes of partial desiccation. From a paleogeographic viewpoint the brackish environments in both proximal and distal regions of the Mediterranean "*made it impossible to realize a direct connection with the Atlantic Ocean during the terminal Miocene*" [96].

5.2 When did the sea level begin to fall?

In advance of the Utrecht symposium Forese Wezel and Arvedo Decima had created a stratigraphic schema for the evaporite deposits in the Caltanissetta Basin in Sicily [6] (Fig. 16). In map view the successive beds of selenite assigned by Selli to the 'lower evaporite' Cattolica formation were offset from the halite and only present on its margins. However, in cross-section the selenite beds were instead placed beneath the halite and thus precede the halite. The halite in the Decima and Wezel schema was divided into four units, A though D, with an erosional unconformity (#1 in Fig. 16) separating the Cattolica and Pasquasia formations.

However, at a later conference in Erice, Sicily in 1975, with the objective of bringing the sea-going and land geologists together for discussions on the same outcrop, Decima took the participants to the Realmonte salt mine. There they went down though the

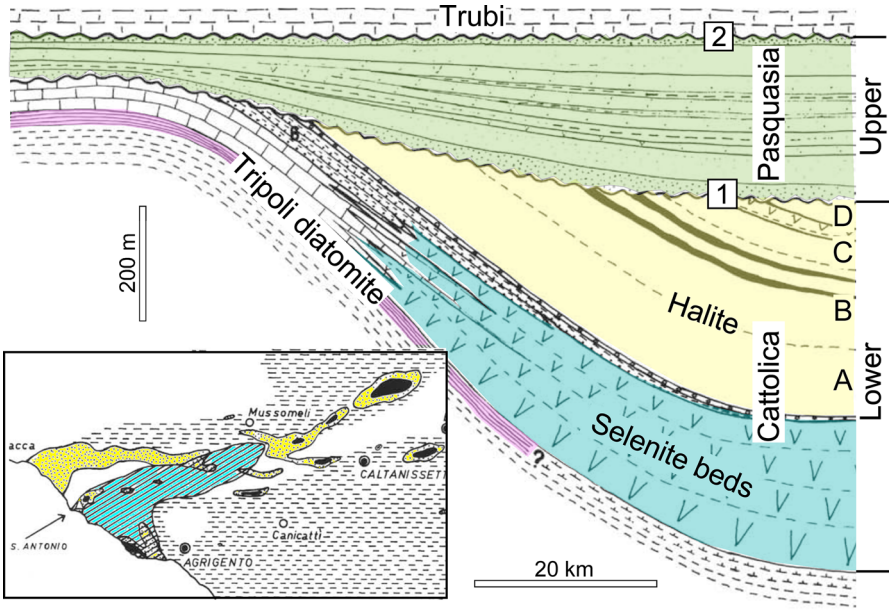

Fig. 16 Stratigraphic schema of Decima and Wezel [6, 7]. The wiggly lines labeled 1 and 2 denote presumed unconformities

salt body in an open cargo elevator. Decima stopped the elevator at the top of his Unit B and pointed to a recently discovered surface that he suspected was once subaerial. The measurements of the bromine content from samples in Units A and B had uniform values in the range of 400 ppm [104] and thus were precipitated from a deep (i.e., thick) body of brine supplied by the evaporative concentration of saltwater, presumably entering from the Atlantic. However, his measurements in Unit C above were no greater than 20 ppm. He advocated that this abrupt drop in the bromine could only be explained by a substantial shoaling of the brine body. Exposure of halite as margins became exposed to rain would lead to its dissolution and the recycling of the solutes into the subsequent Units C and D. In his fieldtrip guide Decima revised his earlier schema to place the major exposure surface as truncating Units A and B (#1 Fig. 17), with Unit C and D halite precipitated in the only the deepest regions of the basin during maximum regression.

Decima's hypothesis of subaerial emersion was confirmed two decades later by findings of spectacular vertical fissures spaced at intervals of up to 5 m apart, extending down to a depth of 6 m into the top of Unit B, and filled with red mud. The salt surface cut by the fissures was upturned and buckled.

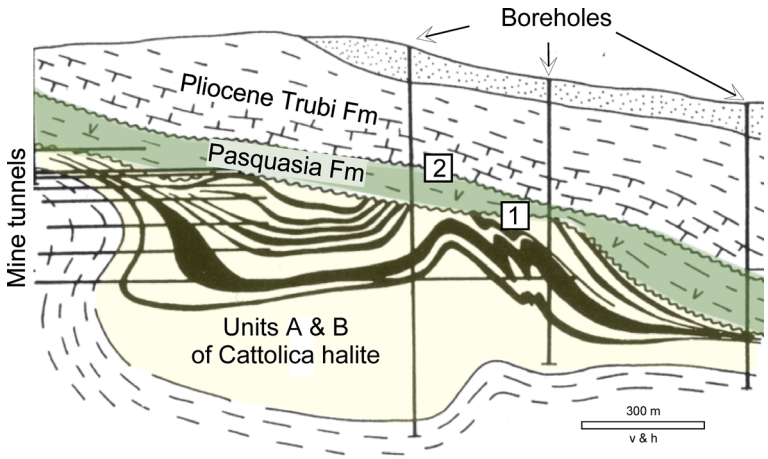

Fig. 17 Revised schema on the thick Cattolica formation halite [105] based on mine shafts, tunnels (horizontal lines) and boreholes (vertical lines) with absence of selenite beds below the Cattolica halite and truncation of the halite, prior to the upper evaporite Pasquasia Formation. Drawn to true scale: vertical and horizontal distances are the same

5.3 Relevance of erosion surfaces

At the 1976 Messinian Seminar on the shore of Lake Garda in the Italian Alps the theme was Messinian erosion surfaces. The Southern Alpine Lakes are crypto-depressions, so deep that their floors lie below mean sea level. With new reflection and refraction measurements, Peter Finckh showed the elevation of bedrock surface beneath the sediment in axis of Lake Garda lay at 1260 mbsl [106]. For him and Alfredo Bini such extreme deepening could not have derived from glacial erosion alone. It was better explained by entrenchment of rivers during extreme Messinian lowstands [107].

Antonio Rizzini and Luciano Dondi built upon this hypothesis when presenting evidence from commercial oil and gas exploration of thick alluvial deposits belonging to the Sergnano Gravel Formation. The gravel was encountered as deep as 1600 m beneath the Lombardian Plain just south of the Alpine Lakes. They proposed that the gravel was alluvial and originated from the excavation of up-stream gorges occupied by the present-day lakes. The gravel had been incised by an even younger network of fluvial valleys. These valleys were filled by Pliocene sand and clay.

In a second presentation Rizzini announced new results from commercial exploration in the subsurface of the Nile Delta [108]. There the Messinian consisted of three formations. Ranging from older to younger they were: the Qawasim Fm of brackish-water fluvial-deltaic sands containing lenses of peat and coal; the Rosetta Fm with beds of anhydrite; and the Abu Madi Fm fluvial sand. The Abu Madi was encountered between 3100 and 3600 mbsl in boreholes. According to Rizzini, the appearance of the Qawasim Formation was sudden and accompanied by "*drastic changes in the faunal assemblage from marine to lacustrine*". Ruling out explanations of lateral migration of proto-Nile mouth or a tectonic phase, Rizzini concluded that the changes were most likely initiated "*by a great lowering of sea level… that would have adjusted the*

fluvial processes to a new base level, deeply entrenching the old channels and alluvial plains."

Attention then turned to erosion surfaces revealed in seismic reflection profiles [109]. Offshore the Ebro delta on the Castellon coast of Spain exploration boreholes had passed through a regional unconformity corresponding the Reflector 'M' separating Castellon sands of Miocene age from Ebro clays of Pliocene age [110, 111]. Messinian sediments were missing beneath the shelf, but present as evaporites in the more distal Valencia Trough (Fig. 18). The erosion surface extended beneath the evaporites sampled at DSDP Site 122 at a depth > 2500 mbsl.

On the Levant margin of the eastern Mediterranean the top of the salt layer in Fig. 19 displayed the same truncation as shown in Fig. 17 for the Caltanessetta Basin of Sicily [112]. However, at this location in the easternmost Mediterranean there was

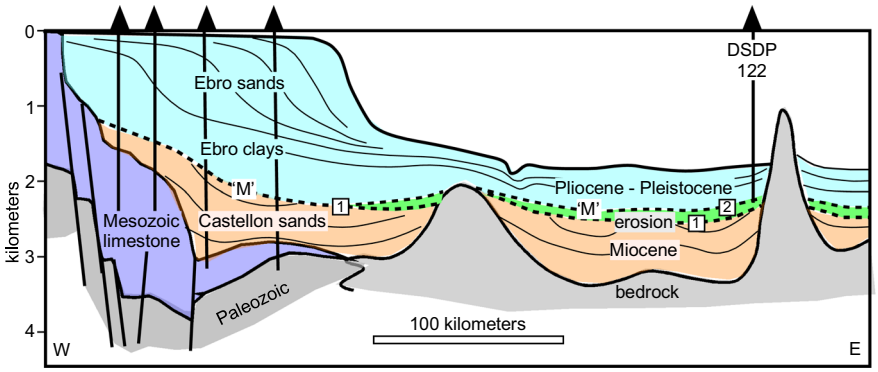

Fig. 18 Reflection profile from the Ebro River margin of Spain to DSDP Site 122. Stratigraphic ages and lithologic formations are based on subsurface drilling [111]. The Messinian erosional surface corresponding to Reflector 'M' can be followed from the margin eastward to beneath the 'upper evaporates' (colored violet). Unconformity numbers are the same as in Figs. 16 and 17

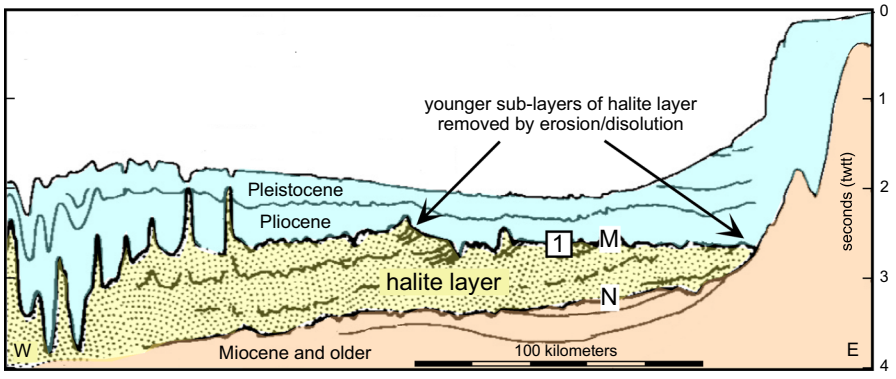

Fig. 19 Tracing of a reflection across the Levant Basin in the eastern Mediterranean showing truncation of the top of the salt layer. Unconformity numbering same as in Figs. 16, 17 and 18

no observable equivalent to the Unit C and D halite layers in Sicily and the younger Pasquasia gypsum beds.

6 New findings from additional Mediterranean deep-sea drilling

There have been four subsequent deep-sea drilling expeditions: 42A in 1975, 107 in 1986, 160 and 161 in 1995.

6.1 Expedition DSDP 42A in the eastern Mediterranean

When re-evaluating the magnitude of sea level fluctuations and the sabkha origin for nodular sulfates belong to the Upper Evaporite member of the Mediterranean Evaporite formation two drill sites in the eastern Mediterranean are of particular relevance (Fig. 9). Site 374, in the center of Messina Abyssal Plain in the Ionian Basin is the deepest (4088 mbsl). In reflection profiles its Unit 1 gypsum beds are continuous with little elevation change over distances exceeding 80 km (Fig. 20, Left). Sites 376 and 375 on the flank of the Florence Rise in the Levantine Basin are considerable shallower (2117 and 1914 mbsl) (Fig. 20, Right). Their Unit 1 gypsum beds were mostly detrital with gypsarenite, gypsiferous sandstone and gypsiferous breccias, but also containing bottom-growth 'swallow-tail' selenite and cumulates in the laminated gypsum 'balatino' facies interbedded with nodular anhydrite with occasional 'chicken-wire' textures. Scattered vugs in the anhydrite were filled with halite. At both of the Florence rise sites the base of Unit 1 is a flat-pebble conglomerate consisting of scattered elongate gypsum clasts similar to those described by Hardie and Eugster [113] from the Caltanissetta Basin as "*formed when storm waves ripped up mud-cracked, algal-bound laminated sediment*."

The flat-pebble conglomerate rests on erosion surface #1 at both the deepest and shallower Florence Rise drill sites. The flat-pebble conglomerate was interpreted by

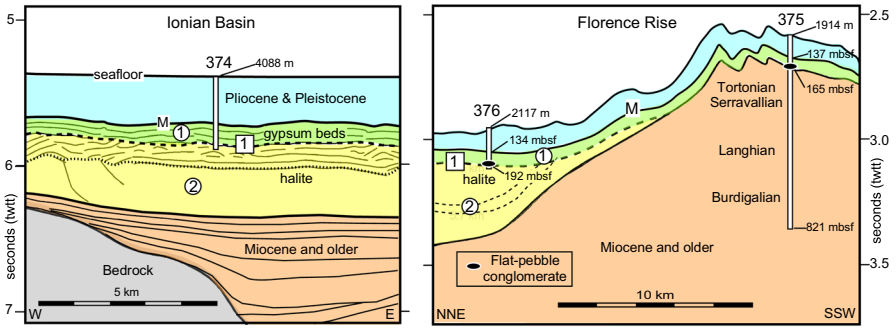

Fig. 20 Left: Tracing of a reflection profile across the center of the flat Messina Abyssal Plain in the Ionian Basin with location of Site 374 Right: Tracing of a reflection profile on northern flank of Florence Rise with locations of Sites 376 and 375 [114]. Dashed line is erosion surface #1, separating Units 2 and 1

those onboard the drillship to be the consequence of a drop in brine surface during the passage from a subaqueous to subaerial environment [115].

The mudstone in Unit 1 was barren of microfossils at Site 374, but contained the brackish to freshwater ostracod *Cyprideis pannonica* and shallow-water *ammonia beccardii* at Sites 375 and 376. The $\delta^{18}O$ isotope measurements on the sulfate at Site 374 showed a progressive upward trend from + 15 to + 19‰, whereas those from the higher site remained more or less constant (Fig. 21) [116]. The marked increase in the sulfate $\delta^{18}O$ at Site 374 could not have derived from bacteriological reduction, because such reduction of sulfate ions produces an accompanying enrichment in $\delta^{34}S$, that was not observed. Besides, bacteria activity is drastically reduced or completely poisoned in brines concentrated to the level for sulfate precipitation [117]. Therefore, the increase in the sulfate $\delta^{18}O$ (Fig. 21, Left) signaled a state of progressive evaporation of a thick brine body. Additional evidence of progressive evaporative concentration is the heavy $\delta^{18}O$ (+ 9.7‰) and $\delta^{13}C$ (+ 13.8‰) in the interbedded dolomitic sediments (Fig. 28) [116, 118]. Because continuing enrichment could only be achieved under conditions of a steadily evaporating brine body, it became difficult with this post-expedition data to maintain the hypothesis that each of the nodular anhydrites or gypsums beds at sites of different elevations had formed on tidal flats (Fig. 22).

The drilling at Sites 374 and 376 terminated in halite. In the Ionian Basin the bromine content varied between 114 to 218 ppm, confirming a thick layer of brine. In comparison on the Florence Rise bromine content was no greater than 30 ppm, suggestive of shallow salt pans [119].

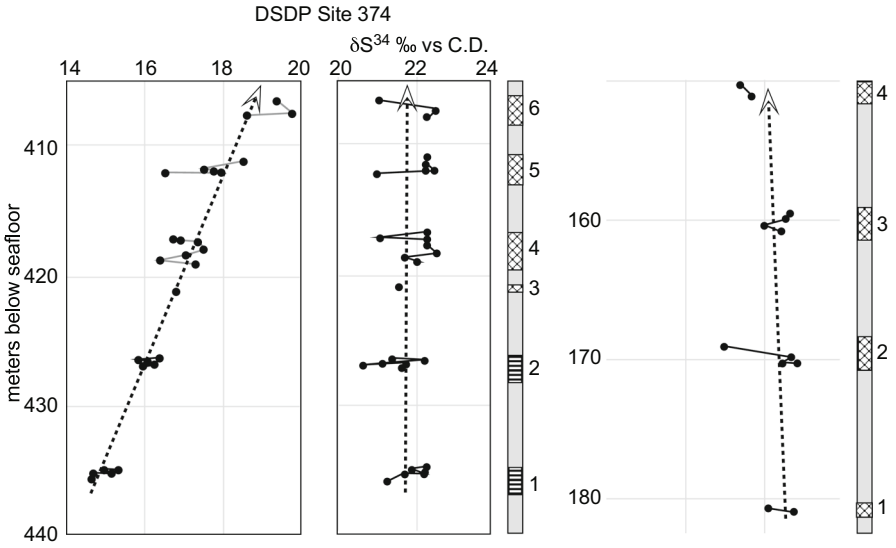

Fig. 21 Isotopic measurements from sulfate beds at Sites 374 (deeper Ionian Basin) and 376 (shallower Florence Rise in the Levantine Basin). The numbers denote beds of anhydrite (parallel stripes) and gypsum (cross hachures)

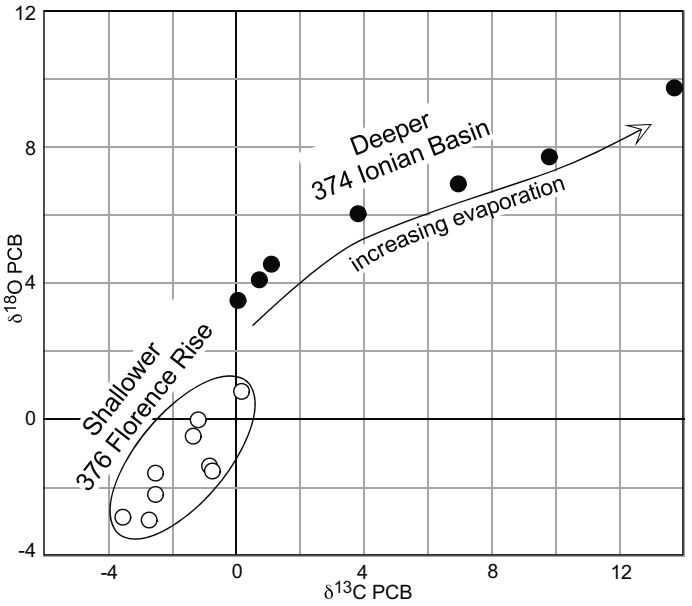

Fig. 22 Oxygen versus carbon isotopes at the deeper 374 and shallower 376 drill sites in eastern Mediterranean sites [118]

The reflection profile (Fig. 20) crossing Site 374 displayed a halite layer with two styles of internal bedding: an acoustically transparent layer succeeded by one with internal reflections. This observation raised the likelihood that the transparency was indicative of the pure (> 98%) halite belonging to Unit A of the Cattolica Formation in Sicily [7] and the upper layer with internal reflections containing beds of kainite, sylvite and bischofite similar to those in Unit B in Sicily. Furthermore, the rubidium measurements in the kainite at Site 374 were in the same ranges as in the kainite of Unit B [119].

In Caltanissetta Basin in Sicily, on the Florence Rise, and in the Levant Basin the physical erosion or chemical dissolution had truncated the top of salt layer prior to accumulation of the overlying upper evaporite gypsum beds. However, in the deepest region of the Ionian Sea the brine had not evaporated to completion, as indicated by the extreme positive values for the both the sulfates SO_4 and dolomites $CaMg(CO_3)$ in the remaining brine. Over time its dilution by freshwater reduced the salinity to a threshold suitable for radiolarians, sponge spicules and diatoms [120], yet the residual brine remained anoxic and thereby excluded ostracods and benthic foraminifera.

6.2 Ocean Drilling Program expedition 107 in the Tyrrhenian sea

There were two additional drill sites in the Tyrrhenian Sea (Fig. 23) of significance when evaluating changes in Messinian water level: namely the shallower Site 654 (2218 mbsl) and deeper Site 652 (3446 mbsl).

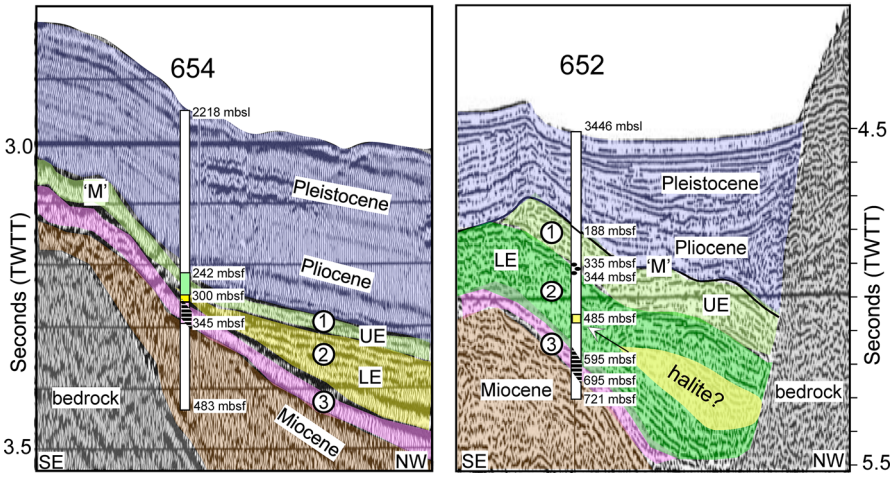

Fig. 23 Reflection profiles at Site 654 and 652 in the Tyrrhenian Sea are colored with the same notation as in Figs. 5, 9, 11 and 20. *UE* upper evaporites, *LE* lower evaporites

At Sites 654 and 652 a breccia and conglomerate were sampled at the depth corresponding to the transition between Unit 1 and Unit 2. Whereas Unit 2 onlaps Unit 3 at Site 654, Unit 2 drapes Unit 3 at Site 652. In the Site 652 reflection profile Unit 2 displays an internal bed (yellow), located down-dip and remote from the drill site. The up-dip conformity from this bed points to 485 mbsf where the downhole increase in porewater chlorinity reached a peak value of nearly three times that of seawater.

At the deeper Site 652 the downhole electric logs showed the top of the Messinian to be a 2-m-thick iron-rich, indurated clay of increased bulk density and decreased porosity. The sediment below was mudstone with occasional sand and silt beds containing detrital gypsum, plant debris and alga spores [121]. The presence of *Cyprideis pannonica* and *Ammonia beccarii tepida* (Fig. 24) confirmed a brackish-water environment [122]. A substantial depletion of the strontium isotope 87 [123] and strongly negative $\delta^{18}O$ (− 4 to − 5‰) in calcites confirmed that the water in which the foraminifera and ostracods had lived had been continently derived [124].

The drilling at both sites encountered beds of anhydrite (v symbol) below the discontinuity in Fig. 24. The $\delta^{34}S$ measured on the anhydrite displayed an oceanic composition. Farther below were thinly laminated black shales rich in organic carbon (3–11%) at Site 652 and rich in diatoms at Site 654.

The clay mineral content above the discontinuity was abundant in smectite [127]. Smectites are a dominant component of the Pasquasia Formation in Sicily, whereas in the preceding Cattolica Formation, the mineralogical composition had only minor smectite [127]. At the drill sites the strontium and calcium contents were low above and high below [123]. Based on fauna, isotopes, chemistry and mineralogy the sediments above the discontinuity were assigned to the 'upper evaporites', sediments below to the 'lower evaporites', and the finely laminated anoxic shale and diatomite to the precursor Tripoli Formation [121].

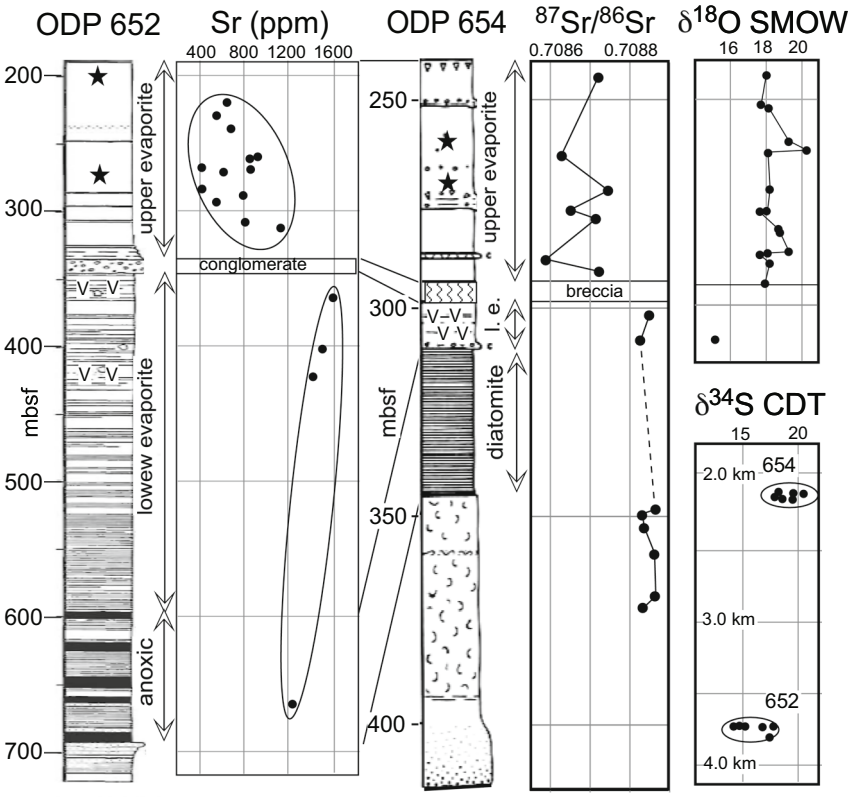

Fig. 24 Comparisons between Sites 652 (3470 mbsl) and 654 (2218 mbsl) in the Tyrrhenian Sea [125, 126]. Depths are meters below seafloor

As a consequence of the observed discontinuity in the reflection profiles now firmly located between the upper and lower evaporites, the conglomerate and breccia came into focus as potential indicators of possible sea level drop. Quoting from the expedition report, the rounding and in some cases flattening of the pebbles at Site 652 may have indicated "*a temporary fluviatile or beach environment*" [125]. If so, its stratigraphic position makes the discontinuity an equivalent to the surface that truncated Units A and B in the Cattolica halite in Sicily (Fig. 17). The pebble's composition of limestone of Oligocene to early Miocene age, quartz arenite, calcareous phyllite, and calcareous sandstone with fragments of Bryozoa and mollusks is more similar to the local bedrock than to source terrains in Sicily and the Apennines [128].

The sampling in reflection Unit 3 of anoxic shales at Site 652 and diatomite at Site 654 confirmed for the first time that the band of strong reflections directly beneath the ductile halite layer was not 'lower evaporite" selenite or its stratigraphic equivalent, but instead the Formazione Peliti Eusiniche.

6.3 Ocean Drilling Program expedition 160: eastern Mediterranean

There are four drill sites in the eastern Mediterranean (Fig. 25) of further relevance to the elevation of the sea surface during the MSC. The shallowest (966) is close to the crest of the Eratosthenes Seamount at a depth 923 mbsl and the deepest (967) on northern toe at 2687 mbsl. Six holes were investigated at the shallowest site. All were offset within a few tens of meters from each other. The deposit beneath a relatively thin and soft Pliocene–Pleistocene cover was described shipboard as a compact calcareous limestone breccia or para-conglomerate [129]. There was a wide range of carbonate lithologies, including limestone derived from the underlying formation. Some clasts displayed signs of dissolution and recrystallization. The most common clast type was clotted micrite, a typical product of soil formation on Quaternary carbonate substrates [130]. Some clasts exhibited polygonal cracking [131]. Porewater measurements showed a downhole decrease in salinity indicative of freshwater aquifers.

This somewhat pebbly deposit rested with an erosive contact on shallow-water limestone that upon microscopic analysis revealed a coralgal, oncolitic, and oolitic facies. Although benthic foraminifers, echinoids, bryozoa and mollusks were present, a late Miocene (Tortonian) was confirmed on the basis of the strontium isotopic composition and its similarity to shallow-water carbonates of known age exposed on Cyprus (Koronia Member of the Paskhna Formation) [132].

Based on the offset drilling, the depth to its top of the breccia varied by more than 20 m between holes spaced only a few tens of meters apart. The very irregular relief was suggestive of pot holes of karst origin. Since the drill site is on a local

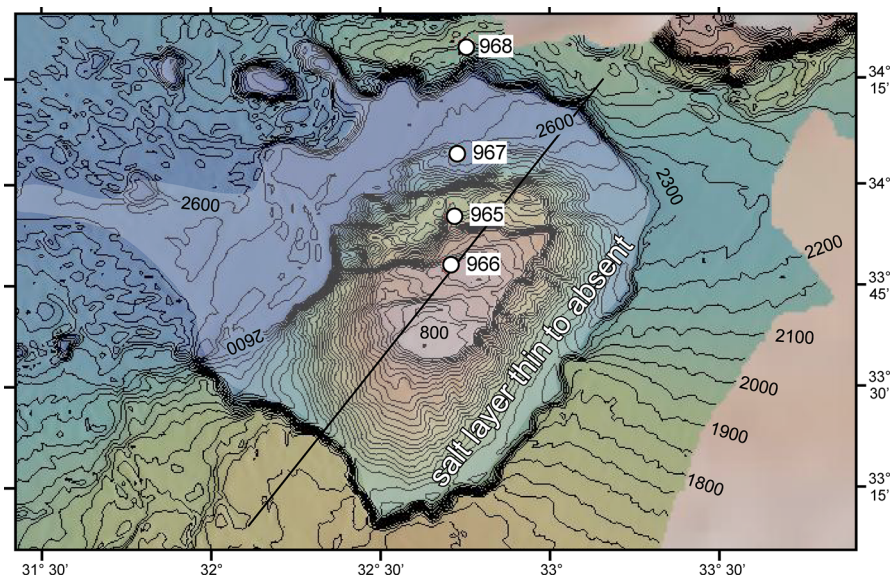

Fig. 25 Location of a drill site transect from the crest of the Eratosthenes Seamount to the foot of the southern margin of Cyprus. Bathymetric contours are numbered in units of mbsl. The seamount is nestled in a depression rimmed by steep scarps where the surrounding subsurface salt layer is thin or absent

topographic high, the clasts in the breccia could not have been transported downslope from elsewhere.

Late Miocene karst surfaces had previously been reported on reef limestone in the Santa-Pola basin of southeastern Spain [133], the island of Mallorca [134], the Melilla peninsular in Morocco [135] and the Koronia reef on the south coast of Cyprus [132]. Karstification of these reef platforms to depths of 60 m is indicative of a long duration of subaerial exposure. The growth of almost all coral reefs along the margins of the western Mediterranean ended with truncated surfaces [136], resulting in a deposit called the Terminal Complex. The Terminal Complex is commonly made up of oolite shoals and both evaporitic and fresh-to-brackish limestone. The Terminal Complex is considered a lateral equivalent to the 'upper evaporites' and shows clear evidence of long periods of emersion such as karst, terra rossa soil with rizocretions and caliche.

At the intermediate depth Site 965 (1506 mbsl) on the northern slope of Eratosthenes Seamount the Pliocene–Pleistocene foraminiferal ooze covered a ~ 5-m-thick bed of indurated clay containing calcareous nodules and caliche that were interpreted as components of a desert soil [137, 138]. Shallow-water limestones of indeterminate age, similar to those at Site 966, underlay the calcareous clay, again with an erosive top surface.

The latest Miocene limestones on both the crest and flank of Eratosthenes Seamount show extensive moldic and vuggy porosity with cavities forming after dissolution of aragonitic mollusk shells. The Formation Micro Scanner (FMS) images of the borehole wall and mechanical caliper logs of the drill hole diameter revealed voids up to a meter in size [131]. The voids came from dissolution of limestone by meteoric water at times of subaerial exposure.

The deepest Site 967 on the seamount (2553 mbsl) had another relatively thin bed of calcareous clay with ostracod carapaces indicative of Lago-Mare fresh-to-brackish waters. However here the clay rested conformably on a single bed of gypsum that was also captured with the Formation Micro Scanner [139] (Fig. 26, Right). Noteworthy

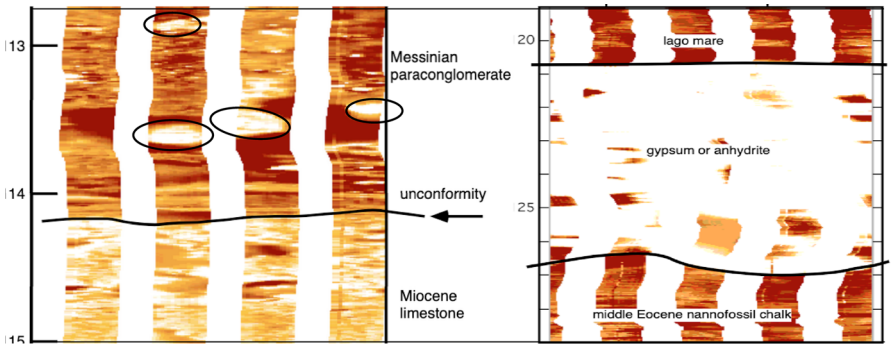

Fig. 26 Left: Formation Micro Scanner Image strips 90° apart of the wall of the drill hole at Site 966. Highlighted are large rounded clasts in the breccia and the sharp erosive boundary separating it from the underlying shallow-water limestone. Right: FMS image of a ~ 5-m-thick gypsum bed at foot of the Eratosthenes Seamount at Site. 967, overlying upper Eocene foraminiferal nannofossil chalk along an irregular erosion surface

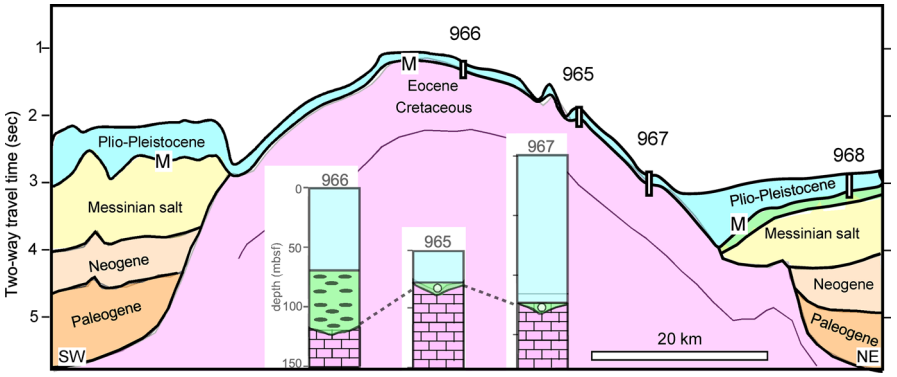

Fig. 27 Tracing of a reflection profile across the Eratosthenes Seamount showing the Eocene and Cretaceous limestone (violet), the thin Messinian breccia, paleosol and gypsum (green) and Pliocene–Pleistocene oozes (blue) at all three drill sites. Track is located in Fig. 25. Drill sites have been projected onto the profile, some at considerable distance. The circle symbol at two sites indicates presence of Lago-Mare ostracods. Black ovals signify clasts in the Site 966 breccia

is the clear sign of erosion on the top of underlying middle Eocene chalk that left a gap of 35 million years in duration.

The onlap of the salt layer and older strata against the flanks of the seamount confirms that the edifice existed as a topographic high prior to the MSC (Fig. 27). The Messinian and Pliocene–Pleistocene sediment cover on the seamount is thin in comparison with its thickness in surrounding deep basins. Although age control at the two shallower sites (965 and 966) is poor over the intervals of interest, the presence of the acme of the pelagic foraminifera *Sphaeroidinellopsis* just above the Lago-Mare ostracods [140] at the deepest site (967) clearly indicates an abrupt change from brackish environments to fully-marine environment at the beginning of the Pliocene.

Site 968 (1963 mbsl) recovered 150 m of mostly clastic sediments attributed to the late Messinian by the presence of gypsum, both as beds of in situ alabaster, but mostly detrital in beds of sand intercalated with calcareous and dolomitic marls containing *Cyprideis pannonica* and *Ammonia beccardii tepida*. The sand included fragments of amphibole and serpentine derived from erosion of the Troodos ophiolite currently outcropping on Cyprus. The steady downhole rise of chloride, sodium and magnesium in the pore waters confirmed the existence of halite beyond the reach of the drilling. An unexpected discovery was the finding of a terrestrial snail, *Brotia* (*Melanidae*) at two levels (224 and 265 mbsf) [141]. If the snail was autochthonous, its occurrence implied an episode of subaerial emergence and development of soil, a sign desiccation.

6.4 Ocean Drilling Program expedition 161: western Mediterranean

Evidence of sea level lowstand also became evident from additional drill sites in the western Mediterranean, especially those in the Alboran Sea. There, the salt layer is not observed in reflection profiles. The salt layer's landward limit is the in westernmost Algero-Balearic Basin at an elevation 3.2 km below the sea surface (Fig. 28). Despite

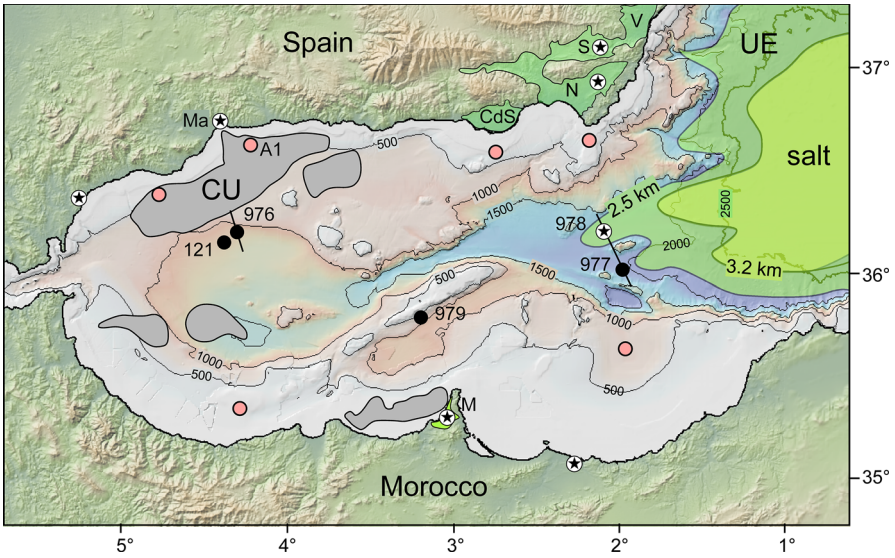

Fig. 28 Neither the upper evaporites (UE), as mapped in reflection profiles, nor the underlying the salt layer reach westward into the Alboran Sea. The only Messinian deposits there are detrital aprons (gray) and sediment associate with gravel at Sites 977 and 978 [142]. Instead of evaporites, the Messinian is expressed by a widespread erosion surface, first confirmed by DSDP Site 121 and since by ODP 161 Sites 976, 977, 978, and 979 [143] (black dots) as well as by commercial exploration wells (pink dots). Onshore time equivalents to the upper evaporites (UE) appear in margin basins of Spain and Morocco (N Nijar; S Sorbos); V Vera; M Mellia; Ma Malaga). Dots with stars denote occurrences of fresh-water ostracods. The elevation of the landward limit of the salt is ~ 3200 mbsl, deeper than most of the buried bedrock surface in the Alboran Sea. Seabed contours are in units of mbsl at a 500 m spacing

the absent of a halite layer, downcore increases in sodium and chloride were observed at all the Alboran sites [32, 47]. The average molar Na/Cl ratio of the interstitial water samples was equivalent to the seawater ratio of 0.86. If the pore waters increase had derived from dissolution of buried halite at these locations, the Na/Cl ratio would be expected have had a value of 1 because of equal amounts of Na and Cl in halite. The seawater ratio implied that the elevated porewater salinity in the Pliocene–Pleistocene sediment cover originated from concentrated Messinian seawater that had seeped into and had become stored in the underlying Miocene strata.

In every case, when drilling at Sites 121, 976, 977, 978 and 979 (Fig. 28), the 'M' reflector corresponded to a resistant formation. At Sites 977 and 978 the formation turned out to be a 10-m thick gravel containing pebbles of volcanic and sedimentary rocks [143]. Pebbles had smooth and rounded surfaces. Cement coatings, scalloped indentations, and adhesion of some pebbles indicated that they were most likely broken apart during drilling. Cementation of the gravel formation was further supported by downhole logging that showed high resistivity due to lack conducting porewater (Fig. 29).

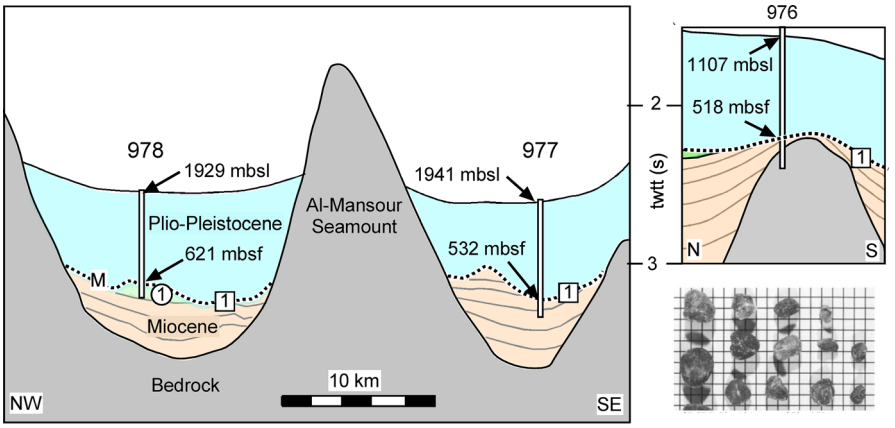

Fig. 29 Tracing of reflection profiles across ODP drill sites showing the erosion surface #1, separating the Pliocene–Pleistocene cover from Miocene sediments. The erosion surface at sites 977 and 978 is strewn with partly cemented gravel containing pebbles eroded from exposed bedrock and Middle Miocene sandstone. Gravel is displayed on a grid with 0.5 cm spacing. Unit #1 at Site 978 has Lago-Mare fauna

Most of the pebbles were of volcanic origin and could have been derived locally from the Al-Mansour Seamount separating Site 978 from Site 977 (Fig. 39). The non-volcanic pebbles consisted of chert, limestone, quartzite and metamorphic rocks of the type sampled from the bedrock at Site 121 [144] and Site 976 [145].

At Site 978 the gravel rested directly on a 68-m thick bed of silt and sand with shallow-water *Ammonia tepida*, and ostracods (*Candona* sp., *Loxoconcha mülleri, Cyprideis* sp.), indicative of either a fluvial or lacustrine environment [122].

The erosion surface upon which the gravel resides is pervasive throughout the sub-bottom of the Alboran Sea. Silvia Iaccarino and Alessandro Bossio, participants in the drilling expedition, concluded in their report that at the end of the MSC "*the area of Site 978 would have been occupied by an alluvial fan, which was drowned and subsequently covered directly by marl ooze with typical planktonic marine fauna of the early Pliocene*." [122]

7 Obtaining an age for the Mediterranean Salinity Crisis

After completion of the first deep-sea drilling in the Mediterranean in 1970, the next task was to obtain the age of the onset and the end the MSC and then estimate its endurance, including the run-up to evaporation expressed by the Tripoli diatomite, and the stages expressed by the 'lower evaporites' and 'upper evaporites'.

7.1 Miocene/Pliocene boundary

The Miocene/Pliocene boundary had been recovered in 1970 at three drill sites and its age became a challenging task [146]. Five published and unpublished K/A dates

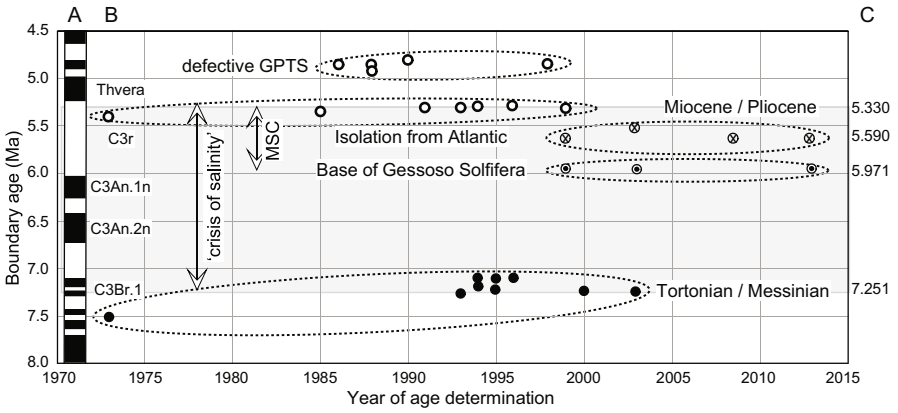

Fig. 30 History of dating the biostratigraphic and paleomagnetic boundaries of Raimando Selli's original 'crisis of salinity' (shaded) and the more commonly referred to Messinian Salinity Crisis (MSC). **A** Reversal boundaries. Black: normal polarity, white: reversed [150, 151]. **B** Magnetic chrons [152]. **C** Currently accepted ages of the boundaries (Ma)

had been derived from volcanic rocks in contact with Pliocene sediments in Italy that also contained planktonic foraminifera [147]. Using the biostratigraphic ranges of these foraminifera in combination with those from Pliocene/Pleistocene sediments from the Tyrrhenian Sea at Site 132 and correlating them with equivalent datums from continuously cored marine sections at DSDP Sites 62 and 77 from the western and eastern equatorial Pacific [148, 149] the Miocene/Pliocene boundary was placed at ~ 5.4 Ma [146] (Fig. 30).

A decade later attention turned to the age of the Miocene/Pliocene boundary as expressed in outcrops in Sicily [153, 154]. There in the Capo Rossello section the boundary was located below the Thvera normal polarity subchron of the Gilbert Chron. According to the geomagnetic timescale in use at that time [155] the boundary was set earlier at 4.86 Ma.

Sediments from ODP Site 652 and 654 in the Tyrrhenian Sea provided the first opportunity for reliable geomagnetic measurements on actual Mediterranean deep-sea sediments [156]. These measurements showed that the Messinian lithologies at these two locations were also confined to the reversed magnetic polarity interval of the lowermost Gilbert Chron that had recently been named subchron 3r. The Miocene/Pliocene boundary was again young at 4.80 Ma. Its youth raised doubt on the validity of the geomagnetic timescale being used at that time [155].

To address the reliability of these young ages, a new astronomically calibrated (polarity) timescale was created [157]. Late Pliocene to early Pleistocene sapropel-carbonate couplets in southern Italy and Crete repeated at the Earth's precession frequency modulated by eccentricity. The alignment of the couplets with orbital calculations provided an innovative method of interpolation between the K/A dated magnetic reversal boundaries [158]. When extended downward from the Thvera subchron to the base of the Pliocene Trubi marls in the Capo Rossello composite section in Sicily, the counted cycles provided an age of 5.32 Ma [157], some 0.5 my older than

the previously accepted age. This date has since been extended to 5.33 Ma, bringing it closer to the original 5.4 Ma from derived from K/A calibrated foraminifera datums applied to DSDP Site 132 [146].

7.2 Dating the base of the Messinian Stage of the late Miocene

According to Selli the Messinian stage was "*characterized throughout the Mediterranean and the Paratethys by a crisis of salinity*" [101]. Therefore, in deference to his definition, the crisis (sensu*latu*) encompasses all of the Messinian stage (i.e., Peliti Eusiniche, Gessoso Solfifera and Colombacci formations) with its base coincident with the onset of the diatomite beds of the Tripoli Formation.

At the time of the first DSDP expedition in the Mediterranean the age of the boundary between the Tortonian and Messinian was poorly constrained (as early as 11.8 Ma [159] and as young as 8.0 my [160]. In the first attempt to access the duration of the Messinian stage, the marine sediments at DSDP Sites 62 and 77 in the western and Pacific equatorial Pacific were investigated for their nannofossil content [161, 162]. Using the *Ceratolithus tricorniculatus* Zone in the Pacific cores and its range at Site 132 in the Tyrrhenian Sea, an extrapolation was made to the next earlier *Discoaster quinqueramus* Zone based on an assumption of constant sedimentation rate. This approach positioned top of the Tortonian [34] at 7.5 Ma and provided a duration of approximately 2 my for the Messinian stage [146].

The Tripoli diatomite in the Falconara section in Sicily is ~ 25 m thick [163, 164]. Its base is coincident with the first occurrence datum (FOD) of *Globorotalia conomiozea* [165]. Six Upper Miocene marine diatomite sections on Crete (Greece) were subjected to a detailed magneto-biostratigraphic analysis [166]. Regrettably, the FOD of *G. conomiozea* was inadvertently placed in the reversed interval of chronozone 5 resulting in an age of 5.6 Ma and thereby reducing the duration of the Messinian stage to 0.3 my.

This misfit was corrected a decade later with the first direct radiometric estimate of the Tortonian-Messinian boundary using K/A methods on lavas imbedded in sediments in the northern Apennines. The resulting K/A age of 7.26 Ma was soon affirmed by additional measurements on the Metochaia section on Gavdos and the Gibliscemi section in Sicily [167, 168]. There the FOD of *G. conomiozea* was observed in chron C3Br.1 with an age of 7.24 Ma according to the CK95 geomagnetic polarity timescale [169]. The currently-accepted age is 7.251 [170, 171].

The 1.91 Ma duration of the Messinian stage from the new astronomical (polarity) time scale turned out to be remarkably close to ~ 2.0 my interval derived 22 years earlier using nannofossil datums in Pacific sediments.

7.3 Age of the Gessoso Solfifera and Colombacci Formations

Since the Gessoso Solfifera and Colombacci Formations all fall within the reversed polarity chron 3r, another approach using high-resolution cyclostratigraphy was necessary to refine the boundary ages for 'upper' and 'lower' evaporites. Sapropel/marl couplets in pre-evaporite sequences of the Sorbas basin of SE Spain, Caltanissetta basin

of Sicily, and eastern Gavdos basin of Greece were investigated [172]. Upward tuning of these cycles by calibration to northern hemisphere insolation peaks [173] arrived at an age of 5.96 ± 0.02 Ma for the first gypsum bed at each location, demonstrating that the onset of the 'lower evaporites' was synchronous across the entire Mediterranean. In the course of counting the cycles, nine Mediterranean-wide planktonic foraminiferal bioevents (first occurrences, last occurrences, coiling changes) were recognized and given astronomically calibrated ages.

In the Sorbas basin of SE Spain 55 precession-induced sapropel/marl cycles of the Upper Abad Member of the Caños Formation passed upwards to 14 gypsum/sapropel cycles in the Yesares Member [174]. The cyclic alternation of gypsum and sapropel [175, 176] indicated that these gypsum cycles were also astronomically controlled. Under the assumption that each cycle had a periodicity of 21–24 kyr, an age of 5.6 to 5.54 Ma was obtained for the top of the Yesares Member [177]. Since the same number of gypsum beds appeared in the Gessoso Solfifera in Sicily, it could be established that the Yesares Member took place synchronously with deposition of the 'lower evaporites' in Sicily and the Apennines.

The Yesares Member was followed by the Sorbas Member, consisting of coastal sandstone followed by conglomerates [178, 179]. The Sorbas Member represents the lateral equivalent of a facies association known as the Terminal Carbonate Complex (TCC) [133, 136] that included Porites patch reefs and thrombolites [180, 181]. These elevation of these reefs along the margins of the basins and the TCC established that Yesares and Sorbas Members accumulated when the Mediterranean was filled with brine from 5.96 to 5.60 Ma.

Next in succession, the continental Zorreras Member exhibited 8 sedimentary cycles of alternating terrestrial reddish silts (dry climate) and yellowish sands (wet climate) which matched in number with gypsum/shale cycles in the Pasquasia Formation in Sicily, the limestone/shale couplets in the Colombacci Formation in the Apennines and the gypsum/Lago-Mare facies in the Mediterranean drill cores. Tuning the eight cycles to the isolation peaks provided an age estimate of 5.52 Ma for the initiation of the 'upper evaporites' and left a gap of 20 to 80 kyr for the evaporative drawdown of the Mediterranean [177].

8 Evidence of subaerial exposure on Mediterranean margins

The findings from deep-sea drilling of lacustrine and even fluvial and alluvial environments soon gained the attention not only terrestrial geologists, but also commercial hydrocarbon exploration companies.

8.1 3D seismic reflection imagery of erosion surfaces

The Koninklijke Shell Exploration and Production Laboratory was among the earliest to conduct a 3D seismic survey of the offshore margin of eastern Spain [182]. The location of their survey in 1981 is shown as box 1 in Fig. 3. There they encountered

high-amplitude reflections from a buried erosion surface outlining a landscape possessing a dendritic-style drainage system with broad interfluves and deeply incised valleys. At the seaward margin of the study area the surface flattened to a presumed piedmont plain. Amplitude extraction identified valley fill which well-data confirmed to be sand and conglomerate deposited in Messinian thalwegs before the resumption of marine sedimentation in the early Pliocene. High amplitude reflections from the thalwegs implied cemented conglomerates. Fluvial terraces and braided streams in the 3D imagery were features of a subaerial landscape. Knowledge of the measured relief of the erosion surface in the area surrounding the 3D survey and correction for the effects of post-Messinian compaction and subsidence suggested "*a minimum value of nearly 2000 m for the Messinian seas level fall*" [182].

The subsequent Tortuga 3D survey (Box 2 in Fig. 3) covered a slightly larger area in which there were more than a dozen exploration wells that had encountered the "*Messinian Unconformity Surface*" [183]. Two or possible three orders of stream branching were distinguished. The morphological characterization of the unconformity was highly reminiscent of complex subaerial erosional networks seen in areas of badlands topography, for example in southern Spain or the USA [184, 185]. There was no evidence of repeated infilling and excavation of the subaerial deposits, implying a sustained Messinian lowstand.

A much larger 3D survey (Box 3 in Fig. 3) was conducted in 2002 by British Gas BV [186–188]. Slices from the 3D seismic data afforded an exceptional view of drainage networks with tributaries of at least five orders, channel-bank terraces and meandering thalwegs (Fig. 31). The reflection amplitude map showed meanders with a sinuosity of 1.3. Sonic velocity values from the Fornax-1 well logs identified the largest excursion (> 1 km/s) when crossing the unconformity. The velocity increase was accompanied by a gamma ray decrease as would be expected from cementation of the fluvial deposits during subaerial exposure [182]. The amount of incision into the underlying Miocene Castellón group approached 1.3 km. The erosion surface could be traced as deep as 3 km below sea level before it was onlapped by the 'upper evaporites' of the Valencia Trough.

The initial drawdown of the sea surface induced large-scale destabilization of the continental slope and the deposition of large detrital bodies at the foot of the margin [186, 187, 189]. The continuing fall of the sea surface exposed these deposits to their own subaerial erosion. An even further drop exposed most of the floor of the Valencia Trough [190]. Reflection profiles have confirmed the presence of a widespread Bottom Erosion Surface (BES) under the 'upper evaporites' [191, 192, 192]. The distal limit of the BES marks a maximum lowstand shoreline situated some 3 km below present sea level [193] (Fig. 32). All of the subaerial landscape not covered by the subsequent upper evaporites was given the name Margin Erosion Surface (MES) [191, 194, 195].

As shown in Fig. 33, fossil drainage also exists in the subsurface of the Gulf of Lions, France [191, 196–199]. Few regions were spared from errosion including interfluves. Mesa tops were truncated. At one location the MES cut into Jurassic dolomite. The erosion surface can be traced to an elevation > 3 km below present sea surface where it becomes onlapped by the 'upper evaporites'. Exploration boreholes confirmed the absence of any Messinian residue expect for gravel in the drainage thalwegs. The reflection profile in Fig. 34, top panel displays the rugged nature of the MES, not

Fig. 31 Depth-structure map and margin-parallel reflection profile) of the Messinian erosional unconformity and resulting dendritic drainage network in the subsurface of the Ebro margin of the western Mediterranean [186–188]. Contours at 0.5 km intervals are relative to sea level. Circles are industrial boreholes. The Fornax-1 well encountered fluvial gravel in the thalweg of a major tributary

discernable from contours alone. Fault offsets in the Miocene substrate had been truncated at the interface between the pre-MSC Miocene and the overlying Pliocene strata.

8.2 Elevation range of erosion surface below present sea level

8.2.1 Sardinia margins

Using reflection profiles, the Margin Erosion Surface can be traced down slope to its overlap by the 'upper evaporites.' The western Sardinia margin of the Provençal Basin has presented an illustrative example [200]. There in Fig. 34 (Left panel) the MES extends from the coast to 2.1 kmbsl. Three individual Messinian paleo valleys, separated by interfluves, have been identified down to a depth of 2.5 kmbsl. On shore, a karstic plateau in Oristano Gulf (Fig. 35A) outcrops over an area of 100 km^2. There the erosion surface has been etched by dissolution and brecciation and incised as deep as 5 m into the top of the Terminal Carbonate Complex [133, 201, 202], the final 'lower evaporite' lithology prior to the evaporative drawdown beginning at 5.6 Ma. The karst plateau had been opened by caves and dissolution pipes prior to infill by Pliocene marls and limestones.

Another MES has been observed on the eastern margin of Sardinia (Fig. 35, Right panel) where it can also be traced to > 2.1 kmbsl [203]. There the MES once again

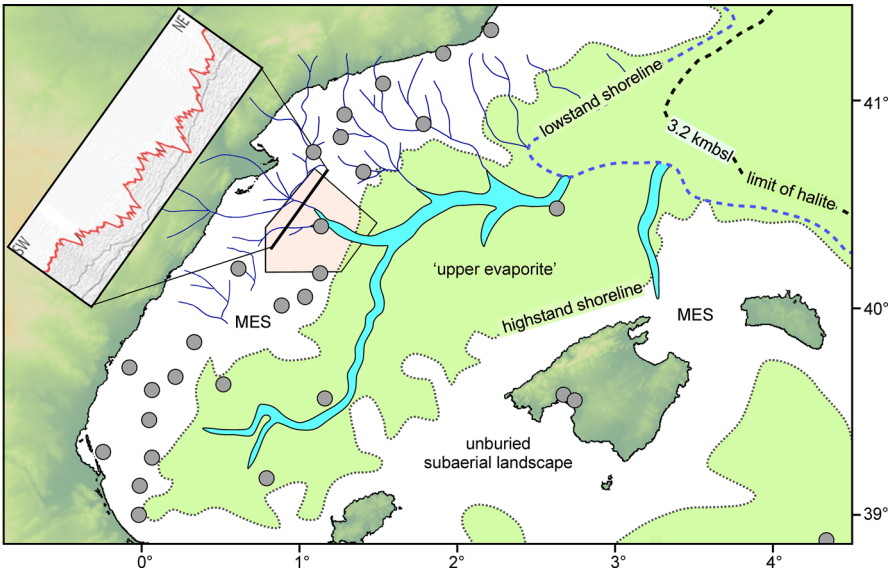

Fig. 32 The Messinian dendritic drainage networks on the Catalan margin of Spain feeding into a 270 km long fluvial valley (blue), later submerged by the upper evaporites (green) [193]. Red line in the reflection profile insert displays the rugged margin erosion surface with no preserved Messinian deposits except fluvial gravel in thalwegs. Solid dots are exploration wells and DSDP drill sites. Vertical scale in the reflection profiles is from − 1 to − 2 km relative to the present sea surface

displays a network of paleo valleys with relief exceeding 250 m. Onshore in the Orosei Gulf (Fig. 35B) the erosion surface had been deeply incised by the paleo-Cedriino river valley and subsequently filled with marine sandy deposits of early Pliocene age [204]. No evidence of sediments belonging to the Lago-Mare stage of the 'upper evaporites' has yet been observed on either margin above 2 kmbsl.

8.2.2 Corsica margin

A Messinian erosion surface exists in the subsurface of the Golo and Orbo basins east of Corsica in the Tyrrhenian Sea (Fig. 35). However, here the MES extends only to ~ 1000 mbsl before continuing as a Top Erosion Surface (TES) across the underlying Messinian evaporites. The exitance of the evaporites suggest that they accumulated in a perched setting, before its lake breached its sill and drained southward into the deeper Tyrrhenian Sea. Again, there is no evidence of latest Messinian deposition on the TES prior to the its Pliocene cover. The drainage of the prior Golko and Orbo lakes cut a valley 3 km wide and > 300-m deep into the evaporites and underlying substrate.

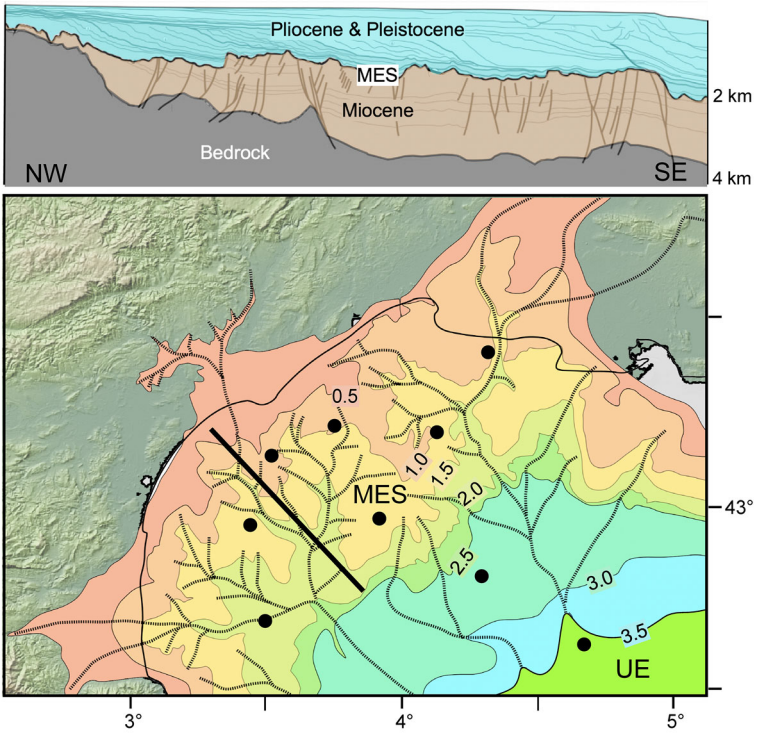

Fig. 33 The Margin erosion surface (MES) in the Gulf of Lions, France [196, 197, 197–199]. Contours at 0.5 km intervals. Solid dots locate exploration boreholes that calibrate the elevations and confirm the absence of any Messinian residue expect for gravel in the drainage thalwegs. The reflection profile (top panel) displays the rugged MES

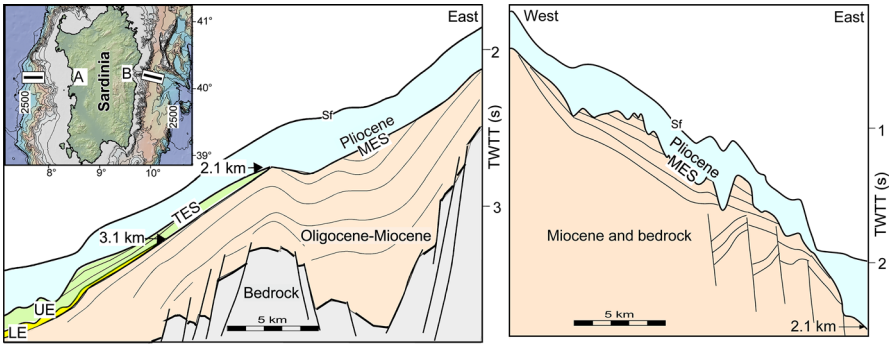

Fig. 34 Tracings of reflection profiles displaying the MES on the western and eastern margins of Sardinia. Bathymetric contours in the map panel are at 250 m intervals [200, 203]. In Map panel: **A** Oriste Gulf; **B** Orosei Gulf

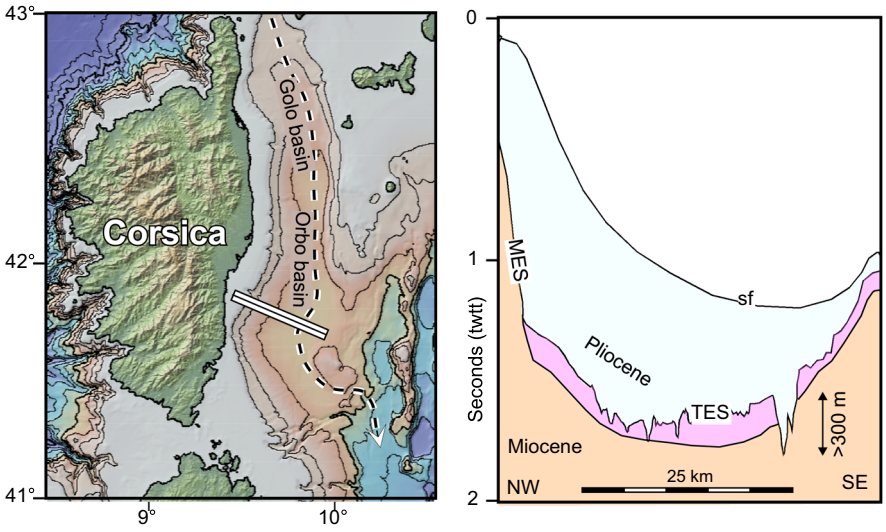

Fig. 35 Tracing of reflection profile (right panel) crossing the Orbo basin east of Corsica [205]. Dashed line in left panel depicts the path of a paleo-river valley cutting an incision > 300-m deep into the Messinian evaporites (purple) and their Miocene substrate at the location of the profile

8.2.3 Subsurface of the northern Adriatic Basin

There was another substantial base-level drop in the Po Plain-Northern Adriatic region of the eastern Mediterranean. The evaporative drawdown resulted in an unconformity with an erosive contact at the Miocene–Pliocene boundary [206, 207]. The unconformity exhibits V-shaped incisions that extend southward from the present-day southern Alpine valleys. These valleys were party-filled with fluvial conglomerates of the Sergnano Formation and then completely filled with Pliocene–Pleistocene turbidites, indicating that the modern drainage network had been inherited from the late Messinian.

The MES has been restored to its original state through flexural-backstripping numerical modeling [206]. The calculations to reconstruct the landscape (Fig. 36) produced a maximum water-level drop of ~ 900 m when assuming that the sea level before the MSC was close to the present elevation. Deeper regions remained as separate lakes, accumulating turbidites of the Fusignano Fm. The 'lower evaporites' are preserved beyond the 500 m level and are directly overlain by Pliocene sediments above a TES that extends to 900 mbsl where the 'upper evaporites' (brackish-water facies) appear in reflection profiles. The enclosed nature of the Po Plain and northern Adriatic Sea and the proximity to substantial fresh water from Alpine drainage are plausible explanations for the lack of halite and potassium-rich salts in these foredeeps.

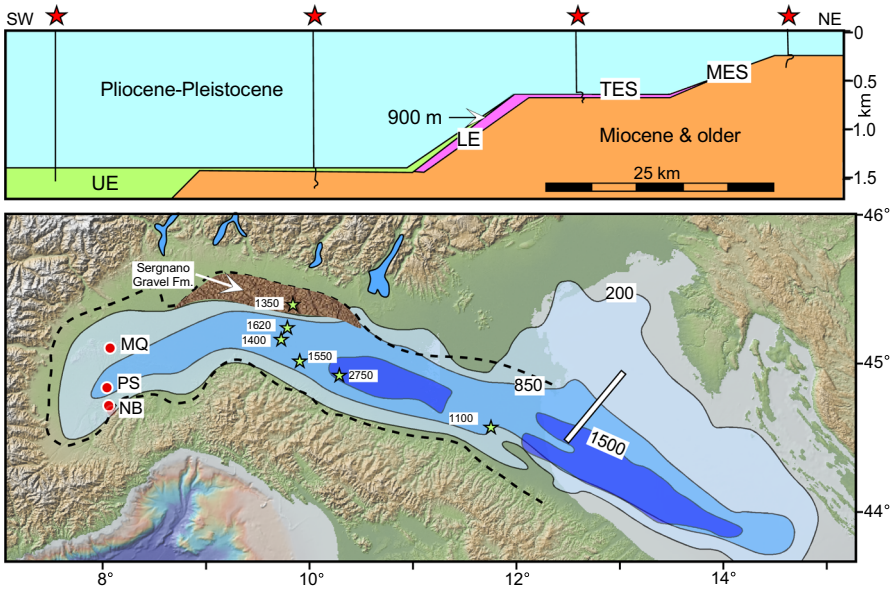

Fig. 36 Lower panel: reconstructed elevation contours (mbsl) of the Po Plain-Northern Adriatic foreland basins for the latest Messinian obtained using an elastic thickness of 20 km [206], extended to include westernmost of the Piedmont Basin. MQ: Moncucco Quarry; PS: Pollenzo Section; NB: Narzole Borehole, discussed in Sect. 13.1.4. Dash line is the outline of the Piedmont Basin based on reflection profiles and exploration wells [208]. Green stars are wells labeled with present depth to the base of the Pliocene (mbsl). The Southern Alpine lakes are shown in blue. Upper panel: SW–NE profile derived from connecting commercial wells (stars) showing the MES, appearance of the 'lower evaporites'(purple) beyond 500 m depth, and 'upper evaporites' (green) below 900 m. The red stars are wells delineated with the resistivity measurements from electric logs

8.2.4 Central Adriatic basin

The gypsum beds of the 'lower evaporite' Gessoso Solfifera Fm were deposited on a pre-MSC substrate of the Adria Plate that had been tilted downward to the SW during its subduction beneath the Apennines [209, 210] (Fig. 37B). The tilting of the 'lower evaporites' gypsum beds provided a slope into which canyons were later cut during falling sea level (Fig. 37C). These gypsum beds were subsequently covered by earliest-Pliocene mudstone as directly calibrated in exploration wells [211]. An erosional unconformity is well-evidenced by truncation of the gypsum beds and an irregular and scattered TES. The base of the gypsum beds showed no evidence of erosion (Fig. 37C). The 'upper evaporites' were either never deposited on the gypsum beds in response to subaerial exposure, or they were removed by subsequent erosion. However, a significant thickness of detrital sediments had accumulated throughout the entire MSC in the adjacent and deeper Apennine foredeep [212, 212, 213].

The finding of the TES at elevations > 2500 mbsl provided substantial evidence of evaporative drawdown of the Mediterranean beginning at around 5.6 Ma and coincident with the event that produced the #1 erosion surface elsewhere.

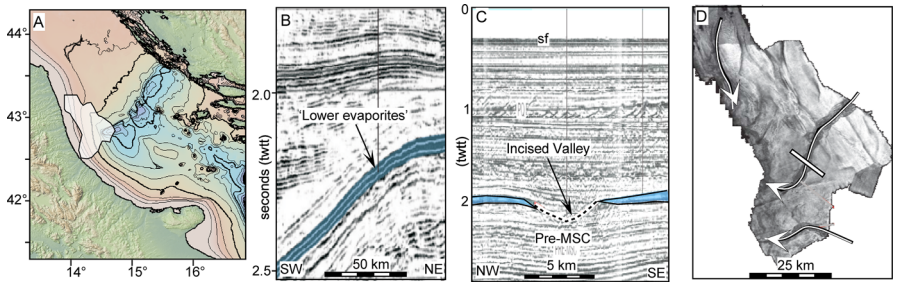

Fig. 37 **A** Present seabed bathymetric contours at 25 m intervals of the Central Adriatic Basin in a region of dense coverage with 2-D and 3D reflection profiles and numerous commercial exploration wells. Region shaded white in the map is displayed in panel **D**. **B** The 'lower evaporites' of the Gessoso Solfifera Fm buried at > 2 km depth in the subsurface of the basin beneath its Pliocene–Pleistocene cover. **C** A 5-km-wide Messinian valley incised through the 'lower evaporites' and filled with earliest-Pliocene sediment. **D** Map of maximum reflectance on the late-Messinian erosion surface showing the paths of the incised valleys. Imagery compiled from [211]

8.2.5 On the Island of Crete

Substantial base-level drop became evident in Crete when examining the MES at five locations across the island (Fig. 38, Left panel) [214]. There the 'upper evaporite' interval of marls with thin beds of gypsum ended with alluvial conglomerate, in places containing bones and teeth of mammals and elsewhere terrestrial snails. Erosion had sculpted ravines in the underlying 'lower evaporite' gypsum beds with relief > 50 m. The breccia interval between the 'lower' and 'upper 'evaporites was interpreted to have resulted in the dissolution of halite, accompanied by collapse of the original bed. The return of saltwater at the onset of the Pliocene was announced by a foraminiferal assemblage indicative of upper-bathyal water depths.

8.2.6 On Cyprus

On Cyprus the passage from the Messinian to Pliocene transition was accompanied by a very rapid environmental [140] change expressed in the lithology, sedimentology, microfaunal assemblages and stable isotope composition [215–217]. The terminal Messinian lakes were colonized by *Cyprideis pannonica* and *Ammonia beccarii* [140]. The feature most evident of a terrestrial landscape was paleosol interbedded with carbonates and conglomerates. Paleosols with preserved casts of plant roots substantiated periods of subaerial exposure of sufficient duration for pedogenesis to have advanced. The topmost soils contained a pollen assemblage composed of *Pistacia* associated with *Olea*, characteristic of dry seasons and mild winters. Conglomerates with basalt, gabbro and Cretaceous-age limestone had been delivered by rivers from the adjacent Troodos Massif and its sedimentary cover.

The uppermost gypsum beds were intensely karstified. Large cavities had been hollowed out by dissolution and subsequently filled with Lago-Mare deposits. As was the case on Crete, the 'lower' and 'upper' evaporites were also separated by an intermediate breccia. The 20-m-thick breccia (also called a mega-rudite) contained

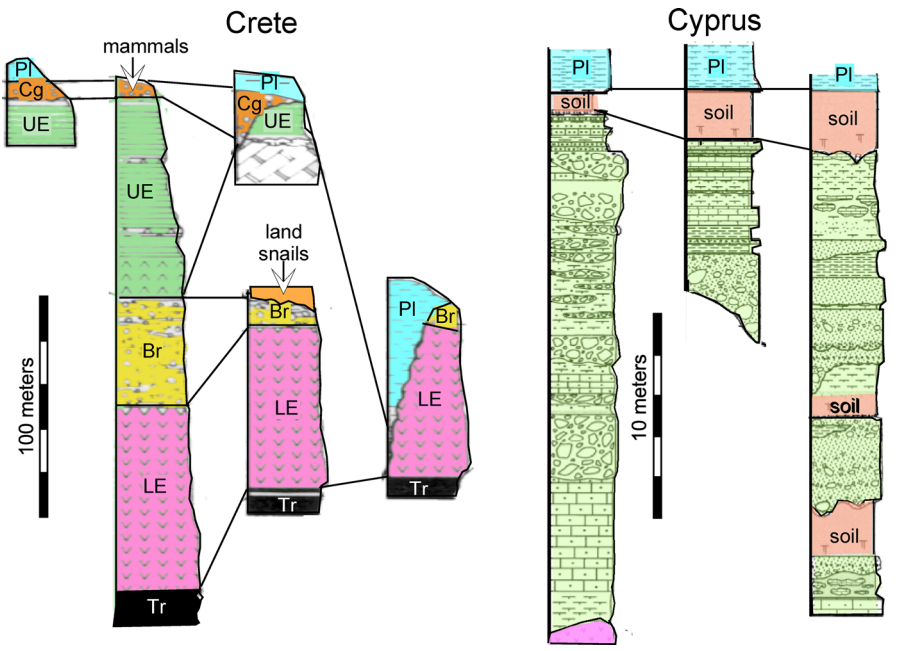

Fig. 38 Left: Five outcrops investigated from the Messinian stage on Crete [214], beginning upwards with the Tripoli diatomite (black), 'lower evaporite' gypsum beds, an intermediate breccia, 'upper evaporite' gypsum bed intercalated with lacustrine sediments hosting brackish-water fauna, terminal alluvial and fluvial conglomerates with clear evidence of belonging to a terrestrial landscape undergoing extensive erosion, and then a blanket cover of earliest-Pliocene-age pelagic marls. Right: Three outcrop sections on Cyprus displaying the latest part of the 'upper evaporites' from its youngest gypsum bed to the earliest-Pliocene marls [217]. Paleosols, alluvial and conglomerates are present at the top of these Messinian successions

meter-sized clasts from both the 'lower' and 'upper' gypsum beds, the precursor diatomite, and olistoliths with stromatolitic layers displaying desiccation cracks. This breccia has been interpreted as a stratigraphically equivalent to the 300 m thick salt unit in the subsurface of the Mesaoria plain north of the Troodos Massif and confirms that halite may have been present in the region of the outcrops illustrated in Fig. 38 (Right panel).

The latest Messinian paleosols were directly overlain by the lowermost Pliocene beige and white marls of the typical 'Trubi' facies in Sicily, deposited in a well-oxygenated marine setting. According to the investigators, the abrupt environment changes at the climax of the MSC showed that the elevations of a late-Messinian terrestrial landscape were several hundred meters below that of the world ocean at the time of the invading Pliocene saltwater [217].

8.2.7 Levant margin in the easternmost Mediterranean

The subsurface of the coastal plain and offshore of the Levant margin has been extensively investigated since the early 1960's with commercial exploration wells and reflection profiling methods [94, 112, 218–235]. The halite layer in the Levant Basin

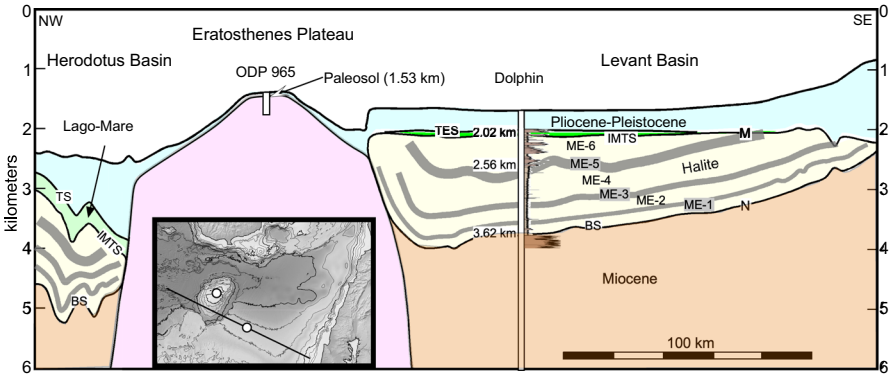

Fig. 39 Tracing with interpretation of a reflection profile from [232] extending westward from the Levant continental margin to the Herodotus Basin. *TES* Top Erosion Surface, *BS* Bottom surface, *IMTS* Intra-Messinian Truncation Surface. Green layer is the stratigraphic equivalent of the 'upper evaporites'. White dots in the map insert are locations of ODP Site 965 and the Dolphin well. The Dolphin gamma-ray log displays the abrupt passage from underlying marine marls below to halite above

exceeds 1.7 km in thickness and extends westward with similar thickness into the more tectonically active and deeper Herodotus Basin (Fig. 39).

The halite layer has been investigated from cuttings and electric logs at the Dolphin well. The succession of planktonic foraminifera bioevents in the sediment immediately below the halite layer has revealed that Levant salt had been deposited synchronously with the 14 to 16 'lower evaporite' gypsum beds of the Cattolica Fm in Sicily and Yesarers Mb in the Sorbas Basin of SE Spain [236].

The top surface of the halite exhibits the truncation of six internal halite layers (ME-1–ME-6) [220, 221, 226, 231]. Although ever-so slightly titled, this surface (Intra-Messinian Truncation Surface—IMTS [225] has remained remarkably flat [234], except at the foot of the continental margin. There the IMTS is pitted with enclosed depressions thought to have been attributed to dissolution [237].

The IMTS has been interpreted both as an erosional unconformity of subaerial origin [220, 226, 229, 234] and the product of halite dissolution [225, 227]. High resolution 3D reflection imagery has since revealed a thin sediment package overlying the IMTS [226, 234] and given the names Nahr Menash [228, 229] and Unit 7 [225]. This layer (Fig. 40, left) has been assigned to the 'upper evaporite' interval of the MSC [234]. It remains unsampled except at well Or-South-1. There the lithology and faunal composition had been described as belonging to the stratigraphic equivalent of the Afiq Member of the Mavqiim Fm [238]. Gamma-ray and density logs indicated the presence of anhydrite and halite (Fig. 40, Right). Deposition of the Afiq Mb ended with a conglomerate located directly above dolomitic marl that contained the brackish-water ostracod *Cyprideis torosa*. The written log described the Late Miocene to include "*evaporite with fluvial clastics*." The conglomerate was followed by the arrival of earliest-Pliocene marls belonging to the *Sphaeroidinellopsis* acme zone. These fully-marine deposits had draped an undulating surface etched with channels 100 m in width and 15 m in relief.

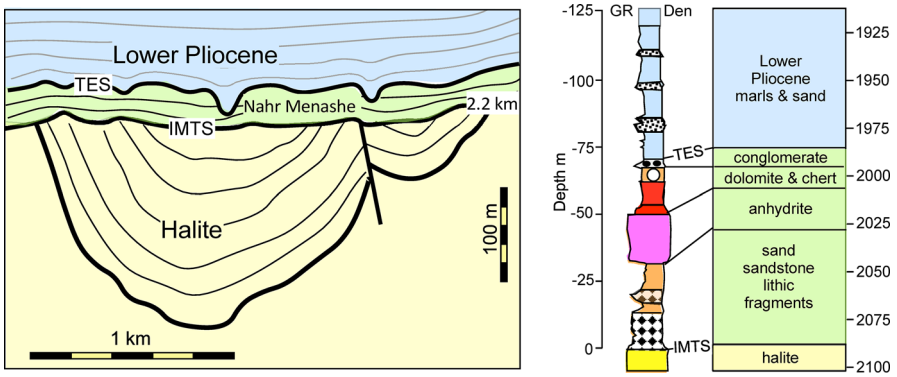

Fig. 40 Left: Tracing of a reflection profile in the Levant Basin of the easternmost Mediterranean. Right: Gamma-ray and density logs from exploration well Or-South-1 [225] correlated with lithologic and faunal descriptions in the well report [238]. White dot is the location of the Cyprideis torosa ostracod. Black ovals depict the terminal conglomerate belonging to the TES

Most intriguing was the necessary gap in time between accumulation of the halite, its deformation into folds, offset of the folds by thrust faults and eventual decapitation to produce the flat surface. The removed halite, even as detritus, was enhanced by dissolution. The solutes were transferred elsewhere into the deeper regions such as the Herodotus Basin [227]. Therefore, top of the salt (IMTS) in the Levant Basin records a substantial fall in relative sea level that most likely coincided in time with the exposure surface between Units B and C in the Realmonte salt mine in Sicily [239].

The Afiq Mb (green in Fig. 40) with its euryhaline ostracod *Cyprideis torosa* had previously been recognized in 18 exploration wells on the Levant Margin ranging from 800 to 2000 mbsl. In all wells it overlies anhydrite (purple) belonging to the Mavqui'im Formation that is equivalent in age to the 'lower evaporites' based on measurements of $^{87}Sr/^{86}Sr$ [240]. The anhydrite on the Levant margin was directly sampled from 1600 to 900 mbsl, and halite (yellow) from 1750 to 1000 mbsl was inferred by unique responses in the electric logs [222, 223] (Fig. 41).

The presence of halite and anhydrite across this large depth range was not surprising since they had been components of the 'lower evaporites' and had accumulated prior to any major fall in sea level. On the other hand, the Afiq Mb raised concerns [241]. If the Afiq Mb had been a lacustrine deposit, it would have implied that the basin may have partly filled to elevations as high as 800 mbsl and then emptied one or more times. However, the Afiq Mb on the margin is a clastic deposit composed of conglomerates with lithoclasts of Cretaceous and Eocene limestone and sandstone as well as earlier detrital anhydrite from the underlying Mavqui'im Formation that had been eroded and redeposited in an alluvial and fluvial setting. These lithologies became subject to erosion with falling sea level during the Lago-Mare Stage 3 of the MSC [219, 242].

Using 3D seismic reflection surveys and boreholes the MES has been recently mapped on the westward dipping continental slope of the Levant margin to reveal

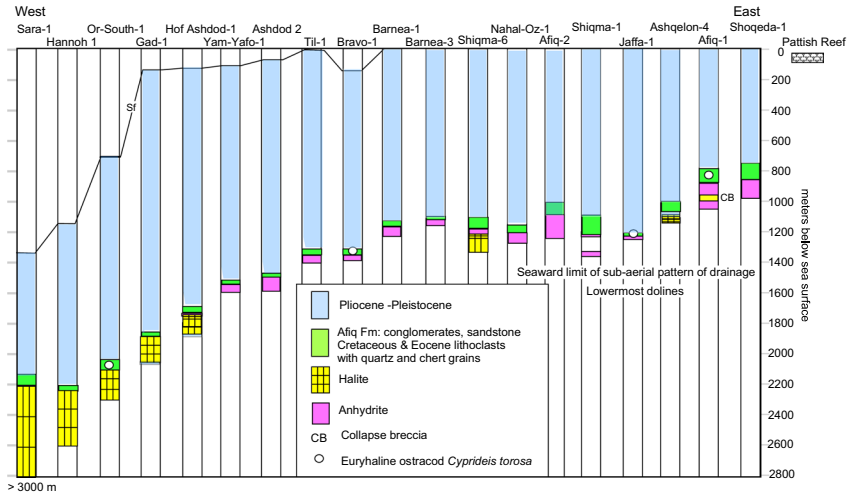

Fig. 41 Composite of exploration wells on the Levant continental margin in passage from offshore (left) to onshore (right). The collapse breccia is a residual from the dissolution of prior salt or gypsum. The pre-evaporite Messinian Patitish Reef at 10 to 50 mbsl provides a stable reference elevation for the pre-MSC sea surface

dendritic channel networks extending downdip to clastic deposits in the Hadrea valley [219] (Fig. 42, Left). The clastic deposits were composed of fragments of 'lower evaporite' anhydrite and pre-Messinian chert and chalk fragments along with distinct Lago-Mare benthic foraminifera. The clastic deposits have also been sculpted by the same upslope drainage. Second and third order channels were cut to a depths >

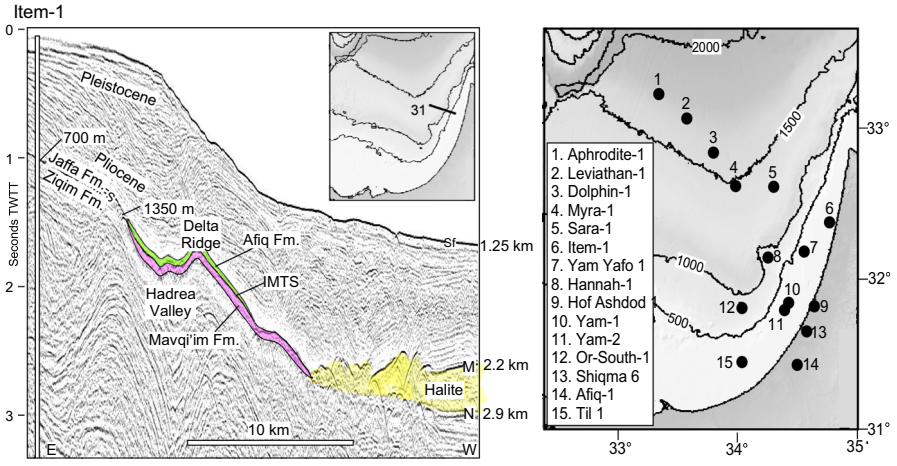

Fig. 42 Left: reflection profile EM-83-31 displaying the Afiq Mb and Mavqi'im Fm in the region of the buried Hadrea Valley and Delta Ridge. Right: Location of exploration wells presented in Fig. 40 and including those discussed elsewhere in the text

5 m below interfluves. The top surface of the clastic deposits display funnel-shaped endorheic depressions interpreted as sink holes and dolines. Although the presumed subaerial pattern of the drainage network disappeared beyond 1350 mbsl, the lowermost dolines extend further down slope to 1530 mbsl.

8.2.8 Nile Delta and its offshore margin

The continental margin of Egypt had experienced severe erosion during the latter part of the MSC when creating a vast drainage system on the southern margin of the Mediterranean [95, 108, 243, 244]. Numerous valley incisions had cut through the entire pre-Messinian Miocene and into the deeper Oligocene and Eocene strata (Fig. 43) [245]. The erosion surface can be followed seaward to elevations approaching 4000 mbsl [246] before arriving at the landward edge of the halite layer buried beneath the Herodotus abyssal plain and the Mediterranean Ridge accretionary prism [247, 248].

One of the incised valleys, the Eonile, has been extensively explored with 3D reflection surveys. More than 50 wells have targeted the Abu Madi sandstones on its floor where they serve as a major hydrocarbon reservoir [244, 245, 249–257]. Beyond the valley's mouth the Eonile evolved into a 6-km wide and slightly-meandering channel cut > 200 m into mudstones and limestones belonging to the brackish-water Qawasim Fm, itself, the stratigraphic equivalent of the 'upper evaporites' [258].

The Eonile channel incision (Fig. 44) has been referred to as an "*intra-Messinian erosional surface*", and the sandstones within it have been attributed to both a "*fluvial to fluvial-deltaic facies*" [252] and a "*braided river deposit*" [259]. On the outside rims of the channel drilling had recovered siltstones and mudstones, intercalated with lagoonal clay rich in coal fragments and soil horizons that have been described as floodplain deposits [108]. These deposits were interbedded with fine-grained sandstones with abundant ripples, presumably deposited during splay-crevassing of a meandering fluvial system. Clastic sediment from the Eonile reached the deepest regions of

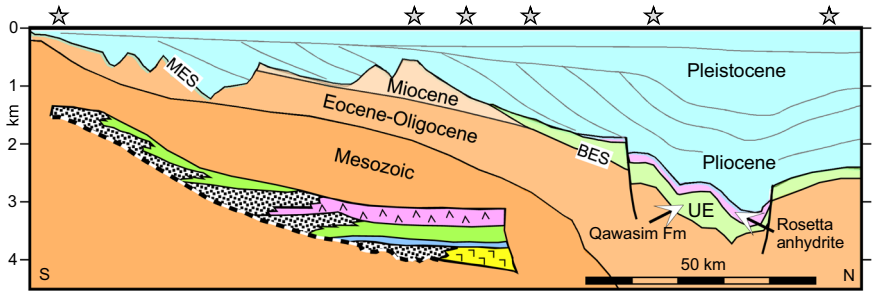

Fig. 43 Adaptation of a generalized south to north cross-section of the western Nile Delta, based on reflection profiles and wells [108]. Stars indicate locations of exploration wells. Insert [256] is a stratigraphic cross-section at the mouth of the EoNile channel displaying the sequence from 'lower evaporite' halite (yellow), to 'upper evaporite' limestone (blue), followed by lacustrine mudstone (green) and ending with the Rosetta Fm. anhydrite (violet). Stipple pattern is for sandstone. Dashed line is the erosion surface cut by the channel. Channel relief > 100 m

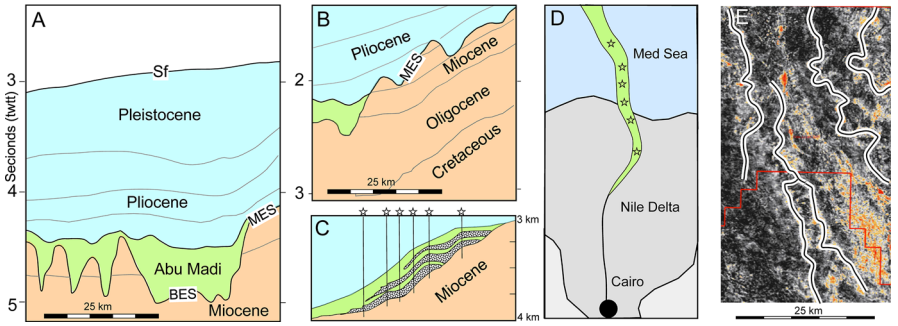

Fig. 44 **A** Tracing of reflection profile showing the 'upper evaporite' Abu Madi Fm. infilling valleys cut into the underlying Miocene by a Bottom Erosion Surface (BES) on the distal margin offshore Egypt [247]. **B** Higher on the margin where valleys have cut through the entire Miocene and into the Oligocene. **C** Sandstone (stippled) interbedded with mudstone of the Abu Madi Fm. within the confines of the Eonile Canyon. **D** Map view of the EoNile Valley with stars locating exploration wells in panel **C** [251, 252]. **E** RMS amplitude map illustrating the meandering channels network within an alluvial to delta plain at the apex of the Nile Messinian lowstand fan 10 km further downdip of the Abu Madi valley mouth [256]

the Herodotus basin where they are recognized in reflection profiles as channel-levee deposits interbedded in the halite layer [246].

The sandstones within the channel contained fragments of igneous rocks (andesite, andesitic tuff, rhyolite, and basalt), limestone and low-grade metamorphic rocks (mica schist and phyllite) that had traveled long distances from their source terrains in Egypt and Sudan. Beyond the mouth of the Eonile Canyon the sand and mudstone of the Abu Madi Fm passed seaward along meandering paths (Fig. 45E) onto a mudstone coastal flat at the edge of a brine lake precipitating anhydrite of the Rosetta Fm.

The overall incised-valley filling pattern of the Abu Madi Formation and the anhydrite accumulation are consistent with a relative sea level fall followed by a stillstand. At the end of the MSC, the incised valley and brine lake became flooded with marine water and the Eonile valley transformed into a > 1000 km long estuary.

8.2.9 Offshore Sirte Basin, Libya

Reflection profiles acquired by CGGVeritas in 2004–2005 have allowed the Messinian on the offshore margin of Libya deposits to be imaged in both cross-section and map view [260–262] (Fig. 45). The coverage has revealed a large tear-shaped apron in the subsurface of the continental margin fed by the EoSahabi River in Libya. The apron accumulated on a rugged erosion surface, labeled in Fig. 43 as the Intra-Messinian Erosion Surface. This apron is part of the 'upper evaporite' series belonging to the late brackish-water Lago-Mare stage of the MSC. Earlier 'lower evaporite' halite had been limited to the interior of the Ionian abyssal plain in the distal Sirte Basin.

The 'upper evaporites' exhibited seven successive layers, interpreted as indicators of periodic fluctuations in base level that had been synchronized to processional cycles. Individual layers had their own deeply incised valley fed by water sourced though the EoSahabi channel from the expansion of Neogene Lake Chad during northern

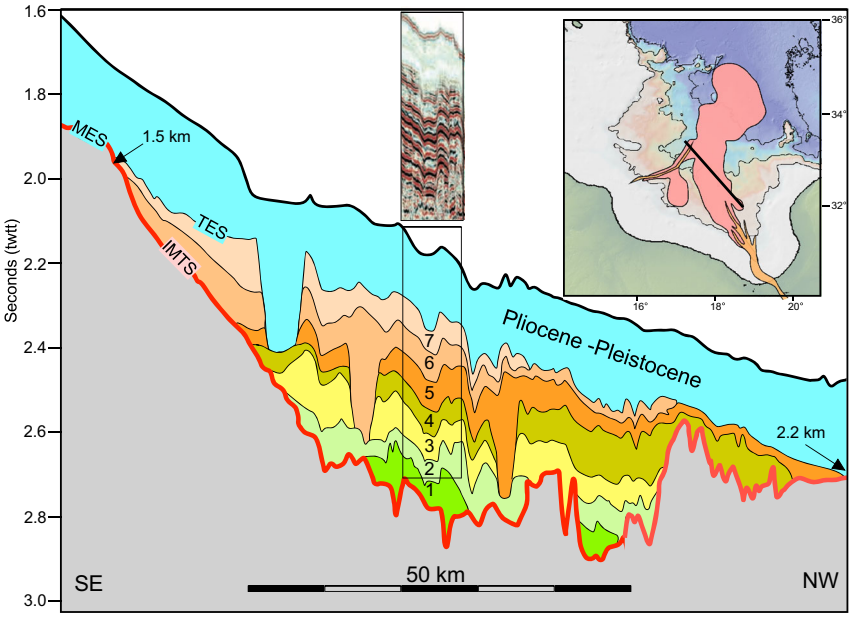

Fig. 45 Tracing of an interpreted reflection profile [260] crossing the large apron of sediment delivered onto the margin of Libya from the Sahabi River during the 'upper evaporite' interval of the MSC. Seven successive layers display episodes of down cutting to created deep valleys followed by refilling. Insert is an example of the original reflection profile. *MES* margin erosion surface, *TES* top erosion surface, *IMTS* Intra-Messinian Erosion Surface

hemisphere insolation maximum. The tear-shaped pattern of the apron indicated that the sediment in the apron had been derived from the river, and not from mass-wasting across the broader margin.

The individual valleys display extremely steep-walls of enormous relief. After being down-cut, each valley had then been refilled by sediment delivered during the next cycle. Each new layer reached higher on the edge of the margin than the previous layer, displaying a pattern of successive coastal onlap. The landward extent of the entire apron coincided with the present-day base of the continental slope at around 1400 mbsl, whereas the basin-ward extent had reached all the way to the southern edge of Sirte abyssal plain at 3600 mbsl.

The high-amplitude reflections (insert in Fig. 45) came from lithified material with high-compressional-wave-velocity and high-density. Well cuttings and logs confirmed these reflections derived from beds of gypsum and anhydrite some 10–20 m in thickness and deposited in a sabkha-like environment [262]. The lower amplitude reflections arrived from sand and clay deposited in a fluvial or lacustrine environment with beds up to 100–200 m in thickness. The extremely-rough IMTS had separated the 'upper evaporites' from the underlying 'lower evaporites' and their deeper substrate. The Margin Erosion Surface corresponds to karst found all across the margin by exploration wells and formed during latest Miocene subaerial exposure [262].

In the profiles, layers 1–4 displayed smaller valleys with a maximum width of 4 km and a maximum relief of 130 m. However, layers 5–7 exhibited the largest valleys with a maximum width of 7.5 km and a maximum relief > 350 m. The flow of water through the larger valleys had been capable of eroding thalwegs down to the base of earlier layers. Analysis of the present-day depth of the 'upper evaporites' indicates that during the terminal stage of MSC sea level had fallen in excess of 1.5 km [260, 261, 263]. During precession maxima and relatively dry periods Neogene Lake Chad would have receded and the flow of the EoSahabi river would have ceased, triggering the lowering of the eastern Mediterranean base level and promoting the precipitation of sulfates from evaporation of residual brine.

8.2.10 Southeast Spain

There are two widespread lowstand erosion surfaces in the marginal basins of southeast Spain [264] (Fig. 46).

End-Messinian unconformity (e-M unc) [263]: The first erosion surface to be recognized in southeast Spain was the previously-overlooked gap that separated the

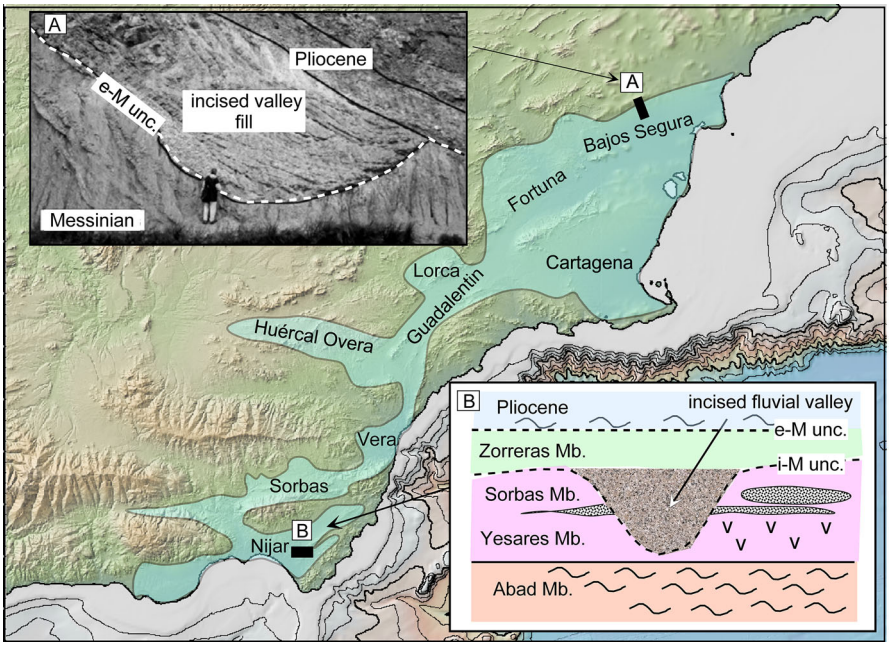

Fig. 46 The interconnected Neogene basins of SE Spain containing Messinian sediments. Insert **A**: The end-Messinian unconformity (e-M unc.) [273] is expressed on the northern margin of the Bajos Segura basin in SE Spain where it had incised fluvial valleys into the 'upper evaporites' lagoonal marls with Lago-Mare brackish-water ostracods and overlain by Pliocene marls. Insert **B**: The intra-Messinian unconformity (i-M unc.) in the Nijar basin was incised into the Sorbas and Yesares Members of the 'lower evaporites' and subsequently filled and covered by the continental Zorreras Member of the 'upper evaporites' [269]

Lago-Mare laminates with the brackish Cyprideis ostracods from the Pliocene open-marine, upper-bathyal foraminifera marls in the Cuevas del Almanzoro section in the Vera Basin [265]. This locality was visited during the third Messinian Seminar in 1977 to test the claim of a continuous Messinian–Pliocene transition [266]. In an outcrop cleared of alluvial soil, a gap appeared on an inclined surface with a veneer of gravel, pebbles and coarse sand overlying mudstone with root casts along the topmost laminae belonging to the *Loxoconcha djaffaroui* zone [265]. At another location visited during the seminar the erosion had cut all the way down into the pre-MSC Abad marls where it left a 4-m-thick boulder bed along the contact. Boulders consisted of reef limestone with Porites from the earlier Terminal Carbonate Complex and the pre-Neogene metamorphic bedrock. Boulders also included large slabs of the Yesares 'lower evaporite' gypsum up to 10 m in diameter [175, 176, 267].

In the adjacent Sorbas Basin to the south (Fig. 46) this erosion surface separated the Zorreras continental deposits with rodent fauna from overlying marine Pliocene marls (Fig. 46). This stratigraphic superposition was considered "*convincing evidence*" for a substantial Messinian lowstand [268]. In the adjoining Nijar Basin the "*almost instantaneous*" Pliocene open-marine flooding occurred above the continental deposits of the Feos Fm along a "*razor sharp contact*" during a "*relatively dry period with lower water levels*" [269].

Farther north in the Bajo Segura Basin on the eastern coast of Spain, the lagoonal marls with *Cyprideis* sp. had been incised by > 30 m-deep fluvial valleys during the latest Miocene terminal lowstand named for the first time the 'End-Messinian unconformity'. Like those in the Vera, Sorbas and Nijar basins, these valleys were also filled with sand and gravel derived from bedrock and with 1-m size boulders from pre-MSC sandstones. Once more, the fill was covered by either earliest-Pliocene pelagic marine marls or coastal sandstones depending upon location within the basin. At one outcrop in the northern sector of this basin, the end-Messinian unconformity rests directly on algal stromatolites interpreted as "*indicators of sudden emersion and subsequent subaerial exposure*" [270]. The End-Messinian unconformity in Spain corresponds to erosion surface #2 and its equivalent TES observed in the Mediterranean reflection profiles.

Intra-Messinian unconformity (i-M unc) [264]: Despite knowledge of the desiccation hypothesis derived from the five Mediterranean drilling campaigns completed in 1995, researchers had not yet found clear evidence for any major erosional hiatus indicative of a large lowstand event in the SE basins of Spain either preceding or during the MSC [178]. If there was any, it was supposedly represented either by local scours occurring at the top of the Sorbas Member [268] or beneath the 'lower evaporites' Yesares member [271]. The most plausible explanation was that the Sorbas Basin had been isolated from the Mediterranean and therefore left unaffected by external sea level changes [177, 272]. However, discoveries in the adjacent Nijar Basin changed this deduction, for there the equivalent to the Sorbas Member had been cut by fluvial valleys later filled by the Feos Fm continental deposits belonging to the MSC Stage 3 Lago-Mare interval [269] (Fig. 46, Insert).

In the afore mentioned Bajo Segura Basin the Intra-Messinian unconformity was occupied by wide and shallow palaeo-valleys on its northern margin [273] and subaerial exposure, such as karstic breccias and caliche-like carbonate crusts, in the south

sector [274]. The overlying sediments included alluvial mudstones, conglomerates, brackish-water lagoon marls with some containing *Cyprideis torosa* and *Ammonia tepida* and others rodent fossils, beach sandstones with stromatolites and up to 7 beds of selenitic gypsum. This composite was interpreted as the product of reflooding after an episode of subaerial emersion [264]. The Intra-Messinian unconformity in Spain most likely corresponds to the IMTS in the eastern Mediterranean and erosion surface #1 observed in the Mediterranean reflection profiles, though some researchers have placed it earlier and separating the 'lower evaporites' from the pre-evaporitic Messinian [275].

8.3 Summary of erosion surfaces

Messinian erosion surface are ubiquitous in the subsurface of all of the margins of the Mediterranean. Their descriptions and interpretations have been presented in two volumes of "Seismic Atlas of the Messinian MSC markers in the Mediterranean Sea—Volumes 1 & 2" with > 50 contributing authors and co-authors [276, 277].

8.3.1 Western Mediterranean surfaces

The common features of western Mediterranean are Margin Erosion Surfaces that display broad dendritic-style drainage systems that continue towards basin depocenters to elevations exceeding 3000 mbsl. There they encounter the onlap limit of the 'upper evaporites'. The onlap onto margins is considered the be the latest Messinian paleo-shoreline [278]. Here the MES splits into Bottom and Top Erosion Surfaces that bracket the 'upper evaporites'. Although the onlap denotes the highest water level during deposition, the top of the 'upper evaporites' shows truncations. The presence of Internal Erosion Surfaces (IES) indicates fluctuations above and below this water level [194].

Flexural-isostatic backstripping using an effective elastic thickness that is dependent upon the age of the bedrock restores the observed onlap elevation to approximately − 1100 ± 100 m at the time of maximum regression [278]. However, a somewhat deeper paleo-shoreline at − 1300 m is required to expose the Ebro margin [188]. A − 1100 m evaporative drawdown implies a ~ 500 m rebound from pre-MSC elevations due to the loss of the weight of water.

Isostatic subsidence, compaction and thermal subsidence since the Messinian have for the most part compensated the accumulation of the Pliocene–Pleistocene cover, implying that the bathymetry of the various basins at the onset of evaporative drawdown was comparable to the present.

8.3.2 Tyrrhenian Sea surfaces

In the Tyrrhenian Sea the Margin Erosion Surface offshore of the Sardinia coast reached to depths a short distance beyond 2000 mbsl (Fig. 47, Left) before being onlapped by the 'upper evaporites' [279]. The three drill sites (132, 652, 654) that recovered brackish-water Messinian sediments containing beds of gypsum and anhydrite came

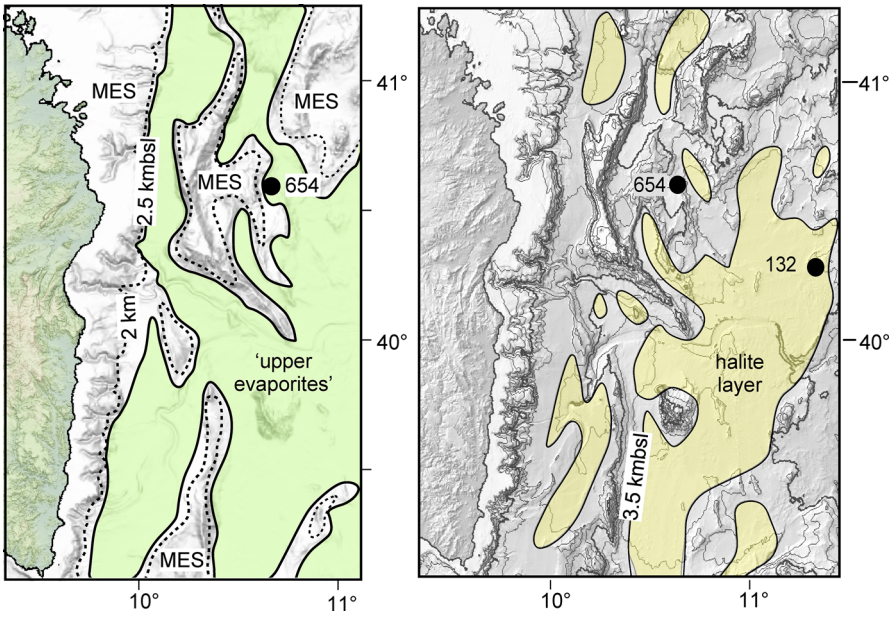

Fig. 47 Left: The regions occupied by the margin erosion surface (white) in the western Tyrrhenian Sea rimmed by the solid line and located close to, but below the 2000 m contour (dashed line). Depths for the 'upper evaporite' onlap are not derived from bathymetry, and come from the observed onlap in reflection profiles. Right: More confined regions are occupied by the halite layer [279, 280]

from elevations below this horizon, but in the case of Site 654 only 400 m deeper. The conglomerate at the base of the 'upper evaporites' at Site 362 lies at 3790 mbsl, or almost 1800 m deeper than the onlap horizon. Therefore, it would have taken an extreme lowstand for the pebbles and gravel to have been a fluvial or alluvial deposit.

The existing underlying halite layer in the Tyrrhenian Sea has been preserved in an even smaller region where it is now confined to the floors of enclosed depocenters (Fig. 47, Right). It is inconceivable that it only precipitated in these depressions, which were at different elevations and separated from each other by sills. It seems more reasonable that the distribution observed today includes the salt that had been dissolved from elsewhere and became reprecipitated in shrinking regions prior to the commencement of the 'upper evaporites'. Such a deduction leads to the question: did the dissolution take place under a fresher body of water, or was the confined salt the residue of extreme evaporative drawdown with all regions without salt having become subaerial? The elevation of the boarder of the salt lies some 100 to 300 m below the onlap of the 'upper evaporites'.

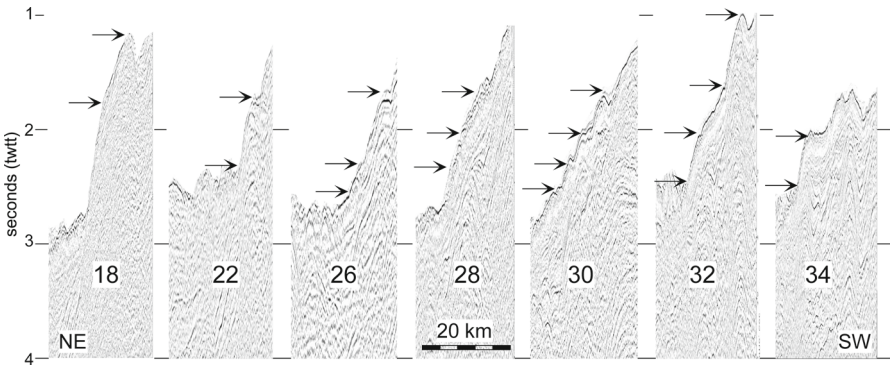

Fig. 48 Reflection profiles on the Levant margin of the eastern Mediterranean with the Pliocene–Pleistocene cover removed to expose the Margin Erosion Surface. Profiles are spaced 10 km apart from north to south along the margin. Arrows show breaks in the slope interpreted as stillstand terraces

8.3.3 Eastern Mediterranean surfaces

At the end of the MSC the Margin Erosion Surface on the Levant margin was left with a rugged relief. Here the surface had been notched by a series of well-defined breaks in its slope, suggestive of wave-cut terraces, presumably created at stillstands of fluctuating shorelines [220]. Many of these breaks align at the same elevation below present sea level (Fig. 48).

A series of enclosed depressions in the top of the salt layer (Fig. 49, Left) had formed a short distance beyond the base of the slope in the region where the upper layers within the salt had been previously truncated (Fig. 49, Left). These depressions, some deeper than 75 m, had been created either from abrasion during exposure of the salt [195, 221, 226, 234, 237, 281], from subaqueous dissolution by an overlying undersaturated body of [225, 227], from down-dip migration of the salt layer away from the margin [282–284] or from later dissolution of the salt beneath its Pliocene–Pleistocene cover.

A 3D reflection survey at the distal end of the Afiq Canyon revealed a fan-shape apron with a thickness > 150 m [285] (Fig. 49, Right). The apron consists of clastic and evaporitic beds. Its lithology and microfossil assemblage were sampled in cuttings and its physical properties obtained from the electric logs of 7 exploration wells [238, 285]. Although initially considered to be the Yafo Sand Fm of earliest-Pliocene age [285], the apron contained latest Messinian ostracods and belonged to the latest Messinian Afiq Fm (Fig. 41, Right).

The lobe had been deposited within the floors and just beyond the mouths of the Afiq and el-Arish canyons. There are no channels with bounding levees crossing the lobe or observed within the lobe interior, as would be the expected for a subaqueous fan [286]. The Or-South-1 well (previously discussed) was located in the middle of the apron. The recovered conglomerate had been interpreted as a fluvial deposit and the underlying anhydrite a sabkha facies emplaced in an environment of subaerial exposure at the conclusion of the MSC [238]. This interpretation is supported by an overwhelming number of allochthonous fossil specimens from Cretaceous to the

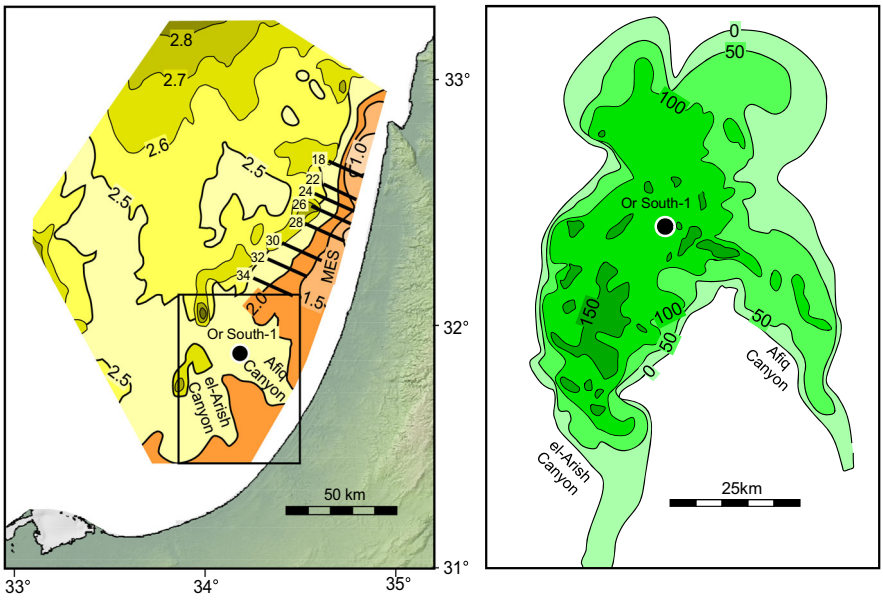

Fig. 49 Left: Contours in seconds (twtt) of the top of the salt layer (yellow colors) and Margin Erosion Surface (orange) on the Levant margin. Labeled lines are locations of reflection profiles in Fig. 48. Right: Fan-shaped apron of the Afiq Fm at the distal end of the Afiq and el-Arish canyons. Contours in meters of the lobe thickness [285]

mid-Miocene strata that were eroded from exposed canyon walls. The allochthonous specimens included > 80% of foraminifera in the sandstones and shale beds in the Afiq Fm [285]. The evidence from the Or South-1 well placed a late-Messinian shoreline in the vicinity of 2 km below present sea level.

Reflection profiles in the far-eastern Mediterranean show that the elevations of base and top of the halite layer is different from basin to basin [287]. The halite base ranges widely from − 2.5 to − 5.9 km with respect to the sea surface, whereas the halite top has a narrower range of − 2 to − 3 km (Table 1, Fig. 50).

The linear relation between the elevation of the salt base and its thickness implies that the halite thickness had been acquired in proportion to the depth of the depocenter in which the halite was collected. If the depth to the top of the halite for the two deepest regions (Anatalya and Herodotus basins) is shifted upwards to − 2.1 km, the trend of increasing thickness with increasing depth to the base of the salt becomes continuous (ghost dots in Fig. 50). The two deepest basins are on the down-bending slab of the African Plate that is currently subducting beneath the Eurasian Plate and have thus been influenced by tectonics since 5 Ma ago [235, 288] (Fig. 51).

The lack of preserved salt above − 2 km in the easternmost Mediterranean basins implies that any halite that had once been precipitated onto seafloors at higher elevations had been removed by the event that left behind the Intra-Messinian Truncation Surface. The cause of this event has been the subject of considerable interest. The competing models for the origin of the surface are (a) subaerial erosion linked with

Table 1 Elevations with respect to present sea level to the top and base of the halite layer and the halite thickness for seven separate basins in the eastern Mediterranean

Basin	Top	Bottom	Thickness	TES	UE
Adana	2116	2487	371	Yes	No
Cilicia	2116	2812	696	Yes	No
Iskenderun/Latakia	2116	2818	702	Yes	No
Florence Rise	2100	3000	900	Yes	Yes
Levant	2100	3700	1600	Yes	Yes
Anatalya	3100	5700	2600	No	Yes
Herodotus	3000	5900	2900	No	Yes

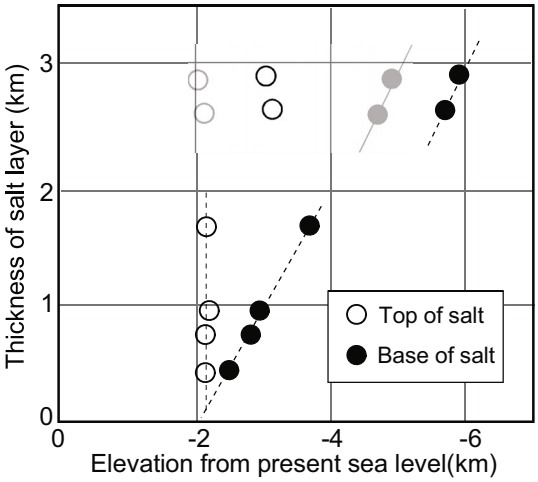

Fig. 50 Salt layer thickness versus the elevations of its top and base. Ghost elevations of the two deepest locations have been adjusted upwards to display an uninterrupted trend

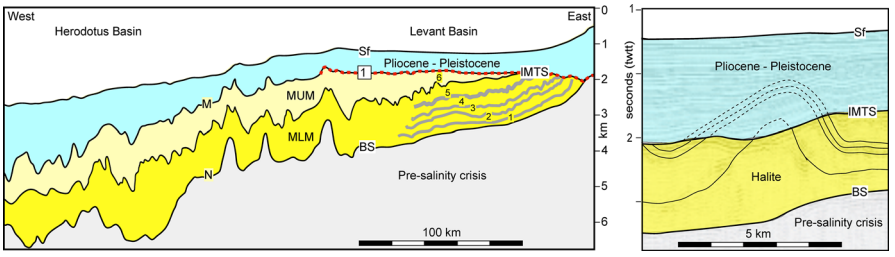

Fig. 51 Left: Tracing of a west to east cross-section through the Herodotus Basin and Levant Basin from (Kirkham, 2020) [227]showing truncation of internal halite layers on the Levant Margin and the western continuation of layer 6 to become the Messinian Upper Megasequence (MUM) above the Messinian Lower Megasequence (MLM) [291]. The IMTS is portrayed as a dashed red line corresponding to unconformity #1 in the Caltanessetta Basin in Sicily. Right: The truncated crest of a fold in the deformed halite layer from the Larnaca–Latalia Basin [281]

relative sea-level fall [112, 220, 226, 234, 281], (b) subaqueous dissolution beneath a stratified body of low-salinity water of substantial thickness [225, 227]. The evidence for dissolution comes from two observations.

First: removal of the crests of the deformed and folded halite layer (Fig. 52, Right) from a reflection profile in the Larnaca-Latakia region SE of Cyprus [281]. Prior to its loss by intra-Messinian truncation, the height of the crest of the folded halite layer above the truncation surface may have reached almost 700 m, unless the crest was dissolving as it protruded into the lower-salinity water.

Second: observation of internal layers within the halite layer that once continued up the Levant margin and were later truncated to become the IMTS. The NaCl removed from all regions of the eastern Mediterranean above the − 2 km elevation was unlikely to have escaped the Mediterranean. Instead, upon further evaporative concentration the Na^{++} and Cl^{--} would have begun to re-precipitate in deeper regions as a rain of hopper crystal originating at the thermocline between the new brine and warmer less-saturated water above, or by direct nucleation on the seabed [289, 290].

The interface between undersaturated brine (epilimnion) above saturated brine (hypolimnion) below is unlikely to have remained stationary in its elevation. As the brine below the interface became consumed into halite, its volume would necessarily

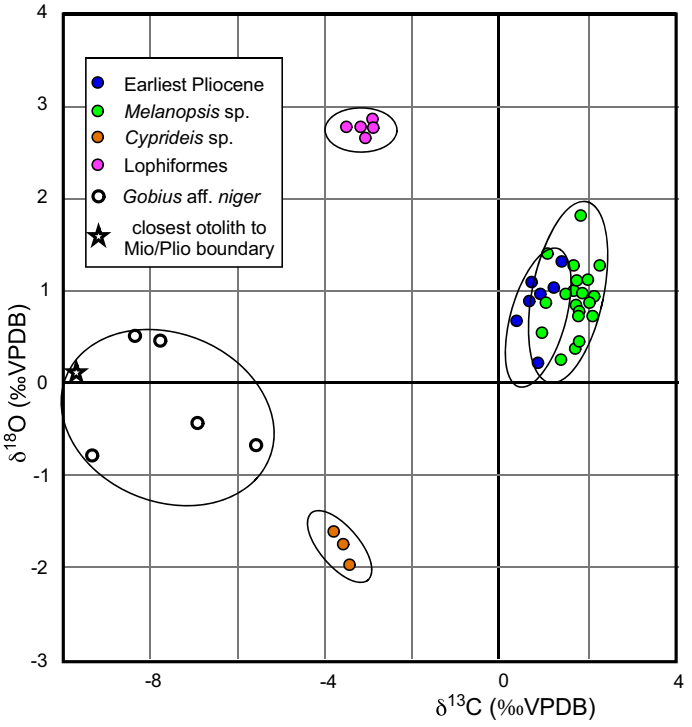

Fig. 52 Stable isotopes of mollusks and fish otoliths from the Podere Torricella gypsum quarry compared to isotopes of earliest-Pliocene marine foraminifera at DSDP Sites 132 and 134

have shrunk, the interface lowered, and the remaining halite on Levant margin exposed and then overlain by the Afiq Fm.

Since, there is little evidence of any further truncation of the halite folds below the − 2 km elevation, the low-salinity water in the epilimnion must have either evaporated, or persisted in lakes confined to the deepest regions of the eastern Mediterranean (the Ionian and Sirte basins and the Hellenic Trough).

Below the 2 kmbsl elevation, the Messinian Upper Megasequence (MUM) became covered by a highly reflective layer that can be attributed to the 'upper evaporite' interval of the MSC [291]. The lithified anhydrite beds in this layer have acted as an effective seal to prevent the halite below from further dissolution.

The tear-shaped apron on the Libya margin has the appearance of a giant alluvial fan with its apex at the mouth of the EoSahabi River. Alluvial fans form when flow exits a feeder channel and is able to spread out in diverging channels or sheet flows. In the proximal fan, where the slope is steepest, the flow is initially confined to a single channel of high relief.

The Libya apron has little in common with subaqueous deep-sea fans such as the Mississippi, Amazon, Rhône and Nile. The Libya margin valleys are far deeper and wider. They lack lateral levees and show no evidence of tight meanders and abandoned oxbows [286, 292–295].

9 Evidence of sea level drop from terrestrial outcrops and wells

9.1 Additional observations supporting desiccation hypothesis

After a period of controversial debate concerning the initial hypothesis of pre-existing the deep basins that had accumulated evaporitic deposits in shallow waters, a near-consensus emerged following the results from the 1975 drilling expedition) [296, 297]. A sequence of five yearly seminars (1975–1979) brought the marine geologists and geophysicists that had been on the drill ship together with terrestrial geologists and paleontologists. The objectives were to examine during fieldtrips the sediments of Messinian age in Sicily, the Apennines, Spain, Calabria, and Cyprus and discuss together each evening their observations and interpretations.

An early publication to emerge from field studies announced the discovery of stromatolites and cryptalgal laminae associated with Messinian gypsum in Cyprus [298]. Preserved algal filaments had been identified in gypsum from the northern Apennines [299, 300] and Sicily [301]. Filamentous (type *Lyngbia* and *Microcoleus*) and coccoid blue-green algae (type *Aphanocapsa*) had also been observed in the dolomitic mudstones of the evaporitic sediments from DSDP Sites 126, 134 and 372 ([65, 302, 303]. Wavy stromatolite bedding became exposed on the walls of gypsum quarries in the Piedmont of northern Italy [304]. Stromatolites with metric scale polygonal desiccation cracks in the Bajo Segura basin of SE Spain are observed directly beneath a subaerial exposure surface corresponding to the intra-Messinian unconformity. Exposure there was followed a sustained drop in Mediterranean sea level, a deep incision of the San Miguel paleovalley, and an abandoned terrestrial basin unable to accumulate Lago-Mare sediments [305].

In Cyprus the cryptalgal laminae and stromatolites appeared in the youngest two gypsum beds of the 'upper evaporites' along with the shallow-water mollusks *Limnocardium*, *Melanopsis*, *Melanoides*, *Congeria* and the ostracod species *Cyprideis*. The alteration between ostracods and mollusks pointed to a switching between brackish and more saline environments that could only have happened on shallow playa lakes fed by the dissolution of earlier sulfates and located below the exterior-ocean sea level [306]. Support for the hypothesis of complete desiccation of these lakes at the end of dry periods came from erosion along the top of each gypsum layer and four levels of paleosols with terrestrial snails interbedded with carbonates and conglomerates [217, 307].

The erosional event at the end of the Messinian also left its imprint in the Vera and Lorca Basins in Spain that became fully continental prior the end of the MSC [265, 308]. There laminated gypsum of the 'balatino' facies passed upwards to a gypsum flat-pebble conglomerate and then on to gypsum with a 'chicken-wire' facies displaying surficial desiccation cracks. Dissolution of deeply buried earlier halite towards the end of evaporite deposition resulted in faults cross-cutting the gypsum and the creation of collapse breccia. All of the accompanying microfossils had arrived from erosion of older Mesozoic to Miocene strata.

9.2 Separation of the MSC into two steps

The Mediterranean Science Commission (CIESM) held a workshop in 2007 with particular focus on the MSC: its deposits and its microbiology. Fifteen scientists from eight countries participated and contributed manuscripts published in the Consensus Report [309].

The method of astrochronology had already been successful in providing consensus ages for the onset of the first gypsum bed of the 'lower evaporites' and the conclusion of the 'upper evaporites' at the Miocene/Pliocene boundary [157, 172, 310]. However, the usage of astronomical tuning to link the closure of the Atlantic gateway to a lowering of the global sea level during the peak glacial stages TG12-14 [311], had led to gap of several precession cycles not accounted for by combination of the 16 to 17 cycles in the 'lower evaporites' and 8 cycles in the 'upper evaporites'. The missing precession cycles left an hiatus of approximately 80 kyr for the evaporitic drawdown, the accumulation of halite that accompanied the drawdown, the isostatic rebound for the loss of the evaporated water, the uplifting of margins in response to the removal of weight of any halite that had accumulated above − 2 km elevation, and the additional loading of the reprecipitated halite in deeper regions [278, 312, 313].

The consensus report envisioned a two-step scenario, in which during Step 1 (5.96–5.6 Ma) the gypsum selenite beds in the Vena del Gesso Basin of the Apennines and Gessi di Cattolica Fm. in Sicily were deposited in shallow regions on Mediterranean margins separated by sills from the exterior deeper Mediterranean lacking preserved sulfates due to its anoxic condition [314, 315]. These selenite beds were labeled the Primary Lower Gypsum (PLG). The PLG was correlated with the western

Mediterranean 'lower evaporites' (LE) that were presumed to exist beneath the acoustically transparent halite based on a set of strong and laterally continuous reflections [191, 194, 316].

Step 2 was divided into two intervals. Step 2.1 (5.6–5.5 Ma) encompassed a brief interval of halite precipitation, followed by evaporitic drawdown, and the shedding of exposed PLG from the margins to become Resedimented Lower Gypsum (RLG). In Step 2.2 (5.53–5.33) the interior of the Mediterranean transformed into a brackish body of water (Lago-Mare) with its'upper evaporites' (UE). Steps 2.1 and 2.2 were separated by a subaerial hiatus corresponding to the erosion surfaces on margins. The placement of halite after the PLG was widely adopted in the Consensus Report despite the envisioned lateral transitions between these deposits that had been proposed by others [317–319].

9.3 The Step 1 early evaporitic facies

As presented in the publications by the attendees at the Consensus Workshop the earliest PLG beds of massive vertical selenite crystals passed upwards into thinner beds of banded selenite before being followed by nodular and lenticular selenite that grew in branches projecting outward from a nucleation zone. All of the PLG beds had been separated by thin euxinic shale layers when undersaturated water during humid periods stopped gypsum precipitation. No evidence of subaerial exposure or evaporite re-sedimentation had been found inside the evaporitic succession. The couplet (gypsum/shale) was explained by evaporite precipitation during falling sea level, producing higher salinity and gypsum growth, followed by dilution during a sea level rise for each shale bed [320, 321]. The driver for the sea level oscillations was inferred to be global eustacy. However, in the late Miocene glacial cycles were pulsed at the obliquity frequency and not the precession frequency of the gypsum beds [322]. The large overall 100 to 200 m thickness of the PLG required substantial pre-existing accommodation space, thus ruling out a very shallow setting for selenite deposition [323].

9.4 The step 2.1 halite facies

The Step 2.1 halite in subsurface of the Caltanissetta basin reached a thickness of 600 m and was divided into four units. The halite unit B contained beds of kainite and carnallite that showed no evidence of dissolution and/or truncation surfaces except on the top of Unit B [324, 325]. However, the upper halite units C and D were peppered by dissolution pipes and displayed halite crystal truncations along bedding surfaces, indicating precipitation in a relatively shallow-water body that had been periodically diluted with fresher water.

The interval layer separating units B and C had also been pierced by closely-spaced dissolution pipes, each filled by clear halite cement and mud. The piped salt layer was upturned to form tepee structures and then cut by vertical fissures interpreted as giant contraction polygons that had dried out on salt flats [239, 326]. According to those presenting at the workshop, the Caltanissetta Basin had been relatively deep at

the location of the Realmonte mine prior to undergoing complete desiccation. After subaerial exposure and re-submergence under a new brine originating from halite that had dissolved from the exposed margins, the halite in units C and D developed in a shallow-water environment.

9.5 The Step 2.2 'upper evaporite' facies

The Step 2.2 'upper evaporites'(UE) also presented a cyclic pattern with thin laminated gypsum cumulates and gypsarenites interbedded with fluvio-deltaic sandstone and shale. The UE beds of selenite did not exceed a few meters in thickness. The rhythmic alternation between the gypsum and sandstone with shale was interpreted as the response to precession-driven arid-wet climate cycles affecting both base level and salinity [327]. During wet climate phases (at insolation maxima) marl and sandstone were deposited in a brackish environment as suggested by the typical Lago-Mare faunal assemblage and negative $\delta^{18}O$ values. During arid phases (at insolation minima) the reduced meteoric supply, registered by higher $\delta^{18}O$ values in the carbonates, led to a negative hydrological interval terminating in evaporite precipitation. The terminal Arenazzolo Fm. with its tabular cross-bedding, climbing ripples, and lenticular bodies of sandstone is genetically different from the thin sandstones and mudstones intercalated with the gypsum beds. Its lithic sand came long distances from terrestrial sources rather than from locally exposed gypsum, and its fossil content consisted of species of Mesozoic, Paleogene and Neogene age that had become extinct long before the MSC. There was little doubt at the workshop that the UE had evolved in a closed Mediterranean isolated from the exterior ocean.

Step 2.2 was itself divided into two sub-units, p-ev1 (5.5–5.42 Ma) and p-ev2 (5.42–5.33 Ma), based on the development of the fauna and flora in the brackish-water environment [328]. Sub-unit p-ev1 contained Lago-Mare species with low-diverse and pioneer taxa belonging to the *Loxoconcha* biozone, whereas p-v2 included fossil assemblages of increasing diversity and complexity which make up the *Loxocorniculina* biozone [329, 330]. The typical Lago-Mare mollusks (*Melanopsis*, *Melanodies*, *Limnocardium*, *Congeria*, and *Dreissena*) became more abundant and diversified in the p-ev2 unit. The calcareous nannofossil assemblages were consistently dominated by specimens reworked from older strata. There existed no convincing evidence from either microfossils or mollusks for any sporadic marine incursion in either of the sub-units [328, 331].

Those attending the Consensus workshop expressed in their published chapters different opinions as to the magnitude of the evaporitic drawdown in the Mediterranean during Step 2.1 and the configuration of the Mare-Lago water body during Step 2.2. Some favored a partial evaporitic drawdown during Step 2.1 [315] and a scenario during Step 2.2 similar to the present-day Caspian Sea with salinity values of 1–14‰ and with adjacent evaporitic conditions as in the Kara–Bogaz Gol, all related to a combination of climate gradient, morphology and areal distribution of the freshwater fluvial input. Others favored a more extreme lowstand in Step 2.1 and persistence of shallow-water conditions during Step 2.2 based on the erosion expressed by the Bottom, Intermediate, and Top Erosion Surfaces visible in reflection profiles from the

Valencia Trough [194] and on the recovery by exploration wells of fluvial sands with seams of coal and paleosols in the deep subsurface of the Nile Delta [255].

9.6 Replacement of the two-step scenario with three Stages

To more clearly distinguish the interval of presumed hypersaline halite precipitation (Step 2.1) from the subsequent hyposaline brackish-water interval (Step 2.2), a new 3-Stage scenario was proposed that is now widely adopted [332]. Step 1 with its 16 to 17 gypsum beds of selenite belonging to the Gessoso Solfifera Fm. became Stage 1 (5.97–5.55 Ma). Step 2.1 with the halite in the Caltanissetta Basin was assigned to its own Stage 2 (5.55–5.53 Ma). Step 2.2 with the 'upper evaporites' was converted to Step 3, itself separated into an earlier Stage 3.1 (5.53–5.42 Ma) with its first 6 gypsum beds in Sicily that was considered more evaporitic and a later Stage 3.2 (5.42–5.33 Ma) with its sandstone beds and terminal Arenazzolo bed indicating an upward increase of fluvial discharge accompanied by the Lago-Mare biofacies along with the presence of paleosols, terrestrial conglomerates and karst.

9.7 A facies cycle for the Upper Gypsum in Stage 3

The Stage 3 'upper evaporites' have seven rhythmically interbedded primary gypsum bodies in Sicily separated by marls, shale and diatomite [327]. The architype depositional cycle begins with sandstone thought to come from prograding deltas as water levels started to drop. The sandstones transitioned into gypsarenite and gypsrudite once former areas of previous gypsum accumulation on the basin margins had become exposed to erosion. The lowstand was announced by a shallow-water gypsum cumulate (the balatino facies). Untruncated crystals were indicative of a permanent cover of saturated brine, whereas flat-pebble conglomerates were diagnostic of polygonal-cracked, alga-bounded laminated sediment that had been ripped up from laminated gypsum by storm waves or surf [113]. Mud-cracked laminae are associated with these conglomerates.

The onset of bottom-growth selenite took place during the deepening of the basin and was accompanied by the creation of substantial new accommodation space to allow for the decimeter-thick beds with increasing crystal size. Domed selenite appeared in the upper portion of the cycle when the growth of crystals was reduced to sparse nucleation points. Similar domes are common in modern marine salina [333]. Maximum flooding at the cycle highstand occurred after the return to undersaturated water conditions and deposition of marl and mudstone recolonized by ostracods, benthic foraminifera in the deeper regions and mollusks in closer proximity to shorelines.

9.8 How dry was the Mediterranean during Stage 3

The dryness of latest Messinian climate was accessed using the hydrogen isotopic composition of the long-chain n-alkanes (δDn-alkanes) derived from higher-plant waxes preserved in the Stage 3 'upper evaporites' from the Caltanissetta Basin in Sicily

[334, 335]. The δD ratios of n-alkanes reflect the δD composition of precipitation. Accordingly, the δDn-alkanes have been successfully used for reconstruction of terrestrial paleo-precipitation. Stage 3 samples came from six beds at the Eraclea Minoa location spanning in age from 5.48 to 5.34 Ma.

The long-chain (C29–C31) n-alkanes had the highest abundances, and displayed a range between − 124‰ and − 150‰, with no differences between samples from evaporites and marls. Values from present-day lakes in Sicily are 40‰ to 60‰ more depleted than those from Stage 3. Three different mechanisms can account for the greater enrichment in the Stage 3 samples: (1) change the water vapor source; (2) distance from the vapor source; (3) increased continental temperatures. All three would have influenced the composition of the higher-plant vegetation [334–338].

In comparison, long-chain alkenones are produced by haptophyte algae living in surface water.

The results from Eraclea Minoa indicated that the hydrogen isotopic composition of the C37 and C38 alkenones had a much higher range than those from the warmest Mediterranean Pleistocene/Holocene interglacial sediments. The very high values (− 125‰ to − 146‰) at Eraclea Minoa confirmed extreme drought. The highest value at − 125‰ in Stage 3 was even more enriched that those from either the kainite beds in Unit B of the Realmonte Salt mine (− 166‰) or from the level of the salt polygons (− 143‰), indicative of desiccation during subaerial exposure [326].

Consequently, climate during Stage 3 had become sufficiently arid during insolation minima to have been able to convert various Lago-Mare lakes into shallow salt pans, especially water bodies at lower latitudes and at elevations such as those in the far-eastern Mediterranean.

9.9 How saline was the Mediterranean surface water at the onset of gypsum precipitation during Stage 1?

Archaea are ubiquitous microbes in the environment. They not only survive but thrive over a broad salinity range from fresh to hypersaline, well beyond that of haptophyte algae and other calcareous or siliceous. The relative amounts of acyclic diether and tetraether membrane lipids synthesized by Archaea correlate with salinity from 0 to 250 practical salinity units (psu) in modern settings. Using this proxy, there is the potential to provide insights into salinity variations within desiccating basins such as the Mediterranean and change the salinity accompanying evaporite precipitation.

Messinian sediments of the Tripoli Formation were collected from two locations in the Caltanissetta Basin in Sicily, affording a continuous record spanning the transition from marine to the hypersaline conditions that signaled the onset of the 'lower evaporites' [339]. The linear salinity correlation deduced from relationship between archaeol, caldarchaeol and salinity (ACE index) and its application to measurements on modern samples to calculate salinity showed relatively low salinities in the range of 20 to 40 psu in the marls and diatomite until just prior to first bed of laminar gypsum, when the lipid-based salinity estimate rose abruptly to ~ 140 psu at one location in the basin and ~ 160 psu at the other, more than four times the earlier salinity and well and within the salinity at which gypsum precipitates (110 psu).

9.10 The Formazione Peliti Eusiniche

As previously mentioned, Raimando Selli included his Formazione Peliti Eusiniche in his 'crisis of salinity'. In the central Sicilian Basin, the microfossils in these deposits, called the Tripoli Formation, evolved from well-oxygenated and ventilated bottom-water conditions to a significant decrease in oxygen concentration and reduced biotic diversity beginning around 7.0 Ma [340]. Deep-dwelling planktonic foraminifers became excluded at 6.7 Ma and were replaced by stress tolerant species. The deterioration of the environment became more extreme at 6.12 Ma, with the development of highly saline, dysoxic bottom-water conditions accompanied by a high preservation of organic matter. A sudden increase of $\delta^{18}O$ in the calcite and dolomite at 6.03 Ma was followed by total anoxia of the seabed, triggering the disappearance of benthic foraminifers and mollusks just below the 1st laminated carbonate at the base of the Primary Lower Gypsum [341]. Although evaporative conditions were reached rapidly, they apparently did not involve changes in prevailing warm and humid climate.

Although pseudomorphs of halite are observed during the trend towards hypersalinity, the increase in salinity did not reach concentrations high enough to precipitate substantial volumes of evaporites prior to 5.97 Ma [342–346]. Still, the $\delta^{18}O$ values of + 4.0 to + 8.5 ‰ in dolomite connote highly evaporated waters [346].

In the previously discussed Falconara section, the Tripoli Fm reaches a thickness of 25 m with 45 cycles of diatomite and marls occurring in synchroneity with the astronomical precession frequency. The dominance of precession in controlling the cyclicity rules out eustatic sea level as the driving mechanism, since glacial cyclicity was obliquity-controlled during the Messinian [347].

The bituminous Tripoli Formation was sampled in the Tyrrhenian Sea at Sites 654 and 652 where it corresponds to refection Unit 3 in Fig. 23. Unlike the halite Unit 2 that onlaps the pre-existing relief at Sit. 654, Unit 3 drapes the relief with a conformable contact on its underlying strata. In the Legnagnone section of the Northern Apennines the bituminous shale was deposited in a coastal shallow environment with no evidence of a sea level drop in the passage from the Tripoli Fm to the Gessoso Solfifera PLG [341]. Therefore, the hypothesis of an early and major drawdown of the Mediterranean seawater before the precipitation of central basins halite layer [196, 348], can be definitely excluded. The sediment beneath the halite layer with a thickness exceeding 1.5 km is the lateral equivalent to the middle to early Miocene marlstones and mudstones recovered at DSDP Site 372 located beyond the foot of the Balearic Platform east of Menorca [349] (Fig. 3).

10 Beginning of a serious pushback against substantial Messinian desiccation

10.1 Evidence from the Levant Margin

A team of five researchers gathered at the Geological Survey of Israel in Jerusalem in 2011 to re-examine cores that had been obtained when drilling through the Afiq and Maviq'im Formations in the subsurface of Israel. Their effort led to the interpretation that the gypsum and anhydrite beds belonged exclusively a clastic sulfate facies [240]. Based on visual appearance and thin-sections, they described the sulfates as gypsrudite and gypsarenite, with some beds laminar and others cross-bedded. The clastic facies was attributed to deposition from subaqueous gravity flows sourced from dismantled Primary Lower Gypsum selenite originally located up dip in the Afiq Canyon. In each of the six wells investigated the gypsum had been deposited directly on Paleogene–Neogene marls and thus on an unconformable surface. The strontium isotopic measurements on the gypsum at elevations > 880 mbsl provided values consistent with those of the Mediterranean 'upper evaporites'.

Therefore, these beds came from the Afiq Fm, not the underlying Mavqui'im Fm, as implied in their publication. Furthermore, the gypsum beds were directly overlain by fully-marine Yafo Fm. of earliest-Pliocene age. The sparce number of gypsum beds in each well (< 4), their overall thinness (< 100 m), and their stratigraphic position sandwiched between pre- and post-MSC strata required only a brief interval of accumulation and not the entire 'upper evaporite' interval. Transitory accumulation is more consistent with fluvial transport or flash-flooding rather than submergence under a water body that had "*persisted even during the acme of the salinity crisis*" [240]. Consequently, the deduction that ancient canyons around the Mediterranean Basin "*may not be necessarily related to a base-level drop*" is as yet unsubstantiated [240].

An earlier publication encompassed a larger set of exploration wells tied to reflection profiles. Their five authors presented more persuasive evidence that "*the final Messinian sea-level drop below the canyon's floor resulted in a subaerial environment in the canyon, the erosion of the upper evaporites, and the subsequent deposition of fluvial and brackish sediments (Afiq Formation)*" [242].

10.2 Re-interpretation of the sulfate facies in the Mediterranean drill cores

Four of the five researchers that had gathered in Jerusalem met again 2 years later at MARUM core repository of the Universität Bremen in Germany to re-examine the evaporite sediments in the Mediterranean drill cores from all five DSDP and ODP expeditions [241]. They once again concluded that the 'upper evaporite' units in both western and eastern deep Mediterranean basins consist mainly of clastics (gypsrudite, gypsarenite). No unequivocal evidence of shallow water or even supratidal (sabkha) deposition was in evidence, suggesting that at the very last phase of the MSC the Mediterranean Sea had not experience any desiccation, but that "*deposition took place under permanent subaqueous conditions*."

In the process of reaching this assessment the authors failed to mention: (1) the bromine measurements on the Site 134 and 376 halite [60, 119]; (2) the photo-synthetic benthic diatoms [39] and coccoid blue-green algae [302, 303] in the dolomitic mud-stones; and (3) the soil horizon at Site 132. In addition, they presented: (1) an incorrect upside-down illustration of the core section with the expansion halite crack (Fig. 12) to dismiss the crack as a desiccation feature; (2) asserted that all anhydrite had formed from gypsum dehydration; and (3) interpreted the elongated and flattened nodular anhydrite as gypsrudite rather than a feature of in situ displacement growth in a sand/silt matrix.

The authors were correct in their critique of the supratidal sabkha facies. The internal reflections in the 'upper evaporites' (Unit #1 in Figs. 5, 10, 11 and 23) are continuous over relatively large distances (> 10 km) and show no geometry of coastal onlap. Consequently, the Ca^{++} and SO_4^{--} that nucleated into anhydrite nodules did not arrive from a nearby offshore region with saltier water and then transit through permeable layers to locations where the brine was drawn upwards through the capillary zone to fill porous layers with nodules in the supratidal environment, as is the case of the modern Persian Gulf. Instead, the Ca^{++} and SO_4^{--} had been delivered by downward reflux into subaqueous sediments from a denser overlying brine as its solute concentrated to saturation under extreme evaporation. The laterally continuous reflections in the profiles are echoes from a succession of individual lithified anhydrite beds (or gypsum) such as those in the drill cores, with their number and order synchronized to the precession frequency. The enlargement of the nodules would still have been by displacement growth within the matrix layer, no matter how thin or thick, with no need for the sulfate to have arrived as sand or clasts in the context of detrital components.

10.3 An alternate scenario for origin of Messinian canyons

In the effort to explain evaporite deposition in a non-desiccated basin rimed by its deeply incised Messinian canyons, a novel mechanism has been proposed, namely energetic erosion of the substate by dense hypersaline brine transiting from the shelf edge into the abyss [350]. Although modern deep-water environments show significant submarine erosion and sediment transport within canyons, the principal processes for erosion are turbidity currents, hyperpycnal flows from river floods, mass wasting, and to a minor degree by shelf water cooled in the winter so as to sink and supply new intermediate and bottom water to ventilate the basin interior.

The published study focused on the latter phenomena called Dense Shelf Water Cascading (DSWC) [351, 352]. Dense water is produced in shallow areas of the continental shelf. Large-scale water cascades from the Antarctic shelves to become Antarctic Bottom Water, the most widespread water mass in the global ocean. Dense water also flows off the Arctic Ocean shelves where it ultimately contributes to the Atlantic Meridional Overturning Circulation (AMOC). Using instrumented moorings, dense shelf water cascading events have been observed passing through the Cap de Creus Canyon in the western Mediterranean with enough energy to create furrows in unconsolidated sediment on the canyon floor [351]. The currents, with velocities up to 1 m/s, support mud and silt in suspension and transport sand as bedload. Furrows

are a common feature on large drift deposits [353, 354]. Although the episodic flows are capable to flush sediment from canyons [355], they lack the energy to excavate bedrock.

To use this process to have deeply incised the Mediterranean canyons such as the forementioned Durance, Rhône and Eonile valleys is considered an overreach. These Messenia valleys are entrenched into Mesozoic limestone, and in the case of the Eonile, had cut through basalt, leaving behind mesas [95]. Furthermore, the incision of valleys now occupied by the south Alpine lakes, the valleys buried beneath the Lombardian Plain and those in northern Adriatic basin are in regions where there is no evidence that salt deposits ever existed during either during Step 1 or Step 2 of the MSC.

10.4 Evidence from fish fossils that the Mediterranean was filled with saltwater during Stage 3.2

Fossil fish assemblages from the 'Stage 3.2 'Lago-Mare' deposits at seven localities in central Italy consisted of marine euryhaline species [356, 357]. These fish assemblages were dominated by taxa of a strict marine affinity [358]. Their presence in the 'upper evaporite' marls was considered "*unambiguous evidence*" that a re-establishment of normal marine conditions in the Mediterranean had occurred before the end of Stage 3.2. Normal marine conditions implied an open connection from the Atlantic and therefore a completely filled the Mediterranean.

In the Podere Torricella gypsum quarry several fossiliferous layers contained abundant mollusks (*Melanopsis*) and ostracods (*Cyprideis*) typically found in Lago-Mare deposits, but also exquisitely preserved otoliths (fish ear bones). Based on sampling location's stratigraphic position and paleontological considerations, the age of the fossiliferous fish was constrained between 5.40 and 5.33 Ma [357]. More than 40 taxa belonging to 15 teleostean family-level groups were identified. Some of these taxa, particularly the *Gobiidae* and *Lophiiformes*, as well as lanternfishes, were documented in multiple localities, although majority of the fish taxa were exclusive to a single locality.

Specimens of mollusks (*Melanopsis* sp.) and otoliths (*Gobius aff. Niger*) and an indetermined *lophiiform* taxon were analyzed for their stable isotope composition and Sr isotope ratios, using samples from the Cava Serredi quarry and spanning a 100 m thick exposure. Fish skeletons were present at two levels, one near the base and the other 10 m below the Pliocene/Miocene boundary. The taxa belonging to the ecological guild of marine seasonal migrants are dominant, with 43% of recognized taxa, followed by estuarine residents that accounted for about 38%. Marine visitors were rare yet present in more than one sample.

The isotopic measurements tell a different story (Fig. 52). Those from the otoliths (*Lopiformes* and *Gobius aff. niger*) have substantially more negative $\delta^{13}C$ than the earliest-Pliocene pelagic foraminifera from DSDP Sites 132 and 134 at a time when the Mediterranean was clearly connected to the Atlantic. Furthermore, the stable isotopic compositions of *Lopiformes* and *Gobius aff. niger* are distinctly different from each other. The sample of *Gobius aff. niger* in the stratigraphic position closest to the

Miocene/Pliocene boundary (star in Fig. 52) has a composition farthest from the that of the earliest-Pliocene foraminifera.

The strontium isotopes provide further confirmation that these fish were not living in or migrating from waters of normal ocean salinity. The $^{87}Sr/^{86}Sr$ on the *lophiiform* otoliths (0.708559) and the *Gobius aff. niger* otoliths (0.708798) is far-removed from the global ocean value (0.709069) measured on the marine Pliocene foraminifera [359]. The $^{87}Sr/^{86}Sr$ measurements on the otoliths are in the very same range bracket as those from the brackish-water ostracod *Cyprideis* (0.7086 to 0.7088).

10.5 Surface-water temperatures in Stage 3 substantially lower than in modern high temperature environments

Abundant fossil organic lipids from Archaea were extracted from anhydrite, halite, and gypsum belonging to the 'upper evaporites' at DSDP Sites 124, 134 and 374 [360]. As mentioned previously, Archaea are ubiquitous microbes in the environment and thrive across temperature, pH, redox and salinity gradients. Distinct differences in the salinity tolerance of Archaea, from fresh water to hypersalinity, produce shifts in the relative dominance of archaeal groups and thus their lipid distributions. Relative abundances of archaeal lipids form the basis for estimating sea-surface temperature [361].

The TEX86 index is defined by the relative abundances of a set of tetraether compounds that are sensitive to water temperature [362, 363]. Archaea that synthesize these compounds live throughout the water column, but thrive at the base of the photic zone. The calibrated TEX86 measurements on the anhydrite, halite, and gypsum showed little variation between 25 and 28 °C [360]. These temperatures were much lower than temperatures such as the modern Dead Sea. The dry atmosphere adiabatic is 9 °C/km and the moist value is around 5 °C/km. Thus, the atmosphere in of a severely desiccated Mediterranean basin would be expected to have been 5 °C to 10 °C warmer than these measurements.

10.6 Surface-water salinities in Stage 3 substantially fresher than in modern high salinity environments

The previously mentioned ACE index was also applied to deduce the paleo-salinity of surface water at the time of the precipitation of the Stage 3 anhydrite, halite, and gypsum at these three drill sites [360]. When converted to marine salinities these ACE values did not exceed 34 psu. These values were far below the saturation levels of ~ 110 psu for gypsum and ~ 250 psu for halite.

As a result, the low salinities were used as an argument for a deep-water evaporitic basin that had been continuously supplied by seawater from the external ocean. Accordingly, the basin must have had a significant volume below wave base and large vertical gradients in density when water levels became balanced by the combined influx of seawater and fresh water from rivers and rain.

However, the gypsum/anhydrite facies, bromine measurements, occasional paleosols, etc., that were present in the 'upper evaporites' are not compatible with a thick

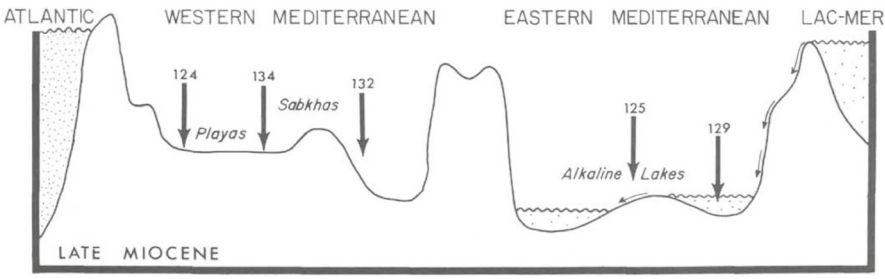

Fig. 53 Contribution of waters from the Paratethys Lac-Mer to the eastern Mediterranean alkaline lakes during the terminal stage of the MSC [146]

body of brine. To explain the discrepancy, it is essential to point out that: (1) the anhydrite, halite, and gypsum contained "*abundant remains of lipids derived from cell membranes of microorganisms of the domain Archaea*" [360] and roughly the same amount in each sample, regardless of its composition; (2) the samples were investigated > 40 years after they were retrieved and stored in core repositories; (3) the cores were initially enclosed shipboard in capped tubes containing sponges wet with Mediterranean seawater; (4) the ACE values indicated normal marine surface water; and (5) Mediterranean surface water with living Archaea was continuously pumped down the drilling pipe and out through the drill bit as the anhydrite, halite, and gypsum was being cut by the drill bit's teeth.

Issues such as these raise the specter of contamination by larger quantiles of modern lipids coming in contact with much lower amounts of Messinian lipids and thereby overwhelming the ACE measurements. Sampling for organic analyses on more recent drilling expedition is accomplished by cutting a section of the core still in its tube, sealing the sample immediately, and then storing the tube in an unlit and frozen condition, and in some cases treated to inhibit new growth. None of these precautions were practiced in 1970 and 1975.

11 Paratethys origin for the Mediterranean's Lago-Mare species

The suggestion that the Paratethys (Lac-Mer) may have contributed to the fresh-to-brackish water prevalent during of Stage 3 of the MSC had already been considered by the participants of the first DSDP expedition in 1970 [146] (Fig. 53). The ostracod, *Cyprideis pannonica*, was well known to have been endemic to not only Pannonian Basin in central Europe but also to the broader Dacian, Euxinic and Caspian-Aral region [10, 50, 52, 55, 364].

11.1 Paratethys endemic fauna

Lake Pannon is thought to have been the cradle for the Ponto-Caspian fauna living in an expansive Paratethys epicontinental seaway between the eastern Alps and modern Kazakhstan [365–367]. Shortly before to the onset of the MSC the species that had evolved in separate lakes became reconnected in a widespread Dacian, Euxinic and

Caspian seaway and gave it a common and distinct faunal assemblage that, when found outside of the Paratethys, implied a Paratethys parenthood [368].

All but a few researchers have proposed that the major supply of brackish water to the Mediterranean came from the Paratethys, either by overspill or through aquifers. However, only the Euxinic basin (paleo Black Sea) had any sizable volume: estimated to have been < 15% of the Mediterranean's capacity [369, 370]. Thus, appreciable delivery of water from the Paratethys would have occurred during episodes of extreme wet climate (insolation maxima). It is more likely that at those times, Mediterranean rivers (Rhone, Po, EoSahabi and Eonile) also played a role, and that their less radiogenic $^{87}Sr/^{86}Sr$ composition would also have contributed to the isotopic signatures of the Mediterranean Lago-Mare ostracods.

Nevertheless, the finding of the Pannonian species (*Cyprideis* and *Loxoconcha djaffarovi*) throughout the entire Mediterranean region and even at locations as distant as the Vera, Nijar and Sorbas basins in SE Spain, led to hypotheses that "*the Mediterranean in the latest Messinian was full of water*" [371]. The $^{87}Sr/^{86}Sr$ ratios from the Spanish and Piedmont marginal basins required an additional external water source with a low Sr isotope ratio. The most available source would have been from "*a near-full Mediterranean*" [372].

11.2 Black Sea and Dacian Basins lowstands

Reflection profiles on the margins of the Black and Azov seas (Fig. 54), calibrated by exploration wells show that during Portaferian and Bosphorian substages of the eastern Paratethys Pontian stage [373–377] the Black Sea experienced a major sea level fall in the range of 700 to 900 m [376–378]. This regression is expressed by erosional surfaces labeled MES, TES and BES in Figs. 55 and 56.

On the Romanian margin, the loss of the weight of the water led to an overpressure buildup in the underlying Oligocene to Lower Miocene sediments. The subsequent gravity failure resulted in up-dip extension and down-dip contraction of the Sarmatian and Meoitian cover along a detachment surface on the top of the Maykopian shales. The extensional depressions became filled by lowstand Portaferian and Bosphorian deltaic sediments and the compressional highs were truncated during subaerial exposure [378].

Using the lack of visible erosion in the reflection profile as indirect evidence of the minimum sea level and 20 km for the effective elastic thickness of the lithosphere, the required sea level fall in was in the range of 700 to 900 m [377]. This magnitude aligned with the elevations of MES, TES and BES surfaces.

11.3 Gap in the Zheleznyi Rog section

The same strong regression created incisions as deep as 400 m into the underlying middle Pontian (substage Novorossian) sediments on the north Scythian shelf in the Sea of Azov. On the nearby Taman Peninsula, the Zheleznyi Rog section (top panel in Fig. 55) exposes in outcrop a passage from the late Miocene Kersonian substage to the Pliocene Kimmerian stage [365, 379–381]. However, a 4 to 6 m interval with a

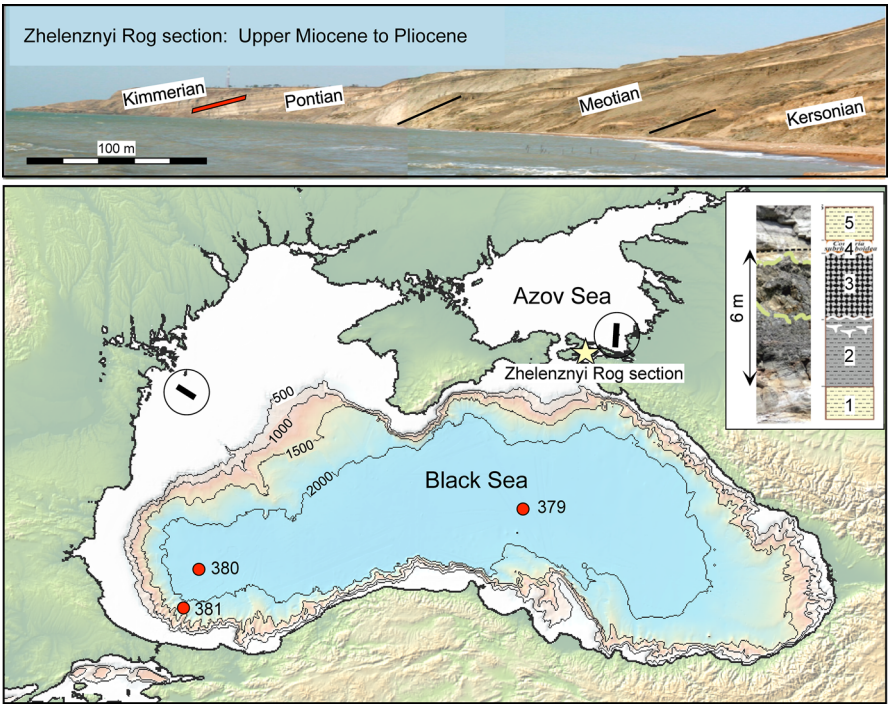

Fig. 54 Black Sea contoured at 500 m intervals with locations of DSDP drill sites and the reflections profiles illustrated in Figs. 55 and 56. The Zhelenznyi Rog section is shown in the upper panel labeled with the late Miocene eastern Paratethys substage names [379]. According to Alena Rybkina and Yuliana Rostovtseva the Portaferian substage is confined to 4 to 6 m thick interval (insert in lower panel) [380, 381]. Red line indicates location of the erosional gap between the Pontian and Kimmerian. Numbers in the insert refer to the sediment type in the gap: (1) Novorossian sandy/silty clay; (2) Portaferian non-calcareous clay with red paleosols; (3) clay breccia; (4) shelly limestone; (5) Bosphorian sandy/silty clay. The clay breccia is bounded by erosional contacts

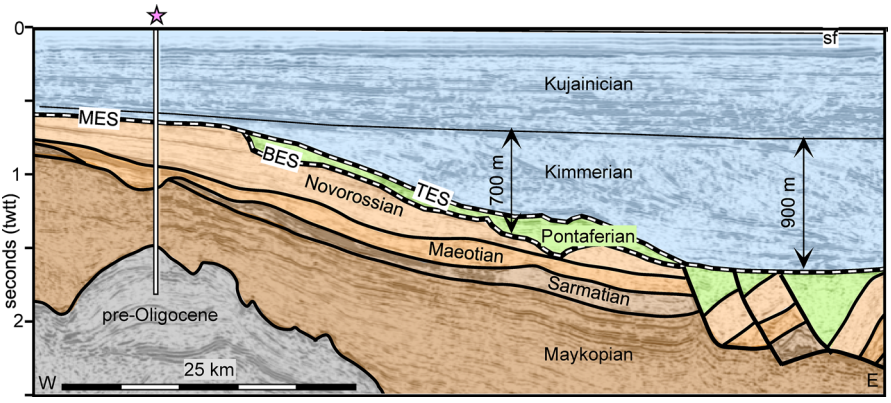

Fig. 55 Reflection profile on the Romanian margin of the Black Sea Azov showing erosional unconformities (MES, TES and BES) bracketing the Portaferian and Bosphorian substages of the Pontian [378]. Arrows show the magnitude of inferred sea level drop during the latest Miocene

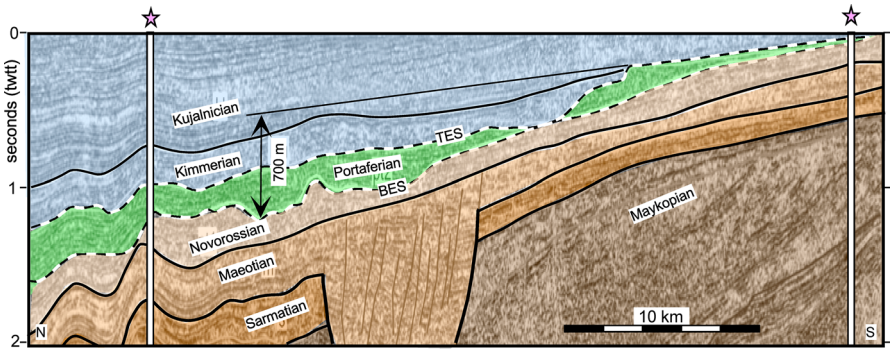

Fig. 56 Reflection profile in the Sea of Azov showing erosional unconformities (TES and BES) bracketing sediments belonging to the Portaferrian and Bosphorian substage of the Pontian [376]

duration of 200,00 years occurs at the same place in two measured sections (between 89 to 92.6 m [379] and 38.4 to 44.4 m [380]).

The gap (located with a red line in upper panel of Fig. 54) has been dated by astronomical tuning methods to span from 5.65 and 5.45 Ma and includes almost the entire Portaferian substage. The sediment includes oolitic shell limestone, clay breccia and paleosols. The clay breccia is bounded with erosional contacts. In the Dacian Basin, a similar drop in sea level also occurred in the Portaferian, which was expressed by a shallow, coastal sediment facies and a switch in the ostracod faunal assemblage from bathyal to littoral, fluvial and lacustrine species.

The coincidence between the timing of the Black Sea's lowstand and the Mediterranean's Stage 2 lowstand is remarkable. Sea level drop in the Mediterranean was in response to closure of the Atlantic gateway. Under the condition of evaporation loss exceeding supply of freshwater, it was expected that drawdown would occur and take place rapidly on a time scale of less than 1 precession cycle.

At the time of deep-sea drilling in the Mediterranean and Black Seas, it was not known if the Paratethys was also in a condition with a negative hydrologic budget in sync with the Mediterranean. However, the thin Portaferian deposit in the Zheleznyi Rog section contains gypsum crystals and jarosite, overlain by 2 m of oolitic limestone that had been stained red with iron oxides [365]. Jarosite occurs during the ultimate stage of pyrite oxidation and has been found as aeolian dust in Antarctic ice cores [382]. It is abundant in the intensely wind-swept oxidizing conditions on the surface of Mars. Oolites seed in agitated shallow, super-saturated saline water. The Babajan Formation that resides in the Bosphorian substage in the Caspian Sea contains shallow marine carbonates and evaporites that have been considered a stratigraphic equivalent of those in the Mediterranean Messinian [383]. The Caspian ostracods include the same Paratethys species as *Leptocythere* and *Loxoconcha* that are diagnostic of the Stage 3 Lago-Mare sediments [329, 330, 368, 384]. All of these indicators align with a parallel regressive setting in the Black, Dacian and Caspian basins at the same time as the evaporative drawdown in the Mediterranean and its conversion to brackish-water lakes with seven cycles of gypsum precipitation.

11.4 Portaferian and Bosphorian substages coincident with Black and Dacian Basin low stands

In the Zheleznyi Rog section on the Taman peninsula the Portaferian resides within the paleomagnetic reversed C3r chron which encompasses the entire MSC [379]. The overlying sediment is positively magnetized and therefore resides in the Gilbert C3n.4n chron. Thus, at this outcrop the first sediment (Kimmerian) above the erosional unconformity must be of Pliocene age. Consequently, the entire latest Miocene Bosphorian substage (upper Pontian) is apparently missing and the Portaferian (middle Pontian) is extremely condensed to a few meters on the northern margin of the Black Sea. The bulk of their accumulation was confined to the lowstand interval observed in the reflection profiles, which makes it nearly impossible for Paratethys water to have overspilled via an outlet sill into the Mediterranean at any time during either Stage 2 or Stage 3 of the MSC.

Had overland spillage occurred through a breach in the sill at an elevation lower than the former Black Sea rim, marine water would have most likely returned to the Black Sea though this opening, following the Pliocene transgression. If escape of water from the Paratethys had actually taken place and been significant, it needed to exploit underground aquifers and passage through karst leading to the Adriatic Sea or by means of other aquifers to the Aegean Sea [385]. In any case, published geophysical and sedimentological evidence indicates that the Black, Dacian and Caspian basins were partly empty during this time interval as the result of evaporation or leakage.

11.5 Eraclea Minoa representation of Stage 3 of the MSC

The 'upper evaporites' environment at Eraclea Minoa in Sicily has been considered to be representative of a moderately deep Messinian basin [38, 386]. The sequence consists of a rhythmic series of seven gypsum beds of different thickness and sedimentological composition, separated by marly clay layers. The series is topped by the Arenazzolo Fm., which marks the limit between the Messinian and the Lower Pliocene (Trubi Formation). The first six beds belong to Stage 3.1 upper gypsum with rare ostracods showing Paratethys affinity [387] (Fig. 57).

The gypsum isotopic composition, measured on samples at different depths in modern, Mediterranean salina has uniform $\delta^{18}O$ (SO_4) values of about + 16.1 ± 0.2‰ [345]. The values on the earlier 'lower evaporites' that had been precipitated when the Mediterranean was receiving salt water from the Atlantic are lower (14.3 ± 0.3‰) and can be considered a typical marine end member.

The $\delta^{18}O(SO_4)$ isotopic composition of each of the Eraclea Minoa upper gypsum beds are more positive by 2 to 4‰ than the those from either the modern salina or the primary lower gypsum and show a progressive decrease of 1 to 2‰ from the bottom to top of each bed [388]. This trend indicates that the conditions prevailing at the beginning of the bed were further from normal seawater evaporating conditions, due to the presence of brackish continental water. In a density-stratified water column, evaporation from the water surface would first thin and then remove the fresher lid followed by the more saline bottom water. As evaporation continued, the salinity

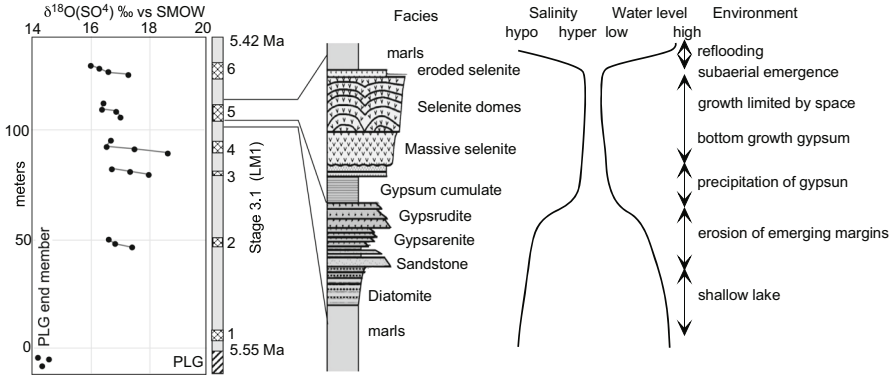

Fig. 57 The first 6 gypsum beds belonging to Stage 3.1 at Eraclea Minoa in Sicily. The $\delta^{18}O$ (SO_4) was measured from the gypsum sulfate [388]. The facies sequence for bed #5 is adapted with modifications from [327, 389]

would increase until it reached saturation for gypsum precipitation, starting first with the cumulate 'balatino' facies and progressing to massive selenite. As the brine body shrunk, accommodation space for the deposit would become reduced and the selenite facies evolved to branching lobes and then domes that were ultimately limited by the thickness of the gypsum-saturated brine layer. Erosion or karstification of the top of the domes, when present, signified subaerial exposure.

The upward trend of the $\delta^{18}O$ (SO_4) towards the Stage 1 Primary Lower Gypsum end member showed that most of the SO_4 was most likely derived from the dissolved and reprecipitated earlier PLG. If the SO_4 had come from the introduction of Atlantic seawater, the decreasing trend would have reached an even lower value of 12‰ for Late Miocene evaporation of ocean [318, 388].

11.6 Does the Eraclea Minoa section show evidence of desiccation?

Figure 58 presents measurements to address this question [388, 390, 391]. Between gypsum bed 6 and 7 there are two intervals (Stage 3.2.1 or p-ev1 and Stage 3.2.2 or p-ev2) separated by a gravel bed. The $\delta^{18}O$, $\delta^{13}C$ and $^{87}Sr/^{86}Sr$ isotopes and Na/Ca ratio measured on ostracods are entirely different in each interval, with no overlap in values above and below the gravel bed. Samples from immediately below and immediately above the gravel have even greater isotopic separation. One can infer that the water body of more or less uniform isotopic composition and higher Na/Ca ratios in Stage 3.2.1 was replaced by an entirely different water body with a different isotopic composition and lower Na/Ca, lower Mg/Ca and higher Sr/Ca in Stage 3.2.2. The only residues of the earlier water reside in the sample directly above the gravel bed. The earlier water body ended with an extremely positive $\delta^{13}C$ and negative $\delta^{18}O$ excursion. In the outcrop, there is an observable gap, compatible with the possibility of erosion and an alluvial or fluvial origin for the gravel bed.

A second unconformity is observed below the Arenazzola Fm. bed with the same isotopic behavior as observed above and below the gravel bed. The $\delta^{18}O$ and $\delta^{13}C$

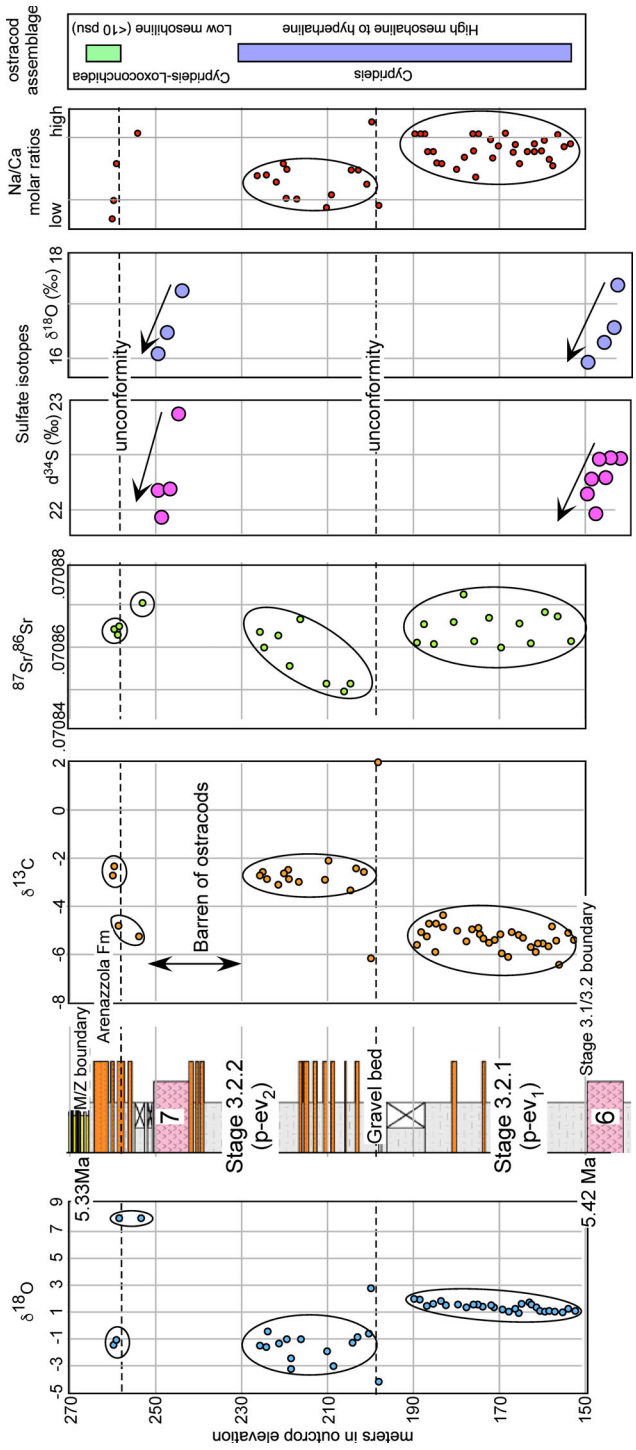

Fig. 58 Isotope measurements of the latest Messinian Stage 3.2 sediments sampled from the Eraclea Minoa section of the Caltanissetta Basin in Sicily [388, 390, 391]. The green rectangle represents the Arenazzolo Bed with its extremely high percentage of long-extinct microfossils

values directly above the younger unconformity are in the same range as below, even though they were separated by a 20 m thick interval barren of ostracods. And once again, the largest isotopic shift occurs just below the unconformity.

Although the ostracod species *Loxoconcha muelleri* had already appeared in Italy below the tephra layer from Colle di Votta as early as 5.5320 ± 0.0074 Ma and is present in Stage 3.2.1 at other Mediterranean locations, at Eraclea Minoa only the single species *Cyprideis agrigentina* is present in Stage 3.2.1, where it is accompanied by the euryhaline benthic foraminifer *Ammonia tepida*. The Cyprideis-Ammonia assemblage is considered an indicator of a mesohaline to hyperhaline shallow waterbody [390, 392]. The appearance of *Loxocorniculina djafarovi* later in Stage 3.2.2 points to a fresher low mesohaline environment. However, in the topmost samples (253–258 m) the assemblage reverts back to the single species *Cyprideis agrigentina*, heralding a return to stronger evaporation as the MSC approaches its end. Throughout Stages 3.2.1 and 3.2.2 the ostracods and benthic foraminifer indicate shallow-water bodies but not necessarily where the sediments were barren [390].

At Eraclea Minoa there are two nearby outcrops displaying the same Arenazzolo bed [393]. In one outcrop of 7.8 m thickness the underlying Lago-Mare sediment had a unique succession of dreissena shells, white sand and more coquina shells sandwiched been gypsum bed #7 and the Arenazzolo Fm. In the other outcrop only 1.5 m of the Lago-Mare sediment was preserved in the window between gypsum bed #7 and the Arenazzolo bed. The second outcrop retains just part of the lower Driessen coquina. Some 6.3 m of the Lago-Mare had been removed before the arrival of the Arenazzolo sediment [394].

The 5.6 m thick Arenazzolo bed is unique with an overwhelming number of microfossils that became extinct long before the MSC [391]. These species range in age from the Cretaceous to the mid-Miocene and occur in silt-sized sediment. The extinct species comprise > 92% of those present in samples, whereas elsewhere in the Lago-Mare the mean reworking is < 15% and consists almost exclusively of Miocene specimens. The Arenazzolo silts had therefore derived from much deeper erosion than the surrounding Lago-Mare and earlier evaporitic strata, yet larger foraminiferal tests are absent. Since the Arenazzolo Fm is the most widespread bed throughout the Caltanissetta Basin and contains minerals from far-away source regions, it raises the question if it is an aeolian deposit concurrent with latest Messinian desiccation. The transition between inner neritic dominated assemblages in the Arenazzolo silts and oceanic dominated assemblages of the earliest-Pliocene Trubi Formation is sharp [395, 396]. Abundant burrows at the boundary between the Arenazzolo and Trubi Formations are filled with the Trubi white biogenic ooze ([397]. The oceanic taxa in these initial oozes (foraminifera, nannoplankton, ostracods and dinoflagellates) became dominant in a deep, distal, open-marine environment with normal sea-surface salinities.

11.7 Other locations with evidence of omission surfaces at the end of the MSC

The unconformity at Eraclea Minoa below the Arenazzolo Bed also appears in the Stingeti quarry in the southern Apennine. Here the upper Messinian post-evaporitic (p-ev2) deposits with abundant mollusks (*Lymnocardiinae, Dreissena, Theodoxus,*

Melanoides, and *Melanopsis*), ostracods (*Cyprideis, Loxoconcha muelleri, Loxocorniculina djafarovi*), and rare shallow euryhaline benthic foraminifera (*Ammonia beccarii* and *A. tepida*) ended with a black clay layer containing the remains of small mammals [398].

A black arenite layer of sand with pebbles re-occurs in the walls of the Moncucco gypsum quarry in the nearby Torino hillside and in the Narzole borehole of the Piedmont basin in northwestern Italy. The black layer overlies paleosols with traces of roots and beds of conglomerates with remains of amphibians, reptiles, birds and large and small mammals, all belonging to Stage 3.2.2 of the MSC (5.41–5.33 Ma) [304, 399–403]. The terrestrial fauna indicated that dry and thinned out forests with well-developed understory were the dominant elements of the late-Messinian landscape. Of the 3,000 gastropod specimens, only 13 were aquatic species dwelling in ephemeral puddles and ponds. The gastropod assemblage is unrelated to coeval Pannonian-Pontian faunas of the Paratethys [404] and included species that are typically found deep under rock rubble, where they could find shelter during desiccation [405].

Like the Arenazzolo Bed, the black layer in the Piedmont Basin was composed of lithic grains from a broad range of source regions (frosted quartz, mica flakes, rounded fragments of metamorphic rocks). Its top corresponded to an omission surface, evidenced by a network of firm-ground burrows filled by the sediments of the overlying earliest-Pliocene Argille Azzurre Fm containing the acme of *Sphaeroidinellopsis* spp. [400]. The occurrence of bathyal benthic foraminifers and deep marine ostracods in the Narzole borehole attests to a sudden re-colonization of the Pliocene Mediterranean at the conclusion of the MSC [401, 402]. Benthic foraminiferal assemblages show a specific composition very similar to the deep marine succession of the Mediterranean area [122, 140, 406, 407]. Taking into account the palaeoecological indications given by the benthic foraminifer and ostracod assemblages, a basin as deep as 1 km was flooded by the introduction of Atlantic seawater. A similar deep submergence is also evident in the Moncucco quarry, as well as in the Maccarone section of the Northern Apennines [400, 402, 408].

In the Cava Serredi quarry (Livorno Province, Italy) a Lago-Mare deposit about 26 m thick was found sandwiched between the uppermost gypsum bed #7 and Pliocene [409]. The Lago-Mare deposit consisted of two beds: a lower 7.50-m thick *dreissena*-rich bed and an upper bed about 18 m thick with *Melanopsis* and *Theodoxus* shells [393]. Over the span of 3 decades the quarry face had retreated from exploitation by 2 km to a location where it exposed only 6.6 m of the lower bed with the dreissena-rich sediments directly capped by the Pliocene clays. The *Melanopsis* and *Theodoxus* bed plus 1 m of top of the *dreissena*-rich sediment were missing. Apparently, more than 17 m of the Lago-Mare deposit had been removed again at the very end of the MSC [393].

In the Monticino gypsum quarry near the town of Brisighella in Ravenna, northern Italy the 'lower evaporite' Gessoso Solfifera Fm had been truncated by an erosion surface displaying deep fissures of a paleokarst origin and then filled with the Stage 3.2.2 Colombacci Fm. [410, 411]. The fossil remains include terrestrial vertebrates, amphibians, and reptiles that have become one of the most important collections of

continental vertebrates in the Late Miocene of Italy. Among the mammals were monkey, aardvark, rhinoceros, hyaenas and the primitive dog living in a warm-temperate to subtropical climate. The entire deposit became sealed beneath the earliest-Pliocene Argille Azzzure Fm, attesting to an abrupt drowning of a terrestrial landscape at the conclusion of the MSC.

Another omission surface occurs along the top of the upper Messinian post-evaporitic sediments on the southern coast of Calabria (Fig. 59). There conglomerates with plutonic and subordinate phyllitic rocks [412, 413] were truncated by an angular unconformity (labeled #1 in Fig. 60). Above are cross-stratified sandstones displaying large-scale, low-angle, bidirectional cross-stratification. At outcrops 2, 3, 4, and 5 of Fig. 60 the cross-bedded sandstones have been truncated by a second erosion surface

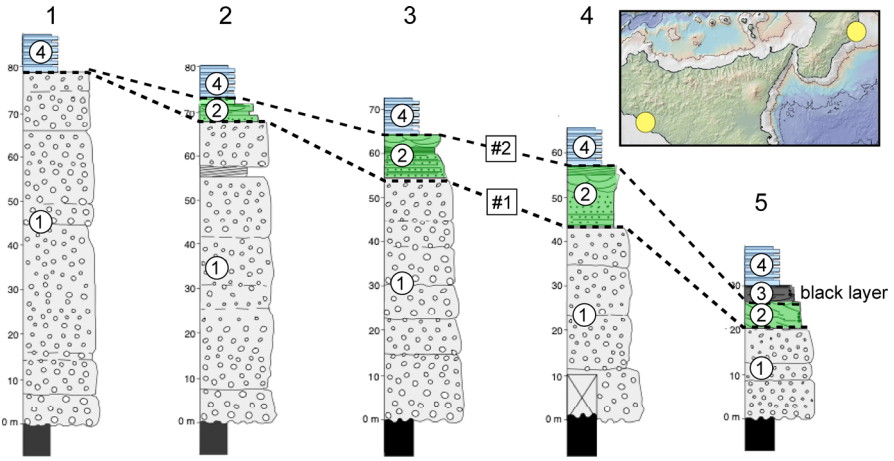

Fig. 59 Five outcrops of the uppermost Messinian on the coast of Calabria [394, 413]. Outcrop locations are spaced apart by ~ 1 km. (1) Uppermost Messinian conglomerates; (2) Cross-bedded sandstones on erosion surface #1; (3) Black layer on erosion surface #2; (4) white Pliocene Trubi Fm marls on erosion surface #2. Dots in location map show the 300 km separation between the Calabria outcrops and those at Eraclea Minoa in Sicily

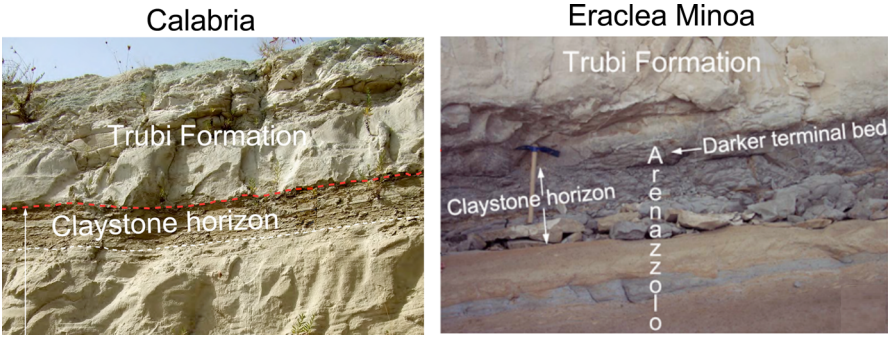

Fig. 60 The dark claystone terminal deposit in the Calabria Eraclea Minoa outcrops [394]

(#2 in Fig. 60). At outcrop 5, the cross-bedded sandstones are covered once again by a dark claystone bed. The dark clayey bed (Fig. 60) stands out in a sharp color contrast to the immediately overlying white first carbonate bed of the Trubi Formation (Fig. 60). The dark claystone bed in Calabria conforms to the same stratigraphic position as the black claystone omission surface in the Stingeti quarry, the Moncucco quary, the Cava Serredi quary, the Buttafuoco, Montepetra, Perticarra sections in the eastern sector of the Romagna Apennines, and the Calabria outcrops and Eraclea Minoa outcrops in Sicily.

The previously mentioned karst in Cyprus [414], conglomerates with remains of plants and mammals in Crete [214], alluvial conglomerates in the Feos Fm in the Nijar Basin in Spain [415], each located at a stratigraphic level just below the Pliocene marls, are further indications of widespread omission surfaces coincident with the end of the MSC.

11.8 The colonization of Mediterranean islands by mainland fauna

The teeth of giant hamster and gerbil from the mainland of Iberia were discovered in the fillings of paleokarst embedded in red-brown silts on the island of Mallorca in the western Mediterranean [416]. The teeth showed a close relationship with the mainland species, an Iberian taxon, from which it differed in size and tooth structure. The giant hamster *Apocricetus darderi* became the first endemic Balearic mammal that could be confidently assigned as having had a direct mainland relative, providing the first solid paleontological evidence of a Messinian origin for the subsequent Pliocene and Pleistocene fauna of Mallorca. The arrival of *Apocricetus* and other mammals, including rats, voles, shrews and rabbits, has been placed at 5.33 Ma [416].

The occurrence of larger mammals and crocodiles in the terrestrial deposits of Moncucco quarry in the Piedmont Basin of Italy affirm even greater distance migrations from Africa by way of terrestrial corridors across the latest Messenian Mediterranean [403, 417]. The mammals in the Moncucco gypsum quarry include the rodent *Paraethomys*; the hippopotamus *Hexaprotodon*, and camel *Paracamelus* [418–423].

Based on reconstructed paleo-bathymetry, and taking into account Pliocene–Pleistocene subsidence, a minimum of 800 to 1200 m evaporative drawdown of the western Mediterranean would have been necessary to allow the colonization of the Balearic Islands by new continental fauna [424]. From an examination of > 100 exposures and numerous boreholes related to the Messinian record in Mallorca, the main desiccation occurred after the accumulation of the Lago-Mare deposits [425].

12 Was the Mediterranean occupied by a single large Lago-Mare lake?

When the Paratethys began to separate into several brackish-water lakes at 9.7 Ma, each new lake developed its own unique endemic fauna in consequence to the diversification of its faunal assemblage [367, 426–428]. Then prior to the Mediterranean MSC these lakes reconnected into a single seaway in which the Lago-Mare assemblage

subsequently evolved [365, 371]. Therefore, when the Lago-Mare ostracods appeared at many widely-separated locations around the Mediterranean during Stage 3 of the MSC, it raised the question: had all of the Mediterranean sites been interconnected with each other by a high-standing shared lake?

Ostracod assemblages have become a useful chronostratigraphic tool for the recognition of the Messinian Lago-Mare event in the whole Mediterranean. The *Loxoconcha* (*Loxocorniculina*) *djaffarovi* Zone was first recognized in Crete [429] where it co-occurred with *Cyprideis pannonica* agrigentina. Also present were several presumed Paratethys immigrants, including *Leptocythere* spp., *Loxocauda* spp., *Loxoconcha* spp. and *Tyrrhenocythere* spp.

The ostracod assemblage in Crete was soon found on the margins of the western Mediterranean (Spain, France, Corsica and Italy) [384, 430]. The species were typical of an oligo-mesohaline environment, which had originated in the recombined Pannonian to the Caspian basins prior to the MSC. However, not all of the species in the Paratethys found their way to the Mediterranean. Instead, only a pioneer contingent became dominant in the Messinian Lago-Mare ostracod assemblage. The pioneers and those who followed gave the Mediterranean its biostratigraphic and palaeogeographic fingerprint.

The Paratethys fingerprints have been expressed differently from one region to another. Community analyses (number of species, Margalef and Shannon–Wiener indexes) and auto/synecological analyses have been performed on deposits at nine sites in Italy and Crete [431]. The community analyses revealed that the post-evaporitic Messinian Stage 3.2.2 was diagnostic of unstable environments, during which salinity and depth changed repeatedly and inhibited the establishment of mature and diversified communities.

The separation between low- and high-diversity ostracod assemblages in the investigated regions turned out not to have been synchronous, even in nearby sites due to the importance of local factors. Many intervals were barren, including the terminal dark layers. Other intervals were interrupted by either paleosols or fluvial/alluvial conglomerates. Thus, the boundary between low- and high-diversity ostracod assemblages cannot be used as a biostratigraphic tool [431].

At present, 68 species have been recognized within the late-Messinian Lago-Mare deposits. Yet, only 36 species are clearly of Paratethyan origin and another 24 are Paratethyan-like taxa [330]. Consequently, the importance of the pioneering Paratethyan contingent within the Mediterranean Lago-Mare ostracod assemblages may have been overestimated when considering the possibility that 10% of the species descended from ancestors which had inhabited the Mediterranean brackish waters before the MSC [432].

The presence of Lago-Mare ostracods in the Mediterranean deep-sea drill cores is astonishing rare. Just a few specimens of either *Candona* sp. or *Cyprideis* sp. were observed at Site 372 in the western Mediterranean, Sites 374 and 652 in the Tyrrhenian Sea and at Site 978 in the Alboran Sea. Specimens of *Loxochonca djaffarovi*, *Euxinocythere praebaquana*, *Amnicythere idonea*, and *Leptocythere limbate* were reported only from Site 975 and found just in intermittent thin white layers of finely laminated micrite indicating discontinuous occupations [122]. In the eastern Mediterranean, closest to a Paratethys spillway, only *Cyprideis pannonica* was present

as a potential Lago-Mare signal, and it was found at merely 3 locations: Site 129 in the Strabo Trench, the two adjacent Sites 375 and 376 on the Florence Rise [433] and at another two adjacent sites Site 969 and 670 on the crest of the Mediterranean Ridge. None of the pioneering species managed to successfully colonize regions of the Messinian Mediterranean except for the westernmost Alboran Sea.

As a test of the interconnectedness of the Lago-Mare lakes, samples with ostracods were collected from interbedded marls separating three distinct laminated limestone horizons (termed Colombacci) at 3 locations in the northern Apennines separated from each other by only 10 to 50 km [432, 434]. The limestones were abiotic, indicating repopulations of ostracods after each Colombacci interruption.

The isotope measurements $\delta^{18}O$ and $\delta^{13}C$ were obtained on three synchronous horizons. Those measurements from Horizon III are shown for three locations in Fig. 61 (S. Donato, Montepetra and Predappio).

In the $\delta^{18}O$ and $\delta^{13}C$ isotopic space the compositions of the three locations are distinct from each other. In addition, the $^{87}Sr/^{86}Sr$ value for S. Donato is 0.70864 and for Montapetra is 0.70875 with a precision of $\pm$ 0.00002 based on repeated analysis of the $SrCO_3$ standard [434]. Furthermore, when comparing the $\delta^{13}C$ for Horizons I and III at the same location (S. Donato), the Horizon I $\delta^{13}C$ values all fall narrowly between $-$ 0.9 and + 0.65‰, whereas the values for Horizon III display a much larger range of $-$ 6.36 to $-$ 0.83 ‰. Therefore, the three horizons were not only isolated from each other at the same time during Stage 3.2.2, but the same location obtained different compositions at separate times. This evidence points to the evolution of separate and intermittent lakes that refreshed with different waters of different compositions after vanishing at times of interruption by conglomerates, azoic limestone and sterile black claystone. The particular ostracod assemblage in each lake developed independently in response to its local environment. The isotopic measurements do not support

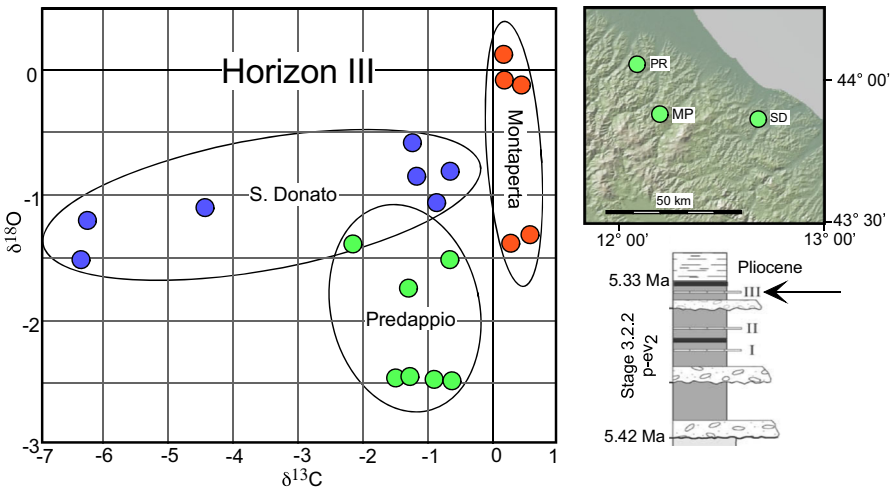

Fig. 61 Comparisons of $\delta^{18}O$ and $\delta^{13}C$ compositions for the same horizon (III) at three different locations in the northern Apennines [432, 434]

the hypothesis that "*some of the major basins formed large water bodies occupying the marginal peri-Mediterranean areas and were probably interconnected during the Lago-Mare phase*" [434].

The observation of different water compositions at different times during Stage 3.2.2 for the northern Apennines is also the case for Eraclea Minoa in Sicily (Fig. 62, Left). As for the Mediterranean deep-sea drill sites, the isotopic compositions are different with no overlap between drill site locations using only Stage 3.2.2 samples within 2 m from the Messinian/Pliocene boundary [435–437] (Fig. 62, Right).

Clearly, the Mediterranean was occupied by separate lakes at different elevations from each other during Stage 3.2.2 of the MSC. These separations prevented ostracod migrations by means of uninterrupted aqueous routes from the Paratethys to the eastern and the western Mediterranean. The diversified ostracod assemblages in Spain, Morocco, Algeria, France and Italy must have arrived by other methods, such as avian transport [438–441]. The environment a kilometer or more below global sea level in the Mediterranean lakes was apparently too extreme, except for *Cyprideis* sp., and *Ammonia* sp. that are more tolerant to a wide range of temperatures, salinity and oxygen concentrations.

As an example of avian transport, Holocene brackish sediments of the former Salziger See and Suesser See in Germany contain *Ammonia tepida*. Because this location had never been directly connected to the ocean, colonization by migratory birds has been assumed as the most viable method of transport [438]. The low diversity

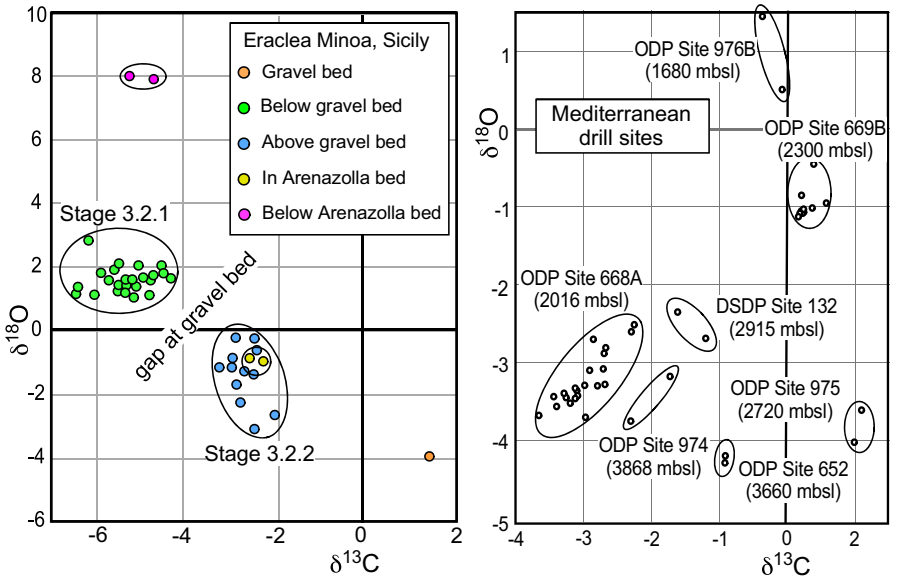

Fig. 62 Left: The $\delta^{18}O$ and $\delta^{13}C$ isotopic space for Eraclea Minoa Right: The $\delta^{18}O$ and $\delta^{13}C$ isotopic space for Mediterranean deep-sea drill sites from the western (974, 975, 976), central (132, 652, 974) and eastern (668, 669) Mediterranean. The measurements are from Stage 3.2.2 samples within 2 m from the Messinian/Pliocene boundary

of the foraminiferal fauna in these lakes is consistent with the > 300 km separation from the natural habitat of foraminifers in the Baltic and North Seas. Since the genus *Ammonia* sp. is unable to withstand complete desiccation [442], these particular benthic foraminifers were most likely transported in wet mud adhered to the feathers or feet of migrating birds.

Ostracods are benthic animals, confined to bottom sediments. Unlike planktonic species, they have no larval stages allowing long-distance transport in circulating waters. They either need to theoretically walk, or be carried intact [443, 444].

13 Contrarians to the hypothesis of > 1 km deep desiccated basins

The contrarians to an intermittently desiccated Mediterranean can be divided into three camps: one objecting on the basis of widespread faunal exchanges with the Paratethys, a second with suggestions of Atlantic seawater connections already occurring in the latest Messinian, and the third with reservations that the observed unconformities in reflection profiles were from dissolution and not subaerial emergence.

13.1 Faunal exchanges and their isotopic signatures

13.1.1: M. J. Brolsma considered the Arenazzolo/Trubi boundary in the Capo Rossello outcrop near the Realmonte mine in Sicily as an indication of "*slow accumulation under very quiet and low energy conditions*" [445–447]. There are no lithologic data to support the supposed "*sudden, catastrophically increasing water depth in the area*." After checking with Brolsma how his samples were taken, and how big they were, it seemed evident that the "*transitional*" character of the faunal assemblages might be accounted for by artificially induced mixing of the white chalks of the Trubi containing open-marine planktonic foraminifera [397]. Taking into account the mixture of the different species, the minimum depth of deposition of the Trubi was alleged to be no more than 40 m [447]. The cross-laminations and parallel laminations in the Arenazzolo were regarded to be the result of deposition from suspension-clouds when the energy of storm waves scoured shallow-water substrates.

13.1.2: Daniela Esu was among the first to use the Lago-Mare mollusk assemblages of Paratethyan affinity in Tuscany and Sicily (specifically the *Lymnocardiinae* and *Dreissenidae*) and their close relationship to upper Pontian species in the Dacian Basin to propose "*diffusion in the larval stage*" throughout a single connected water body [448] (Fig. 63).

13.1.3: Marius Stoica, Wout Krijgsman and co-authors compared the high percentage of Paratethyan ostracods with those in Spanish assemblages as validation for exchange of fauna at high water levels during the final stage of the MSC. Based on this the similarity alone, they concluded that "*the latest Messinian was full of water (comparable to the present Caspian Sea) and that the Zanclean deluge, if happened, only surged some tens, up to a maximum of ~ 200 m, into the Mediterranean"* [371].

Stoica and co-authors Anne Fortuin and Elsa Gliozzi noted the striking similarity in the ostracod distribution patterns in the Cuevas del Almanzora section in Spain with

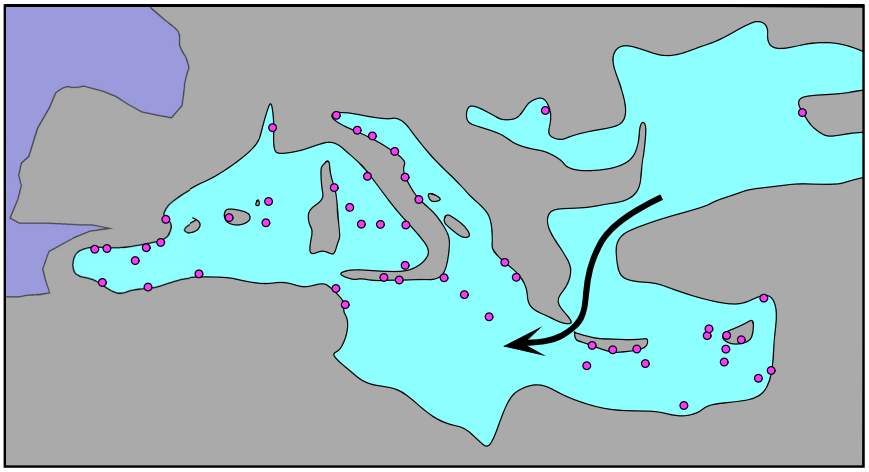

Fig. 63 An example among many of a single water body joining the Paratethys with an expansive Mediterranean Sea [448] with locations containing Lago-Mare assemblages of Paratethyan affinity [372]

those in the Zheleznyi Rog section on the northern Black Sea margin. They found that the Spanish ostracod assemblages had a high percentage of Paratethyan (Pontian) ostracods. By assuming that similar environments had developed synchronously in the western and central Mediterranean marginal basins, they also concluded that there must have been "*intrabasinal exchange at high water level during the final stage of the Lago-Mare* [371]." In each of these publications, there was no mention of the intra-Pontian sea level drop in both the Dacian Basin and the Black Sea coincident with Stage 3 of the MSC in the Mediterranean Sea, even though Krijgsman and Stoica were co-authors of that publication [449].

13.1.4: High Mediterranean water levels during the Lago-Mare phase of the MSC sufficient to enable basin-wide connectivity across the Mediterranean and Paratethys have also been proposed by Federico Andreetto and co-authors based on strontium isotope measurements [372, 450]. The measurements used the valves of the ostracod *Cyprideis sp*. that were picked from Lago-Mare deposits in the Nijar, Sorbas and Vera basins in SE Spain. Most of the $^{87}Sr/^{86}Sr$ measurements from the Nijar and Sorbas ostracods returned ratios above those for coeval external ocean water (0.709025), whereas all measurements from the Vera Basin lay far below ocean water and close to published ratios (< 0.7088) typical of Lago-Mare sediments elsewhere in the Mediterranean during Stage 3.2.2. Measurements on contemporary rivers in the region were all well above 0.7124 and some as high as 0.7265. Those from bedrock were even much higher. With the assumption the $^{87}Sr/^{86}Sr$ ratios from the three Spanish basins cannot be explained by an environment shaped only by local rivers, mass-balance calculations were performed for a mixture of river water combined with a sufficiently low radiogenic end member to replicate the ratios measured on the ostracods. The authors concluded that only an external source of water with a low-radiogenic signature of 0.7085 to 0.7086 as measured elsewhere on Lago-Mare ostracods could

reproduce the Nijar, Sorbas and Vera ratios. Accordingly, they write that the measured $^{87}Sr/^{86}Sr$ was achieved "*with a near-full Mediterranean during the Lago-Mare rather than the hypothesis that these Spanish basins were isolated lakes perched above a deeply desiccated Mediterranean*" [372].

Federico Andreetto and co-authors used similar strontium isotope ratios from the Cassano Spinola Conglomerates in the Pollenzo Section of the Piedmont Basin of NW Italy to state that "*at times during the final stage of the Messinian Salinity Crisis, the Piedmont Basin was hydrologically connected with the main Mediterranean Basin.… (with) … the water level in the Mediterranean Basin relatively high* [451]." However, the Pollenzo Section is only separated by 5 km from the Narzole borehole, previously discussed, where the overlying Pliocene Argille Azzure Fm. contains benthic foraminifer and ostracod assemblages indicative of an epibathyal basin as deep as 500 to 700 in reference to the external global sea [401, 402].

The Cassano Spinola Conglomerates are terrestrial with remains of mammals, birds, amphibian and reptiles and is largely barren of autochthonous microfossils, except for a monospecific ostracod assemblage of *Cyprideis torosa*, known to be a shallow-water dweller (< 10–30-m deep) with high salinity tolerance. Most foraminifera had been eroded from pre-MSC exposures, with many species extinct since the mid-Miocene. The calcareous nannofossil assemblage included species from the Cretaceous, Oligocene and lower-middle Miocene. An in situ ostracod assemblage with *Loxorniculina djafarovi* appeared in MSC Stage 3.3.2 for the first time only in the uppermost 1 m below the black layer omission surface. Its $^{87}Sr/^{86}Sr$ ratio of 0.70875 was used to contend that the surface of the Mediterranean's Lago-Mare lake water, with a similar-less radiogenic isotopic composition, had risen to a sufficiently high elevation that enabled it to submerge the Cassano Spinola Conglomerates in advance of the Pliocene transgression [451].

In the Piedmont region of Italy, the arguments for a late-Messinian Lago-Mare sea level highstand were based entirely on $^{87}Sr/^{86}Sr$ ratios of 0.7085 to 0.7086 that had to have been provided with water of a nearly-filled Mediterranean [451]. However, in earlier Tortonian-age brackish basins in Tuscany (Volterra-Radicondoli, Baccinello-Cinigiano, Valdelsa and Velona basins) the $^{87}Sr/^{86}Sr$ ratios performed on ostracods and mollusks show an almost identical range of 0.7083 to 0.7087 [452, 453]. Their brackish waters came from aquifers of the late Triassic Burano Anhydrite Fm as indicated by Sr/Ca ratios higher than Messinian seawater and $^{87}Sr/^{86}Sr$ ratios around 0.7080. These earlier basins contained high endemic mollusk and ostracod faunas with each lake having its own assemblage, and very few species shared between lakes. The narrow range of $^{87}Sr/^{86}Sr$ ratios came from springs or deep aquifers [452]. For example, modern lake tributaries and some springs located in the Triassic drainage show exceptionally high Sr/Ca ratios in contrast with much lower Sr/Ca in the river waters of the world. Therefore, if using the Tortonian-age brackish basins in Tuscany as an analog, the Lago-Mare $^{87}Sr/^{86}Sr$ ratios of 0.7085 to 0.7086 in the Pollenzo Section of the Piedmont Basin did not necessitate either the mixing of marine and fresh waters, or the mixing of river waters with the brackish waters occupying an expansive Mediterranean lake.

The Piedmont and central Apennine lakes may have been completely isolated from the rest of the Mediterranean at the closure of the MSC, as evidenced by overlying

black layer omission surfaces with root casts and underlying fluvial conglomerates and paleosols [400]. Accordingly, the presence of species referable to the Paratethys does not mandate an aqueous pathway between the central Mediterranean and Paratethyan bioprovinces, but could instead have been achieved by "*passive dispersal through aquatic birds and rapid speciation within each lake*" [453].

13.1.5: The nearly-fully Lago-Mare lake has been put to an additional test using a time-probabilistic approach to evaluate the synchroneity and preservation of the Stage 3 precession-related deposits at 24 circum-Mediterranean sites [454]. Thicknesses and sedimentation rates were calculated for each of the 7 cycles. The filling of the Mediterranean with fresh-to-brackish water would have resulted in landward migrations of deltas and shorelines and caused the burial of antecedent shallow-water clastic deposits by deep-water clays. The latter would have accumulated with significantly lower sedimentation rates engendered by increased distances from sediment sources and by the capture of newly-arriving sediment in flooded estuaries.

Instead, Stage 3 sediment thicknesses were highly variable and spanned three orders of magnitude. Sedimentation rates showed an increasing trend in successively younger intervals that is opposite to expectations from a near-full Mediterranean at the conclusion of the MSC Stage 3.2.2 Lago-Mare interval. On the other hand, sedimentation rates in the earliest Pliocene (5.33 to 3.9 Ma) became not only low at all Mediterranean drill sites [455], but also low in the northern and central Adriatic in close proximity to rivers, once the abrupt sea-level rise of the Pliocene transgression changed the equilibrium between erosion and deposition.

13.2 Early Atlantic sea-water connections

13.2.1: Laurent Londreix and co-authors found the dinoflagellate species *Galeacysta etrusca* with Paratethyan affinity in the Arenazzolo Formation and used it as evidence of the Mediterranean's return to a highstand sea level during the accumulation of the Arenazzolo silts [391]. Instead of an abrupt reflooding, the up to 5 m thick laminated silts implied a gradual transition from Lago-Mare fresh-to-brackish water and to fully-marine saltwater. Londreix and co-authors even conjectured that "*the Arenazzolo silts....might actually belong to the Pliocene series....*" [456]. Considering a shallow-water setting for the silts, they placed the Caltanissetta Basin on the margin of the Mediterranean and alleged that it only deepened after the MSC.

13.2.2: Another early assignment for the change from fresh/brackish water to fully marine came from the appearance of *Galeacysta etrusca* in the uppermost Messinian deposits at Cava Serredi [456]. According to Speranta-Maria Popescu and co-authors the simultaneous occurrence of this fossil cyst in both the Mediterranean and Paratethys implied "*that these two seas communicated during high sea levels*" [393]. Accordingly, they consigned the latest Messinian erosion surface to the boundary between the Lago-Mare clays the Arenazzolo Formation. In agreement with Brolsma [445–447], they attributed the Arenazzolo Formation to a gradual reflooding of the Mediterranean by Atlantic waters.

To strengthen this proposition Popescu and co-authors used the additional presence of planktonic foraminifers and the calcareous nannofossil *Ceratolithus acutus* in the

latest Messinian deposits belonging to the Di Tetto and Colombacci Formations in the northern Apennines to propose that the Atlantic saltwater connection took place as early as 5.40 Ma] [457].

Soon afterwards they re-examined a selection of the Mediterranean drill cores from Sites 976, 977 and 134 in the Alboran and western Mediterranean basins. In these sediments they located the appearance of *Ceratolithus acutus* at levels 2 to 23 m below the conventional Messinian/Pliocene boundary. Its early arrival once again affirmed their hypothesis that the flooding of the Mediterranean took place more than 120 ky prior to the earliest-Pliocene Trubi Formation.

13.2.3: Marco Roveri and co-authors replied to the Popescu publication with a comment that "*the marine signature of uppermost Messinian deposits is weak and still controversial and no significant bio-and magnetostratigraphic events, well-chronologically defined and recognizable at a global scale appear to be available to such a purpose*." [458] They noted that outside the Mediterranean the first occurrence of *Ceratolithus acutus* had already been astronomically calibrated at 5.28 Ma [459], and therefore this species could not have arrived in the Mediterranean as early as 5.40 Ma. As confirmation of its younger first occurrence age, specimens of *Ceratolithus acutus* were subsequently found in a sample from the Pliocene marls at Site 969 in the eastern Mediterranean [460].

Moreover, Mediterranean ostracod and benthic foraminiferal assemblages living in the oligohaline to mesohaline Lago-Mare Stage 3.2.2 are clearly distinguishable from the early Pliocene assemblage living in saltwater at bathyal depths [443]. When species belonging to these assemblages are presence together in the same biostratigraphic formation, those of one assemblage must be allochthonous and the others autochthonous [38]. Only when appearing in an orderly succession, can they be employed as convincing evidence of a transitioning environment.

The $^{87}Sr/^{86}Sr$ ratios of 0.70864 $\pm$ 0.00001 and the $\delta^{13}C$ and $\delta^{18}O$ isotopic measurements on *Cyprideis agrigentina* valves from three levels within the Arenazzolo silts provide a clear indication that the ostracods in this formation retained the same Lago-Mare fingerprint of all the earlier Stage 3.2.2 ostracods (Fig. 63), and thus these silts predated any connection with the open ocean [390].

13.3 The IMTS produced by dissolution rather than subaerial erosion

Zohar Gvirtzman and co-authors have proposed that the IMTS in the Levant Basin of the eastern Mediterranean is best explained by subaqueous dissolution, rather than by a combination of dissolution and erosion under conditions of subaerial exposure [225]. They emphasized that the surface is remarkably flat (Fig. 40). However, flat is a miss-leading term. As observed in reflection profiles the IMTS is inclined downwards from south to north in the Levant Basin with a change in elevation of 0.5 km over a distance of 100 km and east to west with a decline of 0.2 km over a distance of 100 km [226, 247, 461]. The decline of the IMTS in Anatalya Basin approaches 3 km over a distance of 100 km [287].

Their mechanism for dissolution derives from their assumption of a thick and stratified water column having developed during Stage 3 of the MSC. The stratification created a halite-undersaturated epilimnion above a halite-saturated hypolimnion. Accordingly, the truncation of the halite took place within the epilimnion. The Na and Cl dissolved from the truncation surface in the epilimnion would have continued to precipitate as salt elsewhere at deeper elevations in the hypolimnion. The presumed flatness of the IMTS in the Levant Basin was attributed to a persistent sharp interface between the epilimnion and hypolimnion.

What is missing from this argument is any mention to the deep moat-like depression surrounding the Eratosthenes seamount (Figs. 25, 27), where halite is either extremely thin or absent. The timing of the dissolution there is not known. Chris Kirkham and co-authors have suggested that "*dissolution initiated … even prior to the final dilution and emplacement of brackish Lago-Mare and fluvial deposits*" [227]. The Pliocene cover resting conformably on pre-MSC sediments in the depression surrounding the Eratosthenes seamount requires that most of the halite dissolution occurred in the terminal Lago-Mare interval.

Dissolution is still ongoing as attested by porewater salinity increases with sub-bottom depth at deep-sea drill sites and contemporary brine-filled basins (Tyco, Bannock, Urania, Atalante and Discovery) [462]. The chemistry of the brines is strongly variable and suggests dissolution of different levels of the Messinian halite. The brines ponded in the Discovery Basin in the Ionian Sea (Fig. 7) are the saltiest ever recorded in a natural environment. The presence of solutions derived from bischofite ($MgCl_2 \cdot 6H_2O$) "*demonstrated that the eastern Mediterranean had evaporated to near dryness*" [463]. The large bromine contents of 8 mg/g in the Discovery brine can only be obtained when seawater had evaporated to less than 1% of the initial water volume. The abnormally high Br/Cl and Li/Cl ratios in porewaters at DSDP Site 127 in the nearby Hellenic Trench (Fig. 7) added further confirmation of a "*very late stage evaporite deposit or residual liquor*" [49]. A persistent unsaturated epilimnion [225] is inconsistent with a near-complete drying of the deepest regions of the Mediterranean.

13.4 Late Messinian channel systems are marine and not fluvial

Jimmy Moneron and Zohar Gvirtzman have questioned whether the clastic-rich evaporitic unit shown in Figs. 40 and 41 occurred subaerially as a fluvial system on a desiccated seafloor overlying the Intra-Messinian Truncation Surface or, instead, as a network deep-sea turbidite channels in a Mediterranean full or nearly full of fresh-to-brackish water [464]. They based their preference for a deep-water rather than fluvial origin on the aggradation characteristics of the channels (levee height, channel depth, and channel-floodplain coupling).

There is an extensive literature on the characteristics, similarities, dissimilarities, and modes of formation between deep-water and fluvial channels [286, 292, 293, 465, 466]. Among the dissimilarities are vertical aggradation, lateral migration, and channel-bank avulsion in deep-water sinuous channels which are not apparent in the sediments that overlie the IMTS in the Levant Basin [234]. The post IMTS clastic-rich evaporitic layer has been given the name Nahr Menashe [226, 228, 229]. The

Nahr Menashe extends from southern Turkey and western Syria to the Eratosthenes Seamount. The siliciclastic sediments derived from a large ancestor river system draining though the Lebanon Highlands from eastern Anatolia, with some more local contributions from the exposed Latakia Ridge [467]. Its uppermost strata are mostly erosional rather than depositional. Its TES is coincident with the upper boundary of the Abu Madi Formation, offshore Egypt. According to Heidrun Solem the Nahr Menashe sediments (Fig. 64, bottom) are significantly different from the overlying marine Pliocene sediments (Fig. 64, top) (2014) [234]. Based on sonic velocities and formation densities from well logs the Nahr Menashe is composed of materials that are well lithified. Young submarine fans are instead composed of unconsolidated sand and clay.

Although the thalwegs of submarine channels are usually filled with high-amplitude reflecting sands, the channels incised into the Nahr Menashe are filled with low-amplitude Pliocene marls. Channel relief is as large as 100 m and yet widths are no more than 0.5 km. In comparison, the floors of submarine fan channels such as those on the Rhône and Nile fans [87, 468, 469] tend to be wider, are perched above the adjacent submarine fan apron, and are bounded by broad lateral levees. The Nahr Menashe channels lack levees and have lower sinuosity than channels on deep-sea fans. The Nahr Menashe thalweg floors are incised below the elevation of their adjacent aprons.

A gradient is required to develop submarine channels. A gradient comparable to those on distal submarine fans (10 m/km) [293, 466] is not present on the IMTS (< 5 m/km). In the case of subaerial exposure, rainwater gathers in streams. Since the anhydrite, lithified sandstone, limestone and cemented conglomerates in the Or South-1 well are impermeable, water would not have been able to penetrate into the substate

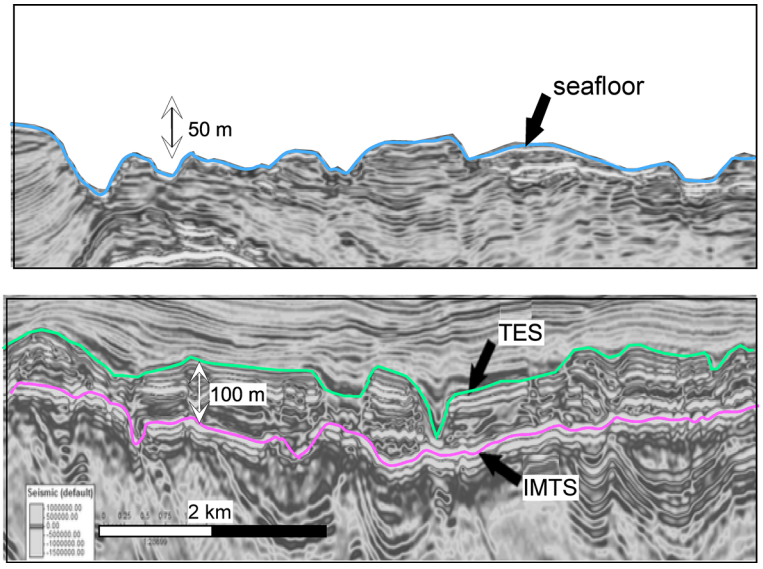

Fig. 64 Top: Seafloor channels in the Levant Basin. Bottom: Channels cut into the Unit 7 Nahr Menashe [234]

and supply aquifers. Nor would water have reached the underlying halite, thereby leaving the distributary trunks of the Nahr Menashe as elevated belts and backstepping lobes [229]. Such topographic inversion [470] is not observed on submarine fans (Fig. 65).

14 What were the magnitudes of Mediterranean desiccations?

Perhaps the most convincing example of extreme desiccation is the exposure surface in the Realmonte Mine with its spectacular vertical fissures (desiccation cracks) separating halite Units B and C (Fig. 65, right). The shrinkage on the exposure surface that accompanied the drying left a network of giant polygons [325, 326]. What is unknown, is the size of the Caltanissetta Basin in which Units A and B precipitated and its depth relative to the surface of the external ocean. One approach is to assume that most of the halite precipitated after the accumulation of the primary lower gypsum and during a brief period of evaporitic drawdown [386, 471, 472]. If the drawdown commenced with the brine already concentrated to saturation for halite (350 kg/m^3) [473] the minimum volume of water (Vmin) needed to precipitate the observed volume of deposits (Vdeposit) can be calculated using the equation below [471].

$$V\_\text{min} = (V\_\text{deposit} \times \rho\_\text{deposit})/\text{c\_saturation},$$

where ρ is the density of halite in (kg/m^3) and c_saturation for halite is 271.1 kg/m^3 [474, 475].

By assuming a hypsometric configuration for the Caltanissetta Basin, basin volume can be related to basin depth and the calculation can be applied to a box shape. With the simplest boundary conditions, a 300 m thick halite layer requires a basin with a

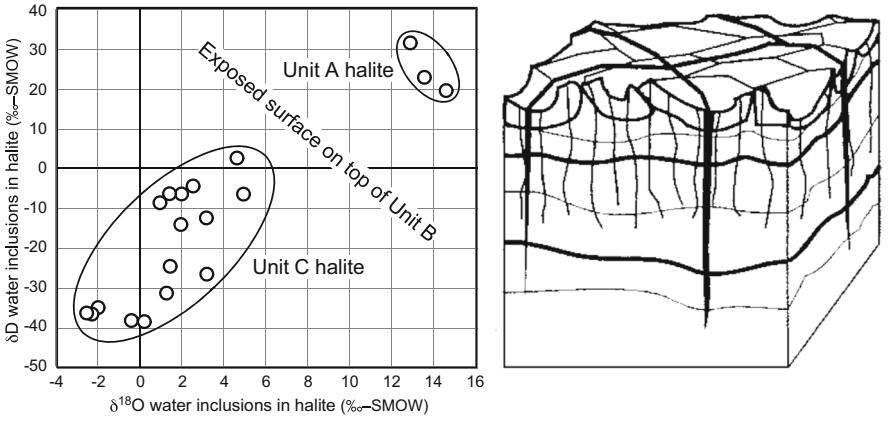

Fig. 65 Left: δD and δ^{18}O values of values of fluid inclusions measured from natural halite in Units A and C from the Realmonte mine, Sicily [476]. Right: The subaerial exposure surface displaying expansion cracks filled with soil separating Units B and C [326]

pre-existing depth of approximately 1.2 km at saturation for halite, if there was no further seawater added during the evaporative drawdown. A disconnected basin with minimal input from rivers would evaporate in less than one precession cycle. One does not know if the entire the Caltanissetta Basin desiccated, only that at the location of the Realmonte mine it became dry. However, the 1.2 km estimate is in the range of mesobathyal and close to the estimate of 800–1400 m for the earliest-Pliocene Trubi marls at Capo Rossello, Sicily [38, 121, 395–397]. The calculated depth also falls with the range of 1000 to 2000 m for the psychrospheric ostracod *Agrenocythere-Krithe* that appeared in the Trubi marls at Pasquasia, Sicily, without evidence of invading shallow fauna that would normally accompany the refilling of warm, shallow basins [443, 444].

Another approach to determining basin depth is to look for the air temperatures when the evaporites were accumulating. The dry atmosphere adiabatic temperature gradient is ~ 7 °C/km. A basin floor at 1400 mbsl would be expected to be roughly 10 °C warmer than one at sea level. Homogenization temperatures of fluid inclusions in halite from the Caltanissetta Basin indicate an average temperature of 34 ± 5 °C for the halite in Unit C of the Realmonte mine and an extreme temperature of 47 °C [476]. Similar homogenization temperatures were obtained for a complete mud–halite–mud cycle in Unit C, presumably formed by precipitation from a shallow non-stratified column of water during a wet–dry–wet cycle [477]. As comparison, fluid inclusions from halite in Death Valley, California are similar to those in the Caltanissetta Basin and average 35 ± 5 °C [478, 479].

The halite fluid inclusions show that the pre-desiccation Unit A halite is distinct from the Unit C halite (Fig. 65, left). The three natural samples from the earlier Unit A are characterized by high water contents and most likely incorporated trace amounts of a hydrated salt, such as kainite or carnallite. The low isotopic values in Unit C indicate that, once the Mediterranean became cutoff from the Atlantic, the source water that precipitated the Unit C halite was residual seawater mixed with at least 50–75% of freshwater [476].

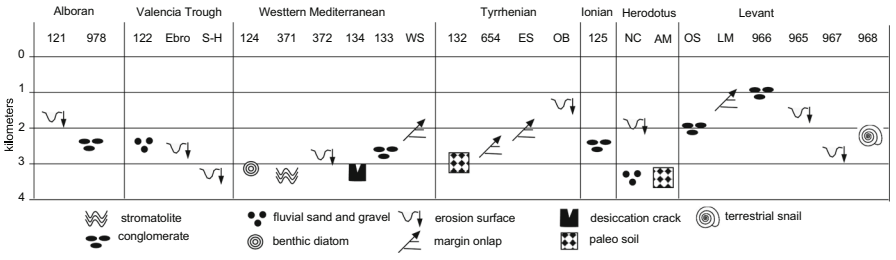

Fig. 66 Paleo-elevation indicators of subaerial emersion for Mediterranean drill sites and margins. Ebro: canyon thalweg at Fornax-1 well [188]; S–H: unconformity on Ebro margin at 2.75 [182]; WS: onlap height on western Sardinia margin [480]; ES: onlap height on eastern Sardinia margin [203]; OB; incised valley in the Orbo Basin east of Corsica [205]; NC: incised depth and fluvial sands in the Eionile canyonp [95]; AM: Abu Madi sands with paleosols [249, 257]; OS: Or-South-1 well [238]; LM: Onlap height of Afiq Fm on the Levant margin [219]

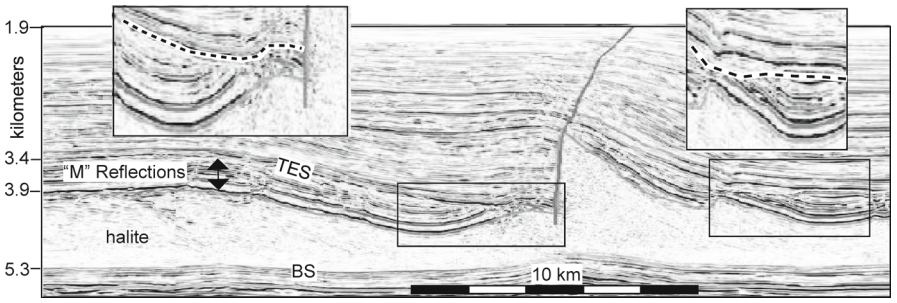

Fig. 67 Local truncation of the "M" reflections ('upper evaporites') by the TES in the Liguro-Provençal Basin of the western Mediterranean

Additional indicators of emergent terrains include paleo soils, alluvial fan deposits, algal filaments and bottom-dwelling diatoms requiring sun light. Figure 66 displays symbols for these types of indicators from Mediterranean drill sites and other locations discussed previously. The symbols are placed at their current elevation with respect to modern sea level. These plotted elevations require some upwards adjustment to account for post-Messinian subsidence. However, from the current elevations alone, it is evident that the western Mediterranean and the Tyrrhenian Sea experienced at minimum 1.3 to 1.9 km of evaporative drawdown and the eastern Mediterranean as much as 2.8 km based on the severe down cutting of the Eonile Canyon and the fluvial nature of the sands of the Abu Madi Formation that are interbedded with paleosols.

An extremely-deep TES is present in the Liguro-Provençal Basin where the mobile salt layer has uplifted the upper evaporite 'M' reflections and allowed them to become truncated (Fig. 67). For this to have happened, desiccation in the western Mediterranean reached a near-completion at the end of the MES.

15 When did the halite layer accumulate?

Two hypotheses have been proposed for the deposition of halite layer in the western, central and eastern Mediterranean.

1. The Mediterranean remained in two-way communication with the Atlantic while becoming hypersaline. Brine reflux delivered the most soluble minerals to regions farthest from the inlet and kept the lesser soluble minerals closer to the inlet [98, 481–483]. Sulfate with interbedded clastic deposits were sedimented on margins, while halite accumulated on basin floors [97, 101]. Early precipitation of the salt took place in deep subaqueous environments [230, 236, 296, 317, 319, 484].
2. Deposition of the halite was delayed until a second stage of the MSC. Precipitation was initiated by a more severe restriction of the Atlantic entryway, which led to evaporative drawdown and shrinkage of brine having already reached saturation for halite [172, 195, 332, 370, 454, 472, 485–487].

15.1 Halite layer thicknesses and volumes

The halite layer is present beneath modern basin floors in all regions of the Mediterranean except for the Adriatic and Alboran Seas and the Valencia Trough. In the western Mediterranean the maximum thickness of the halite layer approaches 1 km and its calculated volume measures at 180×10^3 km^3 [278]. In the eastern Mediterranean the maximum thickness exceeds 2 km and its volume approaches 500×10^3 km^3. Nevertheless, when the halite layer volume is compared to the region's available water volume for storage of potential brine (western vs eastern) the proportions are quite similar (14% and 16%, respectively).

There is a relationship between halite thickness and depth to its base. Deeper regions contain thicker layers. Where former depocenters were flat and undisturbed by tectonics, such as the basins of western Mediterranean, the halite layer thickness is uniform after adjustment for ductile deformation [278, 480]. All six sublayers are observed in each of the far-eastern Mediterranean basins regardless of the elevation of the depositional site [287]. Although each sublayer was originally laterally continuous, halite has been rarely preserved in the eastern Mediterranean at elevations above 1750 mbsl. Halite has survived erosion and dissolution where it had accumulated in enclosed pockets on the crest of the Mediterranean Ridge, however only at depths greater than 2500 mbsl, as attested by reflection profiles [488, 489] and downhole increases in chlorinity at DSDP Site 127 [49].

15.2 Onset of halite in the eastern Mediterranean

Industrial activities targeting hydrocarbon reservoirs in the eastern Mediterranean's Levant Basin have provided abundant 2-D and 3D reflection surveys, well logs, and cuttings from the halite interval. In the Dolphin well the 1.6 km thick halite layer rests on a 2-m-thick anhydrite bed corresponding to Reflector 'N' [236] (Fig. 39). The interval directly beneath the anhydrite bed is composed of bathypelagic calcareous shale and limestone, both containing nannofossils along with benthic and planktonic foraminifera of Late Miocene age. Five of seven reliable biostratigraphic events were recognized (Fig. 68, Left). These events appear in the same order in the sediments directly beneath the PLG in the Sorbas Basin (Spain) [172, 490], in the Falconara Basin (Sicily) ([172], in the Pissouri Basin (Cyprus) [491], beneath the PLG in the 497-Muchamiel well (offshore of SE Spain) [492], and ODP Site 654 (Tyrrhenian Sea) [126]. The biostratigraphic events and well log data from the Dolphin well provide strong support for halite precipitation in the eastern Mediterranean beginning at the same time as the PLG elsewhere in the [230, 236].

The same anhydrite bed at the base of the halite layer in the Dolphin well can be traced up the foot of the Levant margin where it is present in the Yam 1, Yam 2 and Hof Ashdod 1 exploration wells. There it reached elevations above 1750 mbsl. However, on the margin only the first 100 to 200 m of the halite layer survived removal along the IMTS (Fig. 68, Right).

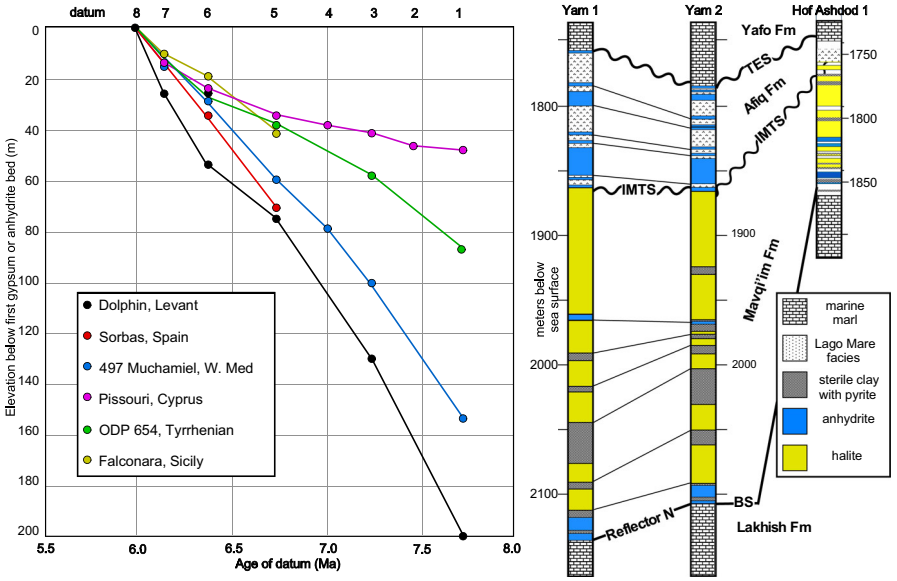

Fig. 68 Left: Datums in sediments from offshore drilling and terrestrial outcrops according to their elevation below the first bed of gypsum or anhydrite belonging to commencement of Stage 1 of the MSC. Convergence at 5.97 Ma marks the passage from marine sediments with planktonic foraminifera to the first evaporites. 8: First PLG bed. 7: First influx of sinistral neogloboquadninds. 6: Sinistral/dextral coiling change of neogloboquadrinids. 5: Top acme of *Globorotalia nicolae*. 4: Base paracme of the *Globorotalia scitula.* 3: First regular occurrence of *Globorotalia miotumida*. 2: Last occurrence of *G. falconarae*. 1: Last regular occurrence of *Globorotalia menardii-4* (sinistral). Right: Halite present in three wells at the foot of the Levant margin where it overlies the same anhydrite bed as in the Dolphin well. The anhydrite bed corresponds to Reflector 'N' and the conformable Bottom Surface (BS)

Halite precipitation continued throughout MSC Stage 1 until 5.56 Ma when the entryway for saltwater from the Atlantic was cut off by obliquity-forced, glacio-eustatic sea level fall accompanying either the TG12 or TG14 glacial cycle [493], depending upon the 16 surviving PLG beds in the Gessoso Solfifera Fm. in the Maiella composite section in the central Apennines [494, 495], or the 17 PLG beds in the Sorbas Basin. If the closure took place in the TG 12 glacial cycle, the duration of the Stage 2 evaporative drawdown was no longer than 28 ± 11 ky [496].

When passing westward from the Levant to the Herodotus Basin sublayer ME-6 thickens and becomes Units D and E in the Messinian Upper Megasequence (MUM) [227, 291]. Deposition of massive halite from a rapidly shirking brine layer would be expected to contain a minor amount of interbedded of detritus. Presumably, it would have been left behind on abandoned shorelines and only later during maximum sea level fall would have been washed into sublayer 7 (the equivalent to the Afiq Fm. sands and conglomerates and Nahr Menashe fluvial deposits [229].

Due to drilling limitations, detritus was only retrieved as downhole "*fallouts*" in the Dolphin well cuttings [230]. The detritus contains a high amount of sub-rounded sand grains, mollusk fragments, ostracods, echinoid spines belonging to the Stage

3 brackish environment, and abundant pre-MSC benthic and planktic foraminifera including Cretaceous, Eocene, Oligocene and early Miocene species derived from the exposed basin margins. The faunal composition is practically identical the reworked assemblages recovered in the wells on the apron located just beyond the mouth of the Afiq and el-Arish canyons [285] (Fig. 49).

In a large depocenter of the Herodotus Basin south of the Florence Rise the halite layer had an original thickness estimated to have been in excess of 4.5 km prior to additional thickening from post-Messiaen tectonic shortening [227]. It is conceivable that this huge deposit not only held the halite removed from above the IMTS, but the solutes precipitated from the Mediterranean brine during evaporative drawdown. The pure halite in sublayer ME-6 would have given it a preferred higher ductility compared with halite burdened with interbeds of clastics, anhydrite and the denser magnesium and potassium salts. The increased ductility of pure halite would allow for its preferred flowage into the diapirs that appear to be sourced from sublayer ME-6, and not from deeper sublayers.

15.3 The halite layer in the western Mediterranean

The halite sublayers in both the Levant Basin of the eastern Mediterranean and the Liguro-Provençal Basin in the western Mediterranean are stacked one the other with conformable bottom boundaries. However, the four sublayers in the western Mediterranean display a pattern of progressive onlap in the direction of the margins, whereas in the eastern Mediterranean they drape pre-MSC sediments. The earliest sublayer MW-1 is confined to the deeper regions. Its Bottom Surface (BS) is conformable with underlying sediments [278]. The youngest sublayer MW-4 extends across the entire basin and reaches as high as 3.2 kmbsl on the margins of the Balearic Platform and western Sardinia (Fig. 34). Sublayer MW-4 is the only sublayer with internal reflectors, while sublayers MW-1 and MW-3 display diffuse internal reflectivity. Sublayer MW-2 is the most acoustically transparent. All of the flowage has occurred in this layer, suggesting a more ductile rheology than in the other sublayers. The equivalent to the IMTS in the Levant Basin is erosion surface #1 at drill sites 124, 132, 374 and 375 and surface #1 separating the Cattolica and Pasquasia formations in the Caltanissetta Basin in Sicily.

Currently, the most widely-accepted timing of the western Mediterranean halite is after deposition of the Stage 1 ‘lower evaporites’ and coincident with either a highly restricted or complete closure of the Atlantic gateway. However, the band of strong reflectors beneath the halite layer and considered to be the stratigraphic equivalent of the ‘lower evaporites’ Stage 1 selenite, has instead been shown to be the Tripoli Fm. diatomite at DSDP Site 654 and euxinic shale of the Formazione Peliti Eusiniche at Site 652. This matching of diatomite and euxinic shale with reflection Unit 3 is evidence that the commencement of halite precipitation most likely occurred at the same time throughout the Mediterranean.

If the brine was still at saturation for halite precipitation following the closure of the saltwater inlet from the Atlantic, evaporative drawdown would have contributed the remaining solutes to additional thickening of the western Mediterranean’s halite

layer. In this circumstance the sublayers MW-1 and MW-2 might be equivalent to the Messinian Lower Sequence (MLM) and sublayers MW-03 and WM-04 to the Messinian Upper Sequence (MUM) observed in the Levant and Herodoitus basins of the eastern Mediterranean.

15.4 Dead Sea analog

Using the Dead Sea as a modern analog with double-diffusive flux of Na and Cl from a warmer upper epilimnion into a colder hypolimnion [497], the accumulation of halite crystals would have become focused into deeper regions of the western Mediterranean basins [290]. As these depocenters filled, the accumulation would spread wider as it transgressed over shallower regions and left behind the observed geometry of progressive landward onlap. The internal reflectors in sublayer MW-4 are likely to be detritus sourced during the enlarging exposure of former seafloors. The observed onlap termination of the sublayer WM-4 has been used as an indicator of a lowstand shoreline [278]. A shoreline at this elevation would have left the deeper Liguro-Provençal and Algero-Balearic Basins still submerged by brine with its halite deposit unaffected by dissolution. The remaining brine would no longer remain at saturation for halite, once losses by diffusion and mixing into the fresher epilimnion were replaced by occasional recharge from the surrounding shallower regions [498]. Thus, an IMTS caused by dissolution would not be anticipated.

The 3.2 kmbsl elevation of the termination of sublayer MW-4 in the Liguro-Provençal and Algero-Balearic Basins and the 3.25 kmbsl at Site 124 (Fig. 5) is within the range of the 3.5 kmbsl onlap termination for the halite in the western Tyrrhenian Sea (Fig. 47) and the 3.2 kmbsl termination at Site 132 (Fig. 10). The Tyrrhenian Sea is younger and has undergone additional thermally driven subsidence during the Pliocene and Pleistocene [280].

The thinner MW-1 and MW-2 sublayers suggests that during Stage 1 seawater from the Atlantic concentrated to saturation for $CaSO_4$ in the western Mediterranean but passed much of its brine over intervening sills to the eastern Mediterranean where under stronger evaporation and a larger surface area it concentrated to saturation for NaCl and crystalized to thicker sublayers there. Its precipitation in the eastern Mediterranean was not focused into the deeper depocenters but occurred at all elevations including those in the shallower Aegean Sea [499]. The eastern Mediterranean's hypolimnion was apparently thick and covered by a relatively thin epilimnion that experienced the seasonal changes in temperatures that effected whether the NaCl crystallization took place at the epilimnion/hypolimnion interface (metalimnion) or as growth on the seabed [289, 290]. Its double-diffusion flux rate though the sharp metalimnion determined the rate of halite crystallization in the hypolimnion. The previously described relationship between the thickness of the halite layer and depth of the basin suggests that the amount of brine residing in the hypolimnion determined the amount of eventually precipitated halite.

The conformable contact (i.e., wet upon wet) between the halite layer in the Liguro-Provençal and Algero-Balearic Basins and Tyrrhenian Sea and their 'upper evaporites'

indicates that the evaporative drawdown did not continue below the 3.2 kmbsl elevation, or if it did, excursions were brief.

15.5 Desiccation limited by sill elevation

As to why the drawdown remained in the range of 3.2 kmbsl is unknown but could have been determined by the height of the deepest sill to the eastern Mediterranean [370, 500–502]. In this case, without continued inflow from the Atlantic, the western basins would only have been refreshed by rivers, rain, and groundwater springs as the basins transform from hypersaline to brackish and freshwater lakes at the commencement of Stage 3. Under this scenario, the magnitude of desiccation in the western Mediterranean was limited by sill elevation. Although rivers alone might not have kept up the higher evaporation rates of fresher waters, substantial evaporative drawdown would have greatly reduced the hydraulic head of margin aquifers, leading to their flushing and additional contributions of large amounts of previously stored ground water.

The permanence of brackish water in the deeper depocenters of the Liguro-Provençal and Algero-Balearic Basins and Tyrrhenian Sea during Stage 3 would have provided an environment for the colonization of ostracods, Radiolaria, diatoms, silicoflagellates and fish that then could have made their appearances in perched lakes at higher elevations. Outlet streams would have served as pathways from the basins to the lakes using fish, reptiles, amphibians, and birds as transport mechanisms.

15.6 Comparisons of the western Mediterranean's sublayer ductility and reflectivity

Sublayer MW-2 in the Liguro-Provençal basin is unique in the lateral flowage that generated the observed diapiric anticlines and domes in Fig. 69, left. Its transparency suggests pure NaCl. Precipitation prior to drawdown assures that there would have been little contamination by detritus derived from exposed margins. Further concentration during drawdown would contribute the mote soluble magnesium and potassium salts to sublayer ME-3. The MW-3 sublayer's diffuse reflectivity could come from interbedded lenses of kainite, bischofite, sylvite, kieserite, and langbeinite as found in Unit B in the Caltanissetta Basin in Sicily [503]. The strongest reflectivity in sublayer MW-4 signals the arrival of interbedded detritus from the exposed margins.

16 Reconnection of the Mediterranean with the Atlantic

Currently there are two divergent scenarios concerning the state of the Mediterranean at the time of its reconnection with the Atlantic [504]. As previously discussed in earlier sections, one scenario postulates that the Mediterranean was full or nearly full of brackish water. Open-marine conditions were reestablished in the Mediterranean interior without major flooding. The second scenario postulates an abrupt flooding of the Mediterranean previously disconnected from the world ocean and severely desiccated.

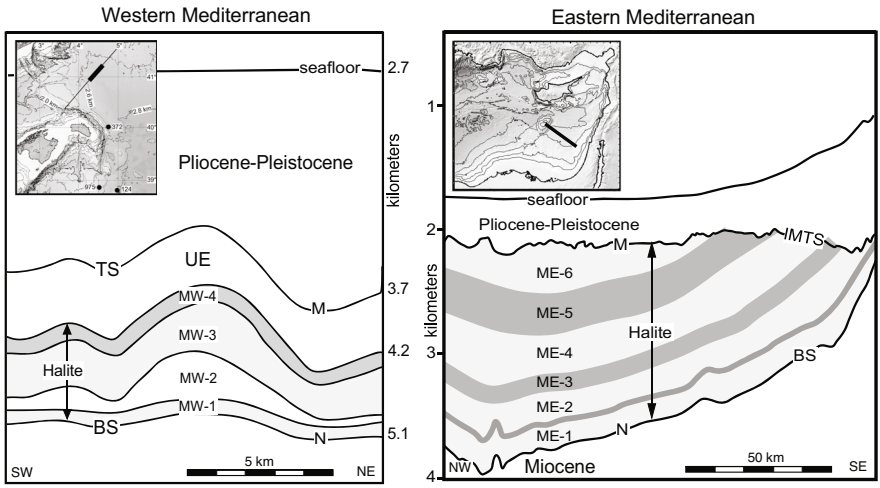

Fig. 69 Differences in the halite sublayers between the western and eastern Mediterranean

To further elucidate the abrupt flooding scenario, a sample was taken a few meters above the Miocene-Pliocene boundary at Site 132 in the Tyrrhenian Sea [505]. This sample of foraminiferal-rich marl had been assigned to the *Sphaeroidinellopsis* Acme zone of the Trubi Fm [56, 395]. Based on calculated sedimentation rates its microfossils would have had an age no younger than the third precession cycle following the opening of the Gibraltar gateway.

Measurements of $\delta^{18}O$ and $\delta^{13}C$ were performed on specimens of planktonic and benthic foraminifera. The oxygen isotopic compositions turned out to be almost identical at $+0.3 \pm 0.1$‰, whereas in the overlying younger sediments the planktonic and benthic compositions differed by as much as -1 to 1.5, with the benthic foraminifera more positive. The value of 0.3‰ for the benthic specimens corresponds to a temperature of 15 °C, if in equilibrium with North Atlantic Deep Water. The identical isotopic composition of the planktonic and benthic foraminifera indicates an early thermal homogeneity of the Mediterranean water column prior to the establishment of a steady-state thermocline. Since the mean surface water temperature of the Atlantic was as warm or warmer than today, a substantial amount of North Atlantic Deep Water was required to bring the average temperature of the Mediterranean interior down to 15 °C.

This experiment was performed again at ODP Site 976 in the Alboran Sea [437]. There the benthic and planktonic values from 0.2 m above the Miocene/Pliocene boundary were also practically the same (+ 0.15 and + 0.19‰) and nearly undistinguishable from those in the Tyrrhenian Sea. However, at the Alboran site additional younger samples of the earliest-Pliocene marls were obtained at 0.1 m intervals over a 2 m interval. In samples where the $\delta^{18}O$ for the benthic and planktonic specimens were the nearly same, the $\delta^{13}C$ were the most divergent (1.2‰) and where the $\delta^{18}O$ for the benthic and planktonic specimens were different (1.0 to 2.0‰), the $\delta^{13}C$ compositions differed by no more than 0.5‰. The strongly negative planktonic $\delta^{13}C$ values were in

organic carbon rich layers with nearly identical $\delta^{18}O$, suggesting continuing Atlantic water renewal to a well-mixed Mediterranean water column capable of stimulating enhanced biological productivity.

A favorable environment for bottom dwellers is observed in the ichnofossil assemblage in the earliest Trubi marls at the Eraclea Minoa site in the Caltanissetta Basin in Sicily [506]). Following the arrival of the cold Atlantic seawater the assemblage became abundant, diverse, well-developed, and symptomatic of a rapid establishment of a deep marine environment with well-oxygenated bottom- and porewaters and the availability of food. Plentiful food stimulated the proliferation of the cold-water-adapted psychrospheric ostracods [443] and the tracemaker communities. The Trubi assemblage differs substantially from that in the underlying Arenazzolo Fm with its unfavorable habitat for tracemaker communities.

A nearly instantaneous restoration of marine conditions in the Mediterranean Sea is registered at many terrestrial locations from Spain [504] to the Apennines [507] as well as in the sediments recovered by deep-sea drilling. At a dozen sites aligned along a west to east transect from the Alboran Sea to the Eratosthenes Seamount in Levantine Basin the $\delta^{18}O$ measurements and $CaCO_3$ content on bulk carbonate exhibited a rapid and progressive increase during the first precession cycle after the introduction of Atlantic seawater [407]. The foraminiferal abundance (P/(P + B) revealed a similar rapid transition to > 80%.

At numerous sampled sections in the northern Apennines more than 12 precession cycles can be recognized in the Trubi marls present above Miocene-Pliocene boundary. The first influx of sinistrally coiled *Neogloboquadrina acostaensis* took place at the boundary between the first and second cycle. The second influx occurred at the base of the 3rd cycle. The base of the *Spheroidinellopsis spp*. acme interval is sandwiched between these two biomarkers. Therefore, when all three biomarkers are present in succession, as they do in the Northern Apennines and elsewhere, they demonstrate that the Mediterranean flooding was not only a synchronous event throughout the entire Mediterranean region, but was accompanied by an abrupt increase in paleodepth estimated at a few hundred meters in the Vera Basin (Spain) [504], 500 m in the Pissouri Basin (Cyprus) [306, 508], 900 m at Eraclea Minoa [509, 510], 950–1400 m in the Alboran Basin [437], 1300 m on the Ebro margin [188], 1300 m on the Florence Rise ([511], 1900 m at the foot of the Gulf of Lions margin [92], and 1800–2000 m in the Ionian Basin [114].

The aforementioned cm/dm-thick dark gray to black layer enriched in organic matter (Fig. 60) is present at the Miocene-Pliocene boundary in many land-based sections (Malaga, Sorbas and Nijar Basins of SE Spain, Northern Apennines, Cyprus, Sicily) and also at Mediterranean drill sites (376, 974, 975). The palaeoenvironmental significance of these dark layers is unclear. In the Northern Apennines and Piedmont Basin, the top of this layer has been placed below the Miocene/Pliocene boundary based on most of the taxa belonging to the uppermost Messinian Stage 3.2.2. However, the presence of some planktonic and rare, poorly diversified benthic foraminifera, almost identical to those found within the lowermost Trubi marls, suggests the possibility of either a transitional environment prior to the definitive re-establishment of open-marine conditions or reworking of the microfossils into the dark layer by the earliest-Pliocene tracemaker communities seeking food in the organic-rich substrate.

The 20-cm-thick bed of sediment at the Miocene/Pliocene boundary in core 22X the Site 374 in the Tyrrhenian Sea has been suggested as a transitional deposit [437, 512]. However, it has the appearance of a breccia mixed with discrete fragments of light olive-gray Trubi clay derived from above and blackish-red silty clay from the Messinian below. This mixture most likely entered the extended core barrel as the weight of drill bit on the formation varied during the passage from softer to firmer lithologies (a routine procedure while adjusting the bearing weight of drill bit when penetration rates suddenly decrease). The uppermost Messinian Lago-Mare Fm at this Tyrrhenian Sea location is distinguished from the overlying Trubi Fm by its parallel laminations, undisturbed by bioturbation and the absence of microfossils.

Others researchers have interpreted the dark gray to black layer as a Pliocene euxinic deposit that developed when the saltwater entered from the Atlantic and sank into the interior of the less saline Mediterranean basins [437]. The resulting stratification reduced the bottom-water oxygen levels. Since the dark layers occur at both deep and shallow margin settings far away from the Gibraltar gateway, a Mediterranean-scale water-mass stratification has been proposed. However, the benthic $\delta^{13}C$ measurements at Site 976 in the Alboran Sea and Site 132 in the Tyrrhenian Sea show that bottom-water renewal rates were high enough to prevent the reduction of $\delta^{13}C$ at the seafloor and development of iron sulfides [437, 505].

17 Conclusions

Wide-spread erosion surfaces on the margins of the Ebro River and Gulf of Lions with patterns of 3 to 5 order dendritic drainage, the gravels containing clasts eroded from the pre-MSC substrate and sampled from a late-Messinian river bed in the Valencia Trough, the cemented gravels in the thalwegs of buried valleys in the Alboran Sea and unconformity hard grounds elsewhere all substantiate a major episode of Mediterranean desiccation at the very end of the MSC. Water levels fell > 1.5 km below the surface of the exterior ocean in the western Mediterranean and > 2 km in the eastern Mediterranean.

The thick pre-MSC Tortonian, Serravallian, Langhian and Burdigalian age (7 to 22 Ma) open-marine sediments in both western and eastern Mediterranean are evidence of pre-existing deep Mediterranean basins, even in the relatively young Tyrrhenian Sea. When restored to their original depths by accounting for flexural isostasy, sediment compaction, and subsidence from the cooling of the lithosphere, these elevations confirmed that the Late Miocene Mediterranean basins were comparable in volume and depth to their modern configurations at the time of the onset of the MSC.

A substantial lowering and shrinkage of Lago-Mare lakes accounts for the terminal alluvial and fluvial conglomerates with remains of mammals and plants in Crete, karst interbedded with soils in Cyprus, black layers with roots of plants and teeth of mammals along both the Adriatic and Tyrrhenian sides of the Apennines, the paleosols in the Tyrrhenian Sea and on the flank of the Eratosthenes Seamount, the exposure of the summit of Eratosthenes Seamount to the development of karst with sink holes, and the development of dolines and notched terraces on the lower margins of the Levant. At the time of the terminal Messinian lowstand, animals of African descent migrated

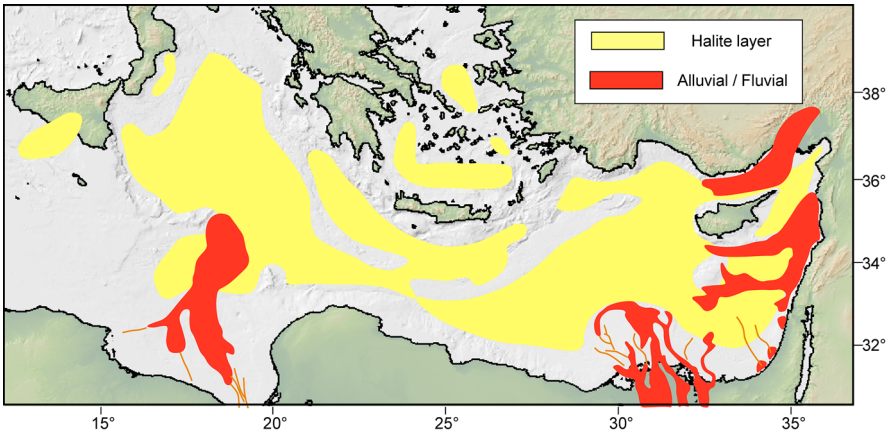

Fig. 70 Large clastic aprons and their fluvial stream beds (red) fed from entrenched continental margin river valleys that spilled onto the top of the massive Messinian halite layer (yellow) in the eastern Mediterranean during Stage 3 of the MSC

to continental Iberia and then traversed the exposed seabed of the Mediterranean to reach the Balearic Islands where they left teeth in karst cavities buried by deep-water earliest-Pliocene marls.

Vast clastic aprons on the African and Levant margins of the eastern Mediterranean attest to the overlooked importance of terrestrial rivers in supplying the Mare-Lago lake water (Fig. 70). These rivers incised deep canyons as they kept pace with falling baselevels. Their meandering distal channels contain sand with minerals from far-away source terranes in Africa, the Near East and Anatolia. The rivers crossed flood plains interbedded with plant roots and coal seams in route to the shores of shrinking playa lakes.

The Paratethys experienced its own lake level fall of 600 to 900 m during the Portaferian substage of the Upper Pontian at the same time as the freshening of the Mediterranean during Stage 3 of the MSC, making it problematic for Paratethan ostracods (with no larval stage) to have been carried into the Mediterranean's Lago-Mare lakes via spillways, instead of transport on the feet and feathers of migrating birds.

When the carbon and oxygen isotopes from the Stage 3.2.2 ostracods, calcite grains from interbedded marls and dolomite grains from mud are plotted separately in their own 2-D space, they show that the Lago-Mare deposits at various locations in the Apennines, Sicily, Spain and at the deep-sea drill sites all had distinctly different isotopic signatures. These differences are further confirmed by strontium isotopes and refute the proposition of a vast single pan-Mediterranean lake at the conclusion of the MSC.

The substantial IMTS became evident in the Caltanissetta Basin in Sicily using hydrogen and oxygen isotopes in H_2O extracted from liquid inclusions on the rims of salt crystals. A combination of isotopic signatures and the extinction levels of calcareous nannofossils and planktonic foraminifera show that the fresh-to-brackish ostracods are in situ in MSC Stage 3, and the calcareous nannofossils and planktonic

foraminifera were reworked from older marine deposits made available by erosion from basin margins when exposed during falling lake levels. The terminal Arenazzolo Formation in Sicily contains the greatest abundance of reworked specimens (> 80%) from strata as old as the Cretaceous and Paleogene.

The 14 to 16 successive beds of selenitic gypsum from the Yesares Member of the Turre and Caños Formations in Spain, the Cattolica Formation in Sicily and the Gessoso Solfifera Formation in the Vena del Gesso Basin in the Apennines corroborate that that gypsum precipitated from a brine that completely filled the entire deep Mediterranean during Stage 1 of MSC. The sulfur, oxygen and strontium isotopes from the sulfates indicate that the major source of the Ca^{++}, $SO_4{}^{--}$ came from the exterior ocean during a time period that preceded the closure of the entrance spillway by 380 ka. The Zorreras Member in Spain, the Pasquasia gypsum beds in Sicily and the Colombacci Formation limestones in the northern Apennines followed the first evaporative drawdown that began at ~ 5.6 Ma. This substantial fall in the brine surface left in its imprint the widespread Intra-Messinian Truncation Surface, a feature attributed to a combination of subaerial erosion and dissolution.

The vast amount of detritus removed by erosion from Mediterranean margins and the interior of the adjacent mainland resides in the alluvial aprons and river beds of the eastern Mediterranean and in the thick 'upper evaporites' in the western Mediterranean and Tyrrhenian Sea.

The band of strong reflections beneath the halite layer in the Liguro Provençal basin and comprising reflection Unit 3 at Mediterranean drill sites 124, 134, 652 and 654 is not from Stage 1 gypsum or shale, but from the preceding Trubi diatomite and equivalent to the Formazione Peliti Eusiniche.

The massive introduction of saltwater from the Atlantic that permanently ended evaporative conditions in the Mediterranean at 5.33 Ma was rapid. This event, known as the Zanclean flood, occurred in the span of a few months or years. Normal marine environments became established and stabilized well before the end of the third precession cycle of the earliest Pliocene.

The contrarians to large-amplitude desiccating events base their reservations on observations of a single feature such as the similarity of Paratethys ostracods with those Mediterranean margin outcrops or on halite dissolution from a single IMTS in the Levant Basin without reference to its absence in the western Mediterranean. A more comprehensive understanding of the MSC desiccation hypothesis comes from the combined integration of all of the geophysical, sedimentological, biostratigraphic, isotopic and geochemical measurements achieved over 50 years by expert teams of sea-going adventurers and terrestrial geologists. These researchers have produced an immense treasure of expedition reports, illustrated guidebooks to field trips, published conference proceedings and > 500 articles in scientific journals, all of which has been a pleasure to review, learn from and appreciate.

Author contributions The author was the sole contributor to the study conception, its design, material preparation, data collection, analysis, preparation of the figures, and the writing of the manuscript.

Funding The author declares that no funds, grants, or other support were received during the preparation of this manuscript.

Data availability All data presented in graphs and illustrations were extracted from published sources cited in the manuscript. Maps were created with the application GeoMapApp (https://www.geomapapp.org) funded by the US National Science Foundation.

Declarations

Conflict of interest Author declares he has no financial interests that are directly or indirectly related to the work submitted for publication.

References

1. G. Ruggieri, The Miocene and later evolution of the Mediterranean Sea, in *Aspects of Tethyan Biogeography*. ed. by C.G. Adams, D.V. Ager (Systematics Association Publisher, London, 1967), pp.283–290
2. G. Ruggieri, Gli esotici neogenici della colata gravitativa della Val Marecchia. Atti Acc Sci Lett Arti Palermo. **17**, 1–169 (1958)
3. C. Lyell, *Principles of Geology* (John Murray, London, 1833)
4. R. Selli, tl bacino del Metauro. Descrizione geologica, risorse minerarie, idrogeologia. Giorn Geol. **24**, 1–268 (1954)
5. R. Selli, Il Messiniano Mayer-Eymar 1867. Proposta di un neostratotipo. Giorn Geol. **28**, 1 (1960)
6. A. Decima, F. Wezel, Observazioni sulle evaporiti messiniane delle Sicilia Centro-meridionale. Riv Min. Sicil. **22**(130–132), 172–187 (1971)
7. A. Decima, F. Wezel, Late Miocene Evaporites of the Central Sicilian Basin, Italy, in *Initial Reports of the Deep Sea Drilling Project*. ed. by W.B.F. Ryan, K.J. Hsü (U.S. Government Printing Office, Washington, D.C., 1973), p.1256
8. Mezzadri: La Serie gessoso-solfifera della Scilia. Lo Zolfa. 30–37 (1962)
9. L. Ogniben, Petrographia della Serie Solfifera-Siciliana e considerazion geotoche relative. Mem Descrit Carta Geol Ital. **33**, 1–275 (1957)
10. G. Ruggieri, Segnalazione di Globoquadrina altispira nei trubi di Buonfornello (Palermo). Riv Min Sicil. **11**, 11 (1960)
11. Alinat, J., Cousteau, J.: Accidents de terrain en mer de Ligurie. Océan. Géologique Geophys. Mediterr. Occident. 121 (1962)
12. J. Alinat, G. Giermann, O. Leenhardt, Reconnaissance sismique des accidents de terrain en mer Ligure. C R Acad. Sci. Paris B. **262**, 1311–1314 (1966)
13. J.B. Hersey, Sedimentary basins in the Mediterranean Sea, in *Submarine Geology and Geophysics*. ed. by W.F. Whittard, R. Bradshaw (Butterworth, London, 1965), pp.75–92
14. O. Leenhardt, Le probléme des domes de la Mediterranée occidentale: étude géophysique d'une colline, la structure A. Bull Soc Géol Fr. **10**, 497–509 (1968)
15. A. Mauffret, Les domes et les structures "anticlinales" de la Mediterranee occidentale au nord-est des Baleare. Rev Lnst Fr Pètrole. **24**, 953–960 (1969)
16. Menard, H.W.: The Rhone deep-sea fan. In: Whittard, W.F. and Bradshaw, R. (eds.) Submarine geology and geophysics: Proceedings 17th Symposium Colston Res. Soc. pp. 271–284. Butterworths, London (1965)
17. W.B.F. Ryan, M. Ewing, J.I. Ewing, Diapirism in the sedimentary basins of the Mediterranean Sea. Am Geophys Union Trans. **47**, 120 (1966)

18. Watson, J.A., Johnson, C.L.: Mediterranean diapiric structures. Geol. Notes. 2247–2243 (1968)
19. H.K. Wong, E.F.K. Zarudzki, Thickness of unconsolidated sediments in the eastern Mediterranean Sea. Bull Geol Soc Am. **54**, 2200–2204 (1969). https://doi.org/10.1130/0016-7606(1969)80[2611:tousit]2.0.co;2
20. W.B.F. Ryan, D.J. Stanley, J.B. Hersey, D.A. Falquist, T.D. Allen, The tectonics and geology of the Mediterranean Sea, in *The Sea*. ed. by A.E. Maxwell (Wiley, New York, 1971)
21. J. Ewing, M. Ewing, Seismic refraction measurements in the Atlantic Ocean basins, in the Mediterranean Sea, on the Mid-Atlantic Ridge and in the Norwegian Sea. Bull Geol Soc Am. **70**, 291 (1959). https://doi.org/10.1130/0016-7606(1959)70[291:smitao]2.0.co;2
22. D.A. Falquist, J.B. Hersey, Seismic refraction measurements in the western Mediterranean Sea. Bull Inst Océan. Monaco. **69**, 1386 (1969)
23. T.F. Gaskell, M.N. Hill, J.C. Swallow, Seismic measurements made by H.M.S. Challenger in the Atlantic, Pacific, and Indian Oceans and in the Mediterranean Sea, 1950–1953. R. Soc Lond. Philos Trans. **251**, 28–83 (1958). https://doi.org/10.1098/rsta.1958.0008
24. T.F. Gaskell, J.C. Swallow, Seismic refraction experiments in the Indian Ocean and in the Mediterranean Sea. Nature **172**, 535–537 (1953). https://doi.org/10.1038/172535b0
25. P. Biscaye, W.B.F. Ryan, F. Wezel, Age and nature of the Pan-Mediterranean sub-bottom reflector M, in *The Mediterranean Sea*. ed. by D.J. Stanley (Dowden, Hutchinson, and Ross, Inc, Stroudsburg, 1972), pp.83–90
26. M. Ewing, J.L. Worzel, C.A. Burk, Regional Aspects of Deep Water Drilling in the Gulf of Mexico, East of the Bahama Platform and on the Bermuda Rise, in *Init. Repts. DSDP*. ed. by M. Ewing, J.L. Worzel, C.A. Burk (U.S. Government Printing Office, Washington, D.C., 1969), pp.624–640
27. A.E. Maxwell, R.P. von Herzen, J.E. Andrews, R.E. Boyce, E.D. Milow, K.J. Hsü, S.F. Percival, T. Saito, Summary and Conclusions, in *Init. Repts. DSDP*. (U.S. Government Printing Office, Washington, D.C., 1970), pp.441–471
28. Shipboard Scientific Party, Boundary of Sardinia slope with Balearic Abyssal Plain-Sites 133 and 134, in *Init. Repts. DSDP*. ed. by W.B.F. Ryan, K.J. Hsü (U.S. Government Printing Office, Washington, D.C., 1973), pp.465–514
29. G. Ferrara, G. Bigazzi, F.P. Bonadonna, O. Giuliani, Radiometric Dating of the Valencia Volcanic Rocks, in *Init. Repts. DSDP*. ed. by W.B.F. Ryan, K.J. Hsü (U.S. Government Printing Office, Washington, D.C., 1973), pp.773–774
30. R.H. Steiger, U. Frick, Isotopic dating of Alboran "basement," in *Init. Repts. DSDP*. ed. by W.B.F. Ryan, K.J. Hsü (U.S. Government Printing Office, Washington D.C., 1973), p.762
31. Shipboard Scientific Party: Cleft in Mediterranean Ridge, Ionian Sea; Site 126. In: Ryan, W.B.F. and Hsü, K.J. (eds.) Init. Repts. DSDP, pp. 219–241. (U.S. Government Printing Office, Washington, D.C., 1973)
32. Shipboard Scientific Party: Western Alboran Basin; Site 121. In: Ryan, W.B.F., Hsü, K.J. (eds.) Init. Repts. DSDP, pp. 43–89. (U.S. Government Printing Office, Washington D.C., 1973)
33. W.H. Blow, Late Middle Eocene to Recent planktonic foraminiferal biostratigraphy. In: Brill (ed.) Proc. I. Intern. Conference Plankt. Microf, p. 199, Geneva (1969)
34. M.B. Cita, W.H. Blow, The biostratigraphy of the Langhian, Serravallian and Tortonian stages in the type- sections in Italy. Riv Ital Paleont Strat. **75**, 549–603 (1969)
35. E. Martini, Standard Tertiary and Quaternary calcareous nannoplankton Zonation. In: Farinacci, A. (ed.) Proceedings Planktonic Conference Rome 1970, pp. 739–785. (Edizioni Tecnoscienza, Rome, 1971)
36. Shipboard Scientific Party: Valencia Trough; Site 122. In: Ryan, W.B.F., Hsü, K.J. (eds.) Init. Repts. DSDP, pp. 91–109. (U.S. Government Printing Office, Washington D.C., 1973)
37. J.G.C.M. Fuller, J.W. Porter, Evaporite formations with petroleum reservoirs in Devonian and Mississippian of Alberta, Saskatchewan, and North Dakota. Bull. Am. Assoc. Pet. Geol. **53**, 909–926 (1969). https://doi.org/10.1306/5d25c809-16c1-11d7-8645000102c1865d
38. M.B. Cita, Mediterranean evaporite: Paleontological arguments for a deep basin desiccation model, in *Messinian Events in the Mediterranean*. ed. by C.W. Drooger (North-Holland Publisher Co, Amsterdam, 1973), pp.206–228
39. M. Hajos, The Mediterranean Diatoms, in *Initial Reports of the Deep Sea Drilling Project*. ed. by W.B.F. Ryan, K.J. Hsü (U.S. Government Printing Office, Washington, D.C., 1973), pp.944–969

40. G.M. Friedman, Petrographic data and comments on the depositional environment of the Miocene sulphates and dolomites at Sites 124, 132 and 134, Western Mediterranean Sea, in *Init. Repts. DSDP*. ed. by W.B.F. Ryan, K.J. Hsü (U.S. Government Printing Office, Washington, D.C., 1973), pp.695–708
41. Shipboard Scientific Party: Balearic Rise; Site 124. In: Ryan, W.B.F., Hsü, K.J. (eds.) Init. Repts. DSDP, pp. 133–174. U.S. Government Printing Office, Washington D.C. (1973)
42. G. Evans, The recent sedimentary focus of the Persian Gulf region. R. Soc. Lond. Philos. Trans. Ser. A. **259**, 291 (1966)
43. D.J.J. Kinsman, Gypsum and anhydrite of Recent age, Trucial Coast, Persian Gulf. Presented at the Second symposium on salt, Cleveland, OH (1966)
44. D.J.J. Kinsman, Modes of formation, sedimentary associations, and diagnostic features of shallow-water and supratidal evaporites. Bull. Am. Assoc. Pet. Geol. **53**, 830 (1969). https://doi.org/10.1306/5d25c801-16c1-11d7-8645000102c1865d
45. K.J. Hsü, Origin of saline giants: a critical review after the discovery ot the Mediterranean evaporite. Earth-Sci. Rev. **8**, 371–396 (1972). https://doi.org/10.1016/0012-8252(72)90062-1
46. K.J. Hsü, *The Mediterranean was a Desert* (Princeton University Press, Princeton, 1984)
47. S.M. Bernasconi, Interstitial water chemistry in the Western Mediterranean: Results from Leg 161, in *Proc. ODP, Sci. Results*, *161*, ed. by R. Zahn, M.C. Comas, A. Klaus (Ocean Drilling Program, College Station, TX, 1999), pp. 413-432
48. F.L. Sayles, L.S. Waterman, F.T. Manheim, Interstitial Water Chemistry: Deep Sea Drilling Project, Leg 13, in *Initial Reports of the Deep Sea Drilling Project*. ed. by W.B.F. Ryan, K.J. Hsü (U.S. Government Printing Office, Washington, D. C., 1973), pp.801–808
49. B.J. Presley, C. Petrowski, I.R. Kaplan, W.B.F. Ryan, Interstitial water chemistry: deep sea drilling project, leg 13, in *Init. Repts. DSDP*. ed. by W.B.F. Ryan, K.J. Hsü (U.S. Government Printing Office, Washington, D.C., 1973), pp.809–811
50. N. Krstić, Ostracodes des couches congériennes: 1. Cyprideis I. Bull. Muséum D'Histoire Nat. Belgrade A **23**, 107–151 (1968)
51. N. Krstić, Ostracode biofacies in the Pannone. In: Oertli, H.J. (ed.) Paleoecologie Ostracodes, p. 391. Bull. Centre Rech. Pau-SNPA (1968)
52. N. Krstić, Ostracodes des couches congériennes: 3. Cyprideis II. Bull. Muséum D'Histoire Nat. Belgrade A. **23**, 153–183 (1968)
53. L.A. Zenkevich, Caspian and Aral Seas. In: Hedgpeth, J.W. (ed.) Treatise on Marine Ecology and Paleoecology, pp. 891–916. Geol. Soc. Am. Memoir (1957)
54. M.L. Colalongo, Ostracodi del Neostratigrafici del Messiniano. Presented at the Coing. Medit. Neog. Strat., IV sess., Bologna (1968)
55. A. Decima, Ostracodi del genere Cyprideis Jones nel Neogene e Quaternario Italiani. Paleontogr. Ital. **57**, 81–133 (1964)
56. Shipboard Scientific Party: Tyrrhenian—Site 132. In: Ryan, W.B.F., Hsü, K.J. (eds.) Init. Repts. DSDP, pp. 403–464. (U.S. Government Printing Office, Washington D.C., 1973)
57. R.W. Thompson, Tidal Flat Sedimentation on the Colorado River Delta, Northwestern Gulf of California. Geol. Soc. Am. Mem. **107**, 133 (1968). https://doi.org/10.1130/MEM107-p1
58. K. Kelts, Texture and Mineralogy of Some Clastic Sediments from Site 133—Western Sardinia Slope, in *Init. Repts. DSDP*. ed. by W.B.F. Ryan, K.J. Hsü (U.S. Government Printing Office, Washington, D.C., 1973), pp.729–731
59. K.J. Hsü, W.B.F. Ryan, B.C. Schreiber, Petrography of a halite sample from Hole 134—Balearic abyssal plain, in *Init. Repts. DSDP*. ed. by W.B.F. Ryan, K.J. Hsü (U.S. Government Printing Office, Washington, D.C., 1973), pp.708–711
60. R. Kuehn, K.J. Hsü, Bromine content of Mediterranean halite. Geology **2**, 213–216 (1975)
61. W.L. Badger, E.M. Baker, *Inorganic Chemical Technology* (McGraw Hill, New York, 1928)
62. L.F. Dellwig, Origin of the Salina Salt of Michigan. J. Sed. Pet. **25**, 83–110 (1955). https://doi.org/10.1306/d4269819-2b26-11d7-8648000102c1865d
63. L.F. Dellwig, R. Evans, Depositional processes in Salina Salt of Michigan, Ohio and New York. AAPG Bull. **53**, 040–956 (1969). https://doi.org/10.1306/5d25c80d-16c1-11d7-8645000102c1865d
64. W.D. Nesteroff, Pétrographie des évaporites messiniennes de la Méditerranée. Comparaison des forages JOIDES-DSDP et des dépôts du bassin de Sicile, in *Messinian Events in the Mediterranean*. ed. by C.W. Drooger (North-Holland Publisher Co, Amsterdam, 1973), pp.111–113

65. B.C. Schreiber, Survey of the physical features of Messinian chemical sediments, in *Messinian Events in the Mediterranean*. ed. by C.W. Drooger (North-Holland Publisher Co, Amsterdam, 1973), pp.101–110
66. N. Fanuko, Possible relation between a bloom of Distephanus speculum (Silicoflagellata) and anoxia in bottom waters in the Northern Adriatic, 1983. J Plankt Res. **11**, 75–84 (1989). https://doi.org/10.1093/plankt/11.1.75
67. R. Kühn, Tiefberechnung des Zechstein meeres nach dem bromgehalt der salze. Dtsch. Geol Gesell Zeitschr. **105**, 646–663 (1955)
68. R. Kühn, Geochemistry of the German potash deposits. Geol Soc Am Spec Pap. **88**, 427–504 (1968). https://doi.org/10.1130/spe88-p427
69. J.C. Fontes, R. Letolle, W.D. Nesteroff, W.B.F. Ryan, Oxygen, carbon, sulfur and hydrogen stable isotopes in carbonate and sulfate mineral phases of neogene evaporites, sediments, and in interstitial waters, in *Init Repts DSDP*. ed. by W.B.F. Ryan, K.J. Hsü (U.S. Government Printing Office, Washington D.C., 1973), pp.788–796
70. J.C. Fontes, C. Lepvrier, F. Mélières, C. Pierre, Isotopes stables dans les carbonates évaporitiques du Miocene supérieur de la Méditerranée oceidentale, in *Messinian Events in the Mediterranean*. ed. by C.W. Drooger (North-Holland, Amserdam, 1973), pp.91–100
71. R.M. Lloyd, K.J. Hsü, K.J. Hsü, Stable isotope investigations of the Miocene evaporites and Pliocene and Pleistocene sedimentary rocks and oozes, in *Init. Repts. Deep Sea Drill Proj*. ed. by W.B.F. Ryan, K.J. Hsü (U.S. Government Printing Office, Washington, D.C., 1973), pp.783–787
72. W.T. Parry, C.C. Reeves, J.W. Leache, Oxygen and carbon isotopic composition of West Texas lake carbonates. Geochim. Cosmochim. Acta. **34**, 825–830 (1970). https://doi.org/10.1016/0016-7037(70)90032-3
73. N. Clauer, 87Sr/86Sr composition of evaporitic carbonates and sulphates from Miocene sediment cores in the Mediterranean Sea (D.S.D.P., Leg 13). Sedimentology **23**, 133–140 (1976). https://doi.org/10.1111/j.1365-3091.1976.tb00043.x
74. E.J. Dash, P.E. Biscaye, Isotopic composition of strontium in Cretaceous-to-recent, pelagic foraminifera. Earth Planet Sci. Lett. **11**, 201–204 (1971). https://doi.org/10.1016/0012-821x(71)90164-6
75. Z.E. Peterman, C.E. Hedge, H.A. Tourtelot, Isotopic composition of strontium in seawater throughout Phanerozoic time. Geochim. Cosmochim. Acta. **34**, 105–120 (1970). https://doi.org/10.1016/0016-7037(70)90154-7
76. R.M. Lloyd, Oxygen isotope composition of oceanic sulfate. Science **156**, 1228 (1967). https://doi.org/10.1126/science.156.3779.1228
77. A. Longinelli, H. Craig, Oxygen 18 variations in sulfate ions in sea water and saline lakes. Science **156**, 56 (1967). https://doi.org/10.1126/science.156.3771.56
78. G. Denizot, Les anciens rivages de la Mediterranee francaise. Bull. Inst. Ocean. Monaco. **992**, 56 (1951)
79. G. Denizot, Le Pliocéne dans la vallée du Rhone. Rév. Géogr. Lyon. **27**, 327 (1952)
80. M.B. Cita, *Inventory of Biostratigraphical Findings and Problems* (U.S. Government Printing Office, Washington, 1973)
81. I.S. Chumakov, Pliocene and Pleistocene deposits of the Nile Valley in Nubia and Upper Egypt. Acad Sci. USSR GeolInstitute Trans. **170**, 5 (1967)
82. I.S. Chumakov, Pliocene and Pleistocene deposits of the Nile valley in Nubia and Upper Egypt, in *Init. Repts. DSDP*. ed. by W.B.F. Ryan, K.J. Hsü (U.S. Government Printing Office, Washington, D.C., 1973), pp.1242–1243
83. F.T. Barr, B.R. Walker, Late Tertiary channel system in Northern Libya and Its Implications on Mediterranean sea level changes, in *Initial Reports of the Deep-Sea Drilling Project*. ed. by W.B.F. Ryan, K.J. Hsü (U.S. Government Printing Office, Washington, D. C., 1973), pp.1244–1251
84. C.W. Drooger, The Messinian events in the Mediterranean, a review, in *Messinian Events in the Mediterranean*. ed. by C.W. Drooger (North-Holland Publ. Co., Amserdam, 1973), pp.263–272
85. W.D. Nesteroff, Un modéle pour les évaporites messiniennes en Méditerranée, bassins peu profonds avec dépot d'évaporites lagunaires, in *Messinian Events in the Mediterranean*. ed. by C.W. Drooger (North-Holland Publ. Co., Amsterdam, 1973), pp.68–81
86. J.-M. Auzende, J. Bonnin, J.-L. Olivet, G. Pautot, A. Mauffret, Upper Miocene salt layer in the Western Mediterranean basin. Nat. Phys. Sci. **230**, 82–84 (1971). https://doi.org/10.1038/physci230082a0

87. G. Bellaiche, Prélèvement par 2000 m de profondeur d'un reflecteur acoustique d'âge pliocene inférieur à faciès peu profond (canyon des Stoechadea, Méditerranée nord-occidentale). Nouvelles données sur le creusement des canyons sous-marins et l'amplitude des mouvements verticaux ponto-plio-quaternaire. C R Acad Sc Paris. **275**, 321–324 (1972)
88. J. Bourcart, La Mediterranée et la révolution du Pliocéne. In: L'evolution paleogeopgraphique et structurale des domaines Mediterranéens et alpins d'Europe. Livre Mém. Prof. P. Fallot. pp. 103–116. Mém. h. sér Soc. géol. France (1962)
89. L. Glangeaud, Les grands ensembles structureaux de la Méditerranée occidental d'aprées les données de Geomede 1. Paris Acad Sci Comptes Rendus. **262**, 2405–2408 (1966)
90. O. Leenhardt, Distribution and thickness of the Messinian evaporites in the Western Mediterranean, in *Messinian Events in the Mediterranean*. ed. by C.W. Drooger (North-Holland Publ. Co, Amsterdam, 1973), pp.39–43
91. P.F. Burollet, P. DeFaure, The Neogene series drilled by the Mistral No. I well in the Gulf of Lion. In: Stanley, D.J. (ed.) The Mediterranean Sea—A Natural Sedimentation Laboratory. pp. 91–98. (Dowden Hutchinson & Ross, Stroudsburg, 1972)
92. W.B.F. Ryan, Quantitative evaluation of the depth of the western Mediterranean before, during and after the Late Miocene salinity crisis. Sedimentology **23**, 791–813 (1976). https://doi.org/10.1111/j.1365-3091.1976.tb00109.x
93. A. Ginzberg, Geophysical studies in the central coastal plain and western Emeg (1960)
94. S. Ginzburg, S.S. Cohen, H. Hay-Roe, A. Rosenzwwg, Geology of Mediterranean Shelf of Israel. Bull. Am. Assoc. Pet. Geol. **59**, 2142–2160 (1975). https://doi.org/10.1306/83D9220D-16C7-11D7-8645000102C1865D
95. P.M. Barber, Messinian subaerial erosion of the proto-Nile Delta. Mar. Geol. **44**, 253–272 (1981). https://doi.org/10.1016/0025-3227(81)90053-0
96. A. Decima, R. Sprovieri, Comments on late Messinian microfaunas in several sections from Sicily, in *Messinian Events in the Mediterranean*. ed. by C.W. Drooger (North-Holland, Amsterdam, 1973), pp.229–234
97. G. Richter-Bernberg, Facies and paleogeography of the Messinian evaporites in Sicily, in *Messinian Events in the Mediterranean*. ed. by C.W. Drooger (North-Holland Publ Co, Amsterdam, 1973), pp.124–141
98. R.F. Schmalz, Deep-water evaporite deposition: a genetic model. AAPG Bull. (1969). https://doi.org/10.1306/5D25C7FD-16C1-11D7-8645000102C1865D
99. A. Mauffret, J.P. Fail, L. Montadert, J. Sancho, E. Winnock, Northwestern Mediterranean sedimentary basin from seismic reflection profile. Bull. Am. Assoc. Pet. Geol. **57**, 2245–2262 (1973). https://doi.org/10.1306/83d912e0-16c7-11d7-8645000102c1865d
100. L. Montadert, J. Sancho, J.P. Fail, J. Debyser, E. Winnock, De l'âge tertiaire de la série salifère responsable des structures diapiriques en Méditerranée occidentale (Nord-Est des Baléares). CR Acad. Sci. Paris. **271**, 812–815 (1970)
101. R. Selli, An outline of the Italian Messinian, in *Messinian Events in the Mediterranean*. ed. by C.W. Drooger (North-Holland Publ. Co, Amsterdam, 1973), pp.150–171
102. G.C. Parea, F. Ricci Lucchi, Resedimented evaporites in the Periadriatic Trough (Upper Miocene, Itlay). Isr. J. Earth Sci. **21**, 25 (1972)
103. F. Ricci Lucchi, Resedimented evaporites: indicators of slope instability and deep-basain conditions-din Periadriatic Messinian (Appennines foreedeep, Italy), in *Messinian Events in the Mediterranean*. ed. by C.W. Drooger (North-Holland Publ. Co, Amsterdam, 1973), pp.142–149
104. A. Decima, Initial data on bromine distribution in the Miocene salt formation of southern Sicily. In: Catalano, R., Ruggieri, G., and Sproveri, R. (eds.) Messinian evaporites in the Mediterranean. pp. 39–43. Mem. Soc. Geol. Ital. (1976)
105. R.W.H. Butler, W.H. Lickorish, M. Grassio, H.M. Pedley, L. Ramberti, Tectonics and sequence stratigraphy in Messinian basins, Sicily: Constraints on the initiation and termination of the Mediterranean salinity crisis. Bull. Geiol. Soc. Am. **107**, 425–439 (1995). https://doi.org/10.1130/0016-7606(1995)107%3c0425:tassim%3e2.3.co;2
106. P.G. Finckh, Are southern Alpine lakes former Messinian canyons?—geophysical evidence for preglacial erosion in the southern Alpine lakes. Mar. Geol. **27**, 289–302 (1978). https://doi.org/10.1016/0025-3227(78)90036-1

107. A. Bini, M.B. Cita, M. Gaetani, Southern Alpine lakes—hypothesis of an erosional origin related to the Messinian entrenchment. Mar Geol. **27**, 271–288 (1978). https://doi.org/10.1016/0025-3227(78)90035-X
108. A. Rizzini, F. Vezzani, V. Cococcetta, G. Almagor, Stratigraphy and sedimentation of a Neogene-Quaternary section in the Nile Delta area. Mar Geol. **27**, 327–348 (1978). https://doi.org/10.1016/0025-3227(78)90038-5
109. W.B.F. Ryan, M.B. Cita, The nature and distribution of Messinian erosional surfaces-Indicators of a several-kilometer-deep Mediterranean in the Miocene. Mar. Geol. **27**, 193–230 (1978). https://doi.org/10.1016/0025-3227(78)90032-4
110. A. Maldonado, O. Riba, Les rapports sédimentaires du Néogène et du Quaternaire dans le plateau continental aux environs du delta de l'Ebre (Espagne). Mem. Inst. Geol. Basin Aquitaine. **7**, 321–329 (1974)
111. W.T. Stoeckinger, Valencian Gulf offers deadline news. Oil Gas J. **29**, 197–204 (1976)
112. W.B.F. Ryan, Messinian badlands on the southeastern margin of the Mediterranean Sea. Mar. Geol. **27**, 349–363 (1978). https://doi.org/10.1016/0025-3227(78)90039-7
113. L.A. Hardie, H.P. Eugster, The depositional environment of marine evaporites: a case for shallow, clastic accumulation. Sedimentology **16**, 187–220 (1971). https://doi.org/10.1111/j.1365-3091.1971.tb00228.x
114. Shipboard Scientific Party: Site 374: Messina Abyssal Plain. In: Hsü, K.J., Montadert, L. (eds.) Init. Repts. DSDP. pp. 176–216. (U.S. Government Printing Office, Washington D.C., 1978)
115. R.E. Garrison, B.C. Schreiber, D. Bernoulli, F.H. Fabricius, R.B. Kidd, F. Mélières, Sedimentary petrology and structures of Messinian evaporitic sediments in the Mediterranean Sea, in *Init. Repts. DSDP*. ed. by K.J. Hsü, L. Montadert (US Government Printing Office, Washington, D.C., 1978), pp.571–612
116. T.E. Ricchiuto, J.A. McKenzie, Stable isotopic investigation of Messinian sulfate samples from DSDP Leg 42A, Eastern Mediterranean seas, in *Init. Repts. DSDP*. ed. by K.J. Hsü, L. Montadert (U.S. Government Printing Office, Washington D.C., 1978), pp.657–660
117. K.H. Wallhauser, U. Puchelt, Sulfate reducing bacteria in sulphur springs and underground waters of Germany and Austria. Contrib. Min. Pet. **13**, 12–30 (1965)
118. J.A. McKenzie, T.E. Ricchiuto, Stable Isotopic Investigation of Carbonate Samples Related to the Messinian Salinity Crisis from DSDP Leg 42A, Mediterranean Sea, in *Init Repts Deep Sea Drill Proj*. ed. by K.J. Hsü, L. Montadert (US Government Printing Office, Washington D.C., 1978), pp.650–655
119. R. Kuehn, K.J. Hsü, Chemistry of Halite and Potash Salt Cores, DSDP Sites 374 and 376, Leg 42A, Mediterranean Sea. In: Hsü, K.J. and Montadert, L. (eds.) Init. Repts. DSDP. pp. 613–619. (U.S. Government Printing Office, Washington D.C., 1978)
120. H. Schrader, R. Gersonde, The late Messinian Mediterranean brackish to freshwater environment, diatom floral evidence, in *Init. Repts. DSDP*. ed. by K.J. Hsü, L. Montadert (U.S. Government Printing Office, Washington, D.C., 1978), pp.761–775
121. M.B. Cita, S. Santambrogio, B. Melillo, F. Rogate, Messinian paleoenvironments: New evidence from the Tyrrhenian Sea (ODP Leg 107). In: Kastens, K.A., Mascle, J. (eds.) Proc. ODP, Sci. Results. pp. 211–227. College Station TX (1990)
122. S.M. Iaccarino, A. Bossio, Paleoenvironment of uppermost Messinian sequences in the western Mediterranean (Sites 974, 975, and 978). In: Zahn, R., Comas, M.C., and Klaus, A. (eds.) Proc. ODP Sci. Res,. pp. 529–541. Ocean Drilling Program, College Station, TX (1999)
123. D.W. Müller, P.A. Mueller, J.A. McKenzie, Strontium isotopic ratios as fluid tracers in Messinian evaporites of the of the Tyrrhenian Sea (Western Mediterranean Sea). In: Kastens, K., Mascle, J. (eds.) Proc. Ocean Drill. Program Sci. Results. pp. 603–614. Ocean DFilling Program, College Station TX (1990)
124. H. Clauren, G. Tardy, Distinction, par la composition isotopique du strontium contenu dans les carbonates, entre le milieu continental des vieux socles cristallins et le milieu marin. C R Hehd Sianc Acad. Sci. Paris. **273**, 2191–2194 (1971)
125. Shipboard Scientific Party: Site 652: Lower Sardinian Margin. In: Kastens, K.A., Mascle, J., Auroux, C., et al. (eds.) Proc., Init. Repts. (Pt. A). pp. 403–597. (Ocean DFilling Program, College Station, 1987)
126. Shipboard Scientific Party: Site 654: Upper Sardinian Margin. In: Kastens, K.A., Mascle, J., Auroux, C., and et al. (eds.) Proc., Init. Repts. (Pt. A). pp. 747–875. Ocean DFilling Program, College Station TX (1987)

127. H. Chamley, P. Debrabant, C. Robert, G. Mascle, J.P. Rehault, J. Aprahamian, Mineralogical and geochemical investigations on latest Miocene deposits in the Tyrrhenian Sea (ODP leg 107). In: Proc. ODP Sci. Results. pp. 153–167. (U.S. Government Printing Office, Washington D.C., 1990)
128. R. Satori, G. Mascle, S. Amaudric du Chaffaut, A review of circum-Mediterranean regional geology. In: Kastens, K.A., Mascle, J. (eds.) Proceedings of the Ocean Drilling Program, Scientific Results. pp. 37–63. College Station TX (1990)
129. F.J. Pettijohn, *Sedimentary Rocks* (Harper Row, New York, 1957)
130. C.J.R. Braitewaite, Calcrete and other soils in Quaternary limestones: structures, processes and applications. Jour Geol Soc Lond. **140**, 351–363 (1983). https://doi.org/10.1144/gsjgs.140.3.0351
131. C.O. Major, W.B.F. Ryan, Eratosthenes seamount: Record of late Miocene sea-level changes and facies related to the Messinian salinity crisis. Mem. Soc. Geol. Ital. **54**, 47–59 (1999)
132. E.J. Follows, Patterns of reef sedimentation and diagenesis in the Miocene of Cyprus. Sed. Geol. **25**, 225–253 (1992). https://doi.org/10.1016/0037-0738(92)90013-h
133. M. Esteban, Significance of the Upper Miocene coral reefs of the western Mediterranean. Palaeogeogr Palaeoclim. Palaeoecol. **29**, 169–188 (1979). https://doi.org/10.1016/0031-0182(79)90080-4
134. L. Polmar, Reef geometries, erosion surfaces and high frequency sea-level changes, Upper Miocene reef complex, Mallorca, Spain. Sedimentology **38**, 243–270 (1991). https://doi.org/10.1111/j.1365-3091.1991.tb01259.x
135. J.M. Rouchy, J.-P. Saint Martin, Late Miocene events in the Mediterranean as recorded by carbonate-evaporice relations. Geology **20**, 629–632 (1992). https://doi.org/10.1130/0091-7613(1992)020%3c0629:LMEITM%3e2.3.CO;2
136. M. Esteban, J. Giner, Messinian coral reefs and erosion surfaces in Cabo de Gata (Almeria, SE Spain). Acta Geol. Hisp. **15**, 97–104 (1980)
137. M.E. Böttcher, Y. Mart, H.-J. Brumsack, Geochemistry of Pliocene and Miocene carbonates from the Eratosthenes Seamount (Site 965). In: Robertson, A.H.F., Emeis, K.-C., Richter, C., Camerlenghi, A. (eds.) Proc. ODP, Sci. Results. pp. 447–452. Ocean Drilling Program, College Station, TX (1998)
138. Shipboard Scientific Party: Site 965. In: Emeis, K.-C., Robertson, A.H.F., Richter, C., et al. (eds.) Proc. ODP, Init. Repts. pp. 125–153. (Ocean Drilling Program, College Station, 1996)
139. C.O. Major, W.B.F. Ryan, M.J. Jurado-Rodríguez, Evolution of paleoenvironments of Eratosthenes seamount based on downhole logging integrated with carbonate petrology and reflection profiles. In: Robertson, A.H.F., Emeis, K.-C., Richter, C., Camerlenghi, A. (eds.) Proc. ODP Sci.Results. pp. 483–508. Ocean Drilling Program, College Station, TX (1998)
140. S. Spezzaferi, M.B. Cita, J.A. McKenzie, The Miocene/Pliocene boundary in the eastern Mediterranean: results from ODP Leg 160, Sites 967 and 969. In: Robertson, A.H.F., Emeis, K.-C., Richter, C., Camerlenghi, A. (eds.) Proc. ODP Sci. Results. pp. 9–28. Ocean Drilling Program, College Station, TX (1998)
141. M.-M. Blanc-Valleron, J.-M. Rouchy, C.J. Allègre, D. Badaut-Ttauth, M. Schuler, Evidence of Messinian non-marine deposition at Site 968 (Cyprus lower slope). In: Emeis, K.-C., Robertson, A.H.F., Richter, C., Camerlenghi, A. (eds.) Proceedings of the Ocean Drilling Program, Scientific Results, Vol. 160. pp. 437–445. Ocean Drilling Program, College Station, TX (1998)
142. D. Do Couto, S.-M. Popescu, J.P. Suc, M.C. Melinte-Dobrinescu, N. Barhoum, C. Gorini, L. Jolivet, J. Poort, G. Jouannic, J.-L. Auxietre, Lago Mare and the Messinian Salinity Crisis: evidence from the Alboran Sea (S Spain). Mar Pet. Geol. **52**, 57–76 (2014). https://doi.org/10.1016/j.marpetgeo.2014.01.018
143. M.C. Comas, R. Zahn, A. Klaus, C. Aubourg, P.E. Belanger, S.M. Bernasconi, W. Cornell, E.P. de Kaenel, F.D. de Larouziére, Proceedings of the Ocean Drilling Program, Initial Reports. Ocean Drilling Program, College Station TX (1996)
144. K.J. Hsü, P.J. Fox, W.B.F. Ryan, Petrography of the Western Alboran Basin "Basement," in *Init. Repts. DSDP*. ed. by W.B.F. Ryan, K.J. Hsü (U.S. Government Printing Office, Washington, D.C., 1973), pp.753–758
145. Shipboard Scientific Party: Site 976. In: Comas, M.C., Zahn, R., Klaus, A., and et al. (eds.) Proc. ODP, Init. Repts. pp. 179–297. Ocean Drilling Program, College Station TX (1996)
146. M.B. Cita, W.B.F. Ryan, Timescale and General Synthesis. In: Ryan, W.B.F., Hsü, K.J. (eds.) Init. Repts. DSDP. pp. 1405–1415 (1973)
147. P. Ambrosetti, A. Azzaroili, F.P. Bonadonna, M. Follieri, A scheme of Pleistocene chronology for the Tyrrhenian side of central Italy. Boll Soc. Geol. Ital. **91**, 169 (1972)

148. J.P. Beckmann, The Foraminifera of Sites 68 to 75, in *Init. Repts. DSDP*. ed. by J.I. Tracey, G. Sutton (U.S. Government Printing Office, Washington D.C., 1971), pp.713–725
149. D.G. Jenkins, W.H. Orr, Planktonic foraminiferal biostratigraphy of the eastern equatorial Pacific-DSDP Leg 9, in *Init. Repts. DSDP*. ed. by J.D. Hays (U.S. Government Printing Office, Washington, D.C., 1972), pp.1–41
150. D.S. Wilson, Confidence intervals for motion and deformation of the Juan de Fuca. J Geophys Res. **98**, 16053–16071 (1993). https://doi.org/10.1029/93jb01227
151. D.S. Wilson, Confirmation of the astronomical calibration of the magnetic polarity timescale from seafloor spreading rates. Nature **364**, 778–790 (1993). https://doi.org/10.1038/364788a0
152. S.C. Cande, D.V. Kent, A new geomagnetic polarity time scale for the Late Cretaceous and Cenozoic. J Geophys Res. **97**, 13197–13961 (1992). https://doi.org/10.1029/92jb01202
153. F.J. Hilgen, C. Langereis, A critical re-evaluation of the Miocene/Pliocene boundary as defined in the Mediterranean. Earth Planet Sci. Lett. **118**, 167–170 (1993). https://doi.org/10.1127/nos/16/1986/169
154. J.D.A. Zijderveld, W.J. Zachariasse, P.J.J.M. Verhallen, The age of the Miocene-Pliocene boundary. Newsl. Strat. **16**, 169–181 (1986)
155. W.A. Berggren, D.V. Kent, J.A. van Couvering, Cenozoic geochronology, in *Geochronology and the Geologic Record*. ed. by N.J. Snelling (Geol. Soc, London, 1985), pp.211–260
156. J.E.T. Channell, M. Torii, T. Hawthorne, Magnetostratigraphy of Sediments Recovered at Sites 650, 651, 652, and 654 (Leg 107, Tyrrhenian Sea). In: Kastens, K.A., Mascle, J., and et al. (eds.) Proceedings of the Ocean Drilling Program, Scientific Results. pp. 335–346. Ocean Drilling Program, College Station TX (1990)
157. F.J. Hilgen, Extension of the astronomically calibrated (polarity) time scale to the Miocene/Pliocene boundary. Earth Planet Sci. Lett. **107**, 349–368 (1991)
158. A. Berger, L.J. Lourens, Insolation values for the climate of the last 10 Myr. Quat. Sci. Rev. **10**, 297–317 (1991). https://doi.org/10.1016/0277-3791(91)90033-q
159. Selli, R.: Report on the Absolute Age. In: Committee Mediterranean Neogene Stratigraphy. p. 51. Giorn. Geol., Bologna (1970)
160. W.A. Berggren, Cenozoic chronostratigraphy, planktonic foraminiferal zonation and the radiometric time scale. Nature **224**, 1072–1705 (1969). https://doi.org/10.1038/2241072a0
161. D. Bukry, Coccolith Stratigraphy, Leg 8, Deep Sea Drilling Project, in *Init. Repts. DSDP*. ed. by J.I. Tracey, G. Sutton (U.S. Government Printing Office, Washington D.C., 1971), pp.791–807
162. D. Bukry, Coccolith stratigraphy, Leg 9, in *Initial reports of the Deep Sea Drilling Project*. ed. by J.D. Hays (US Government Printing Office, Washington D.C., 1972), pp.817–832
163. R. Catalano, R. Sproveri, Biostratigrafia di aicune serie saheliane (Messiniano inferiore) in Sicilia. In: Farinacci, A. (ed.) Proc. II Planktonic Conf. pp. 211–249. Rome (1971)
164. R. Sproveri, E. Di Stefano, A. Caruso, S. Bonomo, High resolution stratigraphy in the Messinian Tripoli Formation in Sicily. Paleopelagos. **6**, 415–435 (1996)
165. M.L. Colalongo, A. Di Grande, S. D'Onofrio, L. Giannelli, S.M. Iaccarino, R. Mazzui, M. Romeo, G. Salvatorini, Stratigraphy of Late Neogene Italian sections straddling the Tortonian/Messinian boundary. Boll. Soc. Paleontol. It. **18**, 258–302 (1979)
166. C.G. Langereis, W.J. Zachariasse, J.D.A. Zijderveld, Late Miocene magnetobiostratigraphy of Crete. Mar Micropaleontol. **8**, 261–281 (1984). https://doi.org/10.1016/0377-8398(84)90017-3
167. F.J. Hilgen, W. Krijgsman, Cyclostratigraphy and astrochronology of the Tripoli diatomite formation (pre-evaporite Messinian, Sicily, Italy). Terra Nova **11**, 16–22 (1999). https://doi.org/10.1046/j.1365-3121.1999.00221.x
168. W. Krijgsman, F.J. Hilgen, A. Santarelli, W.J. Zachariasse, Late Miocene magnetostratigraphy, biostratigraphy and cyclostratigraphy in the Mediterranean. Earth Planet Sci. Lett. **136**, 475–494 (1995). https://doi.org/10.1016/0012-821x(95)00206-r
169. S.C. Cande, D.V. Kent, Revised calibration of the geomagnetic polarity time scale for the Late Cretaceous and Cenozoic. J. Geophys. Res. **100**, 6093–6090 (1995). https://doi.org/10.1029/94jb03098
170. F.J. Hilgen, Integrated stratigraphy and astrochronology of the Messinian GSSP at Oued Akrech (Atlantic Morocco). Earth Planet Sci. Lett. **182**, 237–251 (2000). https://doi.org/10.1016/S0012-821X(00)00247-8
171. F.J. Hilgen, L. Bissoli, S.M. Iaccarino, W. Krijgsman, L.J. Lourens, R. Meijer, A. Negri, G. Villa, Breakthrough made in dating of the geological record. Earth Planet Sci. Lett. **182**, 237–251 (2000). https://doi.org/10.1029/97eo00186

172. W. Krijgsman, F.J. Hilgen, I. Raffi, F.J. Sierro, D.S. Wilson, Chronology, causes and progression of the Messinian salinity crisis. Nature **400**, 652–655 (1999). https://doi.org/10.1038/23231
173. J. Laskar, F. Joutel, F. Boudin, Orbital, precessional, and insolation quantities for the Earth from -20 Myr to +10 Myr. Astron. Astrophys. **270**, 522–533 (1993)
174. F. Gautier, G. Clauzon, J. Cravette, D. Violanti, Age et dureée de la crise de salinité Messinienne. C R Acad. Sci. Paris. **318**, 1161–1167 (1994)
175. H. Dronkert, Late Miocene evaporites in the Sorbas Basin and adjoining areas. Mem. Della Soc. Geol. Ital. **16**, 34–361 (1976)
176. H. Dronkert, Evaporite models and sedimentology of Messinian and Recent evaporites. GUA Pap. Geol. 24 (1985)
177. W. Krijgsman, A.R. Fortuin, F.J. Hilgen, F.J. Sierro, Astrochronology for the Messinian Sorbas basin (SE Spain) and orbital (precessional) forcing for evaporite cyclicity. Sed. Geol. **140**, 43–60 (2001). https://doi.org/10.1016/S0037-0738(00)00171-8
178. T.B. Roep, C.I. Dabrio, A.R. Fortuin, M.D. Polo, Late highstand patterns of shifting and stepping coastal barriers and washover-fans (late Messinian, Sorbas Basin, SE Spain). Sed. Geol. **116**, 27–56 (1998). https://doi.org/10.1016/s0037-0738(97)00111-5
179. T.B. Roep, D. Van Harten, Sedimentological and ostracodological observations on Messinian post-evaporite deposits in some southeastern Spanish basins. Ann. Geol. Pays Hellén. **3**, 1037–1044 (1979)
180. C.J. Dabrio, M. Esteban, J.M. Martín, The coral reef of Níjar, Messinian (uppermost Miocene), Almería province, S.E. Spain. J. Sediment Pet. **51**, 521–529 (1981). https://doi.org/10.1306/212f7cca-2b24-11d7-8648000102c1865d
181. J.M. Martín, J.C. Braga, R. Riding, Siliciclastic stromatolites and thrombolites, late Miocene, S.E. Spain. J. Sediment Pet. **63**, 131–139 (1993). https://doi.org/10.1306/d4267aaa-2b26-11d7-8648000102c1865d
182. G.M. Stampfli, C.F.W. Hocker, Messinian paleorelief from a 3-D seismic survey in the Tarraco concession area (Spanish Mediterranean Sea). Geol. En Mijnb. **68**, 201–210 (1989)
183. J. Frey Martinez, J.A. Cartwright, P.M. Burgess, J. Vincente-Bravo, 3D seismic interpretation of the Messinian Unconformity in the Valencia Basin, Spain, in *3D Seismic Technology: Application to the Exploration of Sedimentary Basins*. ed. by R.J. Davies, J.A. Cartwright, S.A. Stewart, M. Lappin, J.R. Underhill (Geological Society, London, Memoirs, 2004), pp.91–100
184. Y. Canton, F. Domingo, A. Solié-Benet, J. Puigdefãbregas, Hydrological and erosion response of a badlands system in semiarid SE Spain. Jour Hydrol. **252**, 65–84 (2001). https://doi.org/10.1016/s0022-1694(01)00450-4
185. M.A. Gonzalez, Recent formations of arroyo sin the Little Missouri Badlands of southern North Dakota. Geomorphology **38**, 63–84 (2000). https://doi.org/10.1016/s0169-555x(00)00070-2
186. A.L. Cameselle, R. Urgeles, B. De Mol, A. Camerlenghi, J.C. Canning, Late Miocene sedimentary architecture of the Ebro Continental Margin (Western Mediterranean): implications to the Messinian Salinity Crisis. Int. J. Earth Sci. Geol. Rundsch. **103**, 423–440 (2014). https://doi.org/10.1007/s00531-013-0966-5
187. A.L. Cameselle, R. Urgeles, Large-scale margin collapse during Messinian early sea-level drawdown: the SW Valencia trough. NW Mediterranean. Basin Res. **29**, 576–595 (2017). https://doi.org/10.1111/bre.12170
188. R. Urgeles, A. Camerlenghi, D. Garcia-Castellanos, B. De Mol, M. Garcés, J. Vergés, I. Haslam, M. Hardman, New constraints on the Messinian sealevel drawdown from 3D seismic data of the Ebro Margin, western Mediterranean: Messinian sealevel drawdown from 3D seismic data. Basin Res. **23**, 123–145 (2011). https://doi.org/10.1111/j.1365-2117.2010.00477.x
189. M. García, A. Maillard, D. Aslanian, M. Rabineau, B. Alonso, C. Gorini, F. Estrada, The Catalan margin during the Messinian Salinity Crisis: Physiography, morphology and sedimentary record. Mar Geol. **284**, 158–174 (2011). https://doi.org/10.1016/j.margeo.2011.03.017
190. C. Escutia, A. Maldonado, Palaeogeographic implications of the Messinian surface in the Valencia trough, northwestern Mediterranean Sea. Tectonophysics **203**, 263–284 (1992). https://doi.org/10.1016/0040-1951(92)90227-W
191. J. Lofi, C. Gorini, S. Berné, G. Clauzon, A. Tadeu Dos Reis, W.B.F. Ryan, M.S. Steckler, Erosional processes and paleo-environmental changes in the Western Gulf of Lions (SW France) during the Messinian Salinity Crisis. Mar. Geol. **217**, 1–30 (2005). https://doi.org/10.1016/j.margeo.2005.02.014

192. A. Maillard, A. Mauffret, Relationship between erosion surfaces and Late Miocene Salinity Crisis deposits in the Valencia Basin (northwestern Mediterranean): evidence for an early sea-level fall. Terra Nova **18**, 321–329 (2006). https://doi.org/10.1111/j.1365-3121.2006.00696.x
193. R. Pellen, D. Aslanian, M. Rabineau, J.P. Suc, C. Gorini, E. Leroux, C. Blanpied, C. Silenziario, S.M. Popescu, J.L. Rubino, The Messinian Ebro River incision. Glob. Planet. Change. **181**, 102988 (2019). https://doi.org/10.1016/j.gloplacha.2019.102988
194. J. Lofi, J. Deverchère, V. Gaullier, H. Gillet, C. Gorini, P. Guennoc, L. Loncke, A. Maillard, F. Sage, I. Thinon, E. OboneZueObame, The Messinian Salinity Crisis in the offshore domain: an overview of our knowledge through seismic profile interpretation and multi-site approach, in *The Messinian Salinity Crisis from Mega-Deposits to Microbiology—A consensus report*. (CIESM Workshop Monographs, Monaco, 2008), pp.83–90
195. J. Lofi, F. Castorina, J. Acosta, L. Dondi, A. Maillard, V. Gaullier, I. Thinon, H. Gillet, P. Guennoc, C. Gorini, Refining our knowledge of the Messinian salinity crisis records in the offshore domain through multi-site seismic analysis. Bull. Société Géologique Fr. **182**, 163–180 (2011). https://doi.org/10.2113/gssgfbull.182.2.163
196. F. Bache, J.L. Olivet, C. Gorini, M. Rabineau, J. Baztan, D. Aslanian, J.-P. Suc, Messinian erosional and salinity crises: view from the Provence Basin (Gulf of Lions, Western Mediterranean). Earth Planet Sci. Lett. **286**, 139–157 (2009). https://doi.org/10.1016/j.epsl.2009.06.021
197. C. Gorini, J. Lofi, C. Duvail, A.T. Dos Reis, P. Guennoc, P. Lestrat, A. Mauffret, The Late Messinian salinity crisis and Late Miocene tectonism: interaction and consequences on the physiography and post-rift evolution of the Gulf of Lions margin. Mar. Pet. Geol. **22**, 695–712 (2005). https://doi.org/10.1016/j.marpetgeo.2005.03.012
198. P. Guennoc, C. Gorini, A. Mauffret, Histoire géologique du golfe du Lion et cartographie du rift oligo-aquitanien et de la surface messinienne. Géologie Fr. 67–9732 (2000)
199. J. Lofi, La Crise de Salinité Messinienne: Conséquences directes et différées sur l'évolution sédimentaire de la marge du Golfe du Lion (2002)
200. J.-J. Cornée, A. Maillard, G. Conesa, F. Garcia, J.-P. Saint Martin, F. Sage, P. Münch, Onshore to offshore reconstruction of the Messinian erosion surface in Western Sardinia, Italy: implications for the Messinian salinity crisis. Sediment. Geol. **210**, 48–60 (2008). https://doi.org/10.1016/j.sedgeo.2008.06.005
201. J.J. Cornée, J.P. Saint Martin, G. Conesa, P. Münch, J.P. André, S. Saint Martin, S. Roger, Correlations and sequence stratigraphic model for Messinian carbonate platforms of the western and central Mediterranean. Int. J. Earth Sci. Geol. Rundsch. **93**, 621–633 (2004). https://doi.org/10.1007/s00531-004-0400-0
202. J.J. Cornée, S. Roger, P. Münch, J.P. Saint Martin, G. Féraud, G. Conesa, S. Pestrea-Saint Martin, Messinian events: new constraints from sedimentological investigations and new 40Ar/39Ar ages in the Melilla-Nador Basin (Morocco). Sediment Geol. **151**, 127–147 (2002). https://doi.org/10.1016/s0037-0738(01)00235-4
203. A. Maillard, V. Gaullier, C. Lézin, F. Chanier, F. Odonne, J. Lofi, New onshore/offshore evidence of the Messinian Erosion Surface from key areas: the Ibiza-Balearic Promontory and the Orosei-Eastern Sardinian margin. BSGF Earth Sci. Bull. **191**, 12 (2020). https://doi.org/10.1051/bsgf/2020007
204. P. Giresse, M.-A. Bassetti, F. Chanier, V. Gaullier, A. Maillard, I. Thinon, J. Lofi, G. Lymer, J.-Y. Reynaud, A. Negri, M. Saaveda-Pellitero, Depositional environment and age of some key Late Pliocene to Early Quaternary deposits on the underfilled Cedrino paleovalley (Orosei): insight into the Neogene geodynamic evolution of Sardinia. Quat. Int. **357**, 220–236 (2015). https://doi.org/10.1016/j.quaint.2014.11.022
205. I. Thinon, P. Guennoc, O. Serrano, A. Maillard, E. Lasseur, J.P. Réhault, Seismic markers of the Messinian Salinity Crisis in an intermediate-depth basin: Data for understanding the Neogene evolution of the Corsica Basin (northern Tyrrhenian Sea). Mar. Pet. Geol. **77**, 1274–1296 (2016). https://doi.org/10.1016/j.marpetgeo.2016.02.017
206. C. Amadori, D. Garcia-Castellanos, G. Toscani, P. Sternai, R. Fantoni, M. Ghielmi, A. Di Giulio, Restored topography of the Po Plain-Northern Adriatic region during the Messinian base-level drop-Implications for the physiography and compartmentalization of the palaeo-Mediterranean basin. Basin Res. **30**, 1247–1263 (2018). https://doi.org/10.1111/bre.12302
207. M. Ghielmi, M. Minervini, C. Nini, S. Rogledi, M. Rossi, Late Miocene-Middle Pleistocene sequences in the Po Plain – Northern Adriatic Sea (Italy): the stratigraphic record of modification phases affecting

a complex foreland basin. Mar. Pet. Geol. **42**, 50–81 (2013). https://doi.org/10.1016/j.marpetgeo.2012.11.007
208. A. Rizzini, L. Dondi, Messinian evolution of the Po basin and its economic implications (hydrocarbons). Palaeogeogr. Palaeoclim. Palaeoecol. **29**, 41–74 (1979). https://doi.org/10.1016/0031-0182(79)90074-9
209. M. Rossi, S. Rogledi, G. Barbacini, D. Casadei, S. Iaccarino, G. Papani, Tectono–stratigraphic architecture of Messinian piggyback basins of Northern Apennines: the Emilia folds in the Reggio-Modena area and comparison with the Lombardia and Romagna sectors. Boll. Soc. Geol. Ital. **1**, 437–447 (2002)
210. M. Rossi, M. Minevvini, M. Ghielmi, S. Rogledi, Messinian and Pliocene erosional surfaces in the Po Plain-Adriatic Basin: insights from allostratigraphy and sequence stratigraphy in accessing play concepts related to accomodation and gateway turnarounds in tectonically active regions. Mar Pet. Geol. **66**, 192–216 (2015). https://doi.org/10.1016/j.marpetgeo.2014.12.012
211. A. Del Ben, R. Geletti, A. Mocnik, R. Castagner, Central Adriatic Basin. In: Lofi, J. (ed.) Seismic Atlas of the Messinian salinity crisis markers in the Mediterranean Sea. p. 67. Mem. Soc. Géol. Fr., n.s., xx and World Geological Map Commission (2017)
212. M. Roveri, M.A. Bassetti, F. Ricci Lucchi, The Mediterranean Messinian salinity crisis: an Apennine foredeep perspective. Sed Geol. **140**, 201–214 (2001). https://doi.org/10.1016/S0037-0738(00)00183-4
213. M. Roveri, S. Lugli, V. Manzi, B.C. Schreiber, The Messinian salinity crisis: a sequence-stratigraphic approach. GeoActa. **1**, 169–19022 (2008)
214. B. Delrieu, J.M. Rouchy, A. Foucault, La surface d'érosion finimessinienne en Crète central (Grèce) et sur le poutour méditerranéen: rapports avec la crise de salinité méditerranéenne. Comptes Rendus Acad. Sci. Paris. **3165**, 527–533 (1993)
215. F. Orzsag-Sperber, J.M. Rouchy, J.J. Bizon, J. Cravatte, C. Muller, La sédimentation messinienne dans le basin de Polémi (Chypre). Géologie Méditerranéenne. **7**, 91–102 (1980)
216. A.H.F. Robertson, S. Eaton, E.J. Follows, A.S. Payne, Depositional processes and basin analysis of Messinian evaporites in Cyprus. Terra Nova **7**, 233–253 (1995). https://doi.org/10.1111/j.1365-3121.1995.tb00692.x
217. J.M. Rouchy, F. Orszag-Sperber, M. Riviére, N. Combourieu-Nebout, I. Panayides, Paleoenvironmental changes at the Messinian-Pliocene boundary in the eastern Mediterranean (southern Cyprus basins): significance of the Messinian Lago-Mare. Sed. Geol. **145**, 93–117 (2001)
218. Y. Ben-Gai, Z. Ben-Avraham, B. Buchbinder, C.GSt.C. Kendall, Post-Messinian evolution of the Southeastern Levant Basin based on two-dimensional stratigraphic simulation. Mar Geol. **221**, 359–379 (2005). https://doi.org/10.1016/j.margeo.2005.03.003
219. L. Ben Moshe, Z. Ben-Avraham, Y. Enzel, U. Schattner, Estimating drawdown magnitudes of the Mediterranean Sea in the Levant basin during the Lago Mare stage of the Messinian Salinity Crisis. Mar. Geol. **427**, 106–215 (2020). https://doi.org/10.1016/j.margeo.2020.106215
220. C. Bertoni, J.A. Cartwright, Controls on the basinwide architecture of late Miocene (Messinian) evaporites on the Levant margin (Eastern Mediterranean). Sediment. Geol. **188–189**, 93–114 (2006). https://doi.org/10.1016/j.sedgeo.2006.03.019
221. C. Bertoni, J.A. Cartwright, Clastic depositional systems at the base of the late Miocene evaporites of the Levant region, Eastern Mediterranean. Geol. Soc. Lond. Spec. Publ. **285**, 37–52 (2007). https://doi.org/10.1144/SP285.3
222. A. Cohen, Stratification of the Messinian evaporites in Israel. Isr. J. Earth Sci. **37**, 103–203 (1988)
223. A. Cohen, Halite-clay interplay in the Israeli Messinian. Sediment. Geol. **86**, 211–228 (1993). https://doi.org/10.1016/0037-0738(93)90023-X
224. M.A. Gardosh, Y. Druckman, Seismic stratigraphy, structure and tectonic evolution of the Levantine Basin, offshore Israel. Geol. Soc. Lond. Spec. Publ. **260**, 201–227 (2006). https://doi.org/10.1144/GSL.SP.2006.260.01.09
225. Z. Gvirtzman, V. Manzi, R. Calvo, I. Gavrieli, R. Gennari, S. Lugli, M. Reghizzi, M. Roveri, Intra-Messinian truncation surface in the Levant Basin explained by subaqueous dissolution. Geology **45**, 915–918 (2017). https://doi.org/10.1130/G39113.1
226. K.H. Kartveit, H.B. Ulsund, S.E. Johansen, Evidence of sea level drawdown at the end of the Messinian salinity crisis and seismic investigation of the Nahr Menashe unit in the northern Levant Basin, offshore Lebanon. Basin Res. **31**, 827–840 (2019). https://doi.org/10.1111/bre.12347

227. C. Kirkham, C. Bertoni, J. Cartwright, N.G. Lensky, I. Sirota, K. Rodriguez, N. Hodgson, The demise of a 'salt giant' driven by uplift and thermal dissolution. Earth Planet Sci. Lett. **531**, 115933 (2020). https://doi.org/10.1016/j.epsl.2019.115933
228. A.S. Madof, S. Connel, Northern Levant basin (Seismic stratigraphy of a previously unidentified Messinian fluvio-deltaic succession: Implications for pre-Zanclean lacustrine flooding in the eastern Mediterranean). In: Lofi, J. (ed.) Seismic atlas of the Messinian salinity crisis markers in the Mediterranean sea. pp. 57–59. Mém. Soc. géol. fr., n.s., xx, and World Geological Map Commission, 67p. (2017)
229. A.S. Madof, C. Bertoni, J. Lofi, Discovery of vast fluvial deposits provides evidence for drawdown during the late Miocene Messinian salinity crisis. Geology **47**, 171–174 (2019). https://doi.org/10.1130/G45873.1
230. A. Meilijson, F. Hilgen, J. Sepúlveda, J. Steinberg, V. Fairbank, R. Flecker, N.D. Waldmann, S.A. Spaulding, O.M. Bialik, F.G. Boudinot, P. Illner, Y. Makovsky, Chronology with a pinch of salt: Integrated stratigraphy of Messinian evaporites in the deep Eastern Mediterranean reveals long-lasting halite deposition during Atlantic connectivity. Earth-Sci. Rev. **194**, 374–398 (2019). https://doi.org/10.1016/j.earscirev.2019.05.011
231. G.L. Netzeband, C.P. Hübscher, D. Gajewski, The structural evolution of the Messinian evaporites in the Levantine Basin. Mar Geol. **230**, 249–273 (2006). https://doi.org/10.1016/j.margeo.2006.05.004
232. G. Roberts, D. Peace, Hydrocarbon plays and prospectivity of the Levantine Basin, offshore Lebanon and Syria from modern seismic data. GeoArabia. **12**, 99–124 (2007). https://doi.org/10.2113/geoarabia120399
233. C. Skiple, E. Anderson, J. Fürstenau, Seismic interpretation and attribute analysis of the Herodotus and the Levantine Basin, offshore Cyprus and Lebanon. Pet. Geosci. **18**, 433–442 (2012). https://doi.org/10.1144/petgeo2011-072
234. H.B. Solem, Seismic Interpretation of the Messinian Salinity Crisis in the Levant Basin, Eastern Mediterranean Sea, http://hdl.handle.net/11250/240417, (2014)
235. N. Vidal, D. Klaeschen, A. Kopf, C. Docherty, R. Von Huene, V.A. Krasheninnikov, Seismic images at the convergence zone from south of Cyprus to the Syrian coast, eastern Mediterranean. Tectonophysics **329**, 157–170 (2000). https://doi.org/10.1016/S0040-1951(00)00194-3
236. A. Meilijson, J. Steinberg, F. Hilgen, O.M. Bialik, N.D. Waldmann, Y. Makovsky, Deep-basin evidence resolves a 50-year-old debate and demonstrates synchronous onset of Messinian evaporite deposition in a non-desiccated Mediterranean. Geology **46194**, 243–246 (2018). https://doi.org/10.1130/G39868.1
237. C. Bertoni, J.A. Cartwright, 3D seismic analysis of circular evaporite dissolution structures, Eastern Mediterranean. J Geol Soc Lond. **162**, 909–926 (2005). https://doi.org/10.1144/0016-764904-126
238. B. Derin, Stratigraphic and environments of deposition of Or South 1075–2090 m: Derin Consulting & Micropaleontological Services LTD, Ramat Gan, Israel (2000)
239. S. Lugli, Geology of the Realmonte salt deposit, a desiccated Messinian basin (Agrigento, Sicily). Mem Soc Geol It. **54**, 75–81 (1999)
240. S. Lugli, R. Gennari, Z. Gvirtzman, V. Manzi, M. Roveri, B.C. Schreiber, Evidence of clastic evaporites in the canyons of the Levant Basin (Israel): implications for the Messinian salinity crisis. J. Sediment. Res. **83**, 942–954 (2013)
241. S. Lugli, V. Manzi, M. Roveri, B.C. Schreiber, The deep record of the Messinian salinity crisis: evidence of a non-desiccated Mediterranean Sea. Palaeogeogr. Palaeoclim. Palaeoecol. **297**, 201–218 (2015). https://doi.org/10.1016/jpalaeo.2015.05.017
242. Y. Druckman, B. Buchbinder, G.M. Martinotti, R. Simon-Tov, P. Aharon, The buried Afiq Canyon (eastern Mediterranean, Israel), a case study of a Tertiary submarine canyon exposed in Late Messinian times. Mar. Geol. **123**, 167–185 (1995). https://doi.org/10.1016/0025-3227(94)00127-7
243. J.C. Harms, J.L. Wary, Nile Delta, in *The Geology of Egypt*. (Balkema, Rotterdam, 1990), pp.329–344
244. G. Sestini, Nile Delta, a review of depositional environments and geological history, in *Deltas: Sites and Traps for Fossil Fuels*. ed. by M.K.G. Whately, K.T. Pickering (Geol. Soc. London, London, 1989), pp.99–127
245. G. Palmieri, H. Harby, J.A. Marini, F. Hashem, S. Dalla, M. Shash, Baltim fields complex: an outstanding example of hydrocarbon accumulations in a fluvial Messinian incised valley. In: Proceedings of the 13th Petroleum Conference: Cairo. pp. 256–269. (Egyptian General Petroleum Corporation, Cairo, 1996)

246. A. Mousouliotis, K. Albanakis, A. Georgakopoulos, B. Medvedev, Siliciclastic Deposits of the Messinian Nile Canyon, Herodotus Basin, Eastern Mediterranean. In: AAPG Geoscience Technology Workshop. p. 1. AAPG, Tel Aviv (2019)
247. H. Abdul Aziz, C.A.-P. Jackson, A.J. Fraser, Gravity-driven deformation of a youthful saline giant: the interplay between gliding and spreading in the Messinian basins of the Eastern Mediterranean. Pet. Geosci. **22**, 340–356 (2016). https://doi.org/10.1144/petgeo2016-034
248. A. Polonia, A. Camerlenghi, F. Davey, F. Storti, Accretion, structural style and syn-contractional sedimentation in the Eastern Mediterranean Sea. Mar. Geol. **186**, 127–144 (2002). https://doi.org/10.1016/S0025-3227(02)00176-7
249. A. Abdel Aal, A. El Barkooky, M. Schwander, H. Zaki, Tectonic evolution of the eastern Mediterranean basin and its significance for the hydrocarbon prospectivity of the Nile Delta deepwater area. GeoArabia. **6**, 363–384 (2001). https://doi.org/10.2113/geoarabia0603363
250. M.I. Abdel-Fattah, Petrophysical characteristics of the Messinian Abu Madi formation in the Baltim east and north fields, offshore Nile delta. Egypt. J Pet. Geol. **37**, 183–195 (2014). https://doi.org/10.1111/jpg.12577
251. M. Abdel-Fattah, R. Slatt, Sequence stratigraphic controls on reservoir characterization and architecture: case study of the Messinian Abu Madi incised-valley fill, Egypt. Open Geosci. **5**, 497–507 (2013). https://doi.org/10.2478/s13533-012-0144-5
252. S. Dalla, H. Harby, M. Serazzi, Hydrocarbon exploration in a complex incised valley fill: an example from the late Messinian Abu Madi Formation (Nile Delta Basin, Egypt). Lead. Edge. **16**, 1819–1824 (1997). https://doi.org/10.1190/1.1437590
253. M. Leila, A. Moscariello, Off shore Nile Delta: Regional setting. In: Lofi, J. (ed.) Seismic altas oif the Messinian salinity crisis markers in the Mediterranean sea. pp. 51–52. Mém. Soc. géol. fr., n.s., xx, and World Geological Map Commission, 67p. (2017)
254. M. Leila, M.A. Kora, M.A. Ahmed, A. Ghanem, Sedimentology and reservoir characterization of the Upper Miocene Qawasim Formation, El-Tamad Oil Field onshore Nile Delta, Egypt. Arab. J Geosci. **9**, 17 (2016). https://doi.org/10.1007/s12517-015-2088-9
255. W. Ottes, P. Lambregts, A.E. Barkooky, The Messinian Salinity Crisis in the Nile Delta: chasing shallow marine reservoirs in a deep-water basin. In: Briand, F. (ed.) The Messinian Salinity Crisis in the Nile Delta: chasing shallow marine reservoirs in a deep-water basin. pp. 107–109. CIESM Workshop Monographs, Monaco (2008)
256. J.L. Rubino, E. Crouzy, R.M. Campo, C. Jardiné, M. Khalil, T. Rives, T. Rossi, Architecture and stratigraphy of Messinian deposits (Abu Madi Fm.) at the mouth of Messinian Nile Canyon, offshore Egypt. Presented at the 77th EAGE Conference and Exhibition—Workshops, Madrid, Spain June 1 (2015)
257. M.A. Sarhan, High resolution sequence stratigraphic analysis of the Late Miocene Abu Madi Formation, Northern Nile Delta Basin. NRIAG J. Astron. Geophys. **4**, 298–306 (2015). https://doi.org/10.1016/j.nrjag.2015.11.003
258. I. El-Heiny, S. Morsi, Stratigraphic correlation of Neogene sediments in the eastern Nile Delta and Gulf of Suez. In: 11th Exploration and Production Conference, pp. 166–193, Cairo, Egypt (1992)
259. A. Salem, J. Ketser, S. Mora, R. Rizk, I.S. Al-Aasm, Diagenesis and reservoir quality evolution on incised-valley sandstone: evidence from the Abu Madi gas reservoirs (Upper Miocene), the Nile Delta basin, Egypt. J. Sediment. Res. **75**, 572–584 (2005). https://doi.org/10.2110/jsr.2005.047
260. S.A. Bowman, A comprehensive review of the MSC facies and their origins in the offshore Sirt Basin, Libya. Pet. Geosci. **18**, 457–469 (2012). https://doi.org/10.1144/petgeo2011-070
261. T. Sabato Ceraldi, M. Kamel, T. Mason, A. Poole, J. Hossack, J. Slack, ACM Fraser, Messinian seismic facies in offshore Sirt Basin Libya and implications for sub-Messinian seismic imaging. In: TOG 2008, Tripoli, Libya (2008)
262. T. Sabato Ceraldi, M. H. Ali, T. Green, K. Benjamin, M. Bourne, M. Kamel, J. Alexander, K. Coterill, A. Poole, A. Fraser, Messinian facies and Oligo-Miocene slumping in offshore Sirt Basin Libya and sub-Messinian seismic imaging. In: 72nd EAGE Conference and Exhibition incorporating SPE EUROPEC 2010. European Association of Geoscientists & Engineers, Barcelona, Spain, (2010)
263. S.J. Wells, Messinian Drawdown and Flooding in the Offshore Sirt Basin, Libya (2010)
264. J.M. Soria, J.E. Caracuel, H. Corbi, J. Dinares-Turell, C. Lancis, J.E. Tent-Manclus, A. Yébenes, The Bajo Segura Basin (SE Spain): implications for the Messinian salinity crisis in the Mediterranean margins. Stratigraphy. **5**, 257–263 (2008)

265. A.R. Fortuin, J.M.D. Kelling, Th.B. Roep, The enigmatic Messinian-Pliocene section of Cuevas del Almanzora (Vera Basin, SE Spain) revisited—erosional features and strontium isotope ages. Sed. Geol. **97**, 177–201 (1995). https://doi.org/10.1016/0037-0738(95)00009-W
266. C. Montenat, G. Bizon, J.J. Bizon, Continuité ou discontinuité de la sédimentation marine Mio-Pliocène en Méditerranée occidentale. L'exemple du bassin de Vera en Espagne méridional. Rev Inst Fr Pétrole. **31**, 613–663 (1976)
267. H. Dronkert, The evaporites of the Sorbas Basin. Rev. Inst. Inv. Geol. Dip. Prov. Barc. **32**, 55–76 (1977)
268. A.R. Fortuin, W. Krijgsman, F.J. Hilgen, F.J. Sierro, Late Miocene Mediterranean desiccation: topography and significance of the 'Salinity Crisis' erosion surface on-land in southeast Spain: Discussion and reply. Sed. Geol. **133**, 167–174 (2000). https://doi.org/10.1016/S0037-0738(00)00040-3
269. A.R. Fortuin, W. Krijgsman, The Messinian of the Nijar Basin (SE Spain): sedimentation, depositional environments and paleogeographic evolution. Sediment. Geol. **160**, 213–242 (2003). https://doi.org/10.1016/S0037-0738(02)00377-9
270. P.G. Villafañe, H. Corbi, C. Cónsole-Gonella, F.J. Ruiz-Sánchez, J.M. Soria, The Messinian stromatolites of the Sierra del Colmenar (Western Mediterranean): facies characterization and sedimentological interpretation. PeerJ **6**, e5766 (2018). https://doi.org/10.7717/peerj.5766
271. R. Riding, J.C. Braga, J.M. Martin, Late Miocene Mediterranean desiccation: topography and significance of the 'Salinity Crisis' erosion surface on-land in southeast Spain. Sed. Geol. **123**, 1–7 (1999). https://doi.org/10.1016/S0037-0738(98)00115-8
272. M.T. McCulloch, P. De Decker, Sr-isotope constraints on the Mediterranean environment at the end of the Messinian salinity crisis. Nature **342**, 62–65 (1989). https://doi.org/10.1038/342062a0
273. J.M. Soria, J.E. Caracuel, A. Yébenes, J. Fernández, C. Viseras, The stratigraphic record of the Messinian salinity crisis in the northern margin of the Bajo Segura Basin (SE Spain). Sed. Geol. **179**, 225–247 (2005). https://doi.org/10.1016/j.sedgeo.2005.05.011
274. J.M. Soria, J.E. Caracuel, H. Corbí, J. Dinarès-Turell, C. Lancis, J.E. Tent-Manclus, A. Yébenes, The Messinian record in the southern Bajo Segura Basin (Betic Cordillera, Spain). Acta Nat. "L' Ateneo Parm. **422**, A.56SS.1 (2006)
275. H. Corbí, J.M. Soria, Late Miocene–early Pliocene planktonic foraminifer event-stratigraphy of the Bajo Segura basin: a complete record of the western Mediterranean. Mar. Pet. Geol. **77**, 1010–1027 (2016). https://doi.org/10.1016/j.marpetgeo.2016.08.004
276. J. Lofi, J. Déverchère, V. Gaullier, H. Gillet, C. Gorini, P. Guennoc, L. Loncke, A. Maillard, F. Sage, I. Thinon, Seismic Atlas of the Messinian Salinity Crisis markers in the Mediterranean and Black Seas. Mem Soc Géol Fr. 179, (2011)
277. J. Lofi, J. Déverchère, V. Gaullier, H. Gillet, P. Guennoc, C. Gorini, L. Loncke, A. Maillard, F. Sage, I. Thinnon, Seismic atlas of the Messinian salinity crisis markers in the Mediterranean domain. Mém. Soc. Géol. Fr Ns World Geol. Map Comm. **2**, 67 (2018)
278. H. Heida, F. Raad, D. Garcia-Castellanos, I. Jiménez-Munt, A. Maillard, J. Lofi, Flexural-isostatic reconstruction of the Western Mediterranean during the Messinian Salinity Crisis: implications for water level and basin connectivity. Basin Res. **34**, 50–80 (2022). https://doi.org/10.1111/bre.12610
279. G. Lymer, J. Lofi, V. Gaullier, A. Maillard, I. Thinon, F. Sage, F. Chanier, B.C. Vendeville, The Western Tyrrhenian Sea revisited: new evidence for a rifted basin during the Messinian Salinity Crisis. Mar. Geol. **398**, 1–21 (2018). https://doi.org/10.1016/j.margeo.2017.12.009
280. A. Malinverno, M. Cafiero, W.B.F. Ryan, M.B. Cita, Distribution of Messinian sediments and erosional surfaces beneath the Tyrrhenian. Sea: geodynamic implications. Oceanol. Acta. **4**, 489–496 (1981)
281. A. Maillard, C. Hübscher, A. Benkhelil, E. Tahchi, Deformed Messinian markers in the Cyprus Arc: tectonic and/or Messinian Salinity Crisis indicators? Basin Res. **23**, 146–170 (2011). https://doi.org/10.1111/j.1365-2117.2010.00464.x
282. J. Cartwright, M. Jackson, T. Dooley, S. Higgins, Strain partitioning in gravity-driven shortening of a thick, multilayered evaporite sequence. Spec. Publ. Geol. Soc. Lond. **363**, 449–470 (2012). https://doi.org/10.1144/sp363.21
283. Y.E. Feng, J. Steinberg, M. Reshef, Intra-salt deformation: implications for the evolution of the Messinian evaporites in the Levant Basin, eastern Mediterranean. Mar. Pet. Geol. **88**, 251–267 (2017). https://doi.org/10.1016/j.marpetgeo.2017.08.027

284. Z. Gvirtzman, M. Reshef, O. Buch-Leviatan, Z. Ben-Avraham, Intense salt deformation in the Levant Basin in the middle of the Messinian Salinity Crisis. Earth Planet Sci. Lett. **379**, 108–119 (2013). https://doi.org/10.1016/j.epsl.2013.07.018
285. J. Frey-Martínez, J. Cartwright, B. Hall, M. Huuse, Clastic intrusion at the base of deep-water sands: A trap-forming mechanism in the Eastern Mediterranean. In: Hurst, A. and Cartwright, J. (eds.) Sand Injectites: Implications for hydrocarbon exploration and production. pp. 49–63. Am. Assoc. Petrol. Geol. (2007)
286. V. Kolla, H.W. Posamentier, L.J. Wood, Deep-water and fluvial sinuous channels—characteristics, similarities and dissimilarities, and modes of formation. Mar. Pet. Geol. **24**, 388–405 (2007). https://doi.org/10.1016/j.marpetgeo.2007.01.007
287. P. Güneş, A.E. Aksu, J. Hall, Internal seismic stratigraphy of the Messinian evaporites across the northern sector of the eastern Mediterranean Sea. Mar. Pet. Geol. **91**, 297–320 (2018). https://doi.org/10.1016/j.marpetgeo.2018.01.016
288. L. Sage, J. Letouzey, Convergence of the African and Eurasian Plates in the eastern Mediterranean, in *Petroleum and Tectonics in Mobile Belts*. ed. by J. Letouzey (Editions Technip, Paris, 1990), pp.49–68
289. I. Sirota, Y. Enzel, N.G. Lensky, Temperature seasonality control on modern halite layers in the Dead Sea: in situ observations. Geol. Soc. Am. Bull. (2017). https://doi.org/10.1130/B31661.1
290. I. Sirota, Y. Enzel, N.G. Lensky, Halite focusing and amplification of salt layer thickness: from the Dead Sea to deep hypersaline basins. Geology **46**, 851–854 (2018). https://doi.org/10.1130/G45339.1
291. C. Gorini, L. Montadert, M. Rabineau, New imaging of the salinity crisis: dual Messinian lowstand megasequences recorded in the deep basin of both the eastern and western Mediterranean. Mar. Petrol. Geol. **66**, 278–294 (2015). https://doi.org/10.1016/j.marpetgeo.2015.01.009
292. R. Flood, P.L. Manley, R.O. Kowsmann, C.J. Appi, C. Pirmez, Seismic facies and Late Quaternary growth of Amazon Submarine Fan, in *Seismic Facies and Sedimentary Processes of Submarine Fans and Turbidite Systems*. ed. by P. Weimer, M.H. Link (Springer, New York, 1991), pp.415–433
293. R.D. Flood, J.E. Damuth, Quantitative characteristics of sinuous distributary channels on the Amazon deep-sea fan. Geol. Soc. Am. Bull. **98**, 728–738 (1987). https://doi.org/10.1130/0016-7606(1987)98%3c728:qcosdc%3e2.0.co;2
294. L. Loncke, G. Bellaiche, J. Mascle, Recent depositional patterns of the Nile deep-sea fan from echo-character mapping. Bull. Am. Assoc. Pet. Geol. **86**, 1165–1186 (2002). https://doi.org/10.1306/61eedc42-173e-11d7-8645000102c1865d
295. O'Connell, S., Normark, W.R., Ryan, W.B.F., Kenyon, N.H.: An entrenched thalweg channel on the Rhone fan: Interpretation from a Seabeam and Seamarc I survey. In: Osborne, R.H. (ed.) From Shoreline to Abyss: Contributions in Marine Geology in Honor of Francis Parker Shepard. pp. 260–270. SEPM Society for Sedimentary Geology (1991)
296. K.J. Hsü, L. Montadert, D. Bernoulli, M.B. Cita, A. Erikson, R. Garrison, R.B. Kidd, F. Melieres, C. Muller, R. Wright, History of the Mediterranean salinity crisis. Nature **267**, 399–403 (1977). https://doi.org/10.1038/267399a0
297. K.J. Hsü, L. Montadert, D. Bernoulli, M.B. Cita, A. Erikson, R. Garrison, R.B. Kidd, F. Melieres, C. Muller, R. Wright, History of the Mediterranean salinity crisis, in *Init. Repts. DSDP*. ed. by K.J. Hsü, L. Montadert (U.S. Government Printing Office, Washington D.C., 1977), pp.1053–1078
298. J.M. Rouchy, C.L. Monty, Stromatolites and cryptalgal laminites associated with Messinian gypsum of Cyprus, in *Phanerozoic Stromatolites*. ed. by C. Monty (Springer, Berlin, 1981), pp.155–180
299. N. Ciaranfi, L. Dazzaro, P. Pieri, L. Rapisardi, A. Sardella, Preliminary description of some Messinian evaporitic facies along the Abruzzi-Molise boundary, in *Messinian Evaporites in the Mediterranean*. ed. by R. Catalano, G. Ruggeri, R. Sproveri (Mem Soc Geol. Ital, Rome, 1978), pp.251–260
300. G.B. Vai, F. Ricci Lucchi, The Vena del Gesso in northern Apennines: growth and mechanical breakdown of gypsified algal crusts. Mem. Sot. Geol. Ital. **16**, 217–249 (1976)
301. G. Lo Cicero, R. Catalano, Facies and petrography of some Messinian evaporites of the Ciminna basin (Sicily), in *Messinian Evaporites in the Mediterranean*. ed. by R. Catalano, G. Ruggeri, R. Sproveri (Mem. Soc. Geol. Ital, Rome, 1978), pp.55–62
302. J.M. Awramik, Stromatolites with coccoid and filamentous blue-green algae of Messinian age from site 374 ~ Ionian abyssal plain. In: Init. Repts. DSDP. pp. 665–668. U.S. Government Printing Office (1978)
303. F.H. Fabricius, K. Braune, K.O. Heiman, Comparison of site 374 with circum-Ionian land sections: implications for the Messinian "Salinity crisis" on the basis of a "dynamic model." In: Init. Repts. DSDP. pp. 927–942. U.S. Government Printing Office (1978)

304. C. Sturani, Messinian facies in the Piedmont basin. Mem. Soc. Geol. Ital. **16**, 11–25 (1978)
305. H. Corbi, J.M. Soria, C. Lancis, A. Giannetti, J.E. Tent-Manclus, J. Dinarès-Turell, Sedimentological and paleoenvironmental scenario before, during, and after the Messinian Salinity Crisis: the San Miguel de Salinas composite section (western Mediterranean). Mar. Geol. **379**, 246–266 (2016). https://doi.org/10.1016/j.margeo.2016.05.017
306. F. Orszag-Sperber, J.-M. Rouchy, M.-M. Blanc-Valleron, La transition Messinien-Pliocène en Méditerranée orientale (Chypre): la période du Lago-Mare et sa signification. Comptes Rendus Académie Sci. - Ser. IIA - Earth Planet. Sci. **331**, 483–490 (2000). https://doi.org/10.1016/S1251-8050(00)01433-6
307. F. Orszag-Sperber, J.-M. Rouchy, G. Bizon, J.J. Bizon, J. Cravatte, J. Muller, La sedimentation méssinienne dans le bassin de Polemi (Chypre). Geól. Méditerr. **7**, 91–102 (1980). https://doi.org/10.3406/geolm.1980.1130
308. J.M. Rouchy, C. Taberner, M.-M. Blanc-Valleron, R. Sprovieri, M. Russell, C. Pierre, E. Di Stefano, J.J. Pueyo, A. Caruso, J. Dinarès-Turell, E. Gomis-Coll, G.A. Wolff, G. Cespuglio, P. Ditchfield, S. Pestrea, N. Combourieu-Nebout, C. Santisteban, J.O. Grimalt, Sedimentary and diagenetic markers of the restriction in a marine basin: the Lorca Basin (SE Spain) during the Messinian. Sed. Geol. **121**, 23–55 (1998). https://doi.org/10.1016/S0037-0738(98)00071-2
309. CIESM: The Messinian Salinity Crisis from mega-deposits to microbiology—A consensus report. In: Briand, F. (ed.) N° 33 in CIESM Workshop Monographs [F. Briand, Ed.]. pp. 1–168. , Monaco (2008)
310. W. Hilgen Krijgsman, C.G. Langereis, L.J. Lourens, A. Santarelli, W.J. Zachariasse, Extending the astronomical (polarity) time scale into the Miocene. Earth Planet Sci. Lett. **136**, 495–510 (1995). https://doi.org/10.1016/0012-821X(95)00207-S
311. E. van der Laan, E. de Kaenel, F.J. Hilgen, W. Krijgsman, No major deglaciation across the Miocene-Pliocene boundary: integrated stratigraphy and astronomical tuning of the Loulja sections (Bou Regreg area, NW Morocco). Paleoceanogr. Paleoclimatology. (2006). https://doi.org/10.1029/2005PA001193
312. R. Govers, P. Meijer, W. Krijgsman, Regional isostatic response to Messinian Salinity Crisis events. Tectonophysics **463**, 109–129 (2009). https://doi.org/10.1016/j.tecto.2008.09.026
313. W.B.F. Ryan, Geodynamic responses to a two-step model of the Messinian salinity crisis. Bull. Société Géologique Fr. **182**, 73–78 (2011). https://doi.org/10.2113/gssgfbull.182.2.73
314. G.J. de Lange, W. Krijgsman, Messinian salinity crisis: a novel unifying shallow gypsum/deep dolomite formation mechanism. Mar. Geol. **275**, 273–277 (2010). https://doi.org/10.1016/j.margeo.2010.05.003
315. Roveri, M., Lugli, S., Manzi, V., Schreiber, B.C., Briand: The shallow-to deep-water record of the Messinian Salinity Crisis: new insights from Sicily, Calabria and Apennine basins. In: The Messinian Salinity Crisis from mega-deposits to microbiology—a consensus report. pp. 73–82. CIESM Workshop Monographs, Monaco (2008)
316. L. Montadert, J. Letouzey, A. Mauffret, Messinian event: seismic evidence, in *Init. Repts. DSDP*. ed. by K.J. Hsü, L. Montadert (U.S. Government Printing Office, Washington, DC, 1978), pp.1037–1050
317. J.A. van Couvering, W.A. Berggren, D. Garcia-Castellanos, B. De Mol, M. Garcés, J. Vergés, The terminal Miocene event. Mar. Micropalentoloigy. **1**, 263–286 (1976). https://doi.org/10.1016/0377-8398(76)90011-6
318. J. Garcia-Veigas, F. Orti, L. Rosell, C. Ayora, J.M. Rouchy, S. Lugli, The Messinian salt of the Mediterranean: geochemical study of the salt from the central Sicily basin and comparison with the Lorca Basin (Spain). Bull. Société Géologique Fr. **166**, 699–710 (1995)
319. J.M. Rouchy, A. Caruso, The Messinian salinity crisis in the Mediterranean basin: a reassessment of the data and an integrated scenario. Sed. Geol. **188–189**, 35–67 (2006). https://doi.org/10.1016/j.sedgeo.2006.02.005
320. S. Lugli, V. Manzi, M. Roveri, New facies interpretation of the Messinian evaporites in the Mediterranean. Presented at the The Mesinian Salinity Crisis from mega-deposits to microbiology—a Consensus Report, Monaco (2008)
321. S. Lugli, V. Manzi, M. Roveri, B.C. Schreiber, The Primary Lower Gypsum in the Mediterranean: a new facies interpretation for the first stage of the Messinian salinity crisis. Palaeogeogr. Palaeoclim. Palaeoecol. **297**, 83–99 (2010). https://doi.org/10.1016/j.palaeo.2010.07.017
322. W. Krijgsman, PTh. Meijer, Depositional environments of the Mediterranean "Lower Evaporites" of the Messinian salinity crisis: constraints from quantitative analyses. Mar. Geol. **253**, 73–81 (2008). https://doi.org/10.1016/j.margeo.2008.04.010

323. M. Babel, Models for evaporite, selenite and gypsum microbialite deposition in ancient saline basins. Geol. Pol. Acta. **54**, 313–337 (2004)
324. S. Lugli, The Realmonte salt deposit (Agrigento, Sicily): geology and exploitation: Neogene Mediterranean Paleoceanography. In: Excursion Guide Book Palermo–Caltanissetta–Agrigento–Erice (Sicily), 24–27 September 1997. pp. 44–60. Societa Geologica Italiana, Milano, and ESCO Secretariat, Zürich, Erice, Sicily (1997)
325. S. Lugli, B.C. Schreiber, Giant polygons in the Messinian salt of the Realmonte Mine (Agrigento, Sicily): Implications for modeling the "salinity crisis" in the Mediterranean. In: Cita, M.B. and McKenzie, J.A. (eds.) Neogene Mediterranean Paleoceanography. pp. 46–47. Soc. Geol. Ital., Erice, Sicily (1997)
326. S. Lugli, B.C. Schreiber, B. Triberti, Giant polygons in the Realmonte mine (Agrigento, Sicily): evidence for the desiccation of a Messinian halite basin. J. Sed. Res. **69**, 764–771 (1999). https://doi.org/10.1016/j.geobios.2006.10.004
327. V. Manzi, S. Lugli, M. Roveri, B.C. Schreiber, A new facies model for the Upper Gypsum of Sicily (Italy): chronological and palaeoenvironmental constraints for the Messinian salinity crisis in the Mediterranean. Stratigraphy. (2009). https://doi.org/10.1111/j.1365-3091.2009.01063.x
328. M. Roveri, S. Lugli, V. Manzi, B.C. Schreiber, The Messinian Sicilian stratigraphy revisited: new insights for the Messinian salinity crisis. Terra Nova **20**, 483–488 (2008). https://doi.org/10.1111/j.1365-3121.2008.00842.x
329. E. Gliozzi, A late Messinian brackish water ostracod fauna of Paratethyan aspect from Le Vicenne Basin (Abruzzi, central Apennines, Italy). Palaeogeogr. Palaeoclim. Palaeoecol. **151**, 191–208 (1999). https://doi.org/10.1016/S0031-0182(99)00023-1
330. E. Gliozzi, M.E. Ceci, F. Grossi, S. Ligios, Paratethyan ostracod immigrants in Italy during the Late Miocene: Immigrants paratéthysiens parmi les ostracodes au Miocéne supérieur en Italie. Geobios **40**, 325–337 (2007)
331. S.M. Iaccarino, A. Bertini, A.D. Stefano, L. Ferraro, R. Gennari, F. Grossi, F. Lirer, V. Manzi, E. Menichetti, M.R. Lucchi, M. Taviani, G. Sturiale, L. Angeletti, The Trave section (Monte dei Corvi, Ancona, Central Italy): an integrated paleontological study of the Messinian deposits. Stratigraphy. **5**, 281–306 (2008)
332. M. Roveri, R. Bekkali, W. Krijgsman, J. Lofi, S. Lugli, V. Manzi, F.J. Sierro, A. Bertini, A. Camerlenghi, G. De Lange, R. Govers, F.J. Hilgen, C. Hübscher, PTh. Meijer, M. Stoica, The Messinian Salinity Crisis: past and future of a great challenge for marine sciences. Mar. Geol. **352**, 25–58 (2014). https://doi.org/10.1016/j.margeo.2014.02.002
333. J.K. Warren, Evaporites through time: tectonic, climatic and eustatic controls in marine and nonmarine deposits. Earth-Sci. Rev. **98**, 217–268 (2010). https://doi.org/10.1016/j.earscirev.2009.11.004
334. P.I. Polissar, K.H. Freeman, Effects of aridity and vegetation on plant-wax dD in modern lake sediments. Geochim. Cosmochim. Acta. **74**, 5785–5797 (2010). https://doi.org/10.1016/j.gca.2010.06.018
335. D. Sachse, I. Radke, G. Gleixner, δD values of individual n-alkanes from terrestrial plants along a climatic gradient—implications for the sedimentary biomarker record. Org. Geochem. **37**, 469–483 (2005). https://doi.org/10.1016/j.orggeochem.2005.12.003
336. I. Vasiliev, E.M. Mezger, S. Lugli, G.J. Reichart, V. Manzi, M. Roveri, How dry was the Mediterranean during the Messinian Salinity Crisis? Palaeogeogr. Palaeoclim. Palaeoecol. **471**, 120–133 (2017). https://doi.org/10.1016/j.palaeo.2017.01.032
337. S.I. Feakins, N.E. Levin, H.M. Liddy, A.I. Sieracki, T.I. Eglinton, R. Bonnefille, Northeast African vegetation change over 12 m.y. Geology **41**, 295–298 (2013). https://doi.org/10.1130/g33845.1
338. I. Vasiliev, V. Karakitsios, I. Bouloubassi, K. Agiadi, G. Kontakiotis, A. Antonarakou, M. Triantaphyllou, A. Gogou, N. Kafousia, M. Rafélis, S. Zarkogiannis, F. Kaczmar, C. Parinos, N. Pasadakis, Large sea surface temperature, salinity, and productivity-preservation changes preceding the onset of the Messinian Salinity Crisis in the Eastern Mediterranean Sea. Paleoceanogr. Paleoclimatol. **34**, 182–202 (2019). https://doi.org/10.1029/2018PA003438
339. C. Turich, K.H. Freeman, Archaeal lipids record paleosalinity in hypersaline systems. Org. Geochem. **42**, 1147–1157 (2011). https://doi.org/10.1016/j.orggeochem.2011.06.002
340. A.F. Di Stefano, M. Abdel-Fattah, F. Lirer, L. Ferraro, S.M. Iaccarino, S.K. Hüsing, F.J. Hilgen, Paleoenvironmental conditions preceding the Messinian Salinity Crisis in the Central Mediterranean: Integrated data from the Upper Miocene Trave section (Italy). Palaeogeogr. Palaeoclim. Palaeoecol. **297**, 37–53 (2010). https://doi.org/10.1016/j.palaeo.2010.07.012

341. R. Gennari, V. Manzi, L. Angeletti, A. Bertini, U. Biffi, A. Ceregato, C. Faranda, E. Gliozzi, S. Lugli, E. Menichetti, A. Rosso, M. Roveri, M. Taviani, A shallow water record of the onset of the Messinian salinity crisis in the Adriatic foredeep (Legnagnone section, Northern Apennines). Palaeogeogr. Palaeoclim. Palaeoecol. **386**, 145–164 (2013). https://doi.org/10.1016/j.palaeo.2013.05.015
342. A. Bellanca, A. Caruso, G. Ferruzza, R. Neri, J.M. Rouchy, M. Sprovieri, M.M. Blanc-Valleron, Transition from marine to hypersaline conditions in the Messinian Tripoli Formation from the marginal areas of the central Sicilian Basin. Sed. Geol. **140**, 87–105 (2001). https://doi.org/10.1016/S0037-0738(00)00173-1
343. A. Bellanca, S. Calderone, R. Neri, Isotope geochemistry, petrology and depositional environments of the diatomite-dominated Tripoli Formation (Lower Messinian), Sicily. Sedimentology **33**, 729–743 (1986). https://doi.org/10.1111/j.1365-3091.1986.tb01972.x
344. A. Decima, J.A. McKenzie, B.C. Schreiber, The Origin of 'Evaporative limestones: an example from the Messinian of Sicily (Italy). J. Sediment. Petrol. **58**, 256–272 (1988)
345. A. Longinelli, Isotope geochemistry of some Messinian evaporites: paleoenvironmental implications. Palaeogeogr. Palaeoclim. Palaeoecol. **29**, 95–103 (1979). https://doi.org/10.1016/0031-0182(79)90076-2
346. J.A. McKenzie, H.C. Jenkyns, G.G. Bennet, Stable isotope study of the cyclic diatomite-claystones from the Tripoli Formation, Sicily: a prelude to the Messinian salinity crisis. Palaeogeogr. Palaeoclim. Palaeoecol. **29**, 125–141 (1979). https://doi.org/10.1016/0031-0182(79)90077-4
347. D.A. Hodell, R.H. Benson, D.V. Kent, A. Boersma, K. Rakic-El Bied, Magnetostratigraphic, biostratigraphic, and stable isotope stratigraphy of an Upper Miocene drill core from the SaleÂ Briqueterie (northwest Morocco): a high-resolution chronology for the Messinian stage. Paleoceanography **9**, 835–855 (1994). https://doi.org/10.1029/94pa01838
348. F. Bache, S.-M. Popescu, M. Rabineau, C. Gorini, J.-P. Suc, G. Clauzon, J.-L. Olivet, J.-L. Rubino, M.C. Melinte-Dobrinescu, F. Estrada, L. Londeix, R. Armijo, B. Meyer, L. Jolivet, G. Jouannic, E. Leroux, D. Aslanian, A.T.D. Reis, L. Mocochain, N. Dumurdžanov, I. Zagorchev, V. Lesić, D. Tomić, M. Namık Çağatay, J.-P. Brun, D. Sokoutis, I. Csato, G. Ucarkus, Z. Çakır, A two-step process for the reflooding of the Mediterranean after the Messinian Salinity Crisis. Basin Res. **24**, 125–153 (2012). https://doi.org/10.1111/j.1365-2117.2011.00521.x
349. Shipboard Scientific Party: Site 372: Menora Rise. In: Hsü, K.J. and Montadert, L. (eds.) Init. Repts. DSDP. pp. 59–150. U.S. Government Printing Office, Washington D.C. (1978)
350. M. Roveri, V. Manzi, A. Bergamasco, F.M. Falcieri, R. Gennari, S. Lugli, B.C. Schreiber, Dense shelf water cascading and Messinian Canyons: a new scenario for the Mediterranean salinity crisis. Am. J. Sci. **314**, 751–784 (2014). https://doi.org/10.2475/05.2014.03
351. P. Puig, A. Palanques, D.L. Orange, G. Lastras, M. Canals, Dense shelf water cascades and sedimentary furrow formation in the Cap de Creus Canyon, northwestern Mediterranean Sea. Cont. Shelf Res. **28**, 2018–2030 (2008). https://doi.org/10.1016/j.csr.2008.05.002
352. G.I. Shapiro, J.M. Hithnance, V.V. Ivanov, Dense water cascading off the continental shelf. J. Geophys. Res. Oceans. **108**, 3390 (2003). https://doi.org/10.1029/2002JC001610
353. R.D. Flood, Classification of sedimentary furrows and a model for furrow initiation and evolution. Geol. Soc. Am. Bull. **94**, 630–639 (1983). https://doi.org/10.1130/0016-7606(1983)94%3c630:cosfaa%3e2.0.co;2
354. C.D. Hollister, R.D. Flood, D.A. Johnson, P. Lonsdale, J.B. Southard, Abyssal furrows and hyperbolic echo traces on the Bahama outer ridge. Geology **2**, 395–400 (1974). https://doi.org/10.1130/0091-7613(1974)2%3c395:afahet%3e2.0.co;2
355. M. Canals, P. Puig, X. Durrieu de Madron, S. Heussner, A. Palanques, J. Fabres, Flushing submarine canyons. Nature **444**, 354–357 (2006). https://doi.org/10.1038/nature05271
356. G. Carnevale, D. Caputo, W. Landini, Late Miocene fish otoliths from the Colombacci Formation (Northern Apennines, Italy): implications for the Messinian 'Lago-mare' event. Geol. J. **41**, 537–555 (2006). https://doi.org/10.1002/gj.1055
357. G. Carnevale, A. Longinelli, D. Caputo, M. Barbieri, W. Landini, Did the Mediterranean marine reflooding precede the Mio-Pliocene boundary? Paleontological and geochemical evidence from upper Messinian sequences of Tuscany, Italy. Palaeogeogr. Palaeoclim. Palaeoecol. **257**, 81–105 (2008). https://doi.org/10.1016/j.palaeo.2007.09.005

358. G. Carnevale, F. Dela Pierre, M. Natalicchio, W. Landini, Fossil marine fishes and the 'Lago Mare' event: has the Mediterranean ever transformed into a brackish lake? Newsl. Stratigr. **51**, 57–72 (2018). https://doi.org/10.1127/nos/2016/0343
359. M. Roveri, S. Lugli, V. Manzi, R. Gennari, B.C. Schreiber, High-resolution strontium isotope stratigraphy of the Messinian deep Mediterranean basins: implications for marginal to central basins correlation. Mar. Geol. **349**, 113–125 (2014). https://doi.org/10.1016/j.margeo.2014.01.002
360. E.C. Christeleit, M.T. Brandon, G. Zhuang, Evidence for deep-water deposition of abyssal Mediterranean evaporites during the Messinian salinity crisis. Earth Planet Sci. Lett. **427**, 226–235 (2015). https://doi.org/10.1016/j.epsl.2015.06.060
361. S. Schouten, E.C. Hopmans, E. Schefus, J.S. Sinninghe Damste, Distributional variations in marine crenarchaeotal membrane lipids: a new organic proxy for reconstructing ancient sea water temperatures? Earth Planet Sci. Lett. **204**, 265–274 (2002). https://doi.org/10.1016/s0012-821x(02)00979-2
362. A. Pearson, A.E. Ingalls, Assessing the use of archaeal lipids as marine environmental proxies. Annu. Rev. Earth Plant Sci. **41**, 359–384 (2013). https://doi.org/10.1146/annurev-earth-050212-123947
363. S. Schouten, E.C. Hopmans, J.S. Sinninghe Damste, The organic geochemistry of glycerol dialkyl glycerol tetraether lipids: a review. Org. Geochem. **54**, 19–61 (2013). https://doi.org/10.1016/j.orggeochem.2012.09.006
364. N.V. Agalarova, Z.K. Kadyrova, S.A. Kuijeva, Ostracoda from Pliocene and Post Pliocene Deposits of Azerbaijan, Baku. Azerbaijan State Publ. pp 420 (1961)
365. W. Krijgsman, M. Stoica, I. Vasiliev, V.V. Popov, Rise and fall of the Paratethys Sea during the Messinian salinity crisis. Earth Planet Sci. Lett. **290**, 183–191 (2010). https://doi.org/10.1016/j.epsl.2009.12.020
366. M. Stoica, I. Lazar, I. Vasiliev, W. Krijgsman, Mollusc assemblages of the Pontian and Dacian deposits from the Topolog—Arges area (southern Carpathian foredeep—Romania). Geobios **40**, 391–405 (2007). https://doi.org/10.1016/j.geobios.2006.11.004
367. M. Stoica, I. Lazār, W. Krijgsman, I. Vasiliev, D. Jipa, A. Floroiu, Paleoenvironmental evolution of the East Carpathian foredeep during the late Miocene–early Pliocene (Dacian Basin; Romania). Glob. Planet Change. **103**, 135–148 (2013). https://doi.org/10.1016/j.gloplacha.2012.04.004
368. G. Carbonnel, L'ostracofaune du Messinien: une preuve de la vidange de la Paratéthys. Géologie Méditerranéenne. **7**, 19–24 (1980)
369. P.T. Meijer, W. Krijgsman, A quantitative analysis of the desiccation and re-filling of the Mediterranean during the Messinian Salinity Crisis. Earth Planet. Sci. Lett. **240**, 510–520 (2005). https://doi.org/10.1016/j.epsl.2005.09.029
370. W.B.F. Ryan, Modeling the magnitude and timing of evaporative drawdown during the Messinian salinity crisis. Stratigraphy. **5**, 227–243 (2008)
371. M. Stoica, W. Krijgsman, A. Fortuin, E. Gliozzi, Paratethyan ostracods in the Spanish Lago-Mare: more evidence for interbasinal exchange at high Mediterranean sea level. Palaeogeogr. Palaeoclim. Palaeoecol. **441**, 854–870 (2016). https://doi.org/10.1016/j.palaeo.2015.10.034
372. F. Andreetto, K. Matsubara, C.J. Beets, A.R. Fortuin, R. Flecker, W. Krijgsman, High Mediterranean water-level during the Lago-Mare phase of the Messinian Salinity Crisis: insights from the Sr isotope records of Spanish marginal basins (SE Spain). Palaeogeogr. Palaeoclim. Palaeoecol. **562**, 110–139 (2021). https://doi.org/10.1016/j.palaeo.2020.110139
373. L.B. Ilyina, L.A. Nevesskaja, On possible connections of the Maeotian Basin with the adjacent seas and on correlations of the Miocene deposits of Eastern Paratethys and Tethys. Ann Geol Pays Hell, pp. 553–558 (1979)
374. S.V. Popov, I.G. Shcherba, L.B. Ilyina, L.A. Nevesskaja, N.P. Paramonova, S.O. Khondkarian, I. Magyar, Late Miocene to Pliocene palaeogeography of the Paratethys and its relation to the Mediterranean. Palaeogeogr. Palaeoclim. Palaeoecol. **238**, 91–106 (2006). https://doi.org/10.1016/j.palaeo.2006.03.020
375. S.V. Popov, M.P. Antipov, A.S. Zastrozhnov, E. Kurina, T.N. Pinchuk, Sealevel fluctuations on the northern shelf of the eastern Paratethys in the Oligocene-Neogene. Strargr. Geol. Correl. **18**, 200–224 (2010). https://doi.org/10.1134/s0869593810020073
376. S.V. Popov, Y.V. Rostovtseva, T.N. Pinchuk, I.S. Patina, Oligocene to Neogene paleogeography and depositional environments of the Thr Euxinian part of Paratethys in Crimean—Caucasian junction. Mar. Pet. Geol. **103**, 163–175 (2019). https://doi.org/10.1016/j.marpetgeo.2019.02.019

377. Z. Schleder, C. Krezsek, A. Lapadat, Z. Bega, G. Ionescu, G. Tari, Structural style in a Messinian (intra-Pontian) gravity-driven deformation system, western Black Sea, offshore Romania. Pet. Geosci. **22**, 400–410 (2016). https://doi.org/10.1144/petgeo2015-094
378. C. Krezsek, Z. Schleder, Z. Bega, G. Ionescu, G. Tari, The Messinian sea-level fall in the western Black Sea: small or large? Insights from offshore Romania. Pet. Geosci. **22**, 392–399 (2016). https://doi.org/10.1144/petgeo2015-093
379. I. Vasiliev, A.G. Iosifidi, A.N. Khramov, W. Krijgsman, K.F. Kuiper, C.G. Lasngereis, V.V. Popov, M. Stoica, V.A. Tomsha, S.V. Yudin, Magnetostratigraphy and radio-isotopic dating of Upper Miocene-Lower Pliocene sedimentary successions of the Black Sea Basin (Taman Peninsula, Russia). Palaeogeogr. Palaeoclim. Palaeoecol. **310**, 163–175 (2011). https://doi.org/10.1016/j.palaeo.2011.06.022
380. A.I. Rybkina, Y.V. Rostovtseva, Astronomically-tuned Cyclicity in Upper Maeotian Deposits of the Eastern Paratethys (Zheleznyi Rog Section, Taman). Mosc Univ. Geol. Bull. **69**, 72–77 (2014). https://doi.org/10.3103/S0145875214050081
381. Y.V. Rostovtseva, A.I. Rybkina, The Messinian event in the Paratethys: astronomical tuning of the Black Sea Pontian. Mar. Pet. Geol. **80**, 321–332 (2017). https://doi.org/10.1016/j.marpetgeo.2016.12.005
382. G. Baccolo, B. Delmonte, P.B. Niles, G. Cibin, E. Di Stefano, D. Hasmpi, L. Keller, A. Marcelii, J. Michalski, Jarosite formation in deep Antarctic ice provides a window into acidic, water-limited weathering on Mars. Nat. Commun. **12**, 436 (2021). https://doi.org/10.1038/s41467-020-20705-z
383. R.W. Jones, M.D. Simmins, A Review of the Stratigraphy of Eastern Paratethys (Oligocene–Holocene), With Particular Emphasis on the Black Sea. In: Robinson, A.G. (ed.) Regional and petroleum geology of the Black Sea and surrounding region. pp. 39–52. AAPG Mem. (1997)
384. G. Carbonnel, La zone à Loxoconcha djaffarovi Schneider (Ostracoda, Miocène supérieur) ou le Messinien de la vallée du Rhône. Rev. Micropaléontologie. **21**, 106–118 (1979)
385. K.J. Hsü, W.B.F. Ryan, M.B. Cita, Late Miocene Desiccation of the Mediterranean. Nature **242**, 240–244 (1973). https://doi.org/10.1038/242240a0
386. F. Raad, J. Lofi, A. Maillard, A. Tzevahirtzian, A. Caruso, The Messinian Salinity Crisis deposits in the Balearic Promontory: an undeformed analog of the MSC Sicilian basins?? Mar. Pet. Geol. **124**, 104777 (2021). https://doi.org/10.1016/j.marpetgeo.2020.104777
387. D. Cosentino, V. Bracone, C. D'Amico, P. Cipoliari, D. Esu, C. Faranda, V. Frezza, E. Gliozzi, F. Grossi, P. Guerrieri, A. Iadanza, T. Kotsakis, I. Soulié-Märsche, The record of the Messinian salinity crisis in mobile belts: Insights from the T Molise allochthonous units (southern Apennines, Italy). Palaeogeogr Palaeoclim. Palaeoecol. **503**, 112–130 (2018). https://doi.org/10.1016/j.palaeo.2018.04.028
388. J. García-Veigas, D.I. Cendón, L. Gibert, T.K. Lowenstein, D. Artiaga, Geochemical indicators in Western Mediterranean Messinian evaporites: implications for the salinity crisis. Mar. Geol. **403**, 197–214 (2018). https://doi.org/10.1016/j.margeo.2018.06.005
389. B.C. Schreiber, G.M. Friedman, A. Decima, E. Schreiber, Depositional environments of Upper Miocene (Messinian) evaporite deposits of the Sicilian Basin. Sedimentology **23**, 729–760 (1976). https://doi.org/10.1111/j.1365-3091.1976.tb00107.x
390. F. Grossi, E. Gliozzi, P. Anadón, F. Castorina, M. Voltaggio, Is Cyprideis agrigentina Decima a good paleosalinometer for the Messinian Salinity Crisis? Morphometrical and geochemical analyses from the Eraclea Minoa section (Sicily). Palaeogeogr. Palaeoclim. Palaeoecol. **419**, 75–89 (2015). https://doi.org/10.1016/j.palaeo.2014.09.024
391. L. Londeix, M. Benzakour, J.-P. Suc, J.-L. Turon, Messinian palaeoenvironments and hydrology in Sicily (Italy): the dinoflagellate cyst record. Geobios **40**, 233–250 (2007). https://doi.org/10.1016/j.geobios.2006.12.001
392. F. Grossi, E. Gliozzi, D. Cosentino, Paratethyan ostracod immigrants mark the biostratigraphy of the Messinian Salinity Crisis. Joannea Geol. Paleontol. **11**, 66–684 (2011)
393. S.-M. Popescu, F. Dalesme, G. Jouannic, G. Escarguel, M.J. Head, M.C. Melinte-Dobrinescu, M. Süto-Szentai, K. Bakrac, G. Clauzon, J.P. Suc, Galeacysta etrusca complex: Dinoflagellate cyst marker of Paratethyan influxes to the Mediterranean Sea before and after the peak of the Messinian Salinity Crisis. Palynology **33**, 105–134 (2009). https://doi.org/10.2113/gspalynol.33.2.105

394. S.-M. Popescu, W. Cavazza, J.-P. Suc, M.C. Melinte-Dobrinescu, N. Barhoun, C. Gorini, Pre-Zanclean end of the Messinian Salinity Crisis: new evidence from central Mediterranean reference sections. J Geol Soc Lond. **178**, jgs2020-183 (2021). https://doi.org/10.1144/jgs2020-183
395. M.B. Cita, Planktonic foraminiferal biozonation of the Mediterranean Pliocene deep-sea record: a revision. Riv Ital. Paleont. Strat. **81**, 527–544 (1975)
396. M.B. Cita, S. Gartner, The stratotype Zanclean: foraminiferal and nannofossil biostratigraphy. Riv. Ital. Paleont. Strat. **78**, 503–558 (1973)
397. M.B. Cita, L. Colombo, Sedimentation in the latest Messinian at Capo Rossello (Sicily). Sedimentology **26**, 497–522 (1979). https://doi.org/10.1111/j.1365-3091.1979.tb00926.x
398. C. D'Amico, V. Bracone, P. Cipoliari, D. Cosentino, D. Esu, C. Faranda, V. Frezza, E. Gilozzi, F. Grossi, P. Cuerrieri, A. Iadanza, T. Kotsakis, The Late Messinian Lago-Mare Biofacies in the Stingeti Quarry (Southern Apennines, Italy). In: Dela Pierre, F., Aldinucci, M., Lozar, F. (eds.) RCMNS Interim Colloquium. p. 16, Torino, Italy (2014)
399. A. Irace, Il Messiniano piemontese: nuovi dati su due aree campione (2004)
400. S. Trenkwalder, D. Violanti, A. D'Atri, F. Lozar, F.D. Pierre, A. Irace, The Miocene/Pliocene boundary and the Early Pliocene micropalaeontological record: new data from the Tertiary Piedmont Basin (Moncucco quarry, Torino Hill, Northwestern Italy). Boll. Della Soc. Paleontol. Ital. 18 (2008)
401. D. Violanti, S. Trenkwalder, F. Lozar, L.M. Gallo, Micropalaeontological analyses of the Narzole core: biostratigraphy and palaeoenvironment of the late Messinian and early Zanclean of Piedmont (Northwestern Italy). Boll. Della Soc. Paleontol. Ital. 15 (2009)
402. D. Violanti, F. Dela Pierre, S. Trenkwalder, F. Lozar, P. Clari, A. Irace, A. D'Atri, Biostratigraphic and palaeoenvironmental analyses of the Messinian/Zanclean boundary and Zanclean succession in the Moncucco quarry (Piedmont, northwestern Italy). Bull. Geol. Soc. Fr. **182**, 149–162 (2011). https://doi.org/10.2113/gssgfbull.182.2.149
403. S. S. Colombero, D.M. Alba, C. D'Amico, M. Delfino, D. Esu, P. Giuntelli, M. Harzhauser, P.P.A. Mazza, M. Mosca, T.A. Neubauer, G. Pavia, A. Villa, G. Carnealle, Late Messinian mollusks and vertebrates from Moncucco Torinese, north-western Italy. Paleoecological and paleoclimatological implications. Palaeontol. Electron. **20**, 1–66 (2017). palaeo-electronica.org/content/2017/1749-moncucco-torinese-paleoecology
404. T.A. Neubauer, M. Harzhauser, E. Georgopoulou, O. Mandic, A gastropod-based biogeographic scheme for the European Neogene freshwater systems. Earth-Sci. Rev. **143**, 98–116 (2015). https://doi.org/10.1016/j.earscirev.2015.01.010
405. H.D. Boeters, K. Gittenberger, P. Subai, Die Aciculidae (Mollusca Gastropoda, Prosobranchia). Zool. Verh. **252**, 1–234 (1989)
406. E. Di Stefano, R. Sproveri, S. Scarantino, Chronology of bio-stratigraphic events at the base of the Pliocene. Paleopelagos. **6**, 401–414 (1996)
407. C. Pierre, A. Caruso, M.-M. Blanc-Valleron, J.-M. Rouchy, F. Orzsag-Sperber, Reconstruction of the paleoenvironmental changes around the Miocene-Pliocene boundary along a West-East transect across the Mediterranean. Sed Geol. **188–189**, 319–340 (2006). https://doi.org/10.1016/j.sedgeo.2006.03.011
408. D. Cosentino, I. Federici, P. Cipollari, E. Gliozzi, Environments and tectonic instability in central Italy (Garigliano Basin) during the late Messinian Lago–Mare episode: new data from the onshore Mondragone 1 well. Sed. Geol. **188–189**, 297–317 (2006). https://doi.org/10.1016/j.sedgeo.2006.03.010
409. A. Bossio, L. Giannelli, R. Mazzanti, R. Mazzei, G. Salvatorini, Gli strati alti del Messiniano, il passaggio Miocene–Pliocene e la sezione plio-pleistocenica di Nugola nelle colline a NE dei Monti Livornesi. In: Excursion guide-book. pp. 55–90, Pisa, Italy (1981)
410. S. Marabini, G.B. Vai, Geology of the Monticino quarry, Brisighella, Italy. Stratigraphic implications of its late Messinian mammal fauna. Boll. Soc. Paleontol. Ital. **28**, 369–382 (1989)
411. L. Rook, M. Delfino, M. Sami, I vertebrati fos- sili della cava del Monticino di Brisighella: una finestra sui popolamenti continentali del Mediterraneo nel Miocene superiore. Mem. Dell'Istituto Ital. Speleol. **28**, 79–100 (2015)
412. P.G. DeCelles, W. Cavazza, Upper Messinian conglomerates in Calabria, southern Italy: Response to orogenic wedge adjustment following Mediterranean sea-level changes. Geology **23**, 775–778 (1995). https://doi.org/10.1130/0091-7613(1995)023%3c0775:umcics%3e2.3.co;2

413. W. Cavazza, P.G. DeCelles, Upper Messinian siliciclastic rocks in southeastern Calabria (southern Italy): paleotectonic and eustatic implications for the evolution of the central Mediterranean region. Tectonophysics **298**, 223–241 (1998). https://doi.org/10.1016/s0040-1951(98)00186-3
414. F. Orszag-Sperber, Changing perspectives in the concept of "Lago-Mare" in Mediterranean Late Miocene evolution. Sed. Geol. **188–189**, 259–277 (2006). https://doi.org/10.1016/j.sedgeo.2006.03.008
415. F.H. Lu, W.J. Meyers, Lithofacies and water-body record of Messinian evaporites in Nijar Basin, SE Spain. Sed Geol. **188–189**, 115–130 (2006). https://doi.org/10.1016/j.sedgeo.2006.03.001
416. E. Torres-Roig, J. Agustí, P. Bover, J.A. Alcover, A new giant cricetine from the basal Pliocene of Mallorca (Balearic Islands, western Mediterranean): biostratigraphic nexus with continental mammal zones. Hist. Biol. **31**, 559–573 (2019). https://doi.org/10.1080/08912963.2017.1377194
417. S. Colombero, C. Angelonr, E. Bonelli, G. Carnevalle, O. Cavello, M. Delfino, P. Giuntelli, P. Mazza, G. Pavia, M. Pavia, G. REpetto, The upper Messinian assemblages of fossil vertebrate remains of Verduno (NW Italy): another brick for a latest Miocene bridge across the Mediterranean. Neues Jahrb. Für Geol. Paläontol.- Abh. **272**, 287–324 (2014). palaeo-electronica.org/content/2017/1749-moncucco-torinese-paleoecology
418. J. Agusti, Dental evolution in the endemic glirids of the western Mediterranean islands. Mém. Mus Hist. Nat. Paris. **53**, 227–232 (1986)
419. J. Agusti, P. Bover, J.A. Alcover, A new genus of endemic cricetid (Mammalia, Rodentia) from the late Neogene of Mallorca (Balearic Islands, Spain). J. Vertebr. Paleontol. **32**, 722–726 (2012). https://doi.org/10.1080/02724634.2012.652322
420. J. Agusti, M. Garces, W. Krijgsman, Evidence for African-Iberian exchanges during the Messinian in the Spanish mammalian record. Palaeogeogr. Palaeoclim. Palaeoecol. **238**, 5–14 (2006). https://doi.org/10.1016/j.palaeo.2006.03.013
421. P. Bover, J. Quintana, J.A. Alcover, Three islands, three worlds: palaeogeography and evolution of the vertebrate fauna from the Balearic Islands. Quat. Int. **182**, 135–144 (2008). https://doi.org/10.1016/j.quaint.2007.06.039
422. P. Bover, J. Rofes, S. Bailon, J. Agusti, G. Cuenca-Bescos, E. Torres, J.A. Alcover, Late Miocene/Early Pliocene vertebrate fauna from Mallorca (Balearic Islands, Western Mediterranean): an update. Integr. Zool. **32**, 183–196 (2014). https://doi.org/10.1111/1749-4877.12049
423. J. van der Made, J. Morales, P. Montoya, Late Miocene turnover in the Spanish mammal record in relation to palaeoclimate and the Messinian Salinity Crisis. Palaeogeogr. Palaeoclim. Palaeoecol. **238**, 228–246 (2006). https://doi.org/10.1016/j.palaeo.2006.03.030
424. G. Mas, A. Maillard, J.A. Alcover, J.J. Fornós, P. Bover, E. Torres-Roig, Terrestrial colonization of the Balearic Islands: new evidence for the Mediterranean sea-level drawdown during the Messinian Salinity Crisis. Geology **46**, 527–530 (2018). https://doi.org/10.1130/G40260.1
425. G. Mas, J.J. Fornós, The Messinian Salinity Crisis in Mallorca: new insights for a Western Mediterranean stratigraphic scenario. Mar. Pet. Geol. **122**, 104656 (2020). https://doi.org/10.1016/j.marpetgeo.2020.104656
426. I. Czicer, I. Magyar, R. Pipik, M. Böhme, S. Corić, K. Bakrač, M. Sütö-Szentai, M. Lantos, E. Babinszki, P. Müller, Life in the sublittoral zone of long-lived Lake Pannon: paleontological analysis of the Upper Miocene Szak Formation, Hungary. J. Earth Sci. Geol. Rundsch. **98**, 1741–1766 (2009). https://doi.org/10.1007/s00531-008-0322-3
427. M. Harzhauser, T. Kowalke, Sarmatian (Late Middle Miocene) gastropod assem-blages of the Central Paratethys. Facies **46**, 57–82 (2002). https://doi.org/10.1007/bf02668073
428. F.P. Wesselingh, H. Alçicek, I. Magyar, A late Miocene Paratethyan mollusc fauna from the Denizli basin (southwestern Anatolia, Turkey) and its regional palaeobio-geographic implications. Geobios **41**, 861–879 (2008). https://doi.org/10.1016/j.geobios.2008.07.003
429. W. Sissingh, Late Cenozoic Ostracoda of the South Aegean Island Arc. Utrecht Micropaleo Bull. **6**, 1–187 (1972)
430. E. Gliozzi, J. Rodriguez-Lazaro, D. Nachite, M. Martin-Rubio, R. Bekkali, An overview of Neogene brackish leptocytherids from Italy and Spain: biochronological and palaeogeographical implications. Palaeogeogr. Palaeoclim. Palaeoecol. **225**, 283–301 (2005). https://doi.org/10.1016/j.palaeo.2005.06.015
431. F. Grossi, D. Cosentino, E. Gliozzi, Late Messinian Lago-Mare ostracods and palaeoenvironments of the central and eastern Mediterranean Basin. Boll. Della Soc. Paleontol. Ital. **47**, 131–146 (2008)

432. M.A. Bassetti, P. Miculan, F. Ricci Lucchi, Ostracod faunas and brackish-water environments of the late Messinian Sapigno section (northern Apennines, Italy). Palaeogeogr. Palaeoclim. Palaeoecol. **198**, 335–352 (2003). https://doi.org/10.1016/S0031-0182(03)00475-9
433. M.B. Cita, M.L. Colalongo, S. Donofrio, S. Iaccarino, G. Salvatorini, Biostratigraphy of Miocene Deep Sea Sediments (Sites 372 and 375), with Special Reference to the Messinian/Pre-Messinian Interval, in *Init. Repts. DSDP*. ed. by K. Hsü, L. Montadert (U.S. Government Printing Office, Washington D.C., 1978), pp.671–684
434. M.A. Bassetti, V. Manzi, S. Lugli, M. Roveri, A. Longinelli, F. Ricci Lucchi, M. Barbieri, Paleoenvironmental significance of Messinian post-evaporitic lacustrine carbonates in the northern Apennines, Italy. Sed. Geol. **172**, 1–18 (2004). https://doi.org/10.1016/j.sedgeo.2004.07.004
435. J.R. Lawrence, Stable Oxygen and Carbon Isotope Variations in Bulk Carbonates from Late Miocene to Present, in Tyrrhenian Basin—Site 132, in *Init. Repts. DSDP*. ed. by W.B.F. Ryan, K.J. Hsü (U.S. Government Printing Office, Washington, D.C., 1973), pp.796–798
436. C. Pierre, J.M. Rouchy, M.-M. Blanc-Valleron, Sedimentological and stable isotope changes at the Messinian/Pliocene boundary in the Eastern Mediterranean (Holes 968A, 969A, and 969B). In: Robertson, A.H.F., Emeis, K.-C., Richter, C., Camerlenghi, A. (eds.) Proc. ODP, Sci. Results. pp. 3–8. Ocean Drilling Program, College Station, TX (1998)
437. F. Bulian, T.J. Kouwenhoven, N. Anderson, W. Krijgsman, F.J. Sierro, Reflooding and repopulation of the Mediterranean Sea after the Messinian Salinity Crisis: Benthic foraminifera assemblages and stable isotopes of Spanish basins. Mar Micropaleontol. **176**, 102160 (2022). https://doi.org/10.1016/j.marmicro.2022.102160
438. V. Wennrich, S. Meng, G. Schmiedl, Foraminifers from Holocene sediments of two inland brackish lakes in central Germany. J. Foraminifer. Res. **37**, 318–326 (2007). https://doi.org/10.2113/gsjfr.37.4.318
439. B. Bruderer, F. Liechti, Bird migration across the Mediterranean. In: Proceedings of the 22nd International Ornithological Congress, Durban, pp. 1983–1999. BirdLife South Africa, Johannesburg (1999)
440. R.T. Patterson, W.B. McKillop, S. Kroker, E. Nielson, E.G. Reinhardt, Evidence for rapid avian-mediated foraminiferal colonization of Lake Winnipegosis, Manitoba, during the Holocene Hypsithermal. J. Paleolimnol. **18**, 131–143 (1997). https://doi.org/10.1023/a:1007927622654
441. J.M. Resig, Recent foraminifera from a landlocked Hawaiian lake. J. Foraminifer. Res. **4**, 69–76 (1974)
442. J.H. Cann, P. De Decker, Fossil Quaternary and living foraminifera from athalassic (non-marine) saline lakes, Southern Australia. J. Paleontol. **55**, 660–670 (1981)
443. R.H. Benson, Psychrospheric and continental ostracoda from ancient sediments in the Floor of the Mediterranean. In: Ryan, W.B.F., Hsü, K.J. (eds.) Init. Repts. Deep Sea Drill. Proj. pp. 1002–1008. U.S. Government Printing Office, Washington, D.C. (1973)
444. R.H. Benson, An ostracodal view of the Messinian salinity crisis, in *Messinian Events in the Mediterranean*. ed. by C.W. Drooger (North-Holland Publ. Co., Amsterdam, 1973), pp.335–342
445. M. Brolsma, Lithostratigraphy and foraminiferal assemblages of the Miocene-Pliocene transitional strata of Capo Rossello and Eraclea Minoa (Sicily, Italy). Proc Nederl Akad Wetensch B. **78**, 341–354 (1975)
446. M.J. Brolsma, Stratigraphical problems concerning the Miocene/Pliocene boundary in Sicily (Italy). Proc Kon Neder Akad Wetensch. **78**, 94–10778 (1975)
447. M.J. Brolsma, Discussion of the arguments concerning the palaeoenvironmental interpretation of the Arenazzolo in Capo Rossello and Eraclea Minoa (S. Sicily, Italy). Mem Soc Geol Ital. **16**, 153–157 (1978)
448. D. Esu, Latest Messinian "Lago-Mare" Lymnocardiinae from Italy: close relations with the Pontian fauna from the Dacic Basin. Geobios **40**, 291–302 (2007). https://doi.org/10.1016/j.geobios.2006.10.003
449. M. ter Borgh, M. Stoica, M.E. Donselaar, L. Matenco, W. Krijgsman, Miocene connectivity between the Central and Eastern Paratethys: Constraints from the western Dacian Basin. Palaeogeogr. Palaeoclim. Palaeoecol. **412**, 45–67 (2014). https://doi.org/10.1016/j.palaeo.2014.07.016
450. F. Andreetto, G. Aloisi, F. Raad, H. Heida, R. Flecker, K. Agiadi, J. Lofi, S. Blondel, F. Bulian, A. Camerlenghi, A. Caruso, R. Ebner, D. Garcia-Castellanos, V. Gaullier, L. Guibourdenche, Z. Gvirtzman, T.M. Hoyle, P.T. Meijer, J. Moneron, F.J. Sierro, G. Travan, A. Tzevahirtzian, I. Vasiliev, W. Krijgsman, Freshening of the Mediterranean Salt Giant: controversies and certainties around the

terminal (Upper Gypsum and Lago-Mare) phases of the Messinian Salinity Crisis. Earth-Sci. Rev. **216**, 1–47 (2021). https://doi.org/10.1016/j.earscirev.2021.103577
451. F. Andreetto, A.M. Mancini, R. Flecker, R. Gennari, J. Lewis, F. Lozar, M. Natalicchio, F. Sangiorgi, M. Stoica, F. Dela Pierre, W. Krijgsman, Multi-proxy investigation of the post-evaporitic succession of the Piedmont Basin (Pollenzo section, NW Italy): a new piece in the Stage 3 puzzle of the Messinian Salinity Crisis. Paleogeo. Paleoclimatol. Paleoecol. **594**, 110961 (2022). https://doi.org/10.1016/j.palaeo.2022.110961
452. P. Anadón, P. Ghetti, E. Gliozzi, Sr/Ca, Mg/Ca ratios and Sr and stable isotopes of biogenic carbonates from the Late Miocene Velona Basin (central Apennines, Italy) provide evidence of unusual non-marine Messinian conditions. Chem. Geol. **187**, 213–230 (2002). https://doi.org/10.1016/S0009-2541(02)00023-2
453. S. Ligios, P. Anadón, F. Castorina, C. D'Amico, D. Esu, E. Gliozzi, P. Gramigna, M. Mola, G. Monegato, Ostracoda and Mollusca biodiversity and hydrochemical features in Late Miocene brackish basins of Italy. Geobios **45**, 351–367 (2012). https://doi.org/10.1016/j.geobios.2011.10.008
454. A.S. Madof, W.B.F. Ryan, C. Bertoni, F.J. Laugier, A.S. Zaki, S.E. Baumgardner, Time-probabilistic approach to the late Miocene Messinian salinity crisis: implications for a disconnected Paratethys. Terra Nova **34**, 395–406 (2022). https://doi.org/10.1111/ter.12579
455. M.B. Cita, S. Racchetti, R. Brambilla, M. Negri, D. Colombarolu, L. Morelli, M. Ritter, E. Rovira, P. Sala, L. Bertariniu, S. Sanvito, Changes in sedimentation rates in all the Mediterranean drillsites document basin evolution and support starved basin conditions after early Zanclean flood. Mem. Della Soc. Geol. Ital. **54**, 145–159 (1999)
456. D. Corradini, U. Biffi, Etude des dinokystes à la limite Messinien-Pliocènebdans la coupe Cava Serredi, Toscane, Italie. Bull. Cent. Rech. Explor.-Prod. Elf-Aquitaine. **12**, 221–236 (1988)
457. S.-M. Popescu, M.-C. Melinte, J.-P. Suc, G. Clauzon, F. Quillévéré, M. Süto-Szentai, Earliest Zanclean age for the Colombacci and uppermost Di Tetto formations of the "latest Messinian" northern Apennines: new palaeoenvironmental data from the Maccarone section (Marche Province, Italy). Geobios **40**, 359–373 (2007). https://doi.org/10.1016/j.geobios.2006.11.005
458. M. Roveri, A. Bertini, P. Cipollari, D. Cosentino, A. Di Stefano, A.F. Accaino, R.Y. Anderson, E.E. Adams, F. Accaino, S.Bailon, S. Lugli, V. Manzi, "Earliest Zanclean age for the Colombacci and uppermost Di Tetto formations of the « latest Messinian » northern Apennines: New palaeoenvironmental data from the Maccarone section (Marche Province, Italy)" by Popescu et al. (2007) Geobios 40 (359–373). Geobios. **41**, 669–675 (2008). https://doi.org/10.1016/j.geobios.2008.01.002
459. J. Backman, I. Raffi, Calibration of Miocene nannofossil events to orbitally tuned cyclostratigraphies from Ceara Rise. In: Shackleton, N.J., Curry, W.B., Richter, C., Bralower, T.J. (eds.) Proc. ODP, Sci. Results. pp. 83–99. Ocean Drilling Program, College Station TX (1997)
460. D. Castradori, Calcareous nannofossils in the basal Zanclean of the Eastern Mediterranean Sea: remarks on paleoceanography and sapropel formation. In: Robertson, A.H.F., Emeis, K.-C., Richter, C., and Camerlenghi, A. (eds.) Proc. Ocean Drill Prog. Sci. Results. pp. 113–123. Ocean Drilling Program, College Station TX (1998)
461. K.H. Kartveit, K.O. Omosanya, S.E. Johansen, O.E. Eruteya, M. Reshef, N.D. Waldmann, Multiphase structural evolution and geodynamic implications of messinian salt-related structures, Levant basin, Offshore Israel. Tectonics **37**, 1210–1230 (2018). https://doi.org/10.1029/2017TC004794
462. M.B. Cita, Exhumation of Messinian evaporites in the deep-sea and creation of deep anoxic brine-filled collapsed basins. Sed Geol. **188–189**, 357–378 (2006). https://doi.org/10.1016/j.sedgeo.2006.03.013
463. K. Wallmann, G.H. Westbrook, G. Winckler, M.B. Cita, Salty brines on the Mediterranean sea floor. Nature **387**, 31–32 (1997). https://doi.org/10.1038/387031a0
464. J. Moneron, Z. Gvirtzman, Late Messinian submarine channel systems in the Levant Basin: challenging the desiccation scenario. Geology **50**, 1366–1371 (2022). https://doi.org/10.1130/G50583.1
465. V. Kolla, A review of sinuous channel avulsion patterns in some major deep-sea fans and factors controlling them. Mar Pet Geol. **24**, 450–469 (2007). https://doi.org/10.1016/j.marpetgeo.2007.01.004
466. C. Pirmez, J. Imran, Reconstruction of turbidity currents in Amazon Channel. Mar Pet. Geol. **20**, 823–849 (2003). https://doi.org/10.1016/j.marpetgeo.2003.03.005
467. S.M. Kabir, D. Iacopiniu, A. Hartley, V. Maselli, D. Oppo, The role of the Nahr Menashe in the Messinian Salinity Crisis: formation, dissolution and fluvial incision of the top evaporite unit in the NE Levant Basin, Eastern Mediterranean. Presented at the EGU General Assembly 2021, Viena April 19 (2021)

468. L. Droz, G. Bellaiche, Rhône deep-sea fan: morphostructure and growth pattern. AAPG Bull. **69**, 460–479 (1985). (**10-16f7-11d7-8645000102c1865d**)
469. J. Mascle, T. Zitter, G. Bellache, L. Droz, V. Gaullier, L. Loncke, The Nile deep sea fan: preliminary results from a swath bathymetry survey. Mar. Pet. Geol. **18**, 471–477 (2001)
470. C.F. Pain, C.D. Oilier, Inversion of relief—a component of landscape evolution. Geomorphology **12**, 151–165 (1995)
471. F. Raad, Balearic Promontory architecture and history during the formation of the Mediterranean salt giant (2022)
472. F. Raad, R. Ebner, P. Meijer, J. Lofi, A. Maillard, A song of volumes, surfaces and fluxes—the case study of the Central Mallorca Depression (Balearic Promontory) during the Messinian Salinity Crisis. Basin Res. **35**, 1–27 (2023). https://doi.org/10.1111/bre.12702
473. M.A. McCaffrey, B. Lazar, H.D. Holland, The evaporation path of seawater and the coprecipitatioon of Br and K with halite. J. Sed. Pet. **57**, 928–937 (1987)
474. M. Leeder, *Sedimentology and Sedimentary Basins: From Turbulence to Tectonics* (Blackwell Science, Oxford, 1999)
475. R.P.M. Topper, PTh. Meijer, A modeling perspective on spatial and temporal variations in Messinian evaporite deposits. Mar. Geol. **336**, 44–60 (2013). https://doi.org/10.1016/j.margeo.2012.11.009
476. T. Rigaudier, C. Lécuyer, V. Gardien, J.-P. Suc, F. Martineau, The record of temperature, wind velocity and air humidity in the δD and δ18O of water inclusions in synthetic and Messinian halites. Geochim. Cosmochim. Acta. **75**, 4637–4652 (2011). https://doi.org/10.1016/j.gca.2011.05.034
477. S. Lugli, T.K. Lowenstein, Paleotemperatures preserved in fluid inclusions in Messinian halite, Realmonte Mine (Agrigento, Italy). Presented at the Neogene Mediterranean Paleoceanography, Erice, Sicily (1997)
478. T.K. Lowenstein, J. Li, C.N. Brown, Paleotemperatures from fluid inclusions in halite: method verification and a 100,000 year paleotemperature record, Death Valley, CA. Chem. Geol. **150**, 223–245 (1998). https://doi.org/10.1016/s0009-2541(98)00061-8
479. S.M. Roberts, R.J. Spencer, Paleotemperatures preserved in fluid inclusions in halite. Geochim. Cosmochim. Acta. **59**, 3929–3942 (1995). https://doi.org/10.1016/0016-7037(95)00253-v
480. M. Dal Cin, A. Del Ben, A. Mocnik, F. Accaino, R. Geletti, N. Wardell, F. Zgur, A. Camerlenghi, Seismic imaging of Late Miocene (Messinian) evaporites from Western Mediterranean back-arc basins. Pet. Geosci. **22**, 297–308 (2016). https://doi.org/10.1144/petgeo2015-096
481. A. Debenedetti, Messinian salt deposits in the Mediterranean: evaporites or precipitates? Bull. Geol. Soc. Italy. **95**, 941–950 (1976)
482. P. Sonnenfeld, Models of Upper Miocene evaporite genesis in the Mediterranean region, in *Geological Evolution of the Mediterranean Basin*. ed. by D.J. Stanley, F.-C. Wezel (Springer, New York, 1985), pp.323–346
483. P. Sonnenfeld, I. Finetti, Messinian evaporites in the Mediterranean: a model of continuous inflow and outflow, in *Geological Evolution of the Mediterranean Basin*. ed. by D.J. Stanley, F.-C. Wezel (Springer, New York, 1985), pp.347–553
484. J.M. Rouchy, La genèse des évaporites messiniennes de Méditerranée. Bull. Mus Nat. Hist. Paris. **50**, 277 (1982)
485. G. Clauzon, J.P. Suc, F. Gautier, A. Berger, M.F. Loutre, Alternate interpretation of the Messinian salinity crisis, controversy resolved? Geology **24**, 363–366 (1996). https://doi.org/10.1130/0091-7613(1996)024%3c0363:aiotms%3e2.3.co;2
486. D. Garcia-Castellanos, A. Villaseñor, Messinian salinity crisis regulated by competing tectonics and erosion at the Gibraltar arc. Nature **480**, 359–363 (2011). https://doi.org/10.1038/nature10651
487. W.B.F. Ryan, Decoding the Mediterranean salinity crisis. Sedimentology **56**, 95–136 (2009). https://doi.org/10.1111/j.1365-3091.2008.01031.x
488. T.J. Reston, J. Fruehn, R. von Huene, The structure and evolution of the western Mediterranean Ridge. Mar. Geol. **186**, 83–110 (2002). https://doi.org/10.1016/S0025-3227(02)00174-3
489. P.L. Tay, L. Lonergan, M. Warner, K.A. Jones, Seismic investigation of thick evaporite deposits on the central and inner unit of the Mediterranean Ridge accretionary complex. Mar. Geol. **186**, 167–194 (2002). https://doi.org/10.1016/S0025-3227(02)00178-0
490. F.J. Sierro, F.J. Hilgen, W. Krijgsman, J.A. Flores, The Abad composite (SE Spain): a Messinian reference section for the Mediterranean and the APTS. Palaeogeogr. Palaeoclim. Palaeoecol. **168**, 141–169 (2001). https://doi.org/10.1016/S0031-0182(00)00253-4

491. W. Krijgsman, M.-M. Blanc-Valleron, R. Flecker, F.J. Hilgen, T.J. Kouwenhoven, D. Merle, F. Orszag-Sperber, J.-M. Rouchy, The onset of the Messinian salinity crisis in the Eastern Mediterranean (Pissouri Basin, Cyprus). Earth Planet Sci. Lett. **194**, 299–310 (2002). https://doi.org/10.1016/S0012-821X(01)00574-X
492. D. Ochoa, F.J. Sierro, J. Lofi, A. Maillard, J.-A. Flores, M. Suárez, Synchronous onset of the Messinian evaporite precipitation: first Mediterranean offshore evidence. Earth Planet Sci. Lett. **427**, 112–124 (2015). https://doi.org/10.1016/j.epsl.2015.06.059
493. E. van der Laan, F.J. Hilgen, L.J. Lourens, E. de Kaenel, S. Gaboardi, S. Iaccarino, Astronomical forcing of Northwest African climate and glacial history during the late Messinian (6.5–5.5Ma). Palaeogeogr. Palaeoclim. Palaeoecol. **313–314**, 107–126 (2012). https://doi.org/10.1016/j.palaeo.2011.10.013
494. G. Sampalmieri, A. Iadanza, P. Cipollari, D. Cosentino, S. Lo Mastro, Palaeoenvironments of the Mediterranean Basin at the Messinian hypersaline/hyposaline transition: evidence from natural radioactivity and microfacies of post-evaporitic successions of the Adriatic sub-basin. Terra Nova (2010). https://doi.org/10.1111/j.1365-3121.2010.00939.x
495. G. Sampalmieri, P. Cipoliari, D. Cosentino, A. Ladanza, S. Lugli, M. Soligo, Le facies evaporitiche della crisi di salinitá messiniana:radioattivitá naturale della Formazione Gessoso-Solfifera della Maiella (Abruzzo, Italia centrale). Boll. Soc. Geol. Ital. **127**, 25–36 (2008)
496. D. Cosentino, R. Buchwaldt, G. Sampalmieri, A. Iadanza, P. Cipollari, T.F. Schildgen, L.A. Hinnov, J. Ramezani, S.A. Bowring, Refining the Mediterranean "Messinian gap" with high-precision U-Pb zircon geochronology, central and northern Italy. Geology **41**, 323–326 (2013). https://doi.org/10.1130/G33820.1
497. A. Arnon, J.S. Selker, N.G. Lensky, Thermohaline stratification and double diffusion diapycnal fluxes in the hypersaline Dead Sea. Limnol. Ocean. **61**, 1214–1231 (2016). https://doi.org/10.1002/lno.10285
498. L.L. Sloss, Evaporite deposition from layered solutions. Bull. Am. Assoc. Pet. Geol. **53**, 776–799 (1969). https://doi.org/10.1306/5d25c7f9-16c1-11d7-8645000102c1865d
499. P. Proedrou, M.C. Papaconstantinou, Primus basin—a model for oil exploration. Bull. Geol. Soc. Greece. **36**, 327 (2004). https://doi.org/10.12681/bgsg.16675
500. P.-L. Blanc, Of sills and straits: a quantitative assessment of the Messinian Salinity Crisis. Deep-Sea Res. **I**(47), 1429–1460 (2000). https://doi.org/10.1016/S0967-0637(99)00113-2
501. P.-L. Blanc, Improved modelling of the Messinian Salinity Crisis and conceptual implications. Earth Planet Sci. Lett. **238**, 349–372 (2006). https://doi.org/10.1016/j.palaeo.2006.03.033
502. PTh. Meijer, A box model of the blocked-outflow scenario for the Messinian Salinity Crisis. Earth Planet Sci. Lett. **248**, 486–494 (2006). https://doi.org/10.1016/j.epsl.2006.06.013
503. T. Yoshimura, J. Kuroda, S. Lugli, Y. Tamenori, N.O. Ogawa, F.J. Jiménez-Espejo, Y. Isaji, M. Roveri, V. Manzi, H. Kawahata, N. Ohkouchi, An X-ray spectroscopic perspective on Messinian evaporite from Sicily: sedimentary fabrics, element distributions, and chemical environments of S and Mg: an x-ray Spectroscopy of MSC evaporites. Geochem. Geophys. Geosyst. **17**, 1383–1400 (2016). https://doi.org/10.1002/2015GC006233
504. A. Caruso, M.-M. Blanc-Valleron, S. Da Prato, C. Pierre, J.-M. Rouchy, The late Messinian "Lago-Mare" event and the Zanclean reflooding in the Mediterranean Sea: New insights from the Cuevas del Almanzora section (Vera Basin, South-Eastern Spain). Earth-Sci Rev. **200**, 102993 (2020). https://doi.org/10.1016/j.earscirev.2019.102993
505. J. van Donk, T. Saito, N.J. Shackleton, W.B.F. Ryan, Oxygen isotopic composition of benthonic and planktonic foraminifera of earliest Pliocene age at Site 132—Tyrrhenian BasinInit. Repts. DSDP. In: Ryan, W.B.F. and Hsü, K.J. (eds.) Init. Repts. DSDP. pp. 798–800. U.S. Government Printing Office, Washington, D.C. (1973)
506. F.J. Rodríguez-Tovar, G. van Dijk, J. Maars, F. Andreetto, F.J. Hernández-Molina, W. Krijgsman, Ichnological analysis of the Messinian-Zanclean (Miocene-Pliocene) transition at Eraclea Minoa (Sicily): tracemaker response to the Terminal Messinian Flood. Palaeogeogr. Palaeoclim. Palaeoecol. **619**, 111539 (2023). https://doi.org/10.1016/j.palaeo.2023.111539
507. R. Gennari, S.M. Iaccarino, A.D. Stefano, G. Sturiale, P. Cipollari, V. Manzi, M. Roveri, D. Cosentino, The Messinian–Zanclean boundary in the Northern Apennine. Stratigraphy. **5**, 307–316 (2008)
508. P. de Deckker, A.R. Chivas, J.M.G. Shelley, Paleoenvironment of the Messinian Mediterranean "Lago Mare" from strontium and magnesium in ostracode shells. Palios. **3**, 352 (1988). https://doi.org/10.2307/3514664

509. F. Sgarrella, R. Sproveri, E. Di Stefano, A. Caruso, Paleoceanographic conditions at the base of the Pliocene in the Southern Mediterranean basins. Riv. Ital. Paleont. Strat. **103**, 207–220 (1997)
510. F. Sgarrella, R. Sproveri, E. Di Stefano, A. Caruso, R. Sprovieri, G. Bonaduce, The Capo Rossello Bore-Hole (Agrigento, Sicily): cyclostratigraphic and paleocecnographic reconstructions from quantitative analyses of the Zanclean foraminiferal assemblages. Riv. Ital. Paleont. Strat. **105**, 303–322 (1999)
511. Shipboard Scientific Party: Sites 375 and 376: Florence Rise. In: Hsü, K.J., Montadert, L. (eds.) Init. Repts. DSDP. pp. 219–304. U.S. Government Printing Office, Washington D.C. (1978)
512. S.M. Iaccarino, D. Castradori, M.B. Cita, E. Di Stefano, S. Gaboardi, J.A. McKenzie, S. Spezzaferi, R. Sproveri, The Miocene/Pliocene boundary and the significance of the earliest Pliocene flooding in the Mediterranean. Mem. Soc. Geol. It. **54**, 109–133 (1999)